DSE - Challenging Fuselage Shape and Material

Y.M. Blommert	4167996	J.M. Knepper	4178521
R. Bosch	4233441	L. Paškauskas	4273885
G.J.A. van den Eijnden	4224833	T. de Reijer	4306570
R.J.P. Giele	4306317	F.A.A.S.D.T. Rometsch	4277953
P. Goergen	4212657	A. Takken	4212118
		S. van der Velden	4213181

Final Report

Design Synthesis Exercise

TU Delft Delft University of Technology

Aerospace Engineering

January 31, 2017

Preface

This report is written by a team of eleven prospective engineers, in the final stage of their Bachelor Aerospace Engineering at Delft University of Technology. The Design Synthesis Exercise is a 10 week project, where we will explore a new aerospace concept, putting our gathered expertise into practise.
This report is the Final Report of a series where we will challenge the fuselage shape and material of an airliner. Advantages could come from having a non-circular fuselage which has a shape that better conforms to that of the payload.
We are very grateful for the help from the AELS CEO Derk-Jan van Heerden, the devotion and contribution of Patrick Rauhut, the help of dr. ir. Bergsma and ir. Sinke and the valuable advice given by our tutor Joris Melkert and coaches Julie Teuwen and Jibran Khaliq. Last but not least we want to thank dr. Christos Kassapoglou and dr. Steven Hulshoff for the valuable technical advice on structural and aerodynamic topics.

DSE Group 3
Delft, January 2017

Abstract

Pioneering in the aviation is dangerous, but its rewards might be worthwhile. What if the fuselage shape is challenged to be non-circular? A better volume efficiency, easier loading and a new perception of the future aircraft are within reach, but at what costs? Carry-on luggage is expected to increase in the future. Does that result in a new fuselage shape? This report shows the design process of a 200 passenger aircraft while challenging the fuselage shape and its material.

Market analysis showed a great demand for sustainable, single aisle aircraft. The current competitors are the Airbus A320neo, Boeing 737MAX-8 and the Airbus A321neo. With the use of system engineering tools, such as a functional breakdown structure, a functional flow diagram and a budget breakdown, a conceptual design was constructed: the A342 Beeblebrox. It purpose is to be able to outperform state-of-the-art aircraft and remain competitive for the next 50 years. Therefore the propulsion & performance, the electronics and the control & stability were designed to surpass the current aviation standard. To this end, off the shelf geared turbofan engines are used because it has a surpassing specific fuel consumption (SFC) and an overall good performance. The A342 is slightly more stable and controllable, because of its longer fuselage length but its overall tail size is similar to the A321neo. The A342 is an All-Electric-Aircraft to reduce subsystem and fuel weight. Its accessabillity is comparable to state-of-the-art aircraft. The maintainability is slightly worse, because of the revolutionary fuselage shape, that requires more frequent checking. The direct operating costs were calculated to be comparable with the A320neo. And because the A342 can carry more payload over longer distances, this ensures its ability to outperform other aircraft.

The interior is designed such to maximise volume efficiency per passenger. This defined the inner boundaries for the fuselage cross-section, for which a lightweight structure was created. From the pressurisation requirement, it follows, both analytically and using a finite element method, that rounder shapes cope better with stresses. However, the elliptical shapes might still be an option. An elliptical shape was calculated to be roughly 1500 kg heavier than the circular of the same material. The fuselage material will consist mainly of CFRP and AFRP (Carbon/Aramid Fibre Reinforced Plastics), due to their high strength and low density. For the aerodynamics of the fuselage Computational Fluid Dynamics simulation software (CFD) was used to calculate the pressure. Subsequently, the drag was calculated analytically. It can be seen that squarish fuselages decrease the wetted area which reduces the drag. The elliptical shape has an increased L/D-ratio (Lift over Drag ratio) of 2%.

The final conceptual design of the A342 Beeblebrox is a 6-abreast single aisle airliner, featuring an elliptical fuselage shape with conventional tail, better SFC and all electric systems. Each passenger has 0.107 m^3 overhead luggage storage and 0.05 m^3 checked-in luggage. Finally, it can be concluded that the elliptical shape is feasible to compete with state-of-the-art aircraft.

Contents

List of Abbreviations

ACARE	Advisory Council for Aviation Research and Innovation in Europe
AC	Alternating Current
ADFI	Air Data and Flight Instrumentation
AEA	All Electric Aircraft
AELS	Aerospace End of Life Solutions
AFDX	Avionics Full-Duplex Ethernet
AFRP	Aramid Fibre Reinforced Plastic
AGP	Airline Ground Personnel
ALC	Airline Company
AM	Additive Manufacturing
APU	Auxiliary Power Unit
ASME	American Society of Mechanical Engineers
ATP	Average Ticket Price
A320ceo	A320 current engine option
A320neo	A320 new engine option
BLI	Boundary Layer Ingestion
BPR	Bypass Ratio
CAC	Cabin Crew
CAD	Computer Aided Design
CEO	Chief Executive Officer
CDR	Conceptual Design Review
CFD	Computational Fluid Dynamics
CFK	Carbonfaserverstaerkter Kunststoff
CF	Carbon Fibre
CFRP	Carbon Fibre Reinforced Plastic
CFSM	Challenging Fuselage Shape and Material
CGN	Control, Guidance and Navigation
CIS	Commonwealth of Independent States
COC	Cockpit Crew
CO_2	Carbon dioxide
CoM	Centre Of Mass
CS	Certification Specification
CTE	Coefficient of thermal expansion
CW	Criteria Weight
DC	Direct Current
DOC	Direct Operating Costs
DOT	Design Option Tree
DOP	Direct Operating Costs
EASA	European Aviation Safety Agency
ECS	Environmental Control System
EMI	Electronic Magnetic Interference
EOL	End-of-Life
EPNdb	Effective Perceived Noise
ETR	Evaluation & Test Review
EU	European Union
FAA	Federal Aviation Administration
FAR	Federal Aviation Regulations
FDR	Final (critical) Design Review
FEM	Finite Element Method
FML	Fibre Metal Laminate
FPR	Fan Pressure Ratio
FRP	Fibre Reinforced Plastics
GDP	Gross Domestic Product
GFRP	Glass Fibre Reinforced Plastics
GOV	Government
GTF	Geared Turbo Fan
HLFC	High Laminar Flow Control
HLS	High Lift Systems
HLD	High Lift Devices
HUMS	Health and Usage Monitoring System
HWB	Hybrid Wing Body
IATA	International Air Transport Association
ICAO	International Civil Aviation Organisation
IDG	Integrated Drive Generator
IOC	Indirect Operating Costs
IPS	Ice Protection System
ISA	International Standard Atmosphere
ITAKA	Initiative Toward sustainable Kerosene for Aviation
KLM	Koninklijke Luchtvaart Maatschappij
LEAP	Leading Edge Aviation Propulsion
LG	Landing Gear
LS	Lift Surfaces
MCDU	Multifunction Control Display Unit
MOI	Moment of Inertia
MOM	Middle Of the Market
MRO	Maintenance, Repair and Overhaul
MTOW	Maximum Take-Off Weight
NASA	National Aeronautics and Space Administration
NEWAC	New Aero Engine Core
NM	Nautical Mile

NLR	Nederlands Lucht- en Ruimtevaartcentrum
NO_x	Oxides of Nitrogen
OEI	One Engine Inoperative
OEM	Original Equipment Manufacturer
OEW	Operative Empty Weight
OPR	Overall Pressure Ratio
P	Propulsion
PAX	Passenger
PC	Passenger Cabin
PPDU	Primary Power Distribution Units
PUC	Purchase Cost
PDR	Preliminary Design Review
PLF	Passenger Load Factor
RAMS	Reliability, Availability, Maintainability, Safety
RCA	Residents Living Close to the Airport
RCF	Reclaimed Carbon Fibre
RDT	Requirement Discovery Tree
RMC	Repair Maintenance and Cleaning
ROI	Return On Investment
RPK	Revenue Passenger Kilometres
RTO	Research Technical Organisation
RW	Relative Weight
S	System Requirements
S.F	Safety factor
SFC	Specific Fuel Consumption
SME	Small and Medium Enterprise
SPDU	Secondary Power Distribution Units
SST	Shear Stress Transport
STR	Structures
TBD	To Be Determined
TCAS	Traffic Alert and Collision Avoidance System
TOP	Take-Off Parameter
TRL	Technology Readiness Level
UF	Utilisation Factor
US	United States
USD	United States Dollar
VFSG	Variable Frequency Starter Generator
VHU	Vehicules hors d'usage
VOC	Volatile Organic Compound

List of Symbols

Symbol	Description	Unit
A	Cross-sectional area	m^2
A	Aspect Ratio	-
b	Wing span	m
C_D	drag coefficient	-
C_{D_0}	Zero-lift drag coefficient	-
$C_{D_{induced}}$	Zero-lift drag coefficient	-
C_f	friction coefficient	-
C_L	Lift coefficient	-
C_{L_α}	Lift slope curve	-
$C_{L_{v_\beta}}$	Vertical tail lift coefficient derivative w.r.t. side slip angle	rad/s
C_P	Pressure coefficient	-
CTE	Thermal expansion coefficient	-
c	Distance from neutral axis to outer surface	m
c	Climb speed	m/s
$\bar{c}$	wing average chord, MAC	m
c/V	Climb gradient	-
c_j	Specific fuel consumption	kg/Ns
c_{m_0}	Zero lift pitching moment	-
D	Diameter	m
D	Drag	N
$D_{induced}$	Induced drag	N
D_{skin}	Skin drag	N
E	Efficiency factor	-
E	Young's modulus	MPa
EPN	Effective perceived noise	dB
e	Oswald Factor	-
F	Applied load	N
G	Shear modulus	Pa
g	Gravitational acceleration	m/s^2
g	number of galleys	-
H	Flow shape factor	-
H1	Entrainment velocity shape factor	-
I	Moment of inertia	m^4
I_1	Moment of inertia thin strip thickness t_1	m^4
I_2	Moment of inertia thin strip thickness t_2	m^4
I_{xx}	moment of inertia xx-axis	m^4
I_{xy}	moment of inertia xy-axis	m^4
I_{yy}	moment of inertia yy-axis	m^4
K	Compliance Modulus	Pa
k_g	Gust alleviation factor	-
L	Lift	N
L_V	Side load on vertical tail	N
L/D	Lift over drag ratio	-
l	length	m
l_H	Wing 0.25MAC to horizontal tail 0.25MAC	-
l_V	Wing 0.25MAC to vertical tail 0.25MAC	-
M	Mach number	-
M	Bending moment	Nm
Manhr	total hour of men working on	hr
m	Mass	kg

M_{cr}	Critical Mach number	-
m_d	Mass dismantled Parts	kg
m_m	Mass of metal separation step	kg
m_p	Mass pre treatment step	kg
m_{tr}	Mass nonmetallic residue treatment step	kg
m_v	Vehicle mass	kg
N	Number of	-
n	Load Factor	-
$n_{gust_{neg}}$	Maximum negative gust load Factor	-
$n_{gust_{pos}}$	Maximum positive gust load Factor	-
n_{land}	Landing load factor	-
$n_{man_{neg}}$	Maximum negative manoeuvring Load Factor	-
$n_{man_{pos}}$	Maximum positive manoeuvring load factor	-
n_{max}	Maximum load factor	-
P	Passengers	-
P	Pressure	Pa
p	seats across	-
p_{cab}	Internal Cabin Pressure	Pa
p_{op}	Pressure at maximum operating altitude	Pa
R	Range	m
R_{cycl}	Recyclability rate	-
Re	Reynolds number	-
Re_θ	Reynolds number based on theta	-
r	Radius	m
S	Wing area	m^2
S_h	Surface area horizontal tail	m^2
S_{land}	runway landing distance	m
S_{TO}	runway take-off distance 8 m	
S_v	Surface area vertical tail	m^2
S_{wet}	wetted area	m^2
s	Runway length	m
T	Thrust	N
T	Temperature	K
T_4	Exit temperature of combustion chamber	K
T/W	Thrust to weight ratio	-
TOP	Take-off parameter	-
t	number of toilets	-
t	Plate thickness	m
U	Elastic strain energy	J
U_E	Equivalent Gust Airspeed	m/s
V	Volume	m^3
V	Velocity	m/s
V_∞	Free stream velocity	m/s
V_A	Design manoeuvring speed	m/s
V_B	Design speed maximum gust intensity	m/s
V_C	Design cruise speed	m/s
V_D	Design dive speed	m/s
Ve	Free stream velocity over aircraft	m/s
V_E	Equivalent airspeed	m/s
V_F	Design flap speed	m/s
$\bar{V}_H$	Horizontal tail volume coefficient	-
V_{MS}	Minimum stall speed	m/s
V_s	Stall speed	m/s
$\bar{V}_V$	Vertical tail volume coefficient	-
$\bar{x}_{ac}$	Longitudinal location aerodynamic centre	-
$\bar{x}_{cg}$	Longitudinal location centre of gravity	-

$\bar{x}_{ac_{fuselage}}$	Aerodynamic centre shift due to fuselage	-
$\bar{x}_{ac_{nacelles}}$	Aerodynamic centre shift due to nacelles	-
x_{LEMAC}	Distance from nose to leading edge MAC	m
P	Power	Watt
W	Aircraft weight	N
W_{fuel}	Fuel weight	N
W_{skin}	Fuselage skin weight	kg
$W_{str,long}$	Stringer and longerons weight	kg
W_{pay}	Payload weight	N
W_{tfo}	Trapped fuel and oil weight	N
W/S	Wing loading	N/m^2
w	Shear modulus w-direction	Pa
w	number of aisles	-
x	location on fuselage	m
α	Angle of attack	°
β	Side slip angle	°
δ_e	Elevator deflection	°
Δ_{lg}	distance between nose and main landing gear	m
Δ_P	Pressure difference	Pa
δ	Boundary layer thickness	m
δ^*	Displacement thickness	m
λ	fuselage ratio	-
μ	aircraft mass ratio	-
μ	dynamic viscosity	kg/(m s)
ρ	Density	kg/m^3
ρ_0	Air Density on ground level	kg/m^3
σ	Density Ratio	-
σ	Stress	Pa
σ_{allow}	Allowable stress	Pa
σ_{hoop}	Hoop stress	Pa
$\sigma_{0.2}$	Yield strength	Pa
σ_u	Ultimate strength	Pa
τ	Shear stress	Pa
τ_u	Ultimate shear strength	Pa
θ	Angle	°
θ	Momentum thickness	m

1. Introduction

For decades the design of passenger aircraft has been dominated by circular cross-section fuselage concepts. Metals and metal alloys were the primary materials for aircraft manufacturers in the past century. As technology evolved, state-of-the-art aircraft largely consist of composites. This transition did not have an effect on the cross-sectional shape of the fuselage. Airbus would like to know the feasibility of changing a circular cross-section in favour of new shape(s), to increase aircraft performance.

This Final Report is the last in a series of four reports, and will present insights on many aspects of the aircraft. During this phase of the project, a final design has been chosen. Preliminary design decisions are made to derive a feasible design which forms the basis of the final phase.

The report is built up as follows. First the project development will be shown in Chapter 2. This will present a Gantt chart and the management tools used. After this, the market analysis is presented, Chapter 3, followed by Chapter 4, in which the functional breakdown structure and functional flow diagram are presented. Then, in Chapter 5, the approach to make the aircraft competitive will be introduced. In Chapter 6, risks will be assessed and mitigated. It will be followed by an elaborate discussion on the aircraft operations, Chapter 7. The approach on sustainable development, will be shown in Chapter 8. In Chapter 9, the interior allocation will be chosen, which is an important input for the following Chapter, 10. It deals with the structural analysis of the fuselage design. In Chapter 11, the materials for the fuselage and other aircraft parts will be chosen. The aerodynamics of different fuselage shapes will be discussed in Chapter 12. Now there is enough input to do a trade off on the fuselage in Chapter 13. Propulsion and performance choices are discussed in Chapters 14 and 15,respectively. The remaining aircraft subsystems are assessed in Chapter 16. Chapter 17 deals with the control and stability of the aircraft. In Chapter 18, the production plan will be discussed, followed by the manufacturer & airliner economics in Chapter 19. Chapter 20 deals with the integration of the final design. Finally, the compliance matrix will show whether the requirements are met. This will be shown in Chapter 21.

The purpose of this project is to investigate different concepts for the fuselage of a 200 passenger aircraft. After trade-off and optimisation, a factually motivated conclusion is derived why this final design is favourable compared to others. The mission need statement is as follows:

"Challenge the fuselage shape and material choice of a 200 passengers aircraft to set an economic competitiveness benchmark for commercial state-of-the-art aircraft for the next 50 years".

In the Mid-Term Report a trade-off between four concepts was performed. Each was compared against the A320neo. There were concepts which could potentially outperform the A320neo. However, the sensitivity indicated that there is also a possibility that the innovative concepts reduce overall performance. Such conclusions were derived after a research in fields as aircraft performance, propulsion, aerodynamics and structural analysis.

During the Mid-Term Review these results were discussed with the client and mentors. The team provided recommendations to consider alternative planform configurations, as to increase aircraft performance. Objections were made by both the client and mentors. It was indicated that the focus should be on fuselage research and investigation. It was clarified that the requirements should be met with a conventional planform configuration.

This concluded the Mid-Term part. The next part of the project is the finalised conceptual design. The next step is documented within this report and the Final Review. The goal here is to derive a concept with a non-circular fuselage which still meets the requirements. In addition, the jury wants to see a definitive conclusion whether the new shape is the optimum. Can the circle be outperformed by an other shape or is the circle still the best shape for the commercial aviation?

The approach is schematically illustrated in the Figure 1.1. First, the departments analyse their respective

subsystems and move towards the respective trade-off. Second is the trade-off. Structures and aerodynamics departments are both analysing the same thing, a fuselage, hence a collective trade-off is performed. Third, the whole system is integrated. Finally, characteristics, conclusion and recommendations are derived.

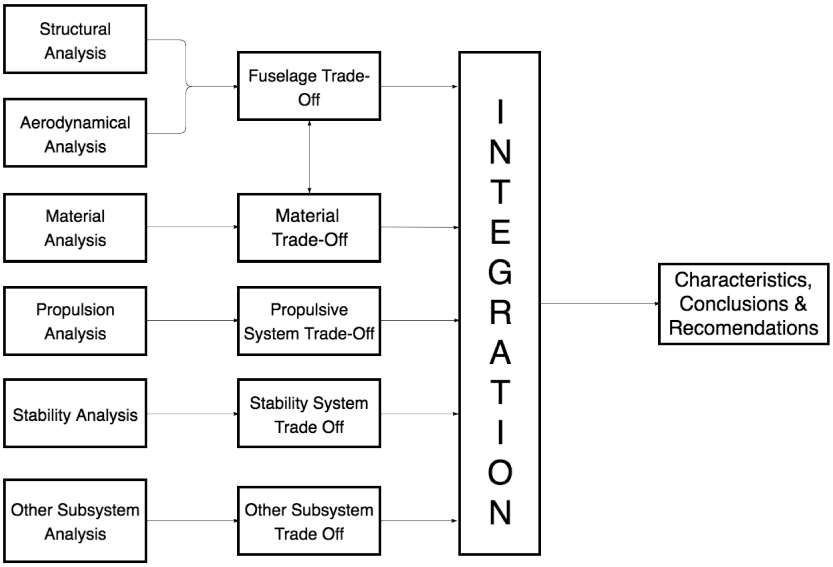

Figure 1.1: Final Report planning strategy

2. Project Development

In this chapter the development of the project is presented. First, the project design & development logic is shown. The purpose of this section is to make the reader familiar with how the project has been and will be carried out in the future. Then, the management approach of the the project is presented. This involves the Gantt chart.

2.1. Project Design & Development Logic

This report marks the end of the conceptual design phase. Conceptual design, in general, is supposed to output a design which is going to be refined and optimised in the preliminary design stage. The previous report was supposed to output a concept for which subsystem level design choices have to be made in this report. However, in the Mid-Term Report none of the concepts were good enough to meet all of the requirements. The main reason for this was that the direct operating costs were estimated to be too high due to the estimated high increase in weight due to the non-circular fuselage.

However, the client still expressed a need for a non-circular fuselage, with a conventional planform. This by definition yielded an early stage conceptual design, even if acquisition of it was somewhat unorthodox. Hence, this report will yield a finalised conceptual design. The current design still has a lot of uncertainty with respect to certain design aspects. For this reason, trade-off on subsystem level is performed later in the report.

Figure 2.1 indicates the industry accepted logic of the aircraft project life cycle. As it can be seen, the next logical step is the preliminary design. In the preliminary design a more detailed analysis of subsystems/components and interfaces is performed, the requirements are expanded and refined. The end of preliminary design phase is reached after the critical design review is carried out. In other words, the design is frozen and now the next step is taken: the detailed design.

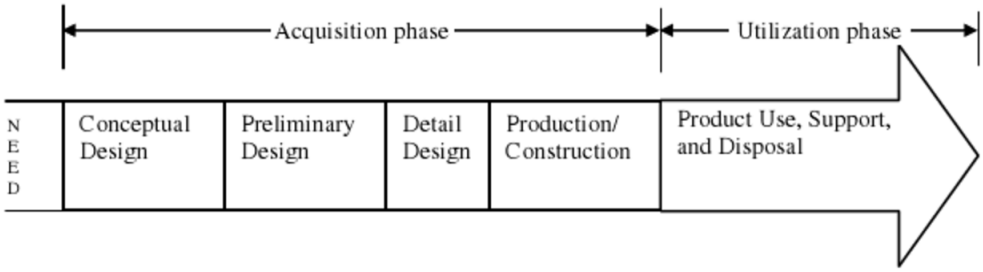

Figure 2.1: Aircraft life cycle illustrated [1]

The goal of the detailed design is to output detailed drawings and manufacturing plans which can be used to produce an aircraft. During the detailed design a physical prototype is produced. There are two reviews during this stage of design: Evaluation & Test Review (ETR) and Final (Detailed) Design Review. ETR is performed after the structural, engine, wind tunnel and flight tests are performed. Results & measurements are evaluated. Improvements then can be made in the design, which is pushed forward in the process. The Final Design Review yields in detailed drawings and manufacturing procedures, in addition to the detailed cost breakdowns. This stage of design has to be in constant validation against the requirements developed in the Preliminary & Conceptual Design stages. The procedure to cope with that is illustrated in Figure 2.2. In addition, a prototype is built. Figure 2.3 indicates design review stages in a flow chart manner to help the reader visualise the logical flow of activities.

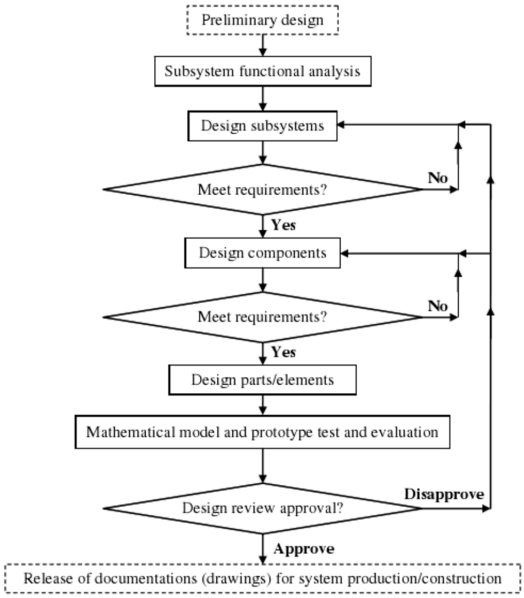

Figure 2.2: Detailed design illustrated [1]

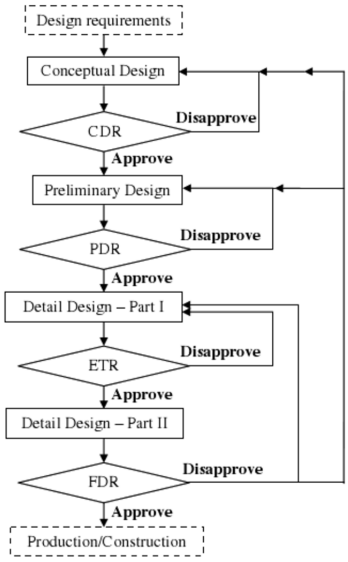

Figure 2.3: Design reviews flow [1]

Also, at the end of the detailed design, the Type Certification is performed. Here the authorities approve the type of the aircraft and the aircraft manufacturer can proceed to the next step: production.

Manufacturing, production & integration follow next. The detailed plan for this procedure in given in Chapter 18. Then, the operations stage follows. This stage is described in detail in Chapter 7. Finally, the end-of-life of the aircraft is investigated in Chapter 8.

2.2. Gantt Chart

In this section the project Gantt chart is presented. Activities that continue after the preliminary design are stated in Figure 2.4.

Figure 2.4: After DSE activities

3. Market Analysis

In this chapter, the market analysis is presented. The goal of performing a market analysis is to set the competitive volume and cost of the market for the aircraft and the services it can offer. First, the identified stakeholders are listed. Then, the current market is presented. Reference aircraft with characteristics similar to the requirements of this project are reviewed from economical and technical points of view, as well as current clients. Third, air traffic and global economy are described. Finally, an analysis of future market is presented. Global demand forecasts and aircraft performance forecasts are introduced. Then regional analysis of major commercial aviation markets is analysed.

3.1. Stakeholder Identification

A project stakeholder is an entity who is directly or indirectly influenced by or involved in the project. In order to satisfy all the stakeholders' needs, it is necessary to first identify the stakeholders of the project. The following stakeholders have been identified to be influential over the final design of this project:

- Cockpit crew
- Passengers
- Cabin crew
- Airport ground personnel
- Airline company
- Aircraft manufacturer
- Aircraft repair, maintenance and cleaning personnel
- Residents living close to the airport
- Governmental aircraft regulators
- Material suppliers
- Aircraft leasing companies
- Financial institutes
- Airline suppliers
- Non-governmental organisations
- Business communities
- Sales channels

3.2. Current Market Situation

In this section an overview on the current market situation is given. In Section 3.2.1, comparable commercial aircraft that are currently on the market are described in economic and in technical terms. Section 3.2.2 will give an insight on the current air traffic situation.

3.2.1. Reference Aircraft

State-of-the-art aircraft should be outperformed by the A324. Hence, it is required to analyse aircraft of similar properties that are currently available. The chosen aircraft closely resemble the range and number of passengers and are relatively new on the market or are still competing with state-of-the-art aircraft:

- Airbus A320neo
- Boeing 737 MAX 8/MAX 200
- Irkut MC-21-300
- Comac C919
- Bombardier CS300
- Airbus A321
- Boeing 757-200
- Boeing 757-300
- Boeing 737-900ER

These aircraft are analysed from two different perspectives. First, economic aspects such as price and maintenance cost are considered. Second, high level performance indicators are presented.

Economic Analysis

Four parameters have been chosen for economic analysis of reference aircraft: the list price, range, total of orders and the total deliveries, both until October 2016. They are compared in Table 3.1[1] [2] [3] [4]. The analysis serves to get an overview of the current market for large single aisle passenger aircraft and their characteristics. As can be seen in Table 3.1 the cost lies in the range of 68 M USD to 115 M USD, while the range in nautical miles varies from 3,200 to 3,900 nm, except for the Comac.

[1] http://planes.axlegeeks.com [accessed on November 23rd 2016]
[2] http://www.rusaviainsider.com/irkut-mc-21-russian-aircraft/ [accessed on November 24th 2016]
[3] http://www.boeing.com/company/about-bca/ [accessed on December 2nd 2016]
[4] http://www.ruaviation.com/docs/2/2010/11/1/7/?h [accessed on December 2nd 2016]

Table 3.1: Economic parameters of the reference aircraft [1] [2] [3] [4]

Aircraft description	List Price [M USD]	Range [nm]	Current Orders	Deliveries 2016
Airbus A320neo	107	3,385	4,800+	32
Boeing 737 MAX 8/MAX 200	110	3,515	1,748	0
Irkut MC-21-300	91	3,240	175	0
Comac C919	68	2,200	517	0
Bombardier CS300	82	3,300	235	0
Airbus A321	115	3,200	2,749	1,247
Boeing 737-900ER	102	3,200	524	229
Boeing 757-200	75	3,900	913	913
Boeing 757-300	80	3,395	55	55

Reference aircraft in this range have been considered since market analysis has shown that a range between 2,000 and 4,000 nm covers nearly 50% of the range preferred by the Middle Of the Market, MOM, operators, Figure 3.1 [5].

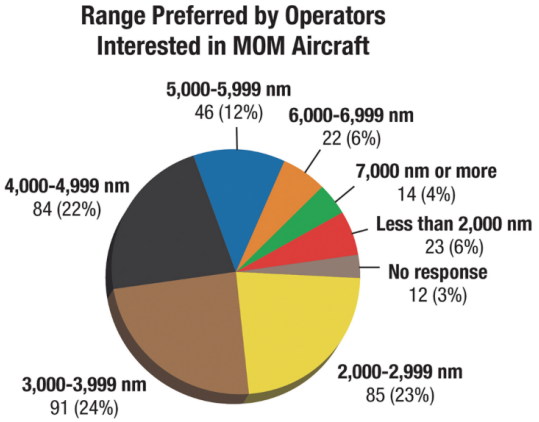

Figure 3.1: Range preferred operators interested in the middle of the market operators

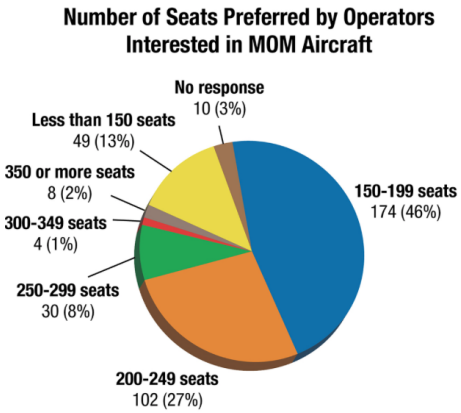

Figure 3.2: Number of seats preferred operators interested in the middle of the market operators

Performance Analysis

To clearly visualise the high-level technical data of the aircraft, a comparison Table 3.2 has been made.

Table 3.2: Performance parameters of the reference aircraft [1]

Aircraft description	Max passenger capacity	Max takeoff weight [10^3 kg]	Fuel Consumption USD per seat per NM in 2016
Airbus A320neo	195	79	0.073
Boeing 737 MAX 8/MAX 200	200	82	0.070*
Irkut MC-21-300	211	79	0.074*
Comac C919	174	77	Not available
Bombardier CS30	160	60	0.051
A321	236	93	0.063
737-900ER	215	74	0.068
757-200	228	116	0.078
757-300	289	124	0.070

*Derived from comparison with A320neo

[5] http://aviationweek.com/site-files/aviationweek.com/files/uploads/2016/07/10/AI29_pie2.jpg [accessed on 23rd January 2017]

Three performance parameters have been chosen to compare aircraft on: the maximum passenger capacity, the maximum takeoff weight, MTOW, and the fuel cost per seat per nm. The maximum passenger capacity is important because it is a direct source of revenue for the commercial passenger aircraft. Reference aircraft in this range of seating capacity have been considered since market analysis has shown that the preferred number of seats by the Middle Of the Market (MOM) operators is between 150 to 249 seats, see Figure 3.2 [6].
The maximum take off weight has a great effect on the fuel efficiency and therefore provides a good indication for off-the-shelf engines capabilities. Fuel cost per seat per nm also is an estimating factor for efficiency.

Unfortunately, Comac does not disclose any factual information regarding their efficiency or how they compare with other aircraft. Boeing and Irkut do not provide any data either for the newer aircraft. The values for the fuel consumption in USD per seat per NM were derived from comparisons with the Airbus A320neo. This should be kept in mind when considering the accuracy/validity of the data.

This data will serve as target values to achieve and preferably outperform. It is worth mentioning that all of the analysed aircraft are considered low to mid range, narrow bodied aircraft with a single aisle. Most of the referenced aircraft allow to adjust seats to accommodate multiple classes, for example business and economic. In practise this can be adjusted to facilitate for a single class, achieving maximum passenger capacity.

Current Clients of The Reference Aircraft

In order to understand the market, the possible customers for the design outcome of this project were assorted. Therefore a look was taken into the customers, who are currently using reference aircraft. For detailed information on the clients of the reference aircraft please refer to one of the previous reports [2]

3.2.2. Current Air Traffic Situation

A high growth in air traffic has been recorded from 2010 until 2015. The Revenue Passengers Kilometres increased by 6.8% compared to 2014 according to ICAO data. In 2015, 3.5 billion passengers used airtravel, an increase of 240 million compared to 2014, on a global fleet counting approximately 26,000 aircraft - averaging 100,000 flights a day over 51,000 regional, national, international and intercontinental network routes. Single aisle aircraft command the largest share of new deliveries. Over the next 20 years it is expected that these numbers double [7].

3.3. Prediction on Future Markets

In this section a prediction on future markets will be presented. This includes a forecast on the world economies, new deliveries, number of fleets and market value, the establishment and development of mega-cities, and on the future air traffic. Special attention is paid to single aisle aircraft.

3.3.1. World Economies

Momentarily, there is a great competition between Airbus and Boeing, the main manufacturers in aerospace. However, the so-called "emerging" economies, namely China, India and Russia have the capabilities of taking market-share. However, the competition on a technological level is going to increase by 2035 and the production and supply of these aircraft can already be performed at highly competitive cost levels [8].

3.3.2. Mega-cities and Future Air Traffic

Gross Domestic Product, GDP, remains one of the most important drivers regarding air transport. However, other drivers can be identified, such as urbanisation. It is crucial to understand how urbanisation will evolve in future in order to understand how the demand for air travel will change. As predicted by Airbus 62% of the world wide population will live in cities by 2035. Major cities require and take advantage from the improved connectivity transportation links provide. Nowadays, efficient transportation links are provided by aviation.

Currently, there are 55 mega-cities, this number is expected to increase to 93 mega-cities by 2035. In fact the forecast indicates that air traffic will double every 15 years [3]. These facts allow aviation to remain strong and

[6] http://aviationweek.com/commercial-aviation/airlines-boeing-get-moving-middle-market-aircraft [accessed on 23rd January 2017]
[7] https://www.youtube.com/watch?v=NlIdzF1_b5M&t=30s [accessed on December 1st 2016]
[8] http://www.cleansky.eu/large-passenger-aircraft [accessed on November 23rd 2016]

resilient to perturbations industry faces at times. It is forecasted that by 2035 Asia-Pacific will lead the world traffic followed by the Middle East. In fact domestic traffic flow is predicted to quadruple in China. [3].

3.3.3. Demand Predictions for 2035

The year 2035 was chosen for two reasons. Firstly, since it usually takes around 10 years to develop an aircraft concept and then 20 years to finally produce and deliver it to the market. Assuming that in 10 weeks the concept will be developed, roughly 20 years are left until 2035.

Secondly, the market research is based on the publicly available documents. Most of the resources are based on Airbus and Boeing predictions for year 2035. Since this market analysis is a tool for an innovative aircraft design rather than for an innovative market analysis, available resources have been exploited.

3.3.4. Global Demand

According to Boeing, world GDP is anticipated to grow at 2.9% annually over the next 20 years. During the same period, passenger traffic is predicted to grow by 4.8% and air cargo traffic by 4.2% [4]. This growth induces a demand for new aircraft. Table 3.3 provides a quantified proof for a need of a more aircraft production.

Table 3.3: Demand and in-service aircraft forecast

Aircraft in service	2015	2035	**Demand by size 2016 to 2035**	New aircraft	Value ($B)
Large widebody	740	700	Large widebody	530	220
Medium widebody	1,640	3,690	Medium widebody	3,470	1,250
Small widebody	2,660	6,060	Small widebody	5,100	1,350
Single aisle	14,870	32,280	Single aisle	28,140	3,000
Regional jets	2,600	2,510	Regional jets	2,380	110
Total	22,510	45,240	Total	39,620	5,930

As can be seen in Table 3.3 single aisle aircraft are by far the most demanded aircraft, with airlines requiring around 28,140 new single aisle aircraft deliveries out of a total of 39,620, and an estimated value of 3 trillion USD. As can be noted in Table 3.3 by 2035, the number of single aisle aircraft in service is predicted to double. By 2035 around 70% of the aircraft in service are expected to be single aisle. Coincidentally, the reference aircraft as analysed in Section 3.2.1 are also single aisle aircraft.

While 20 years is a long period of time to make predictions regarding the technology advancements, the demand for the single aisle aircraft, globalisation, and overall GDP growth indicates that more people will join the global middle class. According to Boeing, this trend indicates that low-fare and network airlines will see an increasing demand as well [4]. This conclusion serves as a proof that operation costs and aircraft manufacturing price should decrease to keep the competitive advantage. In addition, aircraft designers should anticipate what properties of the aircraft one should implement. The following subsections contain analysis of certain properties of the single aisle aircraft and their predictions for 2035. This played a crucial role in the design.

Efficiency

Efficiency plays a crucial role in the aircraft industry. Each region will respond to its unique opportunities and needs with specialised aircraft requirements. Middle East airlines, for example, will continue to favour premium wide-body aircraft due to the geographical advantages and business travel. On the other hand, airlines in Europe and North America are actively responding to growing competition from low-fare carriers by replacing old and inefficient with new and economical single class models such as A320neo [4]. Figure 3.3 indicates how current aircraft are gradually replaced by more efficient Airbus models.The similar trend is projected by Boeing for the future and can be found in Figure 3.4.

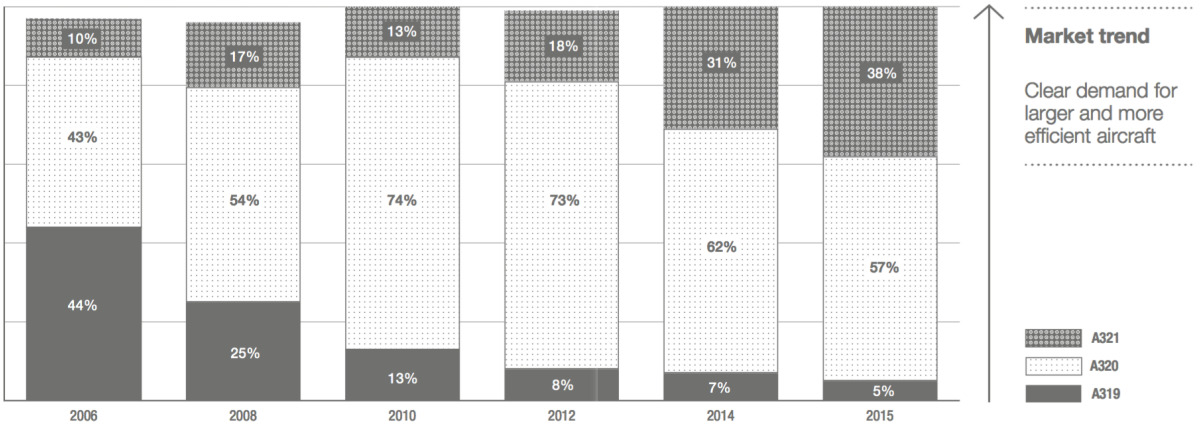

Figure 3.3: Recent airbus aircraft demand dynamics [3]

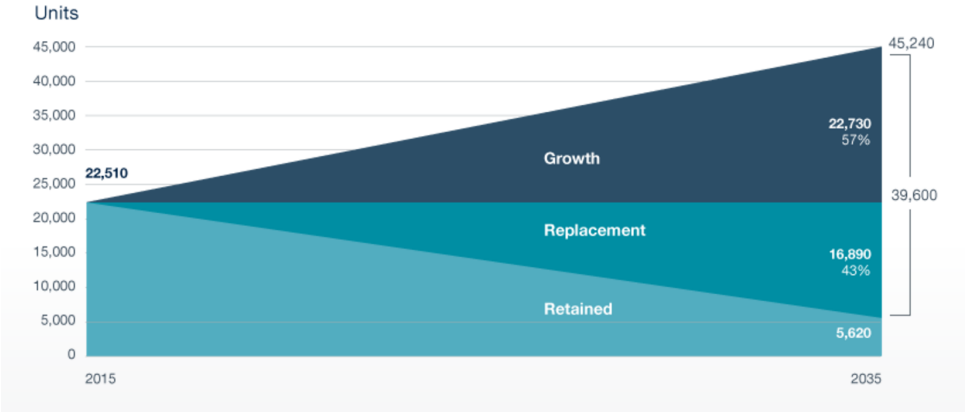

Figure 3.4: Boeing projections for aircraft replacement [4]

Another trend is illustrated by Figure 3.5. It indicates the reduction of fuel consumption per passenger which indicates the overall efficiency of the aircraft. Subsequently, the CO_2 emissions are lower as well.

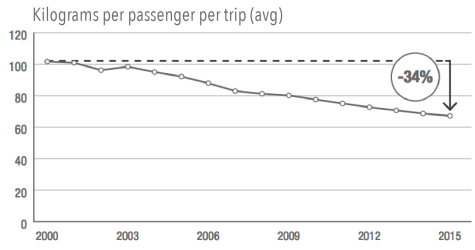

Figure 3.5: Average fuel consumption per passenger per trip in kilograms [3]

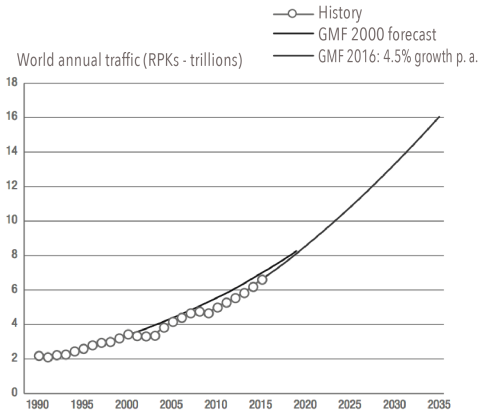

Figure 3.6: Global traffic growth projections [3]

3.3.5. Traffic

From 2010 to 2015 the air traffic has experienced a high growth rate, with a 6.8% increase in Revenue Passengers kilometres in 2015 compared to 2014. Airbus projects a 4.5% global annual air traffic growth rate for the next 20 years. First decade will experience 5% increase annually while the second decade will experience 4.1%

annual growth rate [3]. In Figure 3.6 global air traffic projections can be found. This increasing traffic is a direct source of increasing demand.

Size

Increasing traffic does not just create a need for more efficient aircraft but also for a larger aircraft. There are two factors which, from a business point of view, influence the aircraft size. First, the passenger load factor, or the proportion of the available seats on each flight that are filled, and utilisation, the number of hours a day the aircraft flies. In recent years both of these numbers sky-rocketed to levels which 20 years ago were considered impossible. Figure 3.7 illustrates the average number of seats and Figure 3.8 illustrates the load factor over the years. The projected increase in the air traffic makes it safe to assume similar trends as in these figures.

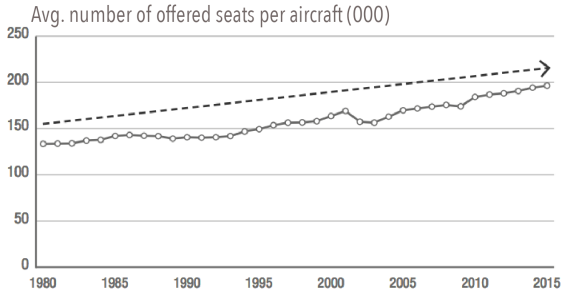

Figure 3.7: Number of average seats over the years [3]

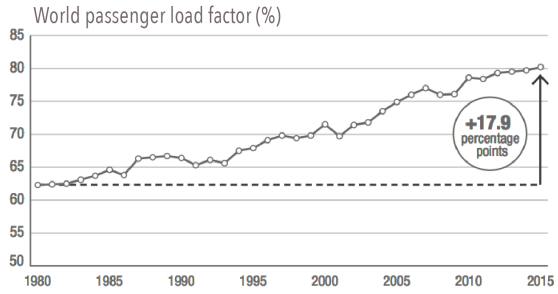

Figure 3.8: Carrier load over past years [3]

Other Considerations

As market analysis already indicates that majority of the clients are going to be the airlines, several other considerations are important. Examples of this are the type of runway on which the aircraft can land, the amount of extra payload it can hold, and range it can cover. However, no trustworthy quantifiable indications of these considerations in the next 20 years have been found. The trend however shows that passengers prefer to carry an increased amount of carry-on luggage compared to checked luggage.

3.4. Market Analysis Conclusion

This section summarises the analysis performed to provide the engineering team with actionable requirements for the aircraft with the challenged fuselage. First, new sustainable and single aisle aircraft have seen a great demand. In addition, it can be seen that a majority of Airbus clients for the single aisle aircraft would be airlines all around the world since demand is forecast to double consistently in every country.

Then, historical data shows that aviation is more or less immune to the economical breakdowns and experienced a steady climb even during the 2008 crisis. By November 2016, records showed 395 orders and 516 deliveries for Airbus [9], 457 orders and 617 deliveries for Boeing [10]. A steady growth in aviation is expected to persist in the foreseeable future.

Global demand for the new aircraft is increasing at a steady pace as well. Airbus predicts a demand of 33,070 new passenger aircraft over the next 20 years. While Boeing is forecasting a need for over 39,600 aircraft by 2035. A fleet forecast conducted by Flight Global [11] states that 26.860 deliveries of single aisle aircraft is forecast. These aircraft are expected to be more efficient, more sustainable and have more seats. A compound annual growth rate of 5% is predicted between 2014-2035 where Airbus is expected to have a 45% market share, Boeing 43%, Bombardier Aerospace 5%, Comac 4% and Irkut Corporation 3%.

Finally, each region is predicted to have unique demands regarding the type of the aircraft. However, as can be seen from future market forecasts released by Airbus and Boeing, single-aisle aircraft are expected to be the most demanded aircraft type by 2035.

[9] http://www.airbus.com/company/market/orders-deliveries/ [accessed on December 2nd 2016]
[10] http://www.boeing.com/commercial/#/orders-deliveries [accessed on December 2nd 2016]
[11] https://www.flightglobal.com/asset/2509 [accessed on December 2nd 2016]

4. Technical Analysis

In this chapter a technical analysis is described. here, the technical funstions of the aircraft are analysed. First, the functional breakdown structure is presented. In the second part the functional flow diagram on a system and subsystem level is shown.

4.1. Functional Breakdown

The functional breakdown structure helps to identify the functions the system has to perform. This helps to derive the required subsystems and system level requirements. In addition, a lower, subsystem level functional breakdown is built. This helps to identify interfaces and expand the requirements. Figure 4.1 shows the main functional breakdown diagram, from which 9 more detailed diagrams are made. Requirements derived from these functions are stated in the baseline report[2]. Figures 4.2 and 4.3 display the breakdown of payload handling and operation functions of the system. Besides being able to handle luggage, passengers and bulk cargo it is also important that accessibility for cleaning purposes is included in the diagram. Interior cleaning is done after each flight, exterior cleaning needs to be done less regularly, though it has to be taken into account.

For safety, the on-ground safety measures and in-flight safety measures are divided into two separate blocks, see Figure 4.4. This division will help determining specific safety measures in both situations. The functions displayed for ensuring safety can be divided in two separate categories; for passengers and for the crew. This is a valid division, since it is impossible to have crew-less passenger aircraft in the near future of aerospace. Safety requirements are already extensively described in the CS-25 regulations, to which the design has to comply in order to be airworthy.

A breakdown of general functions is displayed in Figure 4.5. In order to provide breathable air, pressurisation is needed when flying above certain altitudes. This could be achieved in several ways, as found during dedicated brainstorm sessions. Therefore, thorough research on achieving and maintaining constant pressure will have to be performed. Note that this research should not be constrained to finding an optimum solution for pressurisation; perhaps it is more feasible to fly at lower altitudes without the need for pressurisation.

Besides pressurisation, the system must be capable of protecting itself from the different types of hostile environmental conditions. Requirements regarding customer satisfaction and well-being can be derived from Figure 4.6. As can be observed there is a significant amount of functions that have to be fulfilled in order to guarantee passenger well-being.

Positioning and movement functions are displayed in Figure 4.7. A distinction is made between changing position on ground and in air, since different sub-systems could be responsible achieving the desired results during phases such as taxi, take-off, landing and cruise. As stated in Figures 4.8 and 4.9, different configurations are applied during different phases. This could make the system more efficient in performing its mission. The block stating "ensure efficient flight" has to be interpreted in a broader sense. It should not only be interpreted in a technical way, since efficiency can be improved on different kind of regions.

4.2. Functional Flow Diagram

In the functional flow diagram the functions of the functional breakdown are shown in a logical order. The functional flow diagram is derived from the functional breakdown structure. The functional flow diagram can be found in the Figures 4.10 - 4.15. The top level shows the phases the aircraft goes through. The second level shows the functions in each phase of the top level. The third level works out the functions of the second level if possible. The connection lines between referenced blocks are left out to keep the diagram more clear, but 'REF' is stated in the right-hand corner. Next are the decisions on the diagram that have to be clarified:

- "1.5 Check subsystems" is done throughout the whole flight but more thoroughly at this moment in the ground operation phase. "2.Determine position" is noted because at this moment this function starts.

Figure 4.1: Functional breakdown diagram displaying functions for the system

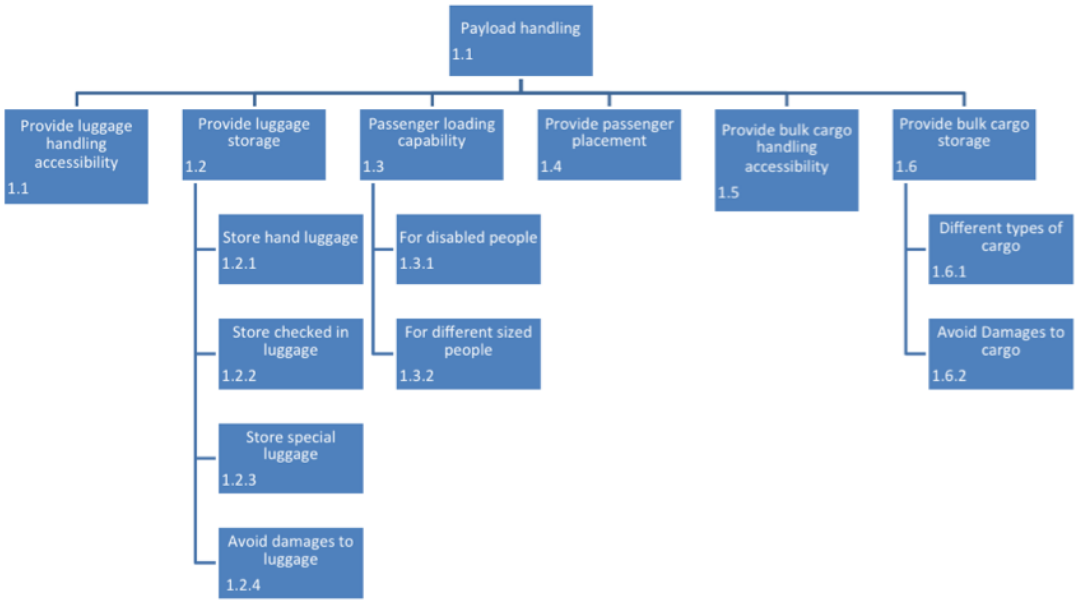

Figure 4.2: Functional breakdown detail for payload handling

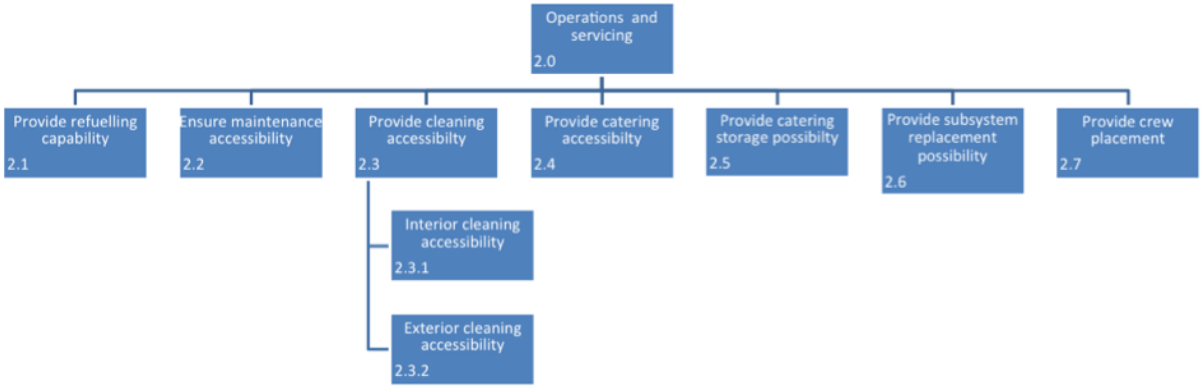

Figure 4.3: Functional breakdown detail for operations and servicing

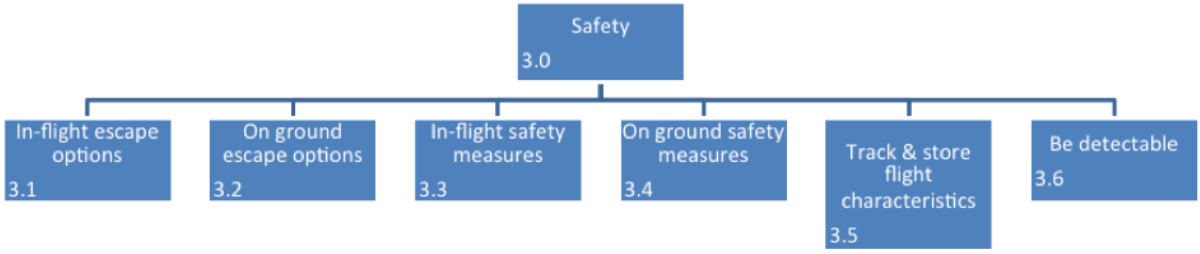

Figure 4.4: Functional breakdown detail for safety

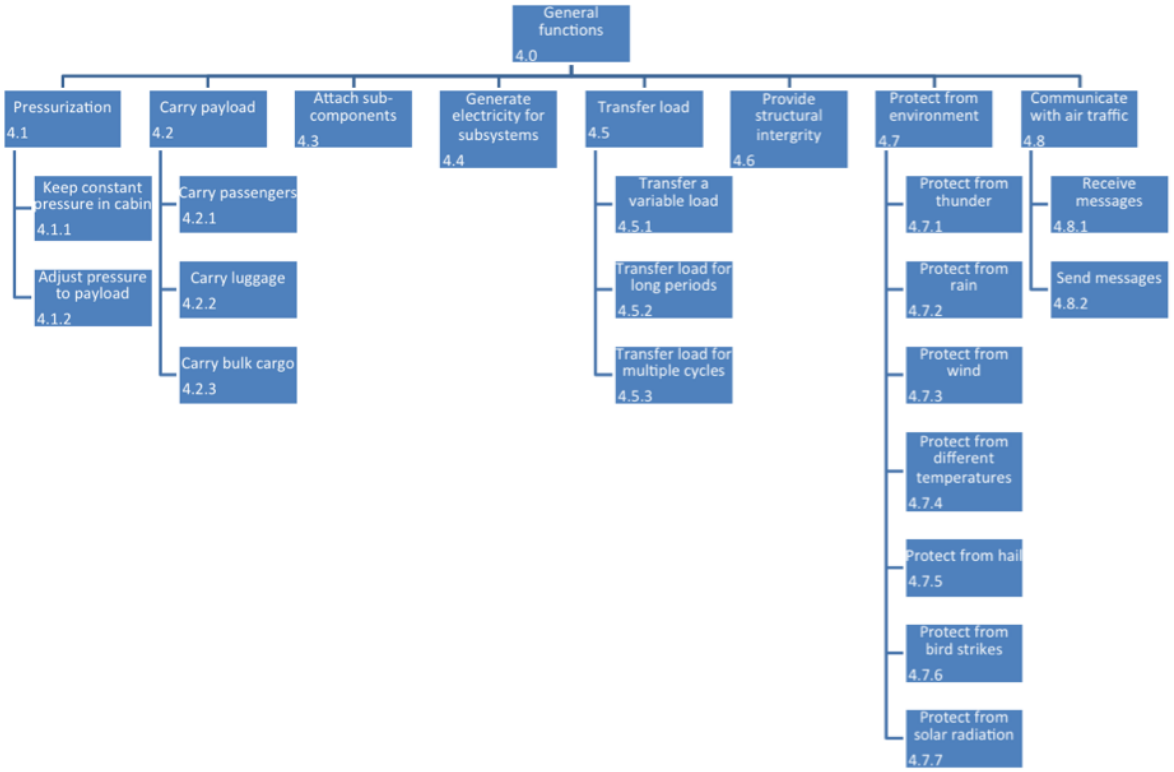

Figure 4.5: Functional breakdown detail for general functions

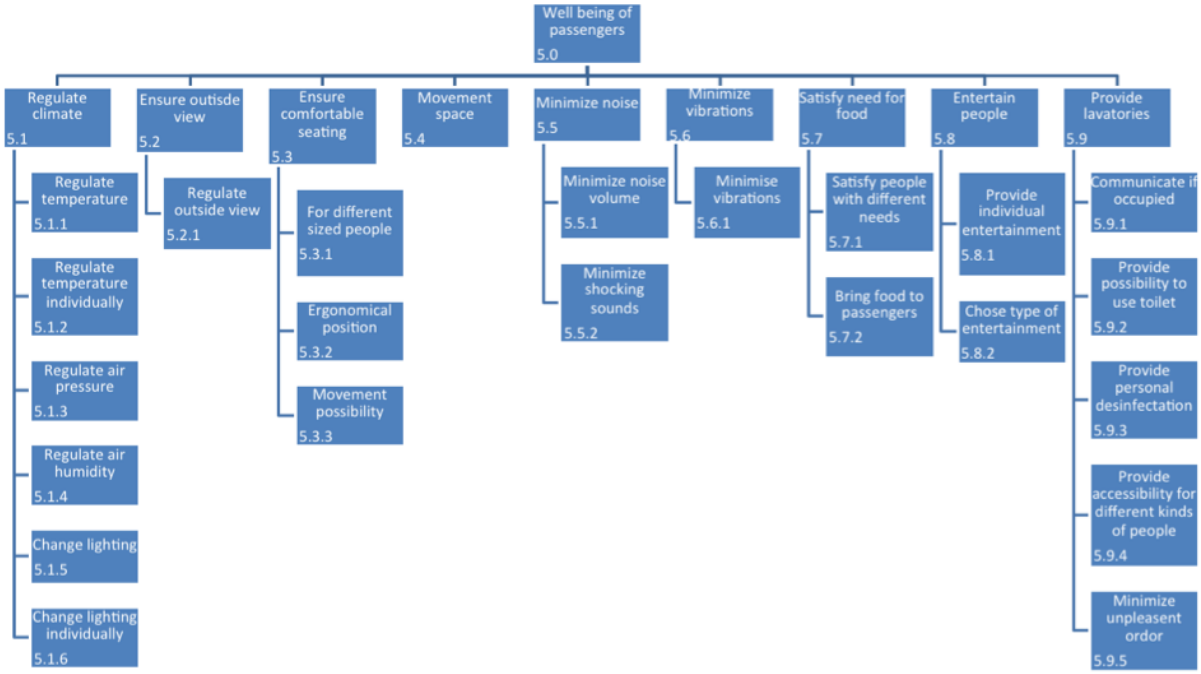

Figure 4.6: Functional breakdown detail for well-being of passengers during the mission

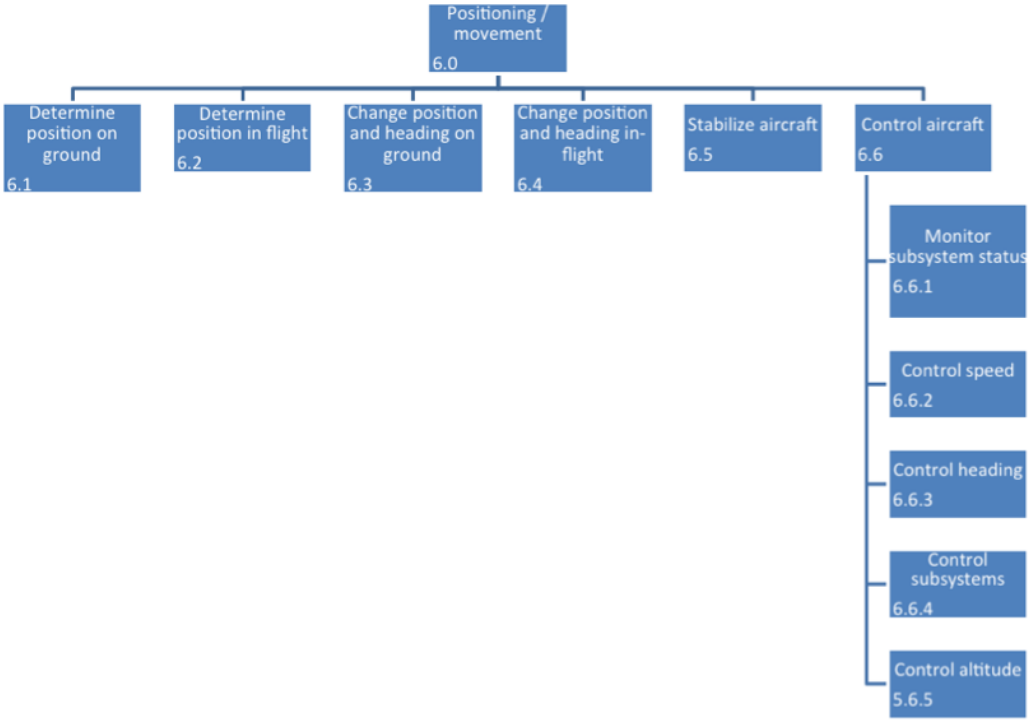

Figure 4.7: Functional breakdown detail for positioning, heading and movement

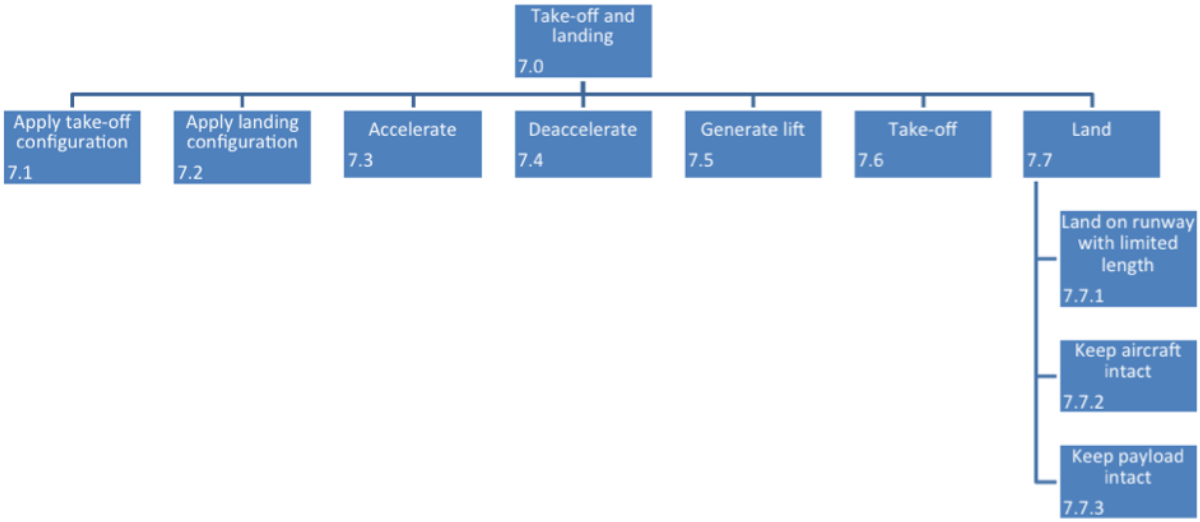

Figure 4.8: Functional breakdown detail for take-off and landing phases

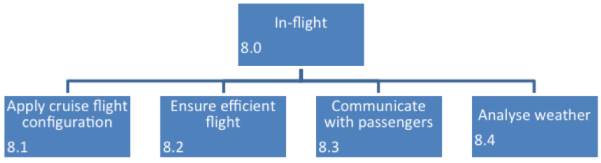

Figure 4.9: Functional breakdown detail for in-flight functions

- The three functions following "4.2 Reach destination" are very general, but carefully selected. The determination of the position and going in the right direction is the only way to reach the destination. Furthermore, protection from environment and a self stabilising aircraft are of high importance during a long flight. Also, a 3rd level after "4.3 Provide passenger well being" could be added with all the function displayed in Figure 4.6, however this would include too many functions to display in this diagram.
- "4.1 Apply cruise flight configuration", "5.2 Apply landing configuration", and "5.5 Taxi" are that much similar to "3.1 Apply take-off configuration" and "2.0 Taxi phase" that the extra level is left out.

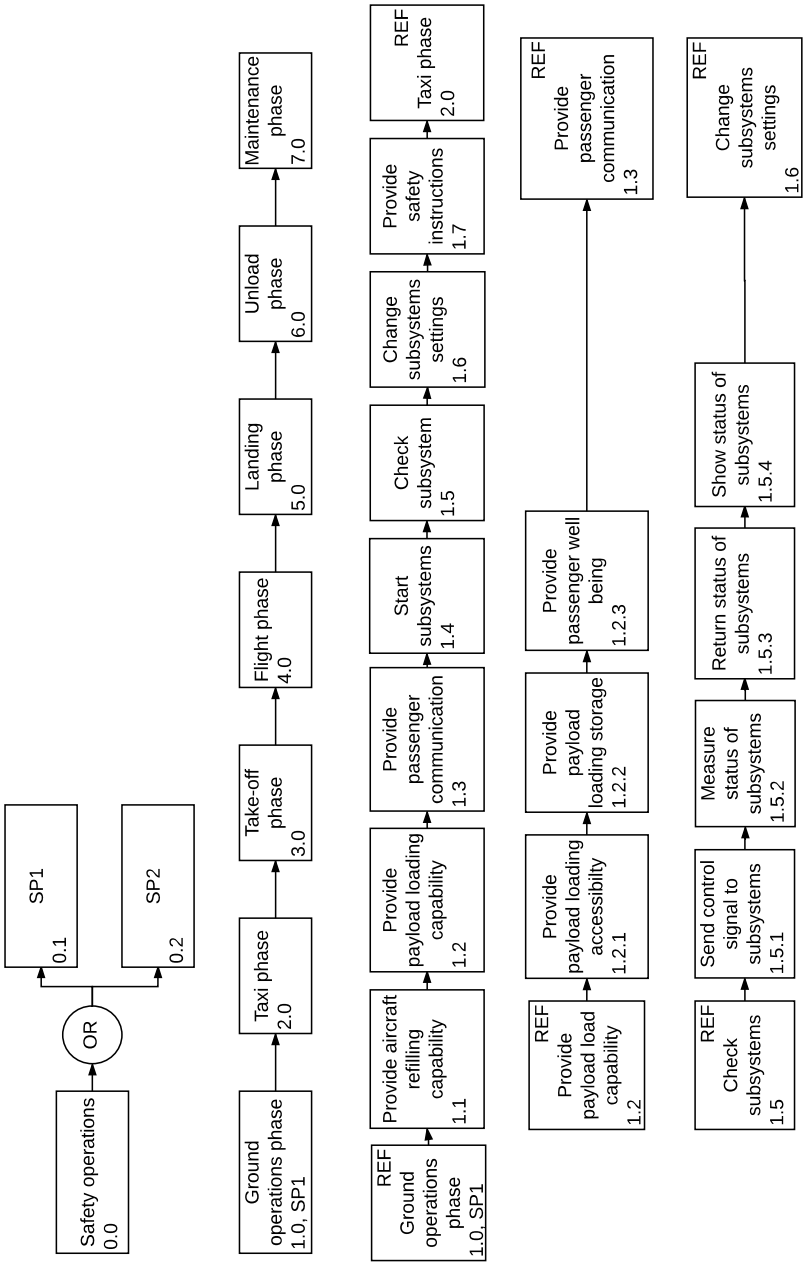

Figure 4.10: The functional flow diagram (part 1) showing the logical order of functions the system must perform

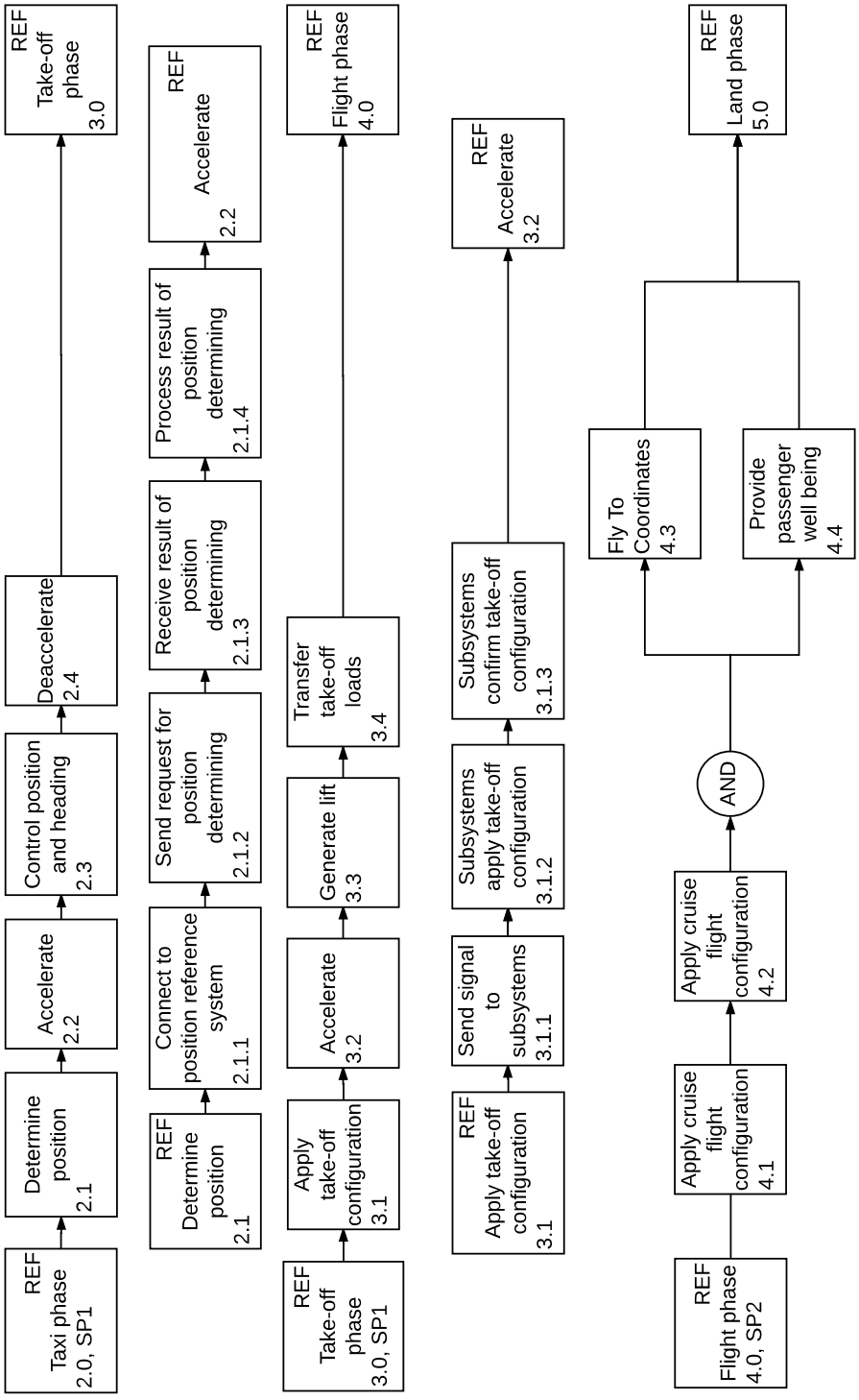

Figure 4.11: The functional flow diagram (part 2) showing the logical order of functions the system must perform

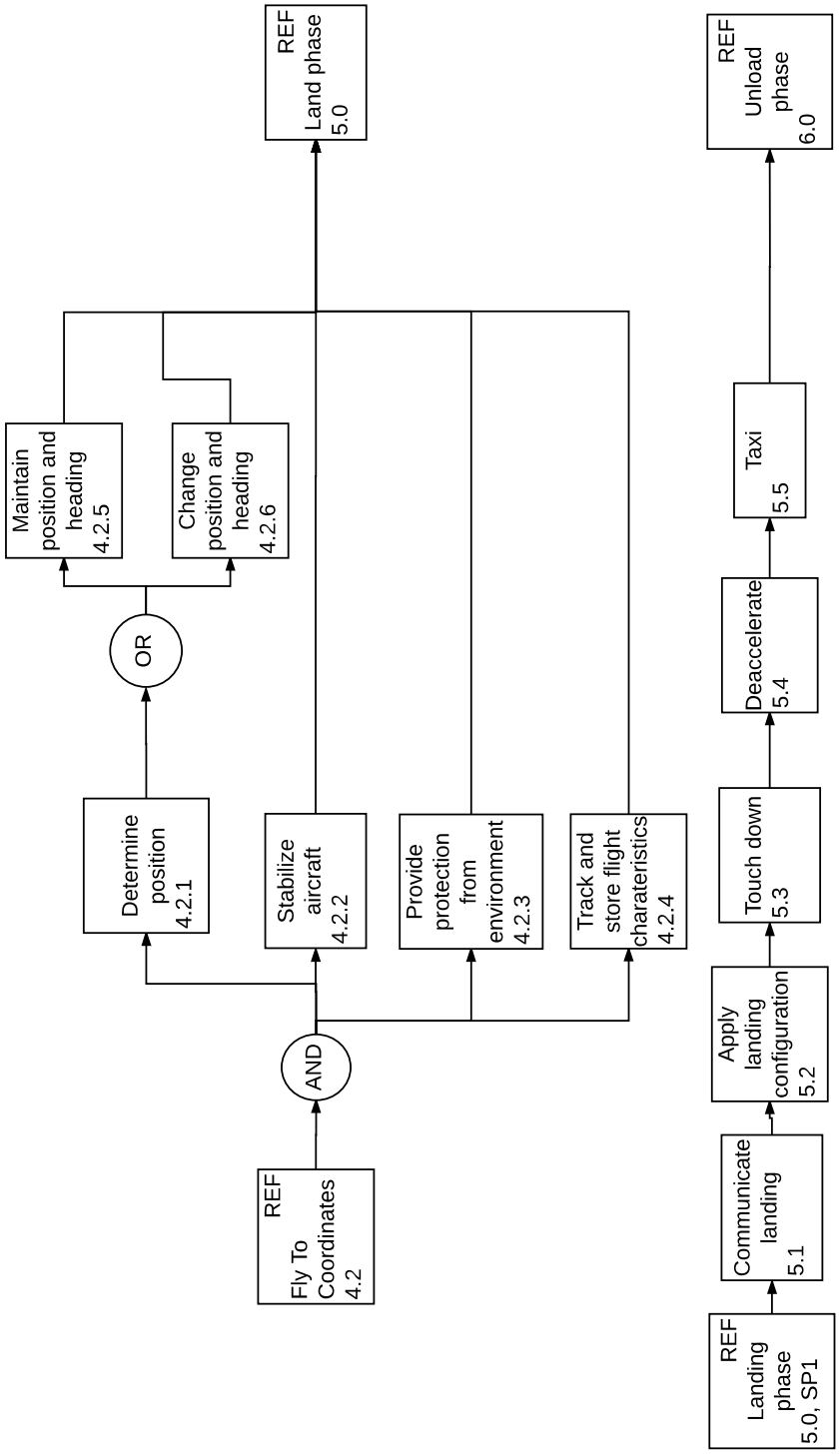

Figure 4.12: The functional flow diagram (part 3) showing the logical order of functions the system must perform

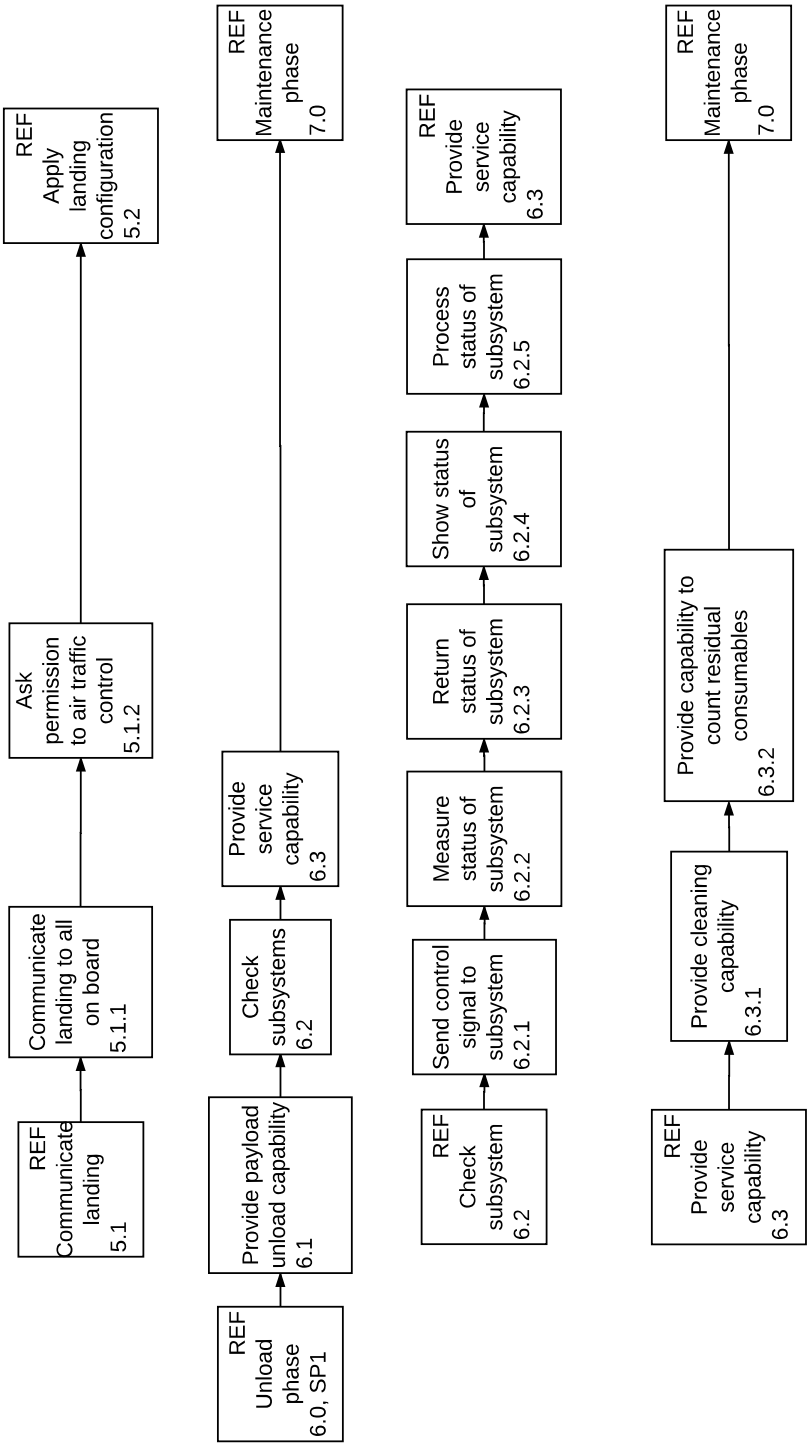

Figure 4.13: The functional flow diagram (part 4) showing the logical order of functions the system must perform

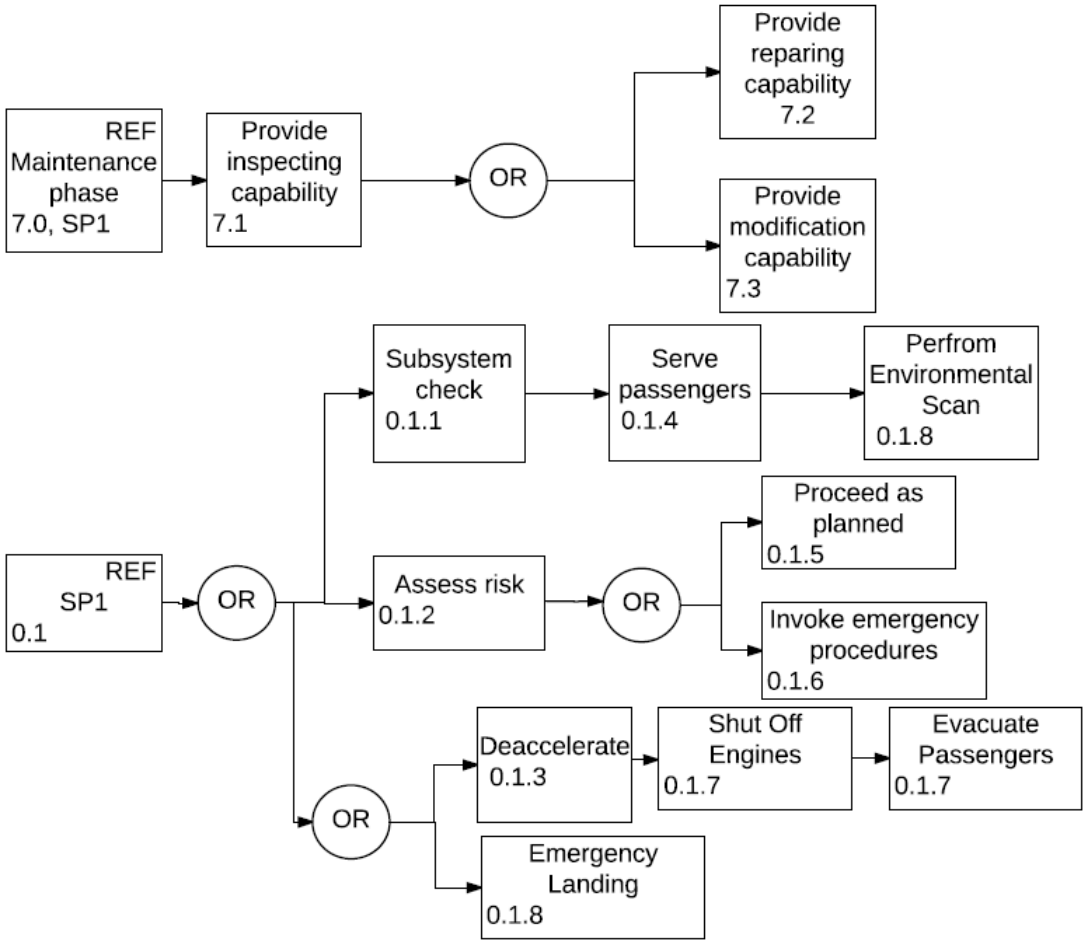

Figure 4.14: The functional flow diagram (part 5) showing the logical order of functions the system must perform

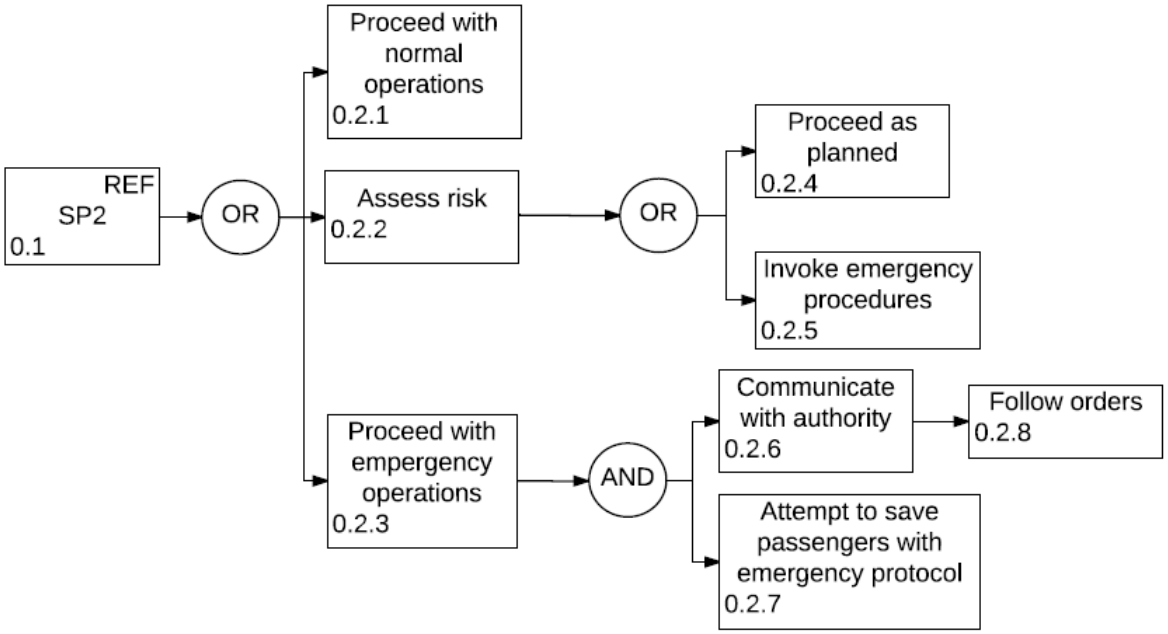

Figure 4.15: The functional flow diagram (part 6) showing the logical order of functions the system must perform

5. Budget Breakdown

In this chapter the budget breakdown, or resource allocation, is discussed. The goal is to manage the technical resources so that constraints can be put on the design. These constraints are called budgets and are updated throughout the design process. First, the budget breakdown values are presented. Then, the explanation of these values is described.

5.1. Budget Breakdown Values

Different budget values have been estimated with contingency. The first estimate was done halfway of the project. Table 5.1 shows if these budgets have been adjusted, and the explanation can be found in the next section.

Table 5.1: Budgets and contingency values

	First estimate	Contingency value [%]	Current estimate	Contingency value [%]
MTOW [kN]	893	6	960	5
OEW [kN]	461	6	495	5
Fuel [kN]	232	-	259	-
Payload [kN]	196	-	206	-
Operating cost [USD/block hour]	8069	10	5747	1
$C_{D_{fuselage}}$ [-]	0.020	10	0.010	10
$C_{D_{fuselage}}$ / C_{D_0} [-]	0.3	10	0.3	10
Thrust Loading [-]	0.32	10	0.28	10
Electric power [kW]	540	225	1500	35

5.2. Budget Breakdown Explanation

The explanation on how the values of the budget breakdown were computed can be found in the next sections.

5.2.1. Mass Budget

The weight & balance of the aircraft is an important factor within the design process. Table 5.1 shows that the weight has increased with respect to the first estimate. It is within the contingency value however. This is mainly because the first estimate was rather optimistic in estimating the weight of the new fuselage. The current expectation is a heavier fuselage, which increases the OEW and MTOW.

The new weight was calculated using a class II weight estimation from Raymer and further details can be found in Chapter 17: Control & Stability. The new weight contingency value, to cope with possible future weight increases, is set on 5%.

5.2.2. Cost Budget

Cost has been regulated through the cost budget. It is important to keep operating cost down, since this largely defines the airlines interest. A stakeholder requirements requires us to have an operating cost comparable to state-of-the-art aircraft, therefore there is not much room for contingency. In Chapter 19 the calculation of direct and indirect operating costs is further discussed. The first estimate proved to be rather inaccurate, compared to the final value. This is due to the fact that the costs of an aircraft are very market dependent and therefore hard to predict. A contingency factor of 1% is used with respect to the new value.

5.2.3. Propulsion Budget

The initial Thrust-to-Weight ratio of T/W = 0.32 was mainly derived from reference aircraft, see Section 15.2. The preliminary performance analysis from Chapter 15, yielded a new value of T/W = 0.28. Since the drag budget is not been limited yet, the same holds for the thrust budget(T=D). That is why this contingency factor is the same as for the drag budget.

5.2.4. Drag Budget

Changes have been made in the estimations for the drag budget. The fuselage drag represents up to 50% of the zero-lift drag C_{D_0} and the zero-lift drag coefficient has been estimated on C_{D_0} = 0.022, based on the 0.020 reference value + 10% margin[5]. Therefore the fuselage zero-lift drag coefficient is estimated at 0.011. The total zero-lift drag coefficient is left unchanged.

5.2.5. Electrical Power Budget

Over the past decades there has been a big shift in aircraft design regarding the power budget. To reduce the OEW and the total amount of power consumed by the subsystems, aircraft manufacturers are slowly moving away from central hydraulic and pneumatic systems, towards more electrical systems. When this concept is implemented in the design it will increase the electric power usage of the aircraft.

For all electric aircraft, which do not use central hydraulics and pneumatics anymore, the increase in electric power consumption is significant. The estimate of 540 kVA, which was made earlier on in the conceptual design phase, is too low. This is because the initial estimate was made using data from conventional reference aircraft, and scaling that data up for all electric aircraft. The scaling factor of 2.25 turned out to be a lot too low though. An improved estimate for secondary power consumption was made. This new value is based on separate estimates for each of the subsystems. The new total electric power consumption estimate is around 1.5 MW. More details on the methods used can be found in Section 16.1.

5.2.6. Computing Resources Budget

Computing power was not expected to be a limiting factor during the conceptual design phase. While working on structural and aerodynamic analysis it became clear though that computing power is in fact a limiting factor even in the conceptual phase. Therefore, in preliminary design computing resources should be managed, and budgets for the use of computing resources will need to be set.

6. Technical Risk Assessment

In this chapter the technical risk assessment is presented. First the risks as well as their impact are identified and mitigation plans are formulated. Second, the risk maps are presented before and after mitigation. These risks are based on the Mid-term Report and are elaborated on as the design progresses.

6.1. Internal Risks

This section contains all risks concerning internal factors that can occur during the design process.

I.1-Technology Readiness Level
The risk 'Technology Readiness Level' comprises all technologies that are very promising, but are not yet proven in flight. An example is recyclable composites. This has been researched, but has not been used in flight yet. Therefore, this poses an uncertainty on the design and performance.

The mitigation plan includes considering only technologies past a certain TRL, others can be shelved for later. To further reduce the impact and consequence risk due to uncertainty, experts can be consulted regularly. Furthermore resources could be invested in testing and optimising the technology. For example, investments could be made into recyclable composites in order to reduce the risk of not meeting the recyclability requirement for the design.

I.2 - Concurrent Designing
Aircraft design is an interdisciplinary project, every decision influences another. Since the aircraft is designed concurrently a certain engine design can pose constraints on wing placement, landing gear, stability, operations and sustainability. The impact of this is a suboptimal overall design.

A mitigation plan includes sufficient communication within departments. This interfacing is done daily in the meeting with the entire group, and individually within the departments when interfaces arise. Also, sensitivity analysis is conducted to see how much certain decisions influence others. This result is also used in the trade-off, to choose the optimal design.

6.2. External Risks

This section contains all risks concerning external factors that can occur during the design process and operational life of the aircraft.

E.1 - Changing Regulations
This risk comprises all events which result in changing regulations, outside control of the engineering department. An example can be noise regulation changes. This leads to an aircraft that is too loud due to for example the engine. The impact of this could be additional fines for the airline, and early retirement of the aircraft because there is no market for it.

A mitigation plan consist of designing an aircraft with a margin on the predicted future noise regulations. This can only be done to a certain extend due to degradation of performance. In case of the engines, sufficient space could be left available in the design in order to later replace them with newer, more quiet models.

E.2 - Changing Market Trends
This risk comprises all events which suddenly change the market trends and introduce unanticipated needs. The impact could be early retirement of the aircraft due to the fact that there will not be a market for it anymore. An example of a changing market trend is the decrease of checked-in luggage. If this is not anticipated, an aircraft might be designed with a lot of unused space. This will result in an aircraft that has much more drag and weight than necessary and the operating cost will be much higher than aircraft that did foresee the trend.

A mitigation plan might include market research in order to anticipate needs. This will increase the probability of selling your aircraft. Also a flexible design could be a solution, so that your design can be adjusted during the process. However, this will also come at a price.

E.3 - External Vendors
Another risk represents the use of products from external vendors. Especially when these components have not been designed yet. An example of this is the incorporation of an engine that has not been developed yet. For the design now an assumption is made about engine parameters, the most important being the specific fuel consumption. An increase in the anticipated SFC negatively affects the aircraft performance.

The mitigation plan includes sufficient communication with the engine manufacturers and clear agreements on what is expected. Furthermore, a sensitivity analysis helps quantify the risks and implications involved in a difference in SFC. During the design process this risk can be taken into account.

6.3. Operational Risks

This section contains all the performance related risks which can occur in flight, or during ground operations.

O.1 - Failure of Fuselage
The risks 'failure of fuselage' comprises all events in which a failure in the load bearing structure occurs. This can be caused by material degradation of a load bearing part due to corrosion or fatigue. The probability of occurrence is high, since every aircraft is susceptible to cyclic loading, and to weather conditions. Another reason is an impact. Examples of these are bird-strikes and hail storms. Also, impacts during ground operations occur very often. The probability of occurrence is therefore very high.

When a failure in the load bearing structure occurs, other components will have to compensate. In the worst case scenario, these will fail as well and the fuselage will lose its ability to carry any loads. One way of mitigating the risk would be to create a design that is fail-safe or impact tolerant, or to work with safety factors. However these measures result in extra mass and thus loss of performance.

A measure to mitigate the degradation of material is to regularly check the condition of the material during service life. This ensures early detection of a part that might fail so that it can be repaired or replaced. Detections are performed as specified according to regulations. Routine checks will be performed every 500 flight hours, while the most extensive check will be performed only every 5 to 6 years [1]. This will have an impact on the direct operating cost.

Lastly, decompression might occur, thus the fuselage has to be equipped with oxygen masks in order for the passengers to survive. Also clear instructions must be provided to them on how to use it.

Using this mitigation plan can change the consequence of loss of fuselage from catastrophic to marginal. With other fail safe components present in the structure and oxygen masks the aircraft should be able to land safely. Also the likelihood of this risk occurring will decrease from high to moderate.

O.2 - Failure of Wing Structure
The risk 'failure of wing structure' comprises all the events in which a loss in lift occurs. A chunk of the wing could break off due to a structural failure, as a result of fatigue or material degradation. In this case the probability of occurrence would be high, according to the same reasoning as risk 1. Another reason could be that the aircraft gets into a extreme stall situation, however with experienced pilots this occurs rarely.

The impact of a loss of lift can be critical. In the worst case scenario suddenly a large part of the wing will break off and lift is lost. If the weight force is larger than the generated lift, the aircraft will crash. Material degradation is mitigated as risk 1. Besides that a warning system for stall will be designed in order to minimise the occurrence of a stall situation.

[1] http://www.wichitech.com/blog/index.php/aircraft-maintenance-checks/ [accessed on December 1st 2016]

O.3 - Failure of Propulsion
The risk 'failure of propulsion' comprises all events in which the propulsion of the aircraft is lost, several reasons are responsible for this. Bird ingestion is one of these. The severity of impact of 'failure of propulsion' depends on the phase of flight the aircraft is in. Loss of propulsion is the most critical in the take-off phase. Next to that the probability of occurrence of bird ingestion is the highest at lowest altitudes [6].

During design, bird strike should be taken into account for nacelle design. This could lower the probability of bird ingestion. Also, the design should incorporate engines that have been tested for bird ingestion, so that the consequence of the risk will decrease. Finally, the consequence of losing one engine during take-off is lowered by designing for the OEI conditions. This means that the aircraft is still able to reach the climb requirements at take-off specified by CS25.

O.4 - Failure of Controls
The risk 'failure of controls' comprises all events in which the controllability of the aircraft is lost. One way this can happen is when the control surfaces become ineffective because they are in the wake of the stall. This is a very dangerous situation because the aircraft can not get out of the stall. Another case for this risk is if the aircraft loses its control surfaces due to structural failure.

A mitigation plan to reduce the risk might include redundancies in design: a fail-safe control surface system, if one part fails, another part can take over its function so that complete control of the aircraft is not lost. For ineffective control surfaces due to stall, the control surfaces should be properly situated on the wing or tail and this process should be monitored well. This mitigation plan reduces the consequence as well as the probability of the risk happening.

6.4. Risk Maps

In this section the risk maps before, Figure 6.1, and after mitigation, Figure 6.2, will be displayed.

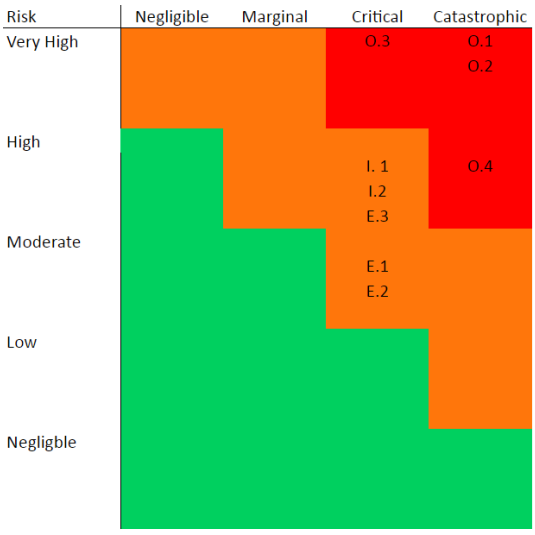

Figure 6.1: Risk map before mitigation

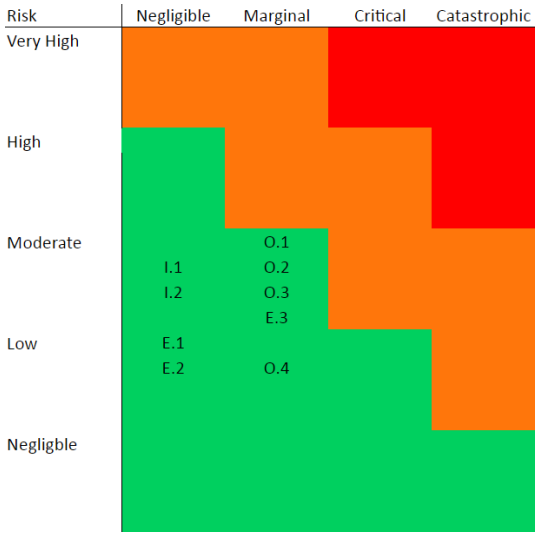

Figure 6.2: Risk map after mitigation

7. Operations and Logistics

In this chapter, aircraft operations are discussed. First, the concept of different operations phases are described. The goal is to have a clear overview of these phases, as the aircraft spends most of the time in operation. Then, the logistics of different phases will be presented, including how the supply chain management for the aircraft should be handled, as well as spare parts and services. Finally, the reliability, availability, maintainability and safety characteristics will be elaborated on.

7.1. Concept of Operations

Operations can be split into different phases. Looking at each of those phases separately will help get a better overview. For each phases a comparison is made with the operations of similar class aircraft that are operated by airlines nowadays.

7.1.1. Flight

The flight phase is the only phase which will produce revenues for the operator. In order to increase the value the aircraft will produce, the fuel consumption has been reduced via several methods. One of those methods is the design of an all electric aircraft (AEA). The subsystems will use less power, and thus less fuel, reducing the operational cost of the aircraft. Furthermore, the weight of the aircraft is not only reduced by the reduced amount of fuel necessary. The electric system itself reduces weight as well, since the power distribution system of an AEA weighs less than the combination of an electric, a pneumatic and a hydraulic system [7]. Without any other modifications an AEA is about 2% lighter than the same aircraft with conventional systems [7]. This reduced weight also reduces the the amount of fuel burned, which induces a snowball effect. After on iterative design cycle the AEA will be about 3% lighter than the original conventional aircraft [7]. This reduction in weight further reduces the amount of fuel necessary, which in turn reduces the operational cost even further.

Furthermore, since the aircraft will fulfill future environmental regulations, the fuel consumption will be further reduced. This is reached by installing fuel efficient engines and reducing the power required from the engines. Noise regulations of 2020 also have to be coped with, meaning travelling will become more comfortable, compared to most state-of-the-art aircraft. Not only the aircraft passengers and crew enjoy the lower noise emissions though, noise will also be reduced for people living close to an airport.

Another important factor in the flight phase is safety. Operating an AEA with a solid-state power distribution system enables the pilots to get information about the aircraft or any of its components during flight [8]. The solid-state power distribution system will be explained in Section 16.3. This makes it easier for pilots to find a fault during an emergency situation, and to land the aircraft safely if necessary. Due to the increased maintainability and reliability of the aircraft and the increased amount of information that is available to the pilot during flight, the operation of the aircraft is safer than operating a conventional aircraft.

7.1.2. Turnaround

In order to maximise the amount of time the aircraft can spend making profit, the turnaround time has to be reduced as much as possible. In order to do so, the access doors and panels are placed in favourable locations around the fuselage. This ensures that most of the turnaround tasks can be completed simultaneously.

The electric taxi system that will be included in the aircraft will also help reduce the turnaround time, as well as turnaround cost. Using the electric taxi system, which is powered by the APU, the airline does not need to rely on the push-back tractors that are usually owned by other companies. This means that push-back will be cheaper, but it will also take a bit less time, since there is no need to wait for the tractor to disconnect from the aircraft.

Refuelling an aircraft usually takes between 15 and 40 minutes depending of the amount of fuel that has to

be put into the tanks [1]. Refuelling is the most time intensive task to be done during a regular turnaround [2]. For that reason turnaround could be reduced by reducing the refuelling time. Of course the refuelling speed is limited by the mass flow the refuelling pumps can handle, but reducing the amount of fuel needed while keeping the pump speed constant will also reduce the refuelling time.

Passenger boarding and de-boarding times will be the same as for conventional aircraft. The fuselage does not allow for faster passenger boarding compared to conventional aircraft, as it still has a quite conventional interior design, with conventional dimensions.

Another aspect about AEA related to the turnaround is that there is no need to connect external hydraulic and pneumatic systems, as the aircraft does not have central hydraulic or pneumatic systems. However, since electric power consumption is higher, the aircraft will need two external electric power supplies instead of just one, in order to supply enough electric power to the aircraft while all engines are shut down.

7.1.3. Maintenance

Designing an AEA with solid-state electronics also have effects on the maintenance of the aircraft. An extended electric power system is easier to maintain than the combination of an electric, a pneumatic and a hydraulic system. Also, since solid-state electronics are used in the power distribution system, as explained in section 16, it is possible to find failed components faster. This will of course decrease the time needed for maintenance, since a search for a fault will not be necessary as often anymore. Furthermore, monitoring components can reveal those that are about to fail. This means components can be replaced before they even fail. This increases safety, reliability and aircraft availability. Furthermore, if components are replaced before they fail, then the old component can still be used until the replacement part arrives. Another aspect is that the solid-state components can withstand a considerably higher amount of cycles before they start failing, when compared to traditional thermo-mechanical circuit breakers.[3]

7.1.4. Training and Technical Support

Making sure a newly designed aircraft handles similar to an aircraft that is already certified and for which there are already training programs in place has several advantages from an operational point of view. If the aircraft controls are similar to those of another aircraft, pilots are allowed to fly both aircraft if they have the certification for one of them, since the certification will be exactly the same. This means airlines can start operating the new aircraft without the need to first train some of their pilots to use the aircraft. Even if pilot certification is still necessary, sometimes aircraft are still similar enough, so that a reduced training program suffices. Furthermore, less technical support is required since some systems are already well known by the operators. Finally, for the people working in technical support understanding the new system is also an easier job.

7.2. Concept of Logistics

Like operations, logistics is a broad term, and a lot of different aspects of logistics can be considered. In this section the main focus will be on the production logistics, the spare part logistics and on the turnaround logistics.

7.2.1. Production Logistics

Production logistics provide quite a broad array of challenges. Some of the parts are small enough to be sent in a parcel by post, while other parts can be large enough to require specialised transport equipment. Since a lot of components in the aerospace industry are produced by other manufacturers, it is really important to synchronise the component and sub-assembly delivery with the main production. Aircraft manufacturers have moved away from stocking a month's worth of components on site, towards a more timed inflow of parts. This means that the requirements for the logistics are a lot higher. Nowadays it is important for aircraft manufacturers to closely work together with the part suppliers, in order to ensure a constant inflow of components that are needed for production. Instead of the part supplier now delivering a fixed amount of parts per time span, the

[1] http://onlinelibrary.wiley.com/doi/10.1002/9780470686652.eae463/full [accessed on January 19th 2017]
[2] http://link.springer.com/article/10.1007/s40622-014-0062-0 [accessed on January 19th 2017]
[3] https://www.expando.se/wp-content/uploads/SSPCvsbreakersWP.pdf [accessed on January 19th 2017]

aircraft manufacturer gives the parts supplier a minimum and a maximum amount of parts of a certain type, and the part supplier is responsible for ensuring the amount of parts of that type in the warehouse always stays within the specified range. [4]

7.2.2. Spare Part Logistics

Aircraft do not make money while they are on ground. In order to make sure aircraft can be repaired quickly in case of damage or a fault, spare-parts need to be readily available. In order to increase the availability of spares, it is a good idea to use parts that are frequently used in commercial aviation. In case this is not possible, like is still the case for some subsystems of AEA, it should be ensured that spares are available as soon as possible, by storing them in warehouses for example. Alternatively, it can also be ensured that spare parts are shipped as fast as possible. At most locations on Earth it is possible to receive parts within one day after ordering them, everywhere on earth. Furthermore storing the spares at a few strategically placed locations will reduce the amount of spares lying around compared to storing them in many different warehouses, but will also reduce the shipping cost and time compared to storing all spares in one single warehouse.

Another way for an aircraft manufacturer to reduce cost of spare part logistics is to outsource maintenance, repair and overhaul (MRO) to independent companies. For the aircraft manufacturer, the cost of outsourcing is less important than the quality of the customer service that will result from outsourcing. [4]

7.2.3. Turnaround Logistics

As mentioned in Section 7.1.2 it is important to keep turnaround as short as possible. In order to reduce the turnaround time it is important that the ground-crew can do its job as quickly as possible. Figure 7.1 shows how an aircraft is usually accessed by the ground-crew during turnaround. As mentioned before, the aircraft's access panels and doors are located such that the ground-crew can access each one of them as efficiently as possible. In the case of the designed aircraft, it is not necessary to place any containers in the fuselage, which makes it easier to place all panels and doors in easily accessible places.

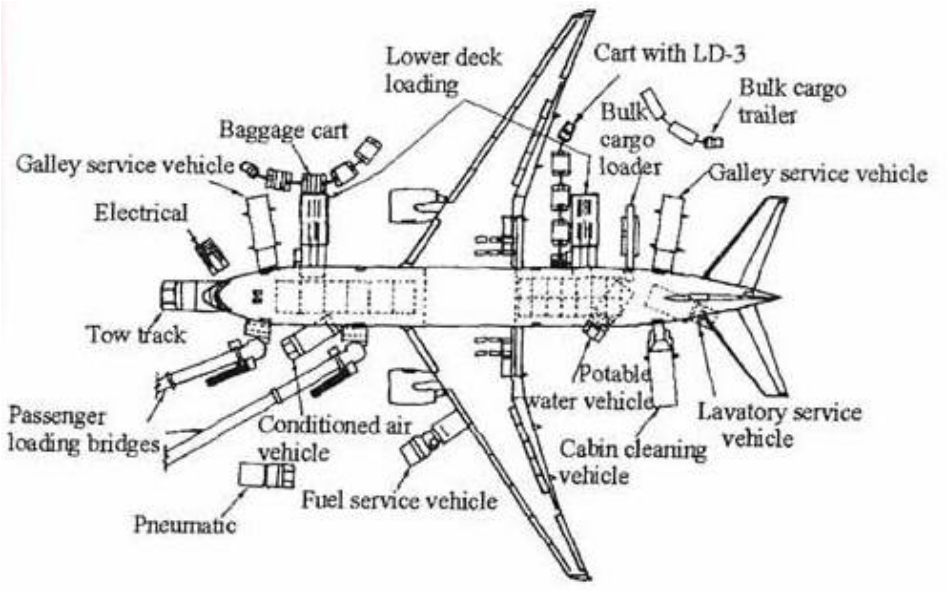

Figure 7.1: Ground operations: aircraft turnaround [5]

[4] http://www.inboundlogistics.com/cms/article/aerospace-logistics-building-for-growth/ [accessed on January 19th 2017]
[5] http://jcfstrategy.com/wp-content/uploads/2015/05/clip_image014.jpg [accessed on January 19th 2017]

7.3. Reliability, Availability, Maintainability and Safety Characteristics

Any product that is designed has an expected life-cycle duration. The reason why a system cannot be used indefinitely is that every system or component fails sooner or later. This is especially true for systems that cannot be excessively over-engineered due to the necessity for lightweight designs. Therefore, in order to design a system that can fulfil its tasks for the whole span of its design life-cycle, it is important to perform a Reliability, Availability, Maintainability and Safety (RAMS) analysis. Over the past decades RAMS analysis methods have evolved from purely qualitative to more quantitative methods. The problem with quantitative methods is that a lot of data about system and subsystem components is necessary. Also, the data should be as specific as possible, meaning it is important to get reliability for the specific part from the specific manufacturer, instead of a general estimate for similar components. Therefore, only a qualitative RAMS analysis is done during the conceptual design phase. [9]

This section discusses the main aspects that have to be taken into account. The focus is on aspects specific to the aircraft that is being designed, when comparing it to conventional aircraft. The main differences of this design compared to conventional ones are the non-circular fuselage shape, the use of composites and sandwich structures, and the all-electric, solid-state power distribution network.

7.3.1. Non-Circular Fuselage

A pressurised non-circular fuselage has to endure higher stresses due to the pressurisation, when comparing it to circular fuselages. This means that, inspections should be carried out more frequently and more thoroughly in order to ensure safety is not compromised. This reduces the availability of the aircraft. For an elliptic fuselage, maintainability should not be influenced by the non-circular shape, except for the increasing frequency of maintenance, because accessibility to the different subsystems does not change much.

7.3.2. Composites and Sandwich Materials

Using more composite and sandwich materials has mainly an influence on the maintainability and safety of the aircraft. A serious issue to watch out for while designing components out of a combination of materials, especially for sandwich structures is the thermal expansion. During the design the thermal expansions of each part have to be analysed in order to make sure the internal stresses resulting from thermal expansion are kept low. If this is not done, the bond between different components might be destroy. This could lead to a complete failure of the structure.

Composites have better fatigue characteristics than metals, which means less inspections might be necessary. However, it is harder to detect cracks in composites, and special equipment might be necessary. Also, depending on the resin used, composite might de-laminate over time due to moisture [10]. In order to avoid this a resin that does not absorb much water should be used.

7.3.3. All-Electric and Solid-State

All-electric aircraft are quite new, though the technology necessary to design such an aircraft has been used for a long time already. Considering this, the safety of a well designed AEA should be the same as for a conventional aircraft. Combining this design choice with the solid-state power distribution choice, means safety as well as reliability are expected to increase compared to conventional aircraft. This is due to the fact that solid-state circuits have a significantly longer life-span than conventional circuits, but also because the solid-state technology enables monitoring of all electric systems in the aircraft. This way, faults can be detected earlier and faster, and sometimes even before they occur. This of course increases safety, reliability, availability and maintainability of the power distribution system.

7.3.4. No Cargo

The only payload that will be carried by the aircraft will be the passengers and their luggage. It is assumed that no extra cargo is carried on passenger flights. Therefore, no space was allocated for extra cargo. This means for a given number of passengers, the airframe can be smaller and thus lighter. This again leads to a reduced fuel consumption, which means less operational cost. Having no extra cargo also has the potential to reduce

the turnaround time. This is only true in case loading/unloading is part of the critical path in the turnaround planning.

7.3.5. Engines

Even though the aircraft is all electric and the engines have to have a low specific fuel consumption, the engine type is still conventional. This means that the implications on operations are not extensive. The lower specific fuel consumption will reduce the amount of fuel necessary to reach a certain range. This will reduce operational cost by reducing fuel cost.

7.3.6. Slender Wings

High aspect ratio wings have two major implications on operations. For the fuel consumption the low induced drag compared to low aspect ratio wings is the main advantage. Because of the reduced drag, fuel consumption is also reduced, which again reduces fuel cost and thus operational cost. Besides fuel cost, the aspect ratio also influences the stability of the aircraft. A higher aspect ratio makes the aircraft more stable, and thus less manoeuvrable. [6]

[6] http://sciencelearn.org.nz/Contexts/Flight/Science-Ideas-and-Concepts/Wing-aspect-ratio [accessed on January 23rd 2017]

8. Sustainable Development Strategy

In this chapter the sustainable development strategy is presented. First, the current regulations are investigated and targets regarding future sustainable aviation identified. Consequently, an approach on how sustainability has been implemented during the design phase and how it will be considered during aircraft operation, is presented. All sustainable development aspects are taken into account during the trade-off by assigning weights to the different design concepts. Furthermore, requirements arising from the strategy chosen were derived and translated into design drivers.

The service life of aircraft can be up to 30 years, depending on its application. Evaluation during the development process of the design options is crucial to systematically and sustainably decrease the ecological impact of aircraft. Aircraft design concepts, suitable materials, manufacturing processes and technologies should be quantitatively analysed. To evaluate the sustainability and relevant parameters of an aircraft, the three main life cycle phases, namely design and production, operation and end-of-life, EOL, will be investigated.

8.1. Sustainable Development Regulations and Targets

Sustainable development has been one of the main objectives in European Union, EU, Treaties. According to the European Directive "VHU 2000/53"[11], regarding the EOL of vehicles, the rate of reuse and recovery should reach 95% by 2015 and 85% for reuse and recycling. The United States (US) does not have regulations and is lagging behind in introducing them[12]. However, regarding aircraft no regulations are available yet on how to design for or deal with EOL, reuse, recovery, or recycling rate[13]. Only rules securing airworthiness of the aircraft that will reuse parts exist. Also, local environmental regulations depending on the recycling location should be considered. The European Directive 2015/1513 called on the Commission to present a proposal for a post-2020 policy. Aiming at creating a long-term perspective for investment in sustainable biofuels with a low risk of causing indirect land-use change and in other ways of decarbonising the transportation sector[14]. The target is to cut emissions by at least 40% below 1990 levels by 2030.

IATA, International Air Transport Association, states that the main objectives of aviation are improving fuel efficiency by 1.5% every year by 2020, and half the emissions by 2050 compared to 2005. A global four pillar strategy to decrease carbon emissions was developed. These pillars focus on new technologies, more fuel efficient aircraft, alternative fuels that are more sustainable than jet fuels, operational efficiency enhancements to reduce emissions, and modernising air traffic management and infrastructure. Furthermore, the implementation of global market-based measures to achieve carbon neutral growth by 2020.

Airbus Smarter Skies prediction for the future is to have 86% aircraft using less fuel and release fewer emissions, 78% aircraft powered by non-fossil fuel and 66% of the aircraft being quieter [1]. The long term aim of the Advisory Council for Aviation Research and innovation in Europe (ACARE) is to reduce CO_2 emissions due to air transport by up to 75% per passenger per kilometre by 2050, reduce fuel consumption by 50% and EPNdB emissions by 65%. These targets are with respect to reference aircraft from the year 2000 [15]. Specific regulations or targets for manufacturing processes and EOL disposal still need to be assessed.

The targets set for 2050 by the European Union [15] on fuel consumption, noise and emissions were translated into design drivers for the engine choice. Furthermore, one of the project requirements was designing an aircraft >97% recyclable, this was considered as a design driver during the material choice, manufacturing and aircraft EOL solutions.

8.2. Engine and Fuel Choice

Major improvements have been seen regarding the reduction of specific fuel consumption, SFC of aircraft engines. There are two options, to increase the propulsive efficiency, or to increase the thermal efficiency.

[1] http://www.airbus.com/fileadmin/media_gallery/photos/aircraft/miscellaneous/infographics/Infographic_Sept2012 [accessed on December 10th 2016]

Improvements in propulsive efficiency can be obtained with an engine that has low specific thrust[16]. For turbofan engines this results in a higher bypass ratio, BPR. However, the reduction in SFC is partially negated by the increase in nacelle mass, pressure losses and drag. For direct drive turbofans the increase in BPR introduces extra mass due to the increase in stages of the low pressure compressor and turbine. A geared turbofan solves this problem. Another option for high propulsive efficiency is an open rotor. These engines have a ultra high BPR without the negative effects of an engine nacelle.

Increasing the engines overall pressure ratio, OPR, results in an increase for thermal efficiency. The exit temperature of the combustion chamber, T_4 is determined by the OPR, and limited by the material capabilities of the combustion chamber and turbine rotor blades. Clearly focus must be placed on new core concepts in order to keep increasing thermal efficiency. Increasing the combustion temperature reduces fuel consumption and thus CO_2 emissions, but it increases the production of NO_x, therefore a trade-off between CO_2 and NO_x has to be found. The EU's research project NEWAC, New Aero engine Core concepts, investigates several core concepts that have the potential to increase thermal efficiency by improving efficiency of components rather than increasing temperatures. These concepts are promising in terms of emission reduction.

In Section 14.2 a trade-off has been performed on advanced open rotor, geared and direct drive turbofan engines. The choice was based on SFC and noise emissions. The geared turbofan engine was chosen. Hence, the engine chosen for the A342 is an off-the-shelf geared turbofan engine with 7.5% reduced SFC compared to the reference aircraft A320neo. For a range of 3,000 nm, the estimated CO_2 emission per passenger-km is 5% lower than values of the A320neo.
The use of alternative fuels is important to reduce the impact of aviation on the global climate and air quality. According to the International Civil Aviation Organisation, ICAO, by 2050, 100% of the international aviation jet fuel demand could be covered with alternative fuels[17]. However, questions are being raised as to the feasibility of biofuel completely replacing kerosene without straining the food chain and environment [2]. Biofuels are able to compete with petroleum, however it is necessary to overcome the economic gap and this is currently done through governmental subsidies and market mechanisms, resulting from mandates that amount 2 USD per gallon. [3]. It is expected that by 2050 the only way to reduce the environmental footprint due to aviation and improve the air quality is by using biofuels, Figure 8.1 [17]. The A342 will be using biofuels, this will be beneficial considering the possibilities of obtaining governmental subsidies making the aircraft more attractive to airlines. Furthermore, restricting regulations on the use of jet fuel might be set in the near future.

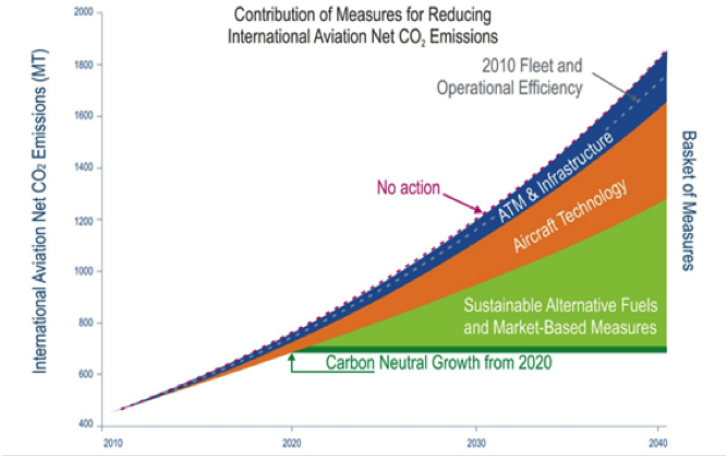

Figure 8.1: The contribution of measures to reduce the international aviation net CO_2 emissions

[2] http://www.ahead-euproject.eu/ [accessed on December 11th 2016]
[3] http://www.masbi.org/content/assets/MASBI_Report.pdf [accessed on January 18th 2017]

8.3. Noise Reduction

Noise has always been one of the major environmental issues and concerns of the public. 2.5 million people have been exposed to critical noise levels at 45 different airports in Europe in 2014 and this will increase by 15% by 2035[18]. Note that a EPNdB level, Effective Perceived Noise, of 80dB is perceived twice as loud as 70dB[4]. Therefore, limiting or reducing the amount of people affected by aircraft noise is crucial. Technologies can be included to lower noise in engine nacelle, jet and exhaust as well as the airframe.

The choice of the type of engine and the location has a major influence on noise. At this stage of the design a conventional location for the engines is assumed. It is recommended to explore other engine locations.

The two largest components of engine noise are fan noise and jet noise. The trend of increasing the BPR, has had a strong impact on jet noise reduction because of decreased jet velocity. Also the reduced fan tip speed of large bypass engines have reduced the fan noise emission [19]. However, the BPR can only be increased up to a certain level, as explained in Section 14.1. Over the years fan noise has become more prominent than jet noise, even at take-off [20]. Therefore, the focus in this section is on reducing fan noise.

The noise of rotating fans increases with speed. Generally two strategies are applied to reduce fan noise: attempting to optimise the blades, or directly regulate the air flow and reduce its velocity. To reduce the noise downstream of the engine liners can be used. Liners are noise absorbing materials, such as honeycombs. They can be implemented in nacelles or fuselages in order to make sure noise does not propagate from the engine. The use of liners on the rotating parts itself is avoided, as it challenges their structural properties [20].

Counter rotating turbofan engines are very promising in terms of noise reduction [21], because aerodynamic loading and tip speed of the blades is reduced. However, if designed incorrectly the two stages of the fan can negatively interact with each other and increase fan noise. The same goes for counter rotating open rotor engines. In this type of engine aft clipping is applied, the rear blades are shorter and therefore unaffected by the vortex created in the first row of blades[22].

The airframe noise represents a significant contribution to the overall aircraft noise. The main contributors include wing and flap trailing edges, flap and slat side edges, landing gears and interactions between aircraft components, leading to turbulent boundary layers. Both active and passive control mechanisms have and are being developed in order to decrease airframe noise.

Fairings will be included on the landing gears. Tests showed that covering the landing gear with one solid fairing led to a noise reduction of 10dB, however this prevents retractability [23]. Covering the individual components led to a noise reduction in terms of overall sound pressure level of -2dB to -3dB and -3.5dB for nose and main landing gear, respectively. Noise levels on parts of the landing gears increase with the 6th power of the locally incident flow speed. High speed flow deflection might occur onto adjacent uncovered parts of the gear erasing the benefits of solid fairings. Low frequency noise related to vortex shedding becomes an issue for landing gears that are covered with solid fairings of relatively large size [23].

Slat cove fillers will be implemented to fill the slat cove, this presented a potential noise reduction of 4-5dB in the broadband frequency range [23]. Sandwich construction present major noise reduction possibility since these materials are noise isolating. This was one of reasons why for the skin of fuselage sandwich construction has been used to make the cabin environment more comfortable for passengers.

One of targets for 2050 was to reduce EPNdB emissions by 65%. Therefore, noise has been an important design driver in the engine choice. The trade-off in Section 14.2 included noise as an important criteria. The geared turbofan engine scored better regarding noise. Furthermore, a higher BPR leads to lower noise emissions as stated earlier in this chapter. The engine chosen has a BPR of 15-20. Currently, geared turbofan engines such as the PW1100G engine used on the A320neo present a cumulative noise margin of 15dB compared to Chapter 4 representing a 50% noise reduction over the A320ceo [5] [6]. The engine of the A342 has a projected cumulative

[4] http://www.industrialnoisecontrol.com/comparative-noise-examples.htm [accessed on December 23rd 2016]
[5] https://www.federalregister.gov/documents/2003/12/01/03-29147/stage-4-aircraft-noise-standards [accessed on January 30th 2017]
[6] http://www.pw.utc.com/Content/PurePowerPW1000G_Engine/pdf/B-1-1_PurePowerEngineFamily_SpecsChart.pdf [accessed on Jan-

noise margin of 25dB with respect to Chapter 4 regulations[24].

8.4. Structural Efficiency

To reduce fuel consumption, structural efficiency of the aircraft plays a crucial role. Higher structural efficiencies can be achieved by a distributed wing loading and large inertia relief dependent on the wing and planform configuration. When the bending moments are reduced the empty weight is reduced, this is the case for Blended-Wing-Body configuration. A lower empty weight results in lower fuel weight. The main goal of this project is to challenge the conventional circular cross-section of the fuselage. Furthermore, the client required a conventional tube and wing configuration. Therefore, concepts regarding the cross-section of the fuselage have been analysed. A trade off has been performed addressing efficient volume usage, weight and costs. It was concluded that the a rectangular cross-section is structurally inefficient since it carries pressurisation loads by out-of-plane stresses while a circular cross-section carries these loads by in-plane stresses. Structural efficiency needed to be considered along with other requirements. In fact, the elliptical cross-section is more volume efficient than a circle but still carries pressurisation loads with out-of-plane stresses resulting in a structurally more inefficient structure.

8.5. Aerodynamic Efficiency

To reach a reduction in fuel consumption, aerodynamic efficiency of the aircraft plays an important role. Winglets, wingtip devices, reduce drag and offer a fuel consumption reductions of 6%. Choosing an aerodynamically efficient planform, for example the Hybrid-Wing-Body can lead to a 15% lower take-off weight and a 27% lower fuel burn per seat and kilometre. A box wing configuration can lead to a reduction in fuel consumption of 9% compared to the A320ceo. However, for a box wing configuration the wing is estimated to be twice as heavy as the A320ceo wing[25]. Sharkskin imitating skin paint can lead to drag reduction without weight increase, saving 4.48 million tons of fuel every year if applied to all aircraft around the world [7]. NASA reports that Near-Term Natural Laminar Flow Transport leads to a 6 to 8% fuel consumption reduction compared to the turbulent wing design [8]. High Lift Systems (HLS) should be considered to fly in combination with a smaller wing which would cause less drag, however this leads to weight and noise increase which need to be compensated, suggestions on this are mentioned in 8.3. The A342-BBB will incorporate winglets and high lift devices, implementing sharkskin imitating skin paint will also be considered. Since the client required a conventional tube and wing configuration the planform could not be optimised.

8.6. Material Choice

Fuel efficient aircraft designs require the use of lightweight materials such as CFRP, carbon fibre reinforced plastics, sandwich constructions with a foam or honeycomb core and prepregs which lead to a reduction in fuel consumption. However, when designing a sustainable aircraft one should consider the environmental impact during the manufacturing of certain materials as well. Whether or not materials lead to noise reduction should be considered.

Nowadays, in the context of sustainable development, manufacturers aim to promote and improve production fields and products. Metal alloys are being replaced by composites since airline operators want to reduce operational costs by improving fuel efficiency. Composites represent a good opportunity, combining high modulus materials with free definition of geometry. The A350 uses 53% composites and the Boeing 787 50% of the total structural weight of the aircraft [26]. The use of GLARE results in weight savings between 15% and 30% compared to Aluminium alloys. Carbon Fibre Reinforced Plastics (CFRPs) and thermoset matrix based composites are very common for aerospace applications. CFRPs are made of non-renewable materials and are expensive approximately 73 EUR/kg [27].

Metals can be recycled without compromising their material properties. While for composites, technology is not yet ready to perform recycling without losing quality. While thermoplastics are relatively easy to recycle,

uary 30th 2017]

[7] https://sites.google.com/a/cornell.edu/sustainable-solutions-for-the-aviation-industry/solution-new-fuel-efficient-planes/environmental-impacts [accessed on December 14th 2016]

[8] http://flight.nasa.gov/pdf/23_kroo_green_aviation_summit.pdf [accessed on December 11th 2016]

thermosets represent a challenge due to their highly cross linked structure. The recycling of CFRPs is mainly concerned with fibres, which will no longer be continuous but chopped and lose value and possible applications. Continuous virgin CF costs around 44 USD per lb while chopped or milled carbon fibre, CF 24-35 USD per lb meaning that looking at the open market it seems unlikely for recycled CF to approach even the lowest figure of this nearest competitor. It is claimed however that in the near future reclaimed CF can be sold at significant lower prices than virgin fibre, remaining profitable when the market applications expand and recycling technologies improve. Momentarily, CFRP recycling infrastructure and logistics costs are very high, this will change when other industries become more interested in composite materials. Tertiary recycling is being investigated to reuse thermoplastics, thermosets and polymeric waste. These can be reused as hydrocarbon fractions, as chemical building blocks for fuels, new polymers or chemicals [9].

Using thermoset prepreg generates a lot of scrap, new processes and technologies are being developed to process this. Prepreg scrap can be upcycled and reused in form of loose chips and used as filling material or roll/sheet stock and structural material [12]. There is an increasing need for composite recycling and reuse to deal with the waste and scrap in a sustainable manner. However, it is not clear how prepreg scrap can be implemented in the aerospace industry.

It becomes clear that recycling would bring great economical and environmental benefits. Several techniques exist for recycling composites: mechanical recycling is cheap but aggressive. It is based on grinding the matrix and fibre. Thermal recycling can be performed by pyrolysis, treatment in molten salt bath or oxidation in a fluidised bed [26]. Chemical recycling based on matrix solvolysis by water under supercritical conditions, includes cold recycling methods with the use of chemicals [28]. Airbus is currently cooperating with specialised companies such as CFK- Valley Stade Recycling GmbH on the development of a pyrolysis - based recycling plant for the recovery of carbon fibres. Adherent Technologies claims that through the innovative wet chemical breakdown procedure 99% clean fibres can be recovered through milder conditions than pyrolysis, retaining more than 95% of their virgin fibre strength [9].

Also noise should be taken into account, both for the passengers and crew as for the surroundings. Different materials have different noise dissipating properties, while structural solutions, such as micro honeycomb, are also an option for reducing noise [10] [11]. As for the moment, porous materials are being used, but the main drawback are their poor structural properties.

Sustainable material for the aircraft interior is available on the market. The current honeycomb panels can be replaced by bio-polymers composites reinforced with natural fibres, and with solid cores. Nevertheless, these solutions need validation regarding material properties with regard to flammability, strength and stiffness, moisture resistance, low weight, durability in the aircraft operation conditions, and compatibility with the adjacent materials. This is due to the fact that natural materials, mainly the ones composed of cellulose, absorb more water and require more energy during manufacturing to keep them stable [12]. However, optimised CF components for shelving units, walls and floor will lead to 75% weight saving compared to metal or wood [13]. The >97% recyclability requirement was the main design driver since the only requirement for the A342-BBB. The A342-BBB will be made to a large extent out of composites, mostly CFRP for the wings, empennage and engines. For the fuselage skin and floor, a sandwich construction is used. Sandwich constructions have been chosen for the fuselage skin due to their low density and high strength properties which leads to up to 50% weight savings compared to Aluminium constructions. Sandwich constructions present better fatigue and corrosion performance, meaning that they are more durable and present a longer service life. This design choice leads to major weight savings hence fuel consumption reduction, posing however a challenge in meeting the recyclability requirement during production and EOL recycling procedures. One has to make sure that most of the aircraft components are recyclable at EOL. As mentioned earlier composite recycling technologies are expected to develop fast. Due to new regulations in the automotive sector, the demand on reclaimed fibres will increase and the recycling industry accordingly.

[9] https://www.adherent-tech.com/recycling_technologies [accessed on January 18th 2017]
[10] http://www.aerospacelab-journal.org/sites/www.aerospacelab-journal.org/files/AL07-01_0.pdf [accessed on December 15th 2016]
[11] https://gtri.gatech.edu/casestudy/reducing-noise-micro-honeycomb [accessed on December 15th 2016]
[12] http://www.scielo.br/scielo.php?script=sci_arttext&pid=S1516-14392016000200339 [accessed on December 14th 2016]
[13] http://dragonplate.com/applications/marine-aircraft-interiors.asp [accessed on January 18th 2017]

8.7. Manufacturing, Production and Maintenance

To reduce the environmental footprint manufacturing, production and maintenance procedures have to be performed in a sustainable manner. During manufacturing processes, several measures can be taken to reduce the energy consumption, waste production, water consumption, use of hazardous chemical substances as well as volatile organic compounds (VOC).

First of all, energy efficiency should be improved by making an audit, this would save costs and reduce carbon emissions as well. Efficient energy cooling, heating and lightning of the factory will be used. LED lighting can be used to replace high bay lighting and the use of renewable energy resources can be implemented. Geothermal systems can be used to retrieve natural heat and biomass-powered boilers will be implemented at the production site. Integrating efficient energy consumption procedures, can lead not only to more sustainable production procedures but also to major cost savings. Secondly, water consumption should be reduced or water should be recycled. Rain water tanks can be used to store the water.

Waste should be reduced during manufacturing procedures. During manufacturing processes of virgin fibre, for which the demand in 2014 was 50,000 metric tonnes, 30% ends up as production waste, resulting in 10,000 metric tonnes ca. of commercial recycled carbon fibre (RCF) before EOL structures are considered [14]. However, recyclers predict that the demand for recycled fibres will increase and the automotive industry will require recycled fibres from carbon fibre waste streams due to restricting EU Regulations.

New technologies can be used during manufacturing in order to reduce waste. One such technology is for example Additive Manufacturing (AM), which offers means of complex geometries part manufacturing reducing waste as well as production and material costs. Powder bed based laser beam melting is a common technology due to high degrees of freedom. The focus is on laser beam melting of Aluminium alloys since these alloys are most common in the Aerospace industry. The aircraft basic weight can be reduced by 4 to 7% when substituting conventional parts with optimised AM lightweight components [29]. AM also contributes to functional integration and part consolidation by decreasing the assembly effort [30]. The possibility of reusing some parts removed from other EOL aircraft such as engines, wings or smaller parts like door handles will be taken into account.

During operational life, measures should be taken to reduce the environmental footprint due to maintenance. The A342-BBB is designed such that easily accessible with easy inspection locations. The detailed external layout can be seen in Chapter 9.2.
The A342-BBB will be to a great extent made out of composite materials. Sustainable manufacturing has to be assured hence several energy, water and waste reduction procedures will be applied at production sites. Furthermore, scrap material and reclaimed fibres from production will be sold to other industries. Furthermore, composites require less maintenance, hence are more sustainable from this point of view.

8.8. End-Of-Life Solutions

Within the next 20 years more than 12,000 aircraft are set to retire from operation, therefore EOL solutions on dismantling and recycling aircraft in an environmentally responsible way becomes crucial [13]. An aircraft that is at EOL loses 75% of its value [26].
There are several options for the reuse of aircraft at EOL. The complete aircraft may be reused or transformed into a freighter. Else components can be reused on other aircraft or for different purposes.

There are two types of recycling: primary and secondary. The first deals with recycling material during production, for example by reusing chips and curls. The latter deals with the recycling of material from the EOL product. In some cases secondary recycling is possible without loosing quality, when it is not, it is referred to as down cycling. In some cases down cycling is the only option when recycling technologies are not available [13].

In order to reuse the components removed from an EOL aircraft one should consider that they have to be classified as serviceable. This can be done by filling in form 1 from the European Aviation Safety Agency (EASA)

[14] http://www.compositesworld.com/articles/recycled-carbon-fiber-update-closing-the-cfrp-lifecycle-loop [accessed on January 20th 2017]

when the aircraft is in service. A component with serviceable tag from the shop has a higher value than a removed serviceable component, this is why the latter are mainly used within the fleet [13]. To increase the recycling rate, possibly all parts of the EOL aircraft should be put on the shelf, ready to be sold. These parts should have all the records telling the status of the component to be assigned the highest value.

Aircraft manufacturers should leverage on developing aircraft consisting of parts and materials that can be down-cycled at EOL. This reduces the waste disposal fees, and increases the attractiveness for airline companies. Hazardous materials should be avoided, because waste disposal fees increase and add to the total manufacturing costs [12]. One of the requirements of this project is to design an aircraft that is by >97% recyclable. The recycling rate of the aircraft at EOL can be determined using Equation 8.1. This equation is however defined for Road Vehicles since no definition is available for the aviation sector.

$$R_{cycl} = \frac{m_p + m_d + m_m + m_{tr}}{m_v} * 100 \tag{8.1}$$

m_v is the vehicle mass, m_p is the mass of the pre-treatment step, m_d is the mass of the dismantled parts, m_m is the mass of the metal separation step and m_{tr} is the recyclable mass of nonmetallic residue treatment step [13]. From Equation 8.1 one can see that for example if all the dismantled parts are going to be put on the shelf at EOL a recycling rate of 100% can already be achieved. It can be concluded that there is a great flexibility and number of possibilities to be able to reach the requirement of a recycling rate above 97%.

The dismantling cost of one aircraft at EOL is estimated to be around $ 4.2 million USD [15]. It is therefore advantageous to obtain the majority of the value back by putting components on the shelf such as the engines, wings, landing gears and the interior components at the EOL The composite materials of components such as ailerons, elevators and rudder are going to be recycled by selling it to other industries to produce phone or laptop cases and lightweight sporting equipment or the automotive industry. Regulations on EOL vehicles are already existing in the automotive industry. As mentioned earlier, in the near future automakers probably will have to ensure that automotive materials are recyclable, hence will take advantage in reusing fibres from EOL aircraft. The rubber from the tyres will be recycled and the rubber granules can then be reused as well as the copper from the electrical wiring.

Concluding, the only specific requirement was to design an aircraft that is >97% recyclable, this will be achieved. At EOL the main components of the aircraft for instance engines, landing gear, wings but also interior components will be put on the shelf certified and ready to be implemented on other aircraft. The other components will be recycled and the reclaimed fibres will be sold to other industries, prominently as forecast to the automotive industry. It should be noted that no regulations regarding sustainability are yet existing in the aviation sector. However, targets set by the European Commission have been translated into design drivers, noise reduction, lower fuel consumption and emissions will be met considering the engine and material that has been chosen.

[15] https://www.skiesmag.com/news/strategies-100-per-cent-recyclable-aircraft/ [accessed on January 18th 2017]

9. General Layout

In this chapter, the fuselage interior configuration design and the external layout will be discussed. The goal was to design a fuselage which primary function is to provide volume for the payload, passenger comfort and overall structural integrity.

9.1. Internal Layout

Fuselage design is based on an inside-out approach meaning that the outer dimensions are determined by inner cabin requirements. Inner cabin requirements include the total number of passengers, the number of seats per row, seat dimensions, cargo and luggage space, as well as requirements for passenger well-being. One of the top-level system requirements for the project was to optimise the fuselage shape to maximise the product payload performance. This has been achieved by first defining the inner cabin layout and after that the outer fuselage shell design has been determined taking into account mainly structural and aerodynamic considerations.

In this section a preliminary analysis following from passenger allocation requirements [31] is presented. It should be noted that some parameters, namely seat pitch, number of toilets, number of aisles and seat width were taken from the reference aircraft A320neo. These parameters still comply with the regulations for an aircraft of 200 passengers.

The total length of the cabin in a unit of accommodation can be calculated with the approximate Equation 9.1 [31].

$$l_{cabin} = [(\frac{P}{p} + g)s + t + 0.8w] \tag{9.1}$$

- l_{cabin} = length of the cabin
- P = number of passengers
- p = number of seats across
- s = seat pitch [m]
- g = number of galleys
- t = number of toilets
- w = number of cross aisles

It should be noted that the number of galleys g, toilets t, and cross aisles w are only counted once [31]. In order to calculate the overall fuselage length l_f, the nose and tail lengths were estimated using a nose length to effective diameter and tail length to effective diameter ratio of 1.5 and 2.6, respectively. This resulted in the nose and tail lengths of 4.7 m and 7.84 m respectively. Please note that an additional 0.5 m has been added to l_{cabin} and hence the l_f. In Table 9.1 the cabin layout dimensions are shown.

Table 9.1: Cabin layout specifications

Cabin Dimensions					
No. of seats across, p	6	No. of cross aisles, w	2	Aisle width [m]	0.5
No. of seats	200	No. of galleys, g	2	Overall diameter, d_f [m]	
Seat width [m]	0.5	Headroom [m]	1.6	l_f/d_f slenderness ratio	12.7
Seat pitch [m]	0.71	Overall length l_f [m]	44.46	Internal cabin width [m]	3.5
No. of toilets along the length, t	1-2	Cabin length [m]	31.92		

Several configurations have been considered, the main variables were the number of aisles, the number of seats abreast and the number of decks. Safety and accessibility were so called killer requirements, meaning that all configurations considered ensured safety and accessibility. Finally, a trade-off was performed on two configurations, 4-seats abreast double-deck, 1 aisle per deck configuration and , 6-seats abreast single deck, single aisle configuration, see Figure 9.1. The main trade-off criteria were comfort, turnaround time and minimum effective cross-sectional area. It should be noted that comfort was defined in terms of noise, personal space available and privacy. The configuration with the minimum area was defined as the one where optimum space usage could be achieved. These criteria were given different weights according to their relative importance. With the minimum area being the most important criterion followed by turnaround and comfort.

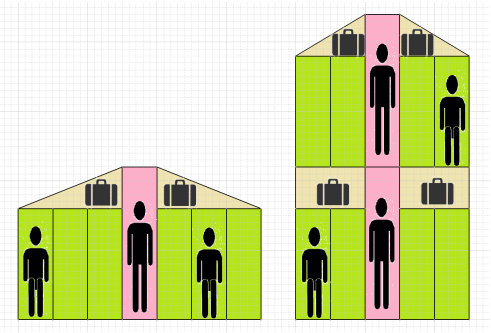

Figure 9.1: Interior layout configurations

Many requirements related to the fuselage pose limits to the designer's range of choice. Drag of the fuselage should be low since it makes up for 20 - 30% of the zero lift drag. For a given dynamic pressure the drag is preponderantly determined by the wetted area S_{wet}, and the shape. An increase of d_{fus} by 10% causes a 1.5-3% increase in total drag. The slenderness ratio is an important parameter that is considered since increasing the diameter increases the drag. For passenger jet aircraft typical slenderness ratios l_f/d_f are between 8-12.5. Therefore, the optimal configuration resulted in six seats across, with a feasible slenderness ratio of 12.7. If the number of seats abreast increases the fuselage gets wider and shorter. The structure should be strong, rigid and light. The fuselage should also be easy to inspect and maintain. The fuselage design has an influence on fuel consumption and manufacturing costs which influence the operating costs. Hence a compact and small fuselage which is within acceptable limits should be designed, meaning that passengers comfort should still be guaranteed to a certain extent such that the passengers do not refuse to fly with the aircraft. Finally, the fuselage does carry the empennage but does also influence the tailplane configuration. The fuselage has a destabilising effect that is more or less proportional to its moments regarding aerodynamic pitching moment and yaw moments. On the other hand the stabilising effect of the tail surfaces depends on the fuselage tail length.

The single aisle aircraft with a 6-seats abreast configuration obtained the best score and was hence chosen, see Figure 9.2. In Table 9.2 the dimension corresponding to this configuration are shown.

Table 9.2: Internal cabin dimensions

Dimensions [m]	**A342-BBB**
A = headroom	1.6
B = seat width	0.5
C = aisle height	2.2
D = floor to seat height	1.04
E = floor to arm-breast height	0.45
F = aisle width	0.5
G = cargo storage height	0.31

A single aisle was considered best when looking at efficient space usage and compactness. FAR 25.817 regulations state that 6-seats abreast is the maximum that can be chosen for a single aisle aircraft. In order to ensure passenger comfort, no more than 2 seats should have to be crossed by a passenger to reach the aisle. More than 6-seats abreast was also considered not favourable for a 200 passengers aircraft since the result would have been a reduced fuselage length and hence a the integration of a large tail surface would have been required for stability.

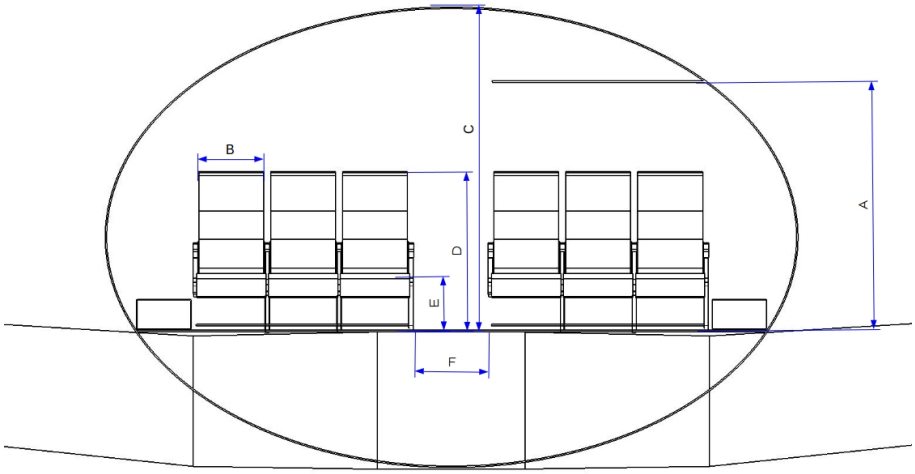

Figure 9.2: Interior configuration for the elliptical cross-section

A seat pitch of 0.71 m was chosen, the minimum possible for high density flights, and a seat width of 0.5 m was set which compensates for the rather limited seat pitch. The personal space for each passenger will then be 0.8 m^2 considering a headroom of 1.6 m and the volume of 0.57 m^3. Compared to the A320neo and A321neo it can be seen that the A342-BBB will offer an increased personal space and hence more comfort (see Table 9.3).Thinner seats will be incorporated giving the passengers more leg room compared to previous generation designs. This also helps compensating for the limited seat pitch. Mirus Aircraft Seating claims that the new Mirus Hawk seat is 40% lighter than conventional economy class seats, with ultra-slim backrests and 10 ° recline to aid ergonomics [1].

Table 9.3: Comparison in terms of personal space

Dimension	A342-BBB	A320neo	A321neo
Seat pitch [m]	0.71	0.71 - 0.74	0.71
Seat width [m]	0.5	0.46	0.46
Area personal space [m^2]	0.8	0.74	0.74
Volumetric personal space [m^3]	0.57	0.52 - 0.54	0.52

The aisle width was chosen to be 0.5 m this value has been taken from the reference aircraft A320neo. It is required that all passengers are able to move their heads freely without touching the cabin walls. Therefore an aisle height of 2.2 m was chosen and a headroom of 1.6 m.

The cabin floor is preferred to be kept level in normal cruise attitude, it should be noted that this is of crucial importance in large passenger aircraft when considering that food and drinks are handled on carts. Furthermore, a flat floor is preferred for safety during emergency situations.

The lavatories, 3 in total since one toilet is required for every 70 passengers, are located such that they are easily accessible and not directly visible from the pantry, for aesthetic reasons. The galleys, 2 in total since one for every 120 passengers ca. are needed [31], will be located one at the rear- and one at front-end of the cabin, to allow for flexibility in the cabin layout.

Regarding the number of emergency exits, from airworthiness regulations one can conclude that for a seating capacity of 200 passengers 2 type I exits and 3 type III exits will have to be included on each side of the fuselage. Two type I and 2 two type III are needed for 179 passengers (see Figure 9.3), however for a 200 passengers aircraft another type III exit is needed (see Figure 9.4).

[1] http://www.futuretravelexperience.com/2016/11/aircraft-seating-innovations-offer-economy-class-hope/ [accessed on January 16th 2017]

Passenger seating configuration (crew member seats not included)	Emergency exits for each side of the fuselage			
	Type I	Type II	Type III	Type IV
1 to 9				1
10 to 19			1	
20 to 39		1	1	
40 to 79	1		1	
80 to 109	1		2	
110 to 139	2		1	
140 to 179	2		2	

Figure 9.3: Emergency exits

Additional emergency exits (each side of fuselage)	Increase in passenger seating configuration allowed
Type A	110
Type I	45
Type II	40
Type III	35

Figure 9.4: Additional emergency exits

If a passenger door is to be certified as an emergency exit it is required to be at least as wide as the relevant type of emergency exit. It should be noted that two doors can be used for up to about 200 passengers and they should be 1.8 x 0.9 m^2 [32]. The windows will be circular due to structural reasons. An average value of 0.5 m is used for the former and window pitch. It should be noted that the window pitch is not always decided by the seat pitch, usually it is decided according to the fuselage formers.

Nowadays, passengers are allowed 17 kg of luggage on average, which can be stored in overhead compartments in a separate compartment in the bottom of the aircraft or along the length of the cabin. However, the client indicated that in the future passengers might want to carry more on-board luggage. Maximising the luggage storage volume in the cabin is one of the main drivers for designing the cabin interior.

From the baggage report of 2015 [33] it can be seen that in 2014 for a total of 3.3 billion passengers, 24.1 million bags were mishandled in total (7.3 bags per 1000 passengers). 80% of the mishandled bags were delayed, 14.3% damaged and 5.5% lost or stolen. Although improvements are being achieved by the airlines and airports, one solution to this problem is to minimise the checked baggage and therefore baggage handling.

Airline companies are allowed to set the limits for carry on luggage and checked luggage themselves. The only international regulation existing is that checked baggage has to weigh less than 23 kg to ensure health and safety of airport workers [2]. From a survey performed in 2009, data on the carry on and checked luggage could be retrieved. The average value for carry on luggage is about 7 kg while the average value for checked luggage changing according to route types vary between 18.3 kg for Non-European flights and 15 kg for domestic flights, on average 16.7 kg are compose checked luggage [3]. However, from the market analysis, Section 3, it can be seen that by 2035, the middle class population will increase, the amount of people that can afford to fly will increase and hence most probably the demand for low cost flights will increase. Since luggage comprises a part of airline business and fees for checked luggage are relatively high, the trend will be that more and more passengers will choose to carry more on board luggage and less checked luggage which is already the case. Carry on luggage not only saves money it is also preferred since accessible at all times during flight, does not get lost or damaged and saves time.

To cope with the safety regulations set by the governments and IATA, International Air Transport Association, which forbid to carry sharp objects and knives in the cabin, space for checked luggage has to be allocated. Furthermore, since the transportation of liquids as well as bulky baggage such as sporting equipment on board is limited, hence the possibility of storing checked luggage is still needed. At the bottom of the fuselage there will be compartments available for the storage of checked baggage. In the overhead compartments the area available for the luggage amounts 0.9 m^2 and the volume 0.64 m^3. This results in a cabin baggage storage volume of 0.107 m^3 per passengers which exceeds the minimal requirements of the client for the total luggage (carry-on and checked luggage) being 0.085 m^3. For checked luggage approximately 1 m^2 of the cross-section is available, if the luggage is allocated two thirds of the cabin length roughly 20 m^3 is available in total. This results in 0.1 m^3 checked baggage for each of the 200 passengers.
Recent events have shown the tendency of passengers to take their luggage with them during emergencies,

[2] http://www.iata.org/whatwedo/ops-infra/baggage/Pages/check-bag.aspx [accessed on January 17th 2017]
[3] https://www.easa.europa.eu/system/files/dfu/Weight%20Survey%20R20090095%20Final.pdf [accessed on January 17th 2017]

delaying evacuation of the aircraft. For this reason, the overhead luggage compartments will incorporate a system that locks the bins automatically during emergencies ensuring more safety.

Several luggage allocation possibilities have been investigated. The placement of the luggage underneath the seat would take away leg space decreasing passenger comfort. Once the perfectly fitting outer shell was chosen, the additional space next the seats was used to fit extra bins where the passengers can place their luggage. This will especially ease the elderly in storing their luggage. In Figure 9.5 the internal layout of the fuselage can be seen.

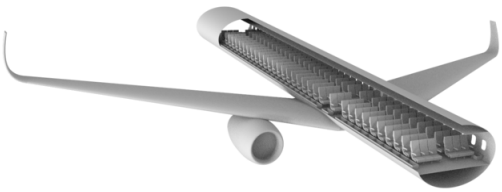

Figure 9.5: Internal configuration of the fuselage

A comparison between current trend and the A342-BBB luggage capacities is given in Table 9.4. Note that the trend carry-on luggage volume is based on standard carry-on luggage size of 55 x 40 x 20 m. And bulk loading volume on the reference aircraft A320neo.

Table 9.4: Comparison luggage capacity A342 BBB and current trend

	Trend 2017	A342 BBB
Carry-on luggage volume per passenger [m^3]	0.04	0.107
Bulk loading volume per passenger [m^3]	0.21	0.1

Please note that a perfectly fitting outer shell has been chosen which does not take into account the placement of the wingbox. However, this can be implemented by adapting the shape and size of the ellipse. This will as a consequence make the ellipse more circular.

9.2. External Layout

In Figure 9.6 the external layout of the aircraft can be seen. The wing location and configuration, empennage location and type, undercarriage, engine location are included. The aircraft will have a span less than 80m, which complies with requirement CFSM-S-17. The aircraft external layout will have the following dimensions, based on class II weight estimation and empirical data [34]:

- Nose has a length of 4.7 m, follows a quadratic formula and ends in a sphere [4]
- Cabin length of fuselage is 31.92 m, based on Section 9.1, and has a elliptical cross-sectional shape with a long axis of 2.125 m and a short axis of 1.409 m. This is the smallest ellipse that could fit around the payload interior
- The tail has a length of 7.841 m, the tip has the same height as the fuselage and it ends in a cone
- Wing area is 135 m^2, based on wing loading graph
- Wing profile is NACA 63A518
- Wing span is 43.47 m; located at 40% aircraft length; root chordlength is 5.17 m; wingtip chord length is 1.03 m; dihedral angle is 5 degrees; sweep @ 1/4 chord is 25 degrees
- Winglets chord length is 0.88; winglets height is 3.07 m
- Wing has a taper ratio of 0.2 and an aspect ratio of 14
- The High Lift Devices (HLD) of the leading edge (LE) are located along the total span, excluding the wing-fuselage section. They take up to 15% of the chord.
- The High Lift Devices (HLD) of the trailing edge (TE) are located from wing-fuselage joint to 11.5 m along the span. They take up to 35% of the chord.
- The TE HLD is a triple slotted flap, the LE HLD is a kruger flap

[4] https://ntrs.nasa.gov/archive/nasa/casi.ntrs.nasa.gov/19930087953.pdf [accessed on January 17th 2017]

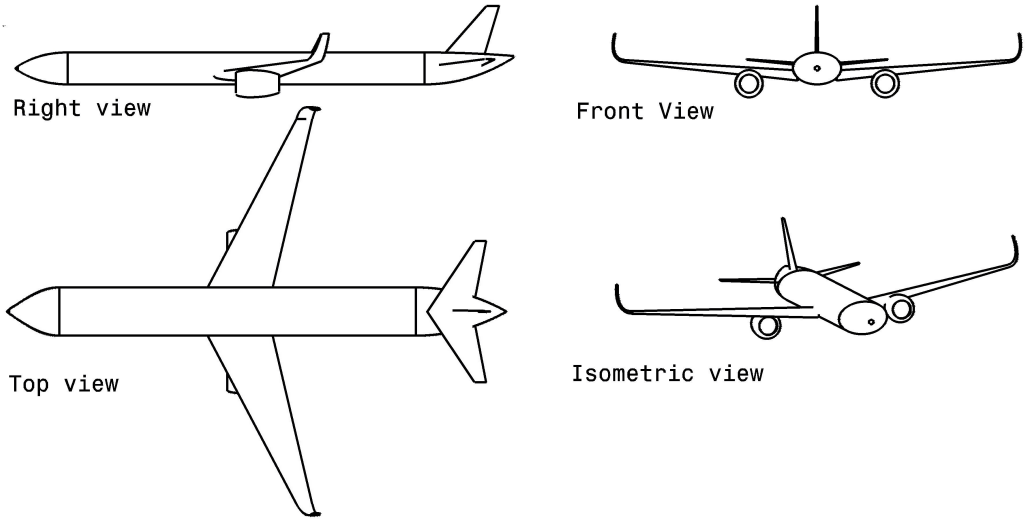

Figure 9.6: Aircraft views

- The distance from the nose to MAC_{LE} 19.3 m; the distance $0.25MAC_{wing}$ - $0.25MAC_{Htail}$ is 18 m; the distance $0.25MAC_{wing}$ - $0.25MAC_{Vtail}$ is 17 m.
- The horizontal tail has an area of 23 m^2; the span is 10.72 m; the sweep @ 1/4 chord is 29 degrees.
- The horizontal tail has a taper ratio of 0.256 and an aspect ratio of 5.
- The vertical tail has an area of 21.5 m^2; the height is 6.26 m; the sweep @ 1/4 chord is 34 degrees.
- The vertical tail has a taper ratio of 0.303 and an aspect ratio of 1.82.

For the analyse of the properties, three different fuselage shapes were computed, see Figure 9.6, 9.8, 9.9 and 9.10. The Rounded rectangle is 100 mm wider than the interior boundary, the ellipse has a semi-major axis of 2125 mm and a semi-minor axis of 1409 mm, and the circle has a radius of 1924 mm.

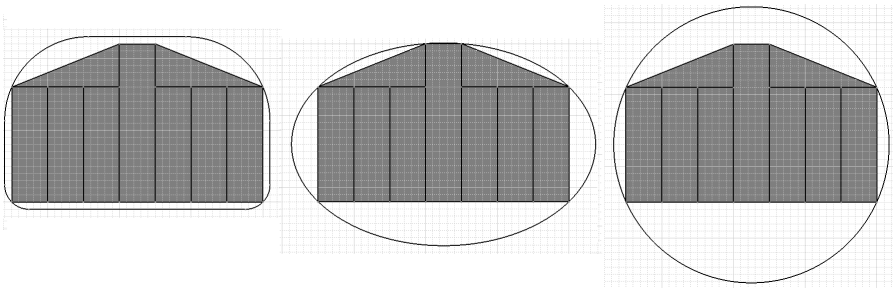

Figure 9.7: Fuselage shapes around interior

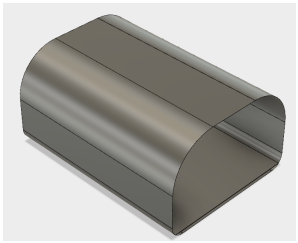

Figure 9.8: Rounded rectangle case

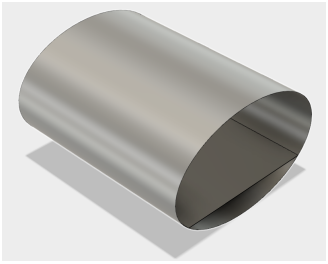

Figure 9.9: Ellipse case

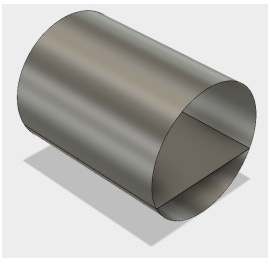

Figure 9.10: Circle case

10. Structural Analysis

In this chapter the structural design of the aircraft will be discussed. Structural design is important to ensure safety and it plays a crucial role regarding cost and performance. First, the main assumptions made are stated. Then, the loads acting on the aircraft are determined and the structural design is investigated. An analytical model and a numerical model have been used in order to find the optimal geometry and thickness distribution of the fuselage, and finally the weight of the fuselage structure. Verification and validation procedures are presented, as well as sensitivity analysis. Finally the conclusions and recommendations are discussed.

10.1. General Assumptions

- The aircraft is in static equilibrium under the given loads.
- Drag and lift forces are negligible during landing.
- Total weight comprising structure and payload can be modelled as a uniformly distributed load.
- The bending moment due to drag force is negligible.
- The lift force is zero when on ground.
- The fuselage can be modelled as a beam.
- Load factor resulting from landing is smaller than n_{max} [35].
- Maximum operating pressure altitude 12,500 m.
- Loads experienced during gust are assumed to be equal to the critical manoeuvring loads [36].
- The fuselage is modelled without cut-outs.

10.2. Forces acting on the fuselage

The main forces acting on an aircraft include:

- Aerodynamic forces
- Gravity forces
- Ground reaction forces
- Pressurisation forces

Lift and drag represent the aerodynamic forces, where the tail lift force, L_h is represented as a point load on the fuselage acting at the aerodynamic centre of the horizontal stabiliser. The wing lift force, L_w is transferred to the fuselage through the front and rear spar and the drag force contributing to the bending moment is considered negligible. The lift force is given by Equation 10.1.

$$L = L_w + L_h = nW \tag{10.1}$$

- n = load factor [-] n equals 1 during horizontal flight and n is not equal to 1 during gust and manoeuvres.
- W is the aircraft weight

The pitching moment M, around an axis through the aerodynamic centre, is given by Equation 10.2 [36].

$$M = M_{ac} + nW(x_{cg} - x_{ac}) - L_h(x_{ac_h} - x_{ac}) \tag{10.2}$$

- M_{ac} = moment around the aerodynamic centre [Nm]
- n = load factor [-]
- W = weight of the aircraft [N]
- x_{cg} = centre of gravity location along the x-axis [m]
- x_{ac} = location of the aerodynamic centre along the x-axis [m]
- x_{ac_h} = location of the aerodynamic centre of the tail along the x-axis [m]

Lift force and pitching moment are defined by Equations 10.3 and 10.4.

$$L = C_L \frac{1}{2} \rho V^2 S \tag{10.3}$$

- S = wing area [m^2]
- V = aircraft velocity [m/s]
- ρ = air density [kg/m^3]

$$M = C_m \frac{1}{2} \rho V^2 S \bar{c} \tag{10.4}$$

- C_m = pitching moment coefficient [-]
- S = wing area [m^2]
- V = aircraft velocity [m/s]
- ρ = air density [kg/m^3]
- $\bar{c}$ = mean aerodynamic chord [m]

The aerodynamic forces specified are to balance the aircraft in steady flight with different load factors or during landing.

Gravity forces include the forces induced on the fuselage due to several component weights. The maximum take-off weight of the whole aircraft, MTOW is given by Equation 10.5.

$$MTOW = OEW + W_{fuel} + W_{pay} \tag{10.5}$$

- MTOW = maximum take-off weight[N]
- OEW = operational empty weight [N]
- W_{fuel} = fuel weight [N]
- W_{pay} = payload weight [N]

When all the forces and weights acting on the fuselage are known, the load distribution can be found.

Ground reaction forces result from manoeuvring on ground. They include braking and landing loads, which are transferred to the fuselage through the rear and front spars. It can be assumed that during landing the fuselage is bent as during in-flight manoeuvring. Furthermore it can be assumed that the landing load factor is lower than the maximum load factor [35].

The fuselage has to maintain a pressure level which is high enough for passenger comfort and well-being. This means that a differential pressure occurs which results in a hoop stress in the fuselage skin. The pressure force is carried by in-plane stresses in case of circular cross-sections and in-plane and out-of-plane stresses in case of non-circular cross-sections. The pressure difference is calculated in Subsection 10.3.2.

10.3. Load Cases

Four different load cases have to be addressed when designing an aircraft. These can be retrieved from airworthiness regulations. These load cases are needed to generate a load distribution among the fuselage structure. The load cases analysed can occur every flight or only once a lifetime. The structure has to withstand the forces for each load case and load case combination without detrimental distortion and should not fail until the ultimate load has been achieved. The limit load cases are:

- Flight Loads (Gust and Manoeuvre)
- Flight Loads and Internal Pressurisation
- Ground Loads (Taxiing, Landing Impact, Turning, Braking, Towing)
- Internal Overpressure Only

Please note that not all load cases have been analysed in this report. Pressurisation was considered the critical load case in this design phase.

10.3.1. Manoeuvre, Gust and Landing Loads

The manoeuvre load factor is the ratio of the aerodynamic force to the weight of the aircraft and it is caused by in-flight manoeuvring. The V-n diagram, Figure 10.1[36], represents the variation of the load factor, n, at different airspeeds during manoeuvring. The maximum load factor is restricted by $C_{L_{max}}$ at low airspeed and given by Equation 10.6 [37] and by FAR regulations at high airspeed in case of civil transport aircraft. The maximum positive load factor, $n_{man_{pos}}$ can be estimated from the Equation 10.7 [37] .

$$n_{man_{pos}} = \frac{C_{L_{max}} \frac{1}{2} \rho V^2 S}{W} \tag{10.6}$$

- $C_{L_{max}}$ = maximum lift coefficient [-]
- V = V_{MS} = minimum stall speed [m/s]

$$n_{man_{pos}} = 2.1 + (\frac{24,000}{W + 10,000}) \tag{10.7}$$

Note that W is the maximum take off weight, MTOW in lbs, $n_{man_{pos}}$ resulted to be 2.2, since it is less than 2.5 $n_{man_{pos}}$ is taken as 2.5 as specified by FAR §25.337 (c.). The minimum manoeuvring load factor, $n_{man_{neg}}$ is taken as -1.0 for the normal aircraft category as stated in FAR regulations. The maximum bending moment on the fuselage is retrieved from the combination of the load factor and the maximum take off weight. The positive load factor combined with the weight distribution causes downward bending of the fuselage. This results in tension at the top panels and compression at the bottom panels and shear at side panels. For the negative load factor the top panels will experience compression and the bottom panels tension.

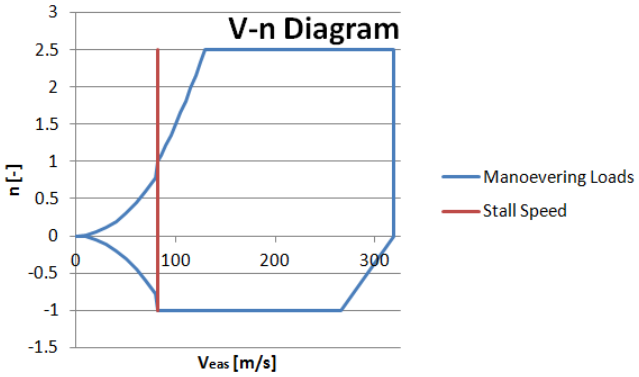

Figure 10.1: V-n diagram

Apart from manoeuvre loads, flight loads also include gust loads. Gust loads have to be determined at different combinations of gust and air speed. In general, large aircraft have a higher wing loading, and are therefore less sensitive to gusts. The highest n_{gust} on the fuselage is computed when the aircraft has the smallest wing loading, hence when the aircraft is empty. A comparison of manoeuvre and gust load case based on the load factor results is difficult. Even if the gust load results to be higher it does not necessarily mean that the bending moment and shear force are highest on the fuselage, since it is empty. Thus the maximum and minimum gust load factor are assumed to be equal to the critical manoeuvre loads, 2.5 and -1.0, respectively [36].
The lateral gust factor is the critical for dimensioning mid and rear section of the fuselage. This will be calculated later on.

The landing loads are calculated from the landing gear geometry, the load and the landing load factor, and the centre of gravity data. Generally, the landing load factor is lower than 2.5 and is now assumed to be equal to 2 [36].

The design speeds are the design manoeuvring speed V_A, the design speed at maximum gust intensity V_B which is generally 43 knots (22.12 m/s) lower than the cruise speed, the cruise speed V_C defined as 230 m/s, the design dive speed V_D and the equivalent airspeed V_E where V_A and V_D can be obtained from Equations 10.8, 10.9 [38].

$$V_A = \sqrt{n_{man_{max}}} V_{MS} \tag{10.8}$$

$$V_D \leq \frac{V_C}{0.8} \tag{10.9}$$

where V_{MS} is the minimum stall speed assumed to be equal to the stall speed V_S which is 50 m/s. V_F is the design flap speed, it depends on the flap position and stalling speeds. It must be greater than $1.6V_{s1}$ at MTOW

and flaps in take-Off position, $1.8V_{s1}$ at maximum landing weight and approach flap, $1.8V_{s0}$ at maximum landing weight and landing flaps. V_{s1} is the stall speed at 1g and V_{s0} at 0g [1]. The design flap speeds will be estimated later on.
The strength requirements must be met at each combination of airspeed and load factor and within the boundaries of the V-n diagram (Figure 10.1). The structural operating limitations are also defined by the manoeuvring envelope. One should note that beyond the maximum manoeuvring speed V_A, if the maximum load factor is exceeded or the maximum velocity of the airframe is exceeded structural failure occurs. Please note that the design speeds are based on stall speeds which have not yet been verified and validated, this will be done further on.

10.3.2. Pressurisation

Pressurisation causes internal pressure forces on the fuselage. The differential pressure depends on the maximum operating altitude and the internal cabin pressure. The cabin altitude has been chosen to be 1,800 m to ensure maximum comfort for the passengers and the maximum operating altitude has been set 12,500 m. The differential pressure is calculated from Equation 10.10. The pressure values have been estimated using the International Standard Atmosphere, ISA Model [37].

$$\Delta P = P_{op} - P_{cab} = 81,486 - 17,859 = 63,627 Pa \tag{10.10}$$

For both the analytical and the numerical model cabin pressurisation was considered to be the most critical load case. The other load cases will be investigated further on.

10.4. Structural Design Aspects

The structural design chosen for the fuselage is a double shell construction, namely a sandwich construction.A sandwich beam or plate is composed of an outer structure which is called the facing and an inner structure, the core. The core and facings can be made out of different materials (see Figure 10.2. The core material carries and transfers the imposed loads to the facings perpendicular to the applied load as stringers and frames do. Placing a core material amongst two facings, can make a part become up to 40 times stronger than the combined strength of the facings [2]. The core thickness of the material determines its ultimate strength.

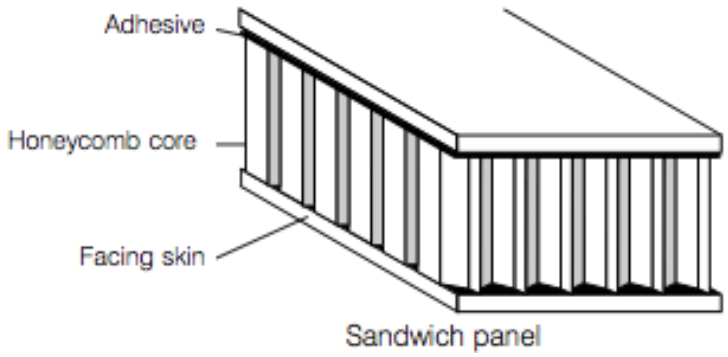

Figure 10.2: Sandwich construction components

The main reason a composite construction has been chosen for the A342-BBB is due to their lightweight properties and structural efficiency resulting from different resin/ reinforcement combinations available and the ability of designing and tailoring differing strength characteristics within a single form allowing for strong and light shapes. In fact, the fibre orientation can be tailored according to the load case the structure is going to be exposed to. However, other favourable properties are enhanced toughness and durability, high fatigue and corrosion resistance and the flexibility in design optimisation. A disadvantage of the thin facings make sandwich structures have low impact tolerance, and when punctured they become highly susceptible to moisture

[1] http://adg.stanford.edu/aa241/supplement/structures2015.pdf [accessed on January 8th 2017]
[2] http://www.aviationpros.com/article/10577549/composites-in-aerospace-a-maintenance-primer [accessed on January 21st 2017]

ingress.

In case of a sandwich fuselage design the major structural aspects that have to be designed for are strength and buckling. Static strength requirements have to be met, this is checked according to the maximum allowable strain for compression, tensile and pressurisation loads. Furthermore bending, shear and torsion buckling requirements have to be met. At this stage of the project no shear or buckling check was performed yet.

10.5. Analytical Model

In this section, the setup of the analytical model is described. First, all specific assumptions made are stated and then the model procedure is discussed. Second, verification and validation procedures, sensitivity analysis and results will be shown.

10.5.1. Assumptions

- The structural design of the fuselage is a double shell construction, specifically a sandwich construction using unidirectional plies.
- The core is assumed not to contribute to the moment of inertia. The core is considered spacing material and not a load bearing component.
- The fuselage skin is assumed to be a long and slender beam. A beam is long and slender when L/t > 10 [3].
- The fuselage skin is discretised into straight beams.
- The cross-section is assumed to be symmetric about the y-axis. $I_{xy} = 0$.
- Castigliano's theorem has been applied to solve for the moment at location 0 and it was assumed that due to symmetry the rotation at location 0 equals zero.
- To evaluate the rotations, θ Castigliano's theorem was applied. It states that when the internal strain energy U_i is expressed in terms of applied loads, then the rotation θ_i at any location equals the partial derivative of U_i w.r.t. the applied moment.
- U_i equals the internal strain energy caused by bending and shear. It was assumed that U_i due to shear is neglected compared to U_i due to bending when the beam analysed is long and slender.
- Only half of the cross-section is analysed this can be done since the cross-section is assumed to be symmetrical about the y-axis 10.5.
- Castigliano's theorem is only valid until Hooke's Law [39].

10.5.2. Skin panel layup

As is explained in Chapter 11.6 carbon fiber reinforced plastic (CFRP) is chosen as the skin material. This is a anisotropic material for which $\sigma_{longitudinal} >> \sigma_{transversale}$. This shows a clear weakness of this type of material. A purely anisotropic laminate will not be suited for multiple load cases. However, it opens the door for the superposition of ply properties in multiple directions at the same time. Adding multiple layers of CFRP plys at angles of 0°, ±45° and 90° wrt. the longitudinal axis of the aircraft a quasi-isotropic material can be created overcoming the previous named downside of these materials.

Because of the non-circularity of some of the investigated fuselage shapes, out of plane moments will be present in the skin. To overcome these moments in a weight efficient way sandwich constructions are introduced. These are constructed from a aramid fibre reinforced plastic (AFRP) honeycomb with on both sides a CFRP facing. Section 11.4 elaborates further on this decision.

If the the load case results in enough layers in every direction and layup transition allow this, plys are symmetrical distributed over the facing thickness. This is done to prevent asymmetric loading of the facings. The same is applicable to the total sandwich construction. An example layup is presented in Figure 10.3. It must be noted that the thickness of the and amount of plys differs throughout the fuselage.

10.5.3. Model Description

For the analytical model, Finite Element Method theory, FEM, has been applied. A flowchart of the tool can be seen in Figure 10.4.

[3] http://www.me.umn.edu/courses/me2011/handouts/beams.pdf [accessed on January 17th 2017]

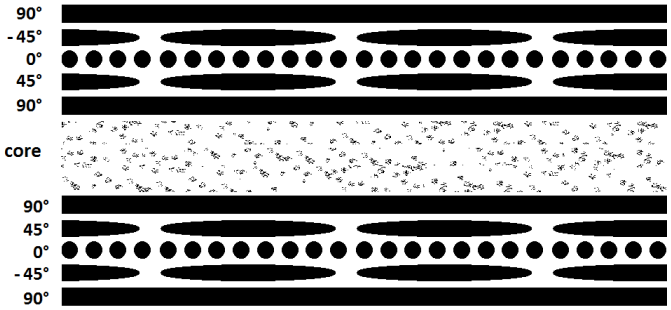

Figure 10.3: Example of lay-up for a sandwich construction

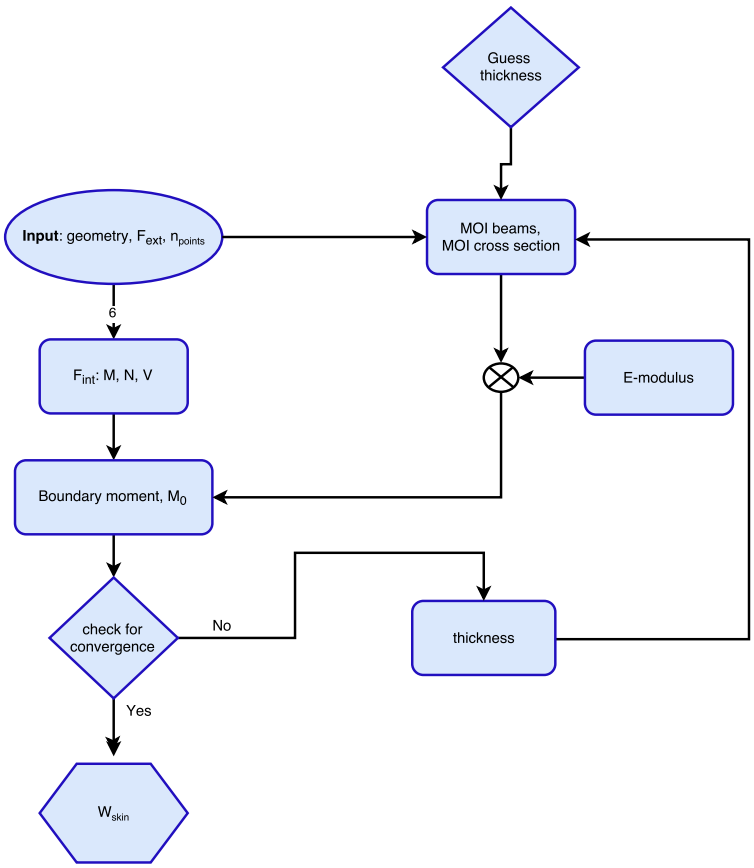

Figure 10.4: Flowchart of analytical model

The model is divided into different steps. First several input parameters can be chosen and entered; the geometry, the pressure difference, and the number of segments the structure is being discretised in. An initial input of the thickness is required. Second, the shear forces, V, membrane forces, N, and moment distribution over each segment is evaluated. After that, the moments of inertia, MOI, of each beam and of the cross-section of the beam are evaluated. The Young's Moduli of the materials used are implemented. Consequently, the moments at 0 are evaluated using Castigliano's theorem, Figure 10.5.

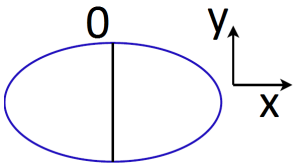

Figure 10.5: Example geometry showing the coordinate system and the 0 location chosen

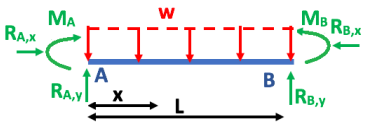

Figure 10.6: Reaction forces on discretised beam

The reaction forces of each beam are determined by applying static equilibrium equations, Figure 10.6. After that the internal moments M_i of each beam are determined. The internal moments are then expressed in terms of the moment at the end section M_n. The total internal energy U_i from Equation 10.11 is obtained by adding the internal strain energies due to bending of each discretised segment.

$$U_i = \int_0^l \frac{1}{2EI} M_i^2 dx \tag{10.11}$$

- U_i = internal strain energy [J]
- l = length of the segment [m]
- E = Young's modulus [MPa]
- I = moment of inertia of the cross-section [m^3]
- M_i = internal moment [Nm]

Consequently, Castigliano's second theorem is applied, Equation 10.12.

$$\theta = \frac{\partial U_i}{\partial M_n} = \int_0^L \frac{\partial M_i}{\partial M_n} \frac{M_i}{EI} dx \tag{10.12}$$

The rotation is set equal to 0, this represents one of the boundary conditions. An expression for the moment, M_0 at the starting location 0 is then determined following from the relation between the moment at the second boundary M_n. In case the moment at the first boundary location, M_0 converges, the stress distribution over the entire discretised structure is determined and the optimal thickness distribution can be found. Specifically, the minimum thicknesses required to withstand the forces acting on the fuselage are evaluated and structural weight can be predicted. From the thickness distribution the weight of the skin, W_{skin} can be calculated using Equation 10.13.

$$W_{skin} = (\rho_c * t_c + \rho_f * (t_{f_1} + t_{f_2})) * A * l \tag{10.13}$$

- ρ_f, ρ_c = density of the facing and the core material respectively [kg/m^3]
- A = circumferential area of the skin for the thin-walled structure [m^2]
- t_f, t_c = thicknesses of the facings and the core, respectively [m]
- l = length of the skin [m]

10.5.4. VERIFICATION

Several unit tests have been performed while the model was being build. Hence, hand calculations on the moment of inertia, MOI have been performed of different cross-sectional shapes 10.1. Also the membrane stresses at two different locations have been evaluated through hand calculations. Furthermore, hand calculations for the shear stresses have been performed 10.4. Then the results from hand calculations, namely the expected values were compared to the computed values from model (see Tables 10.2, 10.3 and 10.4). It can be seen that all results could be verified since either zero discrepancies occurred or the deviation was very low (see shear stress for the ellipse 10.4) between the expected and the computed values. One of the most straightforward case that has been tested is that since the circular cross-section carries pressurisation loads through in-plane stresses, hence for the circular case the moments should be zero and this was the case.

Table 10.1: Verification of Moments of Inertia, MOI

	Height [m]	Width [m]	Thickness [m]	Expected MOI [m^4]	Computed MOI [m^4]	Deviation in %
Square	2	2	0.002	0.0106	0.0106	0%
Circle	2	2	0.002	0.0503	0.0503	0%
Ellipse 1	1	2	0.002	0.0110	0.0265	2.4%
Ellipse 2	1.5	2	0.002	0.0084	0.0266	0.6%
Skin sections	-	-	0.002	6.67E-10	6.67E-10	0%

Table 10.2: Verification of Membrane Forces at location a

	Height [m]	Width [m]	Thickness [m]	Expected Membrane Forces [N]	Computed Membrane Forces [N]	Deviation in %
Square	2	2	0.002	84624	84620	0%
Circle	2	2	0.002	84624	84620	0%
Ellipse	1	2	0.002	42312	42300	0%

Table 10.3: Verification of Membrane Forces at location b

	Height [m]	Width [m]	Thickness [m]	Expected Membrane Forces [N]	Computed Membrane Forces [N]	Deviation
Square	2	2	0.002	19676	119670	0%
Circle	2	2	0.002	84624	84620	0%
Ellipse	1	2	0.002	484624	84620	0%

Table 10.4: Verification of Shear Stresses

	Height [m]	Width [m]	Thickness [m]	Expected Shear Stress [MPa]	Computed Shear Stress [MPa]	Deviation
Square	2	2	0.002	465.77	465.77	0%
Circle	2	2	0.002	0%	0%	0%
Ellipse	1	2	0.002	105.05	105.11	0.1%

10.5.5. VALIDATION

For the validation of the analytical model a stress analysis tool presented in the midterm report was used. This tool originates from and has been validated in pressure vessel code[40]. Membrane forces and out of plane moments where calculated at location A,B and C. These locations and the corresponding loads can be found in Figure 10.7 and Table 10.5 respectively.

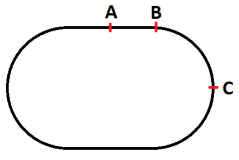

Figure 10.7: Allocation of validation checkpoints

Table 10.5: Validation results

load	location	reference value	computed value	deviation
membrane stress	A	119235.1	119235	0%
membrane stress	B	119235.1	119236	0%
membrane stress	C	179825.8	179826	0%
moment	A	-59221.7	-59221	0%
moment	B	-37530.2	-37530	0%
moment	C	47842.1	47842	0%

As can be seen in Table 10.5 the values computed by the analytical tool do correspond to the validated values from the pressure vessel code. The computed loads can therefore be used as accurate values.

10.5.6. RESULTS

In this section presents the computed skin weights and elaborates on them. As explained in Subsection 10.5.2 the skin panel laminates are composed of fibre laminates in 4 different directions (0°, ±45° and 90°). The laminate weights of the different layers are are presented in Table 10.6, as is the total skin weight. This is done for the different shapes described in Subsection 9.2.

Table 10.6: Results of analytical model: Estimated skin weights

a [m] (height axis)	b [m] (width axis)	a/b [-]	0° ply weight [kg/m]	±45° ply weight [kg/m]	90° ply weight [kg/m]	weight [kg/m]	weight increase
1.924	1.924	1.000	2.0	7.1	3.6	12.7	0%
1.838	1.957	0.939	2.0	7.1	17.8	26.9	112%
1.752	1.991	0.880	2.0	7.1	23.8	32.9	159%
1.667	2.059	0.809	2.0	7.2	30.0	39.2	209%
1.409	2.125	0.663	2.0	7.7	37.0	46.7	268%

A pattern which becomes clear is that the weight of the 0° laminate stays constant for all evaluated shapes. The driving factor for the thickness of the layers is the contribution of the moment. This can be calculated using the following equation.

$$\sigma = \frac{M \cdot y}{I_{xx}} \tag{10.14}$$

The constant weight contribution can be explained by the fact that the $\frac{y}{I_{xx}}_{avr}$ does only vary slightly if the fuselage shape is varied.

It also is clear that the weight of the ±45° layers stays more or less the same for the shape as long as the fuselage cross section has a $\frac{b}{a}$ lower than 1.25.

The biggest weight difference between the shapes comes from the stresses introduced by the pressure difference. A simple circular fuselage ($\frac{b}{a} = 1$) has the best resistance to pressurisation. As was expected. Moving further away from the circular shape introduces bigger and bigger out of plane shear forces and moments. This results the introduction a sandwich construction. Which is suited well for out of plane moments and share forces. However the weights still increases to a large extend as can be seen in Table 10.6.

The skin weight as a function as a function of $\frac{b}{a}$ is show in Figure 10.8. This shows clearly that the weight increases rapidly moving from a circular to sightly eccentric shape. Moving further to more elliptical shapes the weight increase is flattens out.

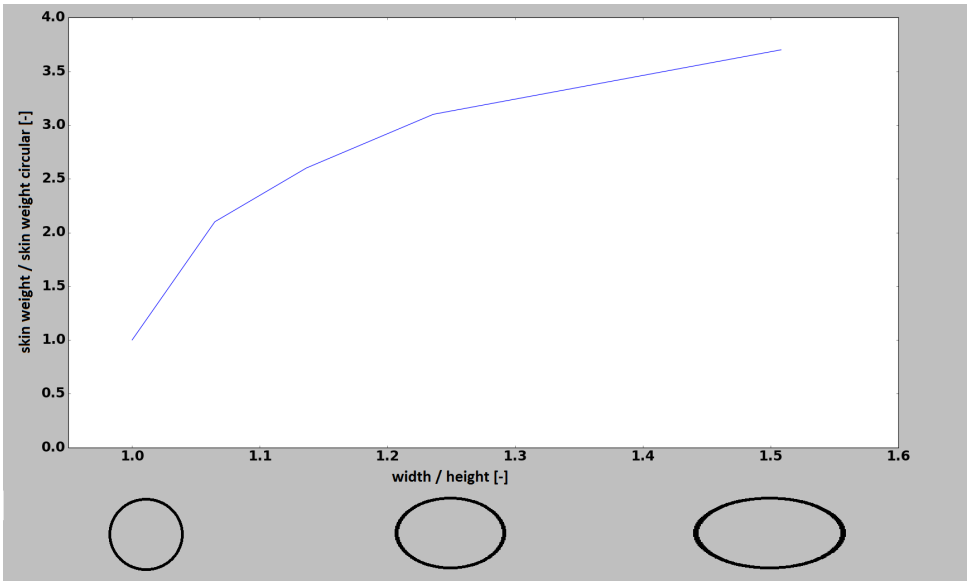

Figure 10.8: Skin weights normalised with respect to skin weight of a circular fuselage

To calculate the the operational empty weight, OEW of the aircraft taking into account the computed skin weights W_{skin} for the elliptical and circular fuselage, the following approach has been taken.
The OEW for the A342-BBB had to be updated for a composite aircraft. Fudge factors were applied for the different aircraft components was applied to account for composite structures (see Table 10.8 [41]), please note than an average has been taken. The new OEW for the A342-BBB is estimated 47800 kg. Then the OEW of the composite elliptical and circular cross-section were estimated. First, the weight of the structural components of the fuselage have been estimated multiplying weight fractions by the OEW of the A342-BBB. The weight fractions of structural fuselage components w.r.t OEW for a composite and aluminium fuselages have been retrieved and can be seen in Table 10.7.

To calculate the OEW of the elliptical cross sections based on the results of the model, the weight of the stringers, longerons and skin based on literature has been subtracted from the OEW and the weight of the skin estimated by the analytical tool has been added. The stringers and longerons weight contribution was subtracted since not needed as the sandwich construction used for the elliptical cross-section will cope for buckling.

To calculate the OEW of the circular cross sections based on the results of the model, only the weight of the skin based on literature has been subtracted from the OEW and the weight of the skin estimated by the analytical tool has been added. Results can be seen in Table 10.9. From this preliminary calculations, it can be seen that the composite elliptical fuselage is only 1.6% heavier in terms of OEW compared to the composite circular fuselage. Note the weight of the fuselage skin of the model outputs the skin kg/m hence the weight of the whole fuselage skin was computed multiplying by the overall length of the fuselage of approximately 44 m. Of the cross-sections analysed the skin weights are retrieved from Table 10.6. The circular cross-section is assumed to have a radius of 1.924 and the elliptical cross-section semi-minor axis 1.409 m and semi-major axis of 2.125 m.

Table 10.7: Weight fractions in terms of OEW

Weight ratios [-]	Composite fuselage
$\frac{W_{skin}}{OEW}$	0.07
$\frac{W_{str,long}}{OEW}$	0.02

Table 10.8: Correction factors

Weight group	Fudge factor (multiplier)
Wing	0.85-0.9
Tails	0.83-0.88
Fuselage, nacelle	0.9-0.95
Landing gears	0.95-1.0

Table 10.9: Computed OEW

Computed OEW	[kg]
OEW A342-BBB composite	47,800
OEW elliptical fuselage	45,560
OEW circular fuselage	44,830

10.5.7. Sensitivity Analysis

A sensitivity analysis has to be performed on the analytical model. During the sensitivity analysis the influence of the inputs on the outputs has to be tested. As can be seen in Section 10.5.4 the output of the model is not sensitive to changes in geometry, it is however sensitive regarding the number of discretisation points chosen. Nevertheless when the number of points is above 501, the error becomes small enough to not affect results. Furthermore, sensitivity analysis has to be performed since very basic load cases have been analysed hence the output of the analytical model might change significantly when looking at real life cases. Furthermore, the approach taken to estimate the weight fractions of structural components using reference data from literature is preliminary, the results might change when using more accurate methods.

10.6. Numerical Model

In this section, the numerical model will be explained. The assumptions will be stated and the model will be described. Afterwards, the verification and validation will be shown.

10.6.1. Assumptions

Here, the assumptions for the numerical tool are listed.

- Only isotropic materials are analysed, which means Hooke's law is applicable.
- The cross-section is assumed to be symmetric about the y-axis. $I_{xy} = 0$.
- The pressure difference is the designing load. Other loads are negligible compared to the pressure difference load.
- The mesh size is fine enough to create an accurate model.

10.6.2. Model Description

The FEM tool Autodesk Fusion 360 was chosen in order to analyse all loads on the fuselage. The tool is a combination of CAD drawing and simulation. Autodesk has purchased the Nastran solver and incorporated that into the Fusion 360 for the sake of software completeness. However, since this convenience seemed almost to good to be true, verification of the software capabilities was initiated.

10.6.3. Verification

In order to verify the tool, three cases were chosen: the hole in plate case, the cantilevered beam case and the pressurised vessel case. They were chosen due to the well known theory and abundance of experimental data to compare the results with.

Hole in Plate case

In the hole in plate case, a tension load was applied to the end of a plate with a hole in the centre. From literature, the maximum stress at the hole will be three times larger than the stress in the rest of the plate, in other

words, the stress concentration factor should be 3.

After running simulations on various settings and dimensions, the results differed 5.6% - 14.3% compared to the theoretical data. The range in these values depends on the change in mesh refinement; a coarser mesh will require smaller solution time, but will have the penalty of less accurate results.

Cantilevered Beam Case

In the cantilevered beam case, a force was applied on a cantilevered beam so it would deflect in the opposite direction. The deflection of the tip of the beam was measured, and compared to the value calculated using Equation 10.15.

$$\Delta = \frac{Pl^3}{3EI} \tag{10.15}$$

- Δ = Deflection of the tip [m]
- F = Applied load [N]
- l = Length of the beam [m]
- E = Young's Modulus [Pa]
- I = Moment of inertia about the longitudinal axis [m^4]

The error in the program's results varied from 0.31% - 3.0% when the deflections were compared.

Pressurised Vessel Case

In the last case, the pressurised vessel, pressure was applied to an open cylinder. The stress in the skin was measured, and compared to the value calculated using Equation 10.16.

$$\sigma_{hoop} = \frac{PR}{t} \tag{10.16}$$

- σ_{hoop} = Hoop stress [Pa]
- P = Applied pressure [Pa]
- r = Radius of the circular cross-section [m]
- t = Thickness of the skin [m]

The error between the values lies in the range of 2.2% - 12.4%.

10.6.4. Set-up

The fuselages that were tested can be seen in Chapter 9 It was found that simulating the fuselage in its full length was impractical for the following reasons. First, the computing time increases greatly with the fuselage length. At a certain point the mesh size becomes too small for the software to even complete the simulation. Second, it was tested that if the mesh is small enough, the stress approaches the same value regardless of the length of the fuselage. In addition, the mesh size can be refined even more for the smaller lengths, which yields more accurate results. Finally, the rounded rectangle could not be successfully simulated by the software for the small thicknesses even with the coarse mesh. With shorter fuselage lengths this appeared to not be an issue any more.

In Figure 10.9 the dimensions for the interior are shown. The bottom line also serves as a floor beam with a thickness of 9.6 mm. The following was done with the dimensions for the cases:

- Rounded rectangle: the inner rectangle has an off-set of 100 mm to the interior. The edges were filleted so that the corners touched the interior design. The outer rectangle has an off-set of 1-10 mm to the inner rectangle.
- Ellipse: the ellipse was chosen so that the interior just fitted inside it. The major axis of the inner ellipse was 2,125 mm, while the minor axis was 1,409 mm. The major and minor axis of the outer ellipse ranged from 2,126-2,135 mm and 1,410-1,419 mm respectively.
- Circle: the circle was chosen so that the interior just fitted inside it. The radius of the inner circle was 1,924 mm, while the radius for the outer circle varied from 1,925-1,934 mm.

The described set-up was then analysed. The stresses and strains were all measured at the top of the fuselage, in the middle of the total length of the fuselage.

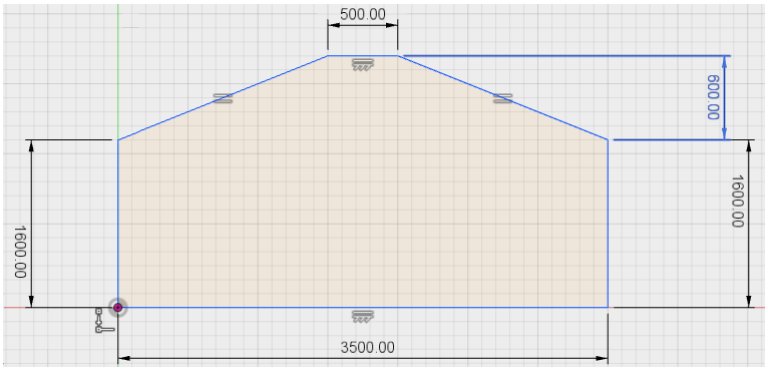

Figure 10.9: The sketch of the interior design, which was used in Fusion 360 to size all cross-sectional cases (all in mm)

10.6.5. Validation

Validation in this case, is checking that the analysis represents the real world case. It is important to stress that only the pressurisation is taken into account at this point. Stresses due to the pressurisation have been validated in subsection 10.6.3. This was done by calculating the pressure with a well established method and by verifying that the pressure simulations in the FEM tool are correct.

However, the team is aware that more stresses than just the one induced by the pressurisation are acting on the fuselage. During manoeuvring the aircraft can experience extreme loads on wings and tail, which would induce even larger stresses in the fuselage. During the landing, the landing gear's reaction force would lead to an another extreme case. However, the main reason why the fuselage is circular is due to the pressurisation. So it is assumed that the fuselage strengthened to cope with the pressure can then be relatively easy refined to cope with the rest of the loads.

To conclude, the discussion above implies that the set-up, and hence results, are validated for the pressure case. Yet, further refinements are required in the subsequent design iterations in order to successfully deal with all present loads throughout the flight envelope.

10.6.6. Results

The results of the simulation are found in Tables 10.10 and 10.11. The stresses and deflections at a midpoint on the fuselage are shown with varying thicknesses. For the simulations, Aluminium 7075 with Young's Modulus of 71,700 MPa was used. Be aware, the tool is designed for linear materials, which means that the stress is linear with regards to the strain. As a result, very large stresses and strains are possible with the program. Because of this, the output values from the program should be handled with care.

Table 10.10: The stresses with varying thicknesses, all measured at the top of the fuselage, in the middle of the total length of the fuselage

Thickness	Stress circle (MPa)	Stress ellipse (MPa)	Stress rectangle (MPa)
1	108.2	183.8	3035
2	55.98	92.29	2471
3	36.02	62.28	1348
4	27.31	46.71	1142
5	22.01	37.61	1288
6	18.09	31.40	907.3
7	15.48	27.25	729.3
8	13.58	24.08	613.8
9	11.75	21.45	475
10	10.85	19.44	361.2

Table 10.11: The strains with varying thicknesses, all measured at the top of the fuselage, in the middle of the total length of the fuselage, in percentage of the vertical height

Thickness	Strain circle (mm)	Strain ellipse (mm)	Strain rectangle (mm)
1	2.732	39.79	23,608
2	1.339	20.15	6,766
3	0.9206	13.31	3,420
4	0.7378	9.711	2,124
5	0.5875	7.809	1,709
6	0.4922	6.452	1,061
7	0.4168	5.593	724.2
8	0.3626	4.896	517.6
9	0.3275	4.340	382.4
10	0.2914	3.860	277.2

The results of the circle and ellipse are also plotted in graphs displayed in Figures 10.10 and 10.12. Unfortunately, the rectangle results cannot be shown in the same graphs, as these values are too large. Instead, these values are plotted in Figures 10.11 and 10.13.

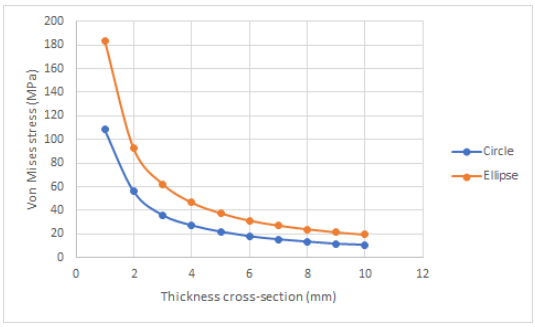

Figure 10.10: Stress against thickness for the circle and ellipse case

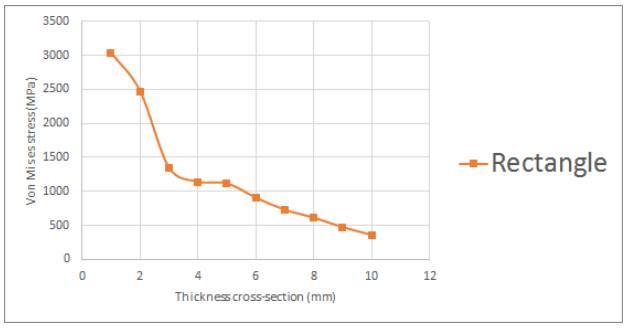

Figure 10.11: Stress against thickness for the rectangle case

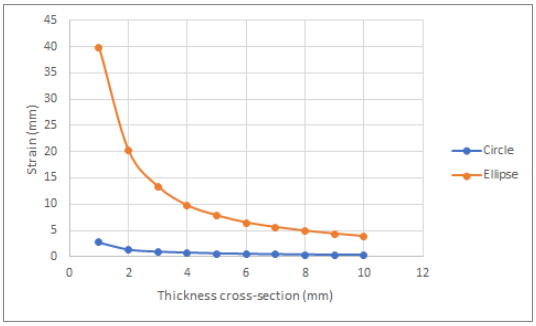

Figure 10.12: Strain against thickness for the circle and ellipse case

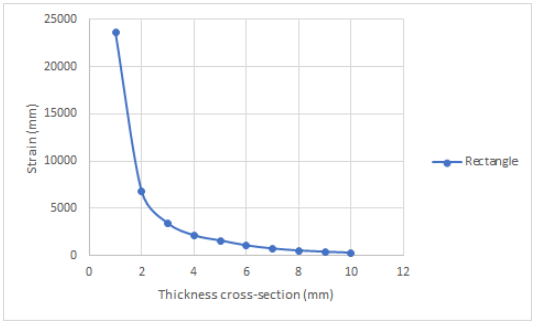

Figure 10.13: Strain against thickness for the rectangle case

Also, the area of the cross-section is plotted against the thickness in Figure 10.14.

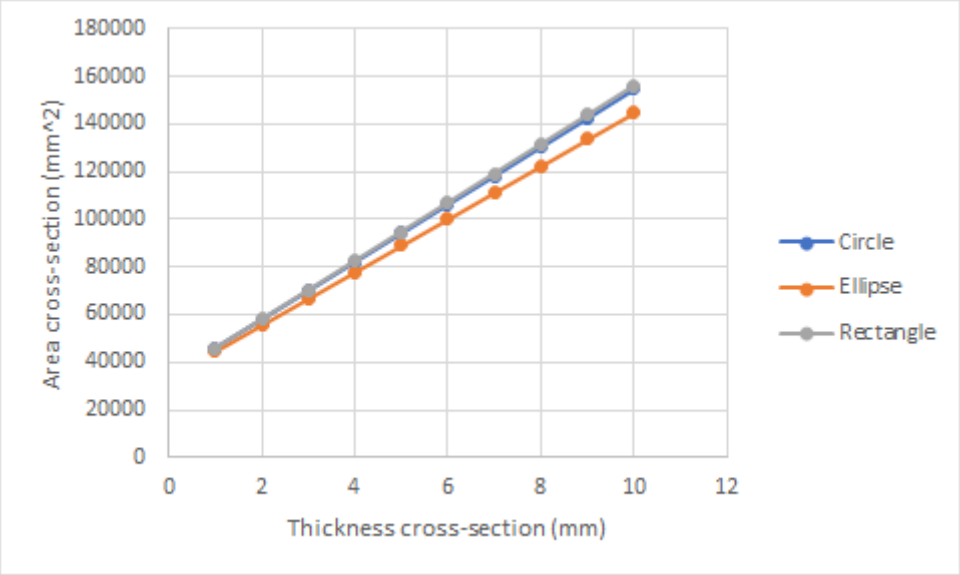

Figure 10.14: Area of the cross-section against the thickness

On top of these results, a case was chosen in which the cross-sectional shape started at a circle. Then, the major axis would be increased, while the minor axis would decrease. In ten equal steps this would result in the elliptical case. Figures 10.15 and 10.16 show the results of these simulations. Eccentricity is defined as the ratio of the minor axis to the major axis.

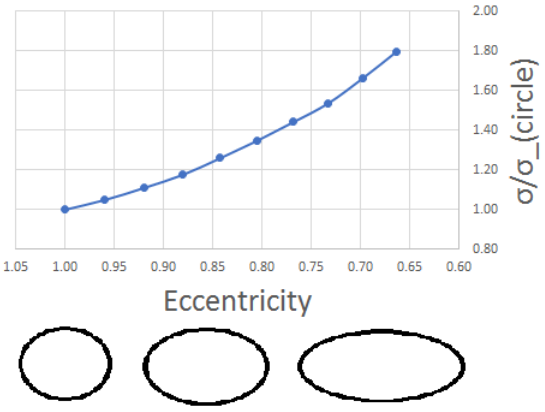

Figure 10.15: Stress ratio against eccentricity for the circle to ellipse case

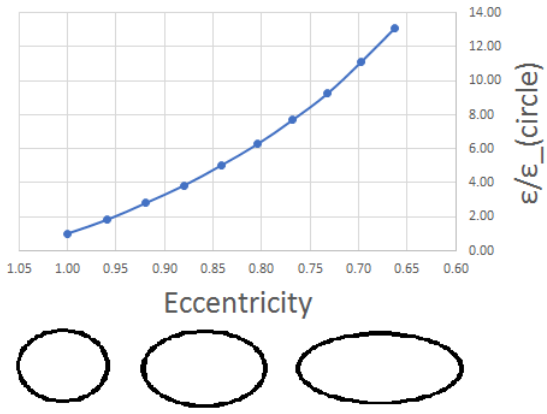

Figure 10.16: Strain ratio against eccentricity for the circle to ellipse case

10.6.7. Sensitivity Analysis

The sensitivity analysis is needed in order to show what varying mesh sizes will do with the results. A circular case is chosen, with the following dimensions:

- Inner radius = 50 mm
- Outer radius = 51 mm
- Length fuselage = 1000 mm

The mesh refinement percentage will be differed from 1-10 %. Then, the stress was measured on top of the fuselage. The results are shown in Figure 10.17. Furthermore, a line is inputted which shows the calculated stress, by Equation 10.16.

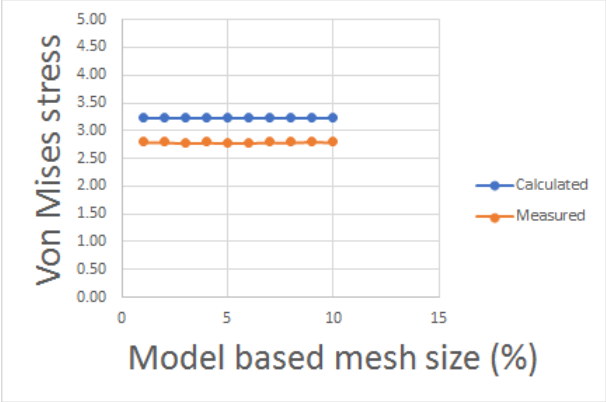

Figure 10.17: Stress against mesh size for the sensitivity case

10.7. Validation against the analytical model

It was not possible to validate the results against the results of the analytical model; the values did not compare. This could be due to the variety of assumptions stated in the numerical model. Furthermore, the numerical model was not thoroughly validated.

10.8. Conclusion

The conclusions from the numerical model are that a circular cross-section is the best option regarding pressure. For the same thickness, its stresses are 55% to 61% of the stresses for the ellipse, and only 2% to 4% of the stresses for the rectangle. At the same time, the area of the cross-section for all the cases only differs by 7% at most. Furthermore, it is shown that the stress decreases as the circular cross-section is changed towards an elliptical cross-section. This indicates that a circular cross-section performs better than an elliptic cross-section.

10.9. Recommendations

The recommendations for the analytical model are as follows:

- The fuselage should be analysed under different load cases.
- A floor should be included when analysing the fuselage cross section.
- The fuselage should be analysed over its full actual length.
- The number and location of the frames should be specified and included in the analysis.
- Shear and buckling checks have to be performed to ensure structural integrity of the skin.
- Design speeds should be estimated and an analysis on structural integrity should be evaluated.
- Lateral gusts should be investigated. A gust envelope for the A342-BBB should be made.
- The effect of stress relief by bionic structures should be further investigated.

The recommendations for the numerical model are as follows:

- More computing time will lead to a finer mesh, hence a more realistic output.
- The fuselage should be analysed under multiple loads.
- The fuselage should be analysed over its full actual length.
- Composites should be analysed.

10.9.1. Stress relief by bionic structures

In Section 10.9 it is recommended to further investigate the effect of stress relief by bionic structures inside of the fuselage. This section provides a short explanation of this recommendation and the possible influence it has on skin weight.

When going from a circular to elliptical fuselage shape, the weight increases. This is because shear loads and moments are introduced in the skin panels for non-circular cross sections under pressure. Adding bionic structures can to take over parts of these loads from the (semi-)monocoque structure.
An example is provided in Figure 10.18. These forces have an influence on both the shear and normal forces in the side panels of the fuselage highlighted with red. Since the shear forces translate into moments and these contribute most to weight increase, this subsection only elaborates on those.

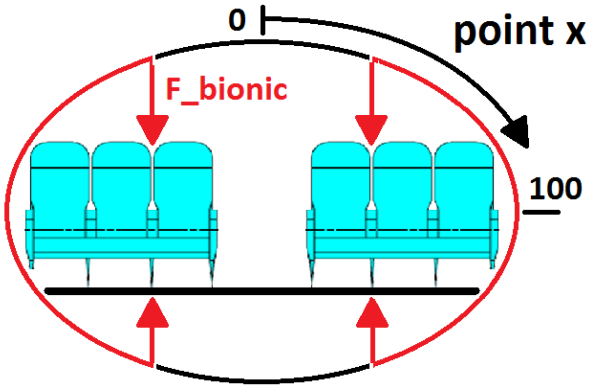

Figure 10.18: Location of bionic forces

Figure 10.19 displays both the shear force with (red) and without (blue) bionic forces. It can been seen that the internal shear force is relieved by the introduction of the bionic forces at location 1.

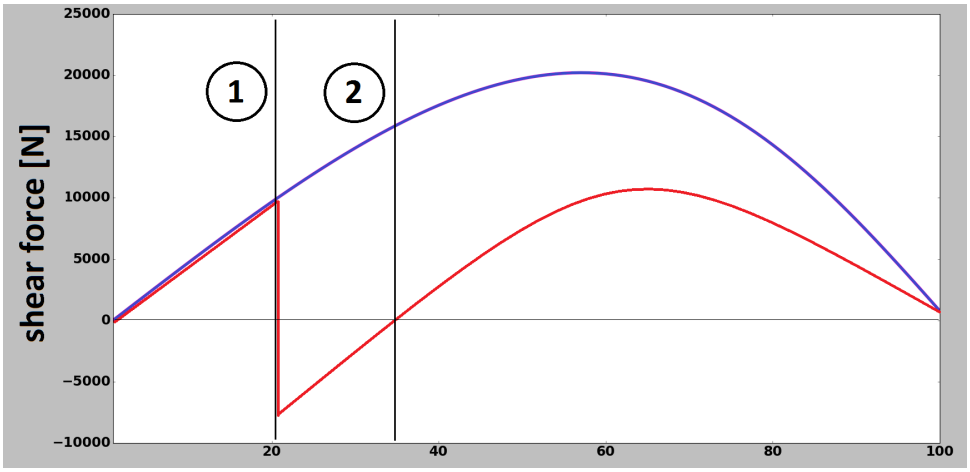

Figure 10.19: Effect of bionics: shear force

Integrating the internal shear force over the circumference provides the internal moment. The reduction of the shear force results in the a lower slope of the moment graph. This also has an influence on the rest of the internal moment. This is shown in Figure 10.20.

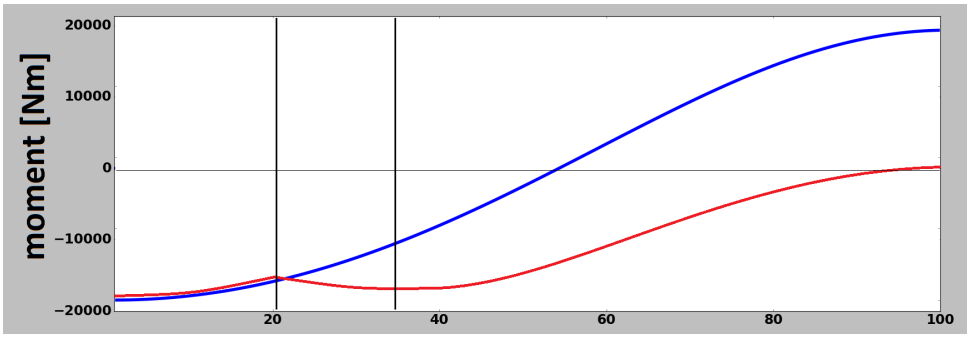

Figure 10.20: Effect of bionics: moment

Since the internal moment directly translates to the internal energy, which itself has an effect on the boundary moment at location 0 shown in Figure 10.18. This results in a translation of the moment graph in Figure 10.20.

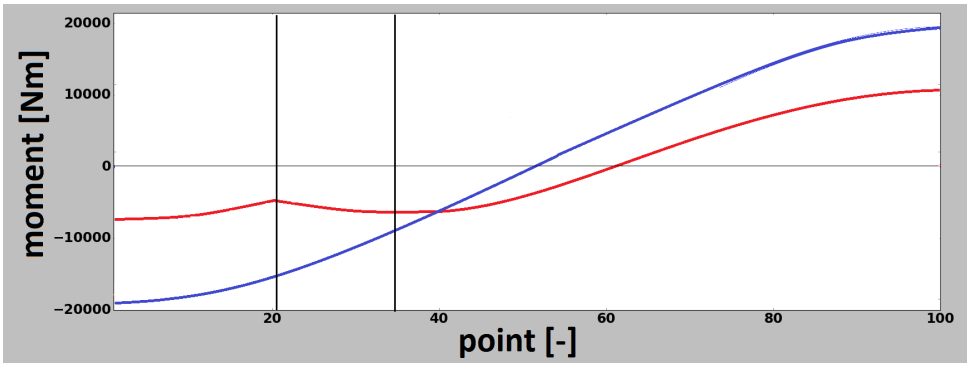

Figure 10.21: Effect of bionics: moment translation

From Figure 10.21 it can be derived that the absolute area under the moment graph is less for the fuselage with bionic structures. While introducing the extra weight of the bionic structure, this will lead to a lower skin weight. It is therefor recommended that trade off on the introduction of bionics is made in the future.

11. Materials

In this chapter the materials choice for the fuselage and the aircraft is discussed. Section 11.1 deals with the most commonly used materials in reference aircraft. Thereafter some general features of metals and composites are discussed, the material properties are also given in Sections 11.2 and 11.3. The sandwich construction is a very efficient way for stiffening a panel, Section 11.4 elaborates on this. In Section 11.5 a cost estimation on different materials is performed. Subsequently, the concept materials for the fuselage are described in Section 11.6. The application of the aircraft materials on the fuselage is given in Section 11.7. At last, a cost estimation of the materials is presented as well as the conclusions and recommendations.

11.1. Materials Used in Fuselage of Reference Aircraft

The Airbus A320neo has a metal semi-monocoque fuselage. A semi-monocoque structure is a skin which is reinforced by stringers, stiffeners, spars and ribs etc. Advanced aluminium alloys are used for this structure. There are some CFRP elements: empennage, landing flaps, sharklets and landing gear doors[1]. The Boeing 737 MAX has a mainly semi-monocoque fuselage structure as well. The materials used for the fuselage are mainly aluminium alloys, except for the radome and the tailcone, which are made from fiberglass. For the fuselage skin aluminium alloy 2024 was used. The frames, stringers, floor beams were made of aluminium alloy 7075 [2]. The Comac C919 has a fuselage structure which is composed of the third generation aluminium-lithium alloy, with a high damage tolerance, and a titanium alloy [3].

The Bombardier CS300 and the Boeing 757 were also analysed. It followed that advanced aluminium alloys are the leading fuselage material. The two most widely used aluminium alloys are Al2024-T4 and Al7075-T6. Aluminium-lithium also seems to be an good alternative. Some smaller components consist of composites. The reason for using composites in these cases is mainly corrosion resistance and weight reduction.

11.2. Metals

Metals are still widely used in aerospace. because of their high strength and stiffness. Aluminium alloys, titanium alloys and steel are numerous options. Although current trends tend more and more towards composites, because of a lower density and better fatigue and corrosion behaviour. Since steel and titanium will be used for some other aircraft components, they are discussed shortly below. Therefore steel and titanium will be discussed here as well. Various mechanical properties of metals are shown in Table 11.1.

Aluminium Alloys 2024-T4 & 7075-T6
Aluminium is relatively light and has good strength at low temperatures. It is easily manufacturable and has a low maintenance. Drawbacks are a bad corrosion and fatigue behaviour compared to composites [4] [42]. Aluminium 2024-T4 is an aluminium alloy with a relatively good fatigue resistance, in particular in thicker plates. This alloy is used in structural elements of aircraft. A drawback of this alloy is that it is sensitive to atmospheric corrosion [43]. Aluminium 7075-T6 has better specific properties compared to aluminium 2024-T4. It is a high strength aluminium alloy. It has a better corrosion resistance than alloy 2024-T4 and a moderate toughness. [44] [45].

Aluminium-Lithium 2090-T8
Aluminium-lithium 2090-T8 has compared to aluminium 7075-T6 a lower density, a higher specific elastic modulus and a better fatigue and corrosion resistance. However, it has a low ductility and low fracture toughness. For micro-structural short cracks there exists a fast crack growth. This means that at locations with high stress concentrations crack growth will happen relatively early. Therefore this will probably not be an optimal material to consider for the fuselage, as there will be high stress concentrations. Furthermore, the costs are

[1] https://aviationvoice.com/airbus-a320-neo-vs-boeing-737-max-201602121522/ [accessed on January 13th 2017]
[2] https://worldairlinenews.com/tag/boeing-737-max/ [accessed on January 13th 2017]
[3] http://english.comac.cc/news/latest/201409/03/t20140903_1895800.shtml [accessed on January 13th 2017]
[4] http://www.aluminiumdesign.net/why-aluminium/properties-of-aluminium/ [accessed on January 13th 2017]

three times higher compared to general aluminium alloys and the manufacturing costs also increase significantly. [5] [46].

Steel (FeD6AC)
Nowadays, steel is a less common material found in aircraft structures because of the relatively high weight. Alternatives were found in composites and other metals, due to the higher specific strength and stiffness. Still, when low-alloyed with carbon, it has a relatively high strength and stiffness. The downside of this is that it has limited toughness, which makes it susceptible to fatigue cracks.

Titanium
Titanium have high specific strengths and high specific stiffness under high temperatures, outperforming aluminium alloys in this regard. When strong and stiff parts are needed, titanium is a good choice. On top of that, titanium has a high compatibility with CFRP, as it will not corrode [6] [7]. The downsides of titanium are that it is a relatively expensive material and it is also hard to manufacture due to the high temperatures it has to be worked at.

Table 11.1: Mechanical properties of metals [45]

Material	ρ (kg/m^3)	σ_y(MPa)	σ_u(MPa)	E (GPa)	σ_u/ρ	E/ρ	$\sqrt[3]{(E)}/\rho$
Aluminium 2024-T4	2,770	325	470	72	0.17	26	0.015
Aluminium 7075-T6	2,700	510	580	72	0.21	27	0.015
Aluminium-Lithium 2090T8	2,590	517	530	76	0.20	29	0.016
Steel (Fe D6AC)	7,870	1,690	1,970	206	0.25	26	0.008
Titanium 6Al-4V	4,500	920	950	118	0.21	26	0.011

- ρ = density of the material [kg/m^3]
- σ_y = yield tensile strength [MPa]
- σ_u = ultimate tensile strength [MPa]
- E = elastic modulus [GPa]

11.3. Composites

Composites are materials that consist out of two or more materials, which are combined together. Usually they consist of fibres surrounded by some resin (polymer). A distinction can be made here between fibre metal laminates (FML) and fibre reinforced plastics (FRP).

11.3.1. Fibre Metal Laminates

FML are composites which consist of alternating layers of metal, fibres and resin. A good example of FML is GLAss REinforced aluminium (GLARE), developed at the TU Delft. It has an excellent corrosion and fatigue resistance [8]. Compared to for instance CFRP, GLARE has better compression properties and it can ensure a more isotropic behaviour.

11.3.2. Fibre Reinforced Plastics

For Fibre Reinforced Plastics (FRP) distinction can be made between three different kind of fibres, carbon fibres, aramid fibres and glass fibres. Therefore these are discussed below.

Carbon Fibre Reinforced Plastic
Carbon Fibre Reinforced Plastic is currently the most used composite in aircraft structures. This is mainly due to its high specific stiffness and strength, but also because of its ability of non-corroding. Furthermore, it has

[5] http://www.totalmateria.com/Article58.htm [accessed on January 11th 2017]
[6] http://www.kobelco.co.jp/english/ktr/pdf/ktr_33/044-049.pdf [accessed on December 12th 2016]
[7] https://www.faa.gov/regulations_policies/handbooks_manuals/aircraft/amt_handbook/media/faa-8083-30_ch06.pdf [accessed on December 12th 2016]
[8] http://link.springer.com/article/10.1007/s11837-005-0067-4 [accessed on December 8th 2016]

excellent fatigue resistance and it reduces the amount of parts needed. Of course there are also limitations; it is susceptible to operational impact damage, not useful in high-temperature environments (depending on resin used) and has a 7 times higher raw material cost when compared to aluminium.

Aramid Fibre Reinforced Plastic
Aramid Fibre Reinforced Plastic is a lightweight, strong and tough composite. Kevlar 49 is the most common aramid fibre in aircraft industry, it has a high stiffness. The biggest advantage of aramid is the high resistance against impact. The main disadvantage is the low resistance against compression. Next to that, aramid can absorb until 8 times of its weight in moisture. Manufacturing processes with aramid fibres are not that easy. Drilling and cutting is difficult due to the fact that the fibres fuzz very easily [9].

Glass Fibre Reinforced Plastic
Glass Fibre Reinforced Plastics (GFRP) have lower costs than other composites, have chemical and galvanic corrosion resistance and do not conduct electricity. It does however have a lower stiffness and specific strength when compared to other composites, which does not make it suitable for primary aircraft structures [47]. However, secondary structures, which are not expected to be under high loads, are made of this material. For example, GFRP is very well suited for interior structures.

Table 11.2: Mechanical properties of composites [48]

Material	ρ (kg/m3)	σ_y(MPa)	σ_u(MPa)	E (GPa)	σ_u/ρ	E/ρ	$\sqrt[3]{(E)}/\rho$
CFRP H-IM6 (UD, longitudinal)	1,600	-	2,860	177	1.8	110	0.035
CFRP H-IM6 (UD, transversale)	1,600	-	49	10.8	0.026	6.8	0.014
AFRP Kevlar 49 (UD, longitudinal)	1,380	-	1,280	87	0.93	63	0.032
AFRP Kevlar 49 (UD, transversale)	1,380	-	30	5.5	0.022	4.0	0.013
GFRP S-glass (UD, longitudinal)	2,000	-	1,280	43	0.64	21.5	0.018
GFRP S-glass (UD, transversale)	2,000	-	49	8.9	0.025	4.5	0.010
GLARE 3 3/2 (0^o /90^o cross-ply, longitudinal)	2,520	305	717	58	0.28	23	0.015
GLARE 3 3/2 (0^o /90^o cross-ply, transversale)	2,520	305	716	58	0.28	23	0.015

11.4. Sandwich Constructions

Sandwich constructions make it possible to deal with high shear and bending loads. The facing and core materials should be able to withstand tensile, compressive and shear stresses. The facings carry the bending and tensile stresses, while the core carries the shear and compressive stresses. Two options are suitable as a core material, a foam core or a honeycomb core. For the facings mainly CFRP can be used or to some extent AFRP, see section 11.4.3.

11.4.1. Foam Core

Foam core is usually applied to interiors, cockpit doors, insulating panels, radomes etc. It is not that common to use foam core in structural and fuselage elements of commercial aircraft. Foam is simply heavier than

[9] https://www.faa.gov/regulations_policies/handbooks_manuals/aircraft/amt_airframe_handbook/media/ama_ch07.pdf [accessed on December 12th 2016]

Table 11.3: Mechanical properties of foam core

Material	ρ (kg/m^3)	σ_{tu} (MPa)	σ_{cu} (MPa)	E (MPa)	E/ρ	τ_u (MPa)	G (MPa)
AIREX R82-60	60	1.7	0.70	45	0.75	0.8	18
AIREX R82-80	80	2.0	1.1	54	0.68	1.1	23
AIREX R82-100	100	2.2	1.4	64	0.64	1.4	30
AIREX C71-60	60	1.5	0.95	42	0.70	0.93	21.5
AIREX C71-80	80	2.2	1.5	60	0.75	1.35	30

honeycomb and has a lower strength. Foam materials have in general a very good strength to weight ratio and a very low moisture absorption. They have typically a high fatigue and impact resistance. There are generally two good possibilities described here, which are AIREX R82 and AIREX C71 [10]. Their properties are summarised in Table 11.3.

AIREX R82 is a closed cell thermoplastic polymer foam. It demands high fire resistance and is well suited for high temperature applications. Next to that it can be used for radomes due to its radar transparency. R82 foam is available in three different densities with its specific properties. The thickness ranges from 3 mm to 60 mm. [49]

AIREX C71 is a closed cell cross-linked polymer foam. It has a high stiffness and strength to weight ratio and a high toughness. C71 foam is available in two different densities. The thickness ranges from 5 mm to 70 mm for a density of 60 kg/m^3 and from 3 mm to 70 mm for a density of 80 kg/m^3. Compared to R82 this one has better specific compression and shear properties. [50].

11.4.2. Honeycomb Core

In order to stiffen a structural panel, a honeycomb core can be used as a material solution. Honeycomb is available in a wide range of different materials and configurations for different specific applications. Honeycomb is very lightweight, it has a high strength and in general good compression and shear properties. Different honeycomb cell configurations exist, as can be seen in Figures 11.1, 11.2, 11.3 below. The hexagonal configuration is the most basic one and commonly used. The OX-configuration is expanded in the W-direction and has therefore better shear properties in that direction. The flex-core has an extreme formability which makes it to a very good application for highly curved panels. This might be very useful for the fuselage structure. A distinction is made below between aluminium honeycomb, aramid fibre reinforced honeycomb and fibreglass reinforced honeycomb. In Table 11.4 all the mechanical properties can be found.

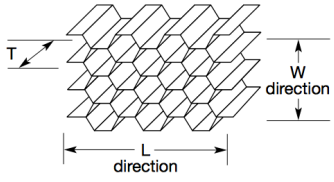

Figure 11.1: Hexagonal core configuration

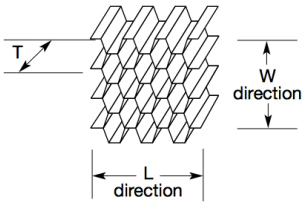

Figure 11.2: OX-core configuration

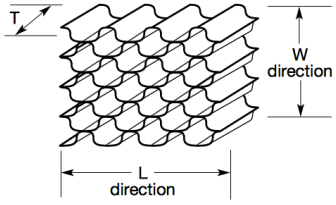

Figure 11.3: Flex-core configuration

Aluminium Honeycomb

Aluminium 5056 honeycomb with CR-PAA (phosphoric acid anodised) coating has a high strength. The CR-PAA coating provides protection against environment affection. It gives also resistance to crack propagation.

[10] https://www.faa.gov/regulations_policies/handbooks_manuals/aircraft/amt_airframe_handbook/media/ama_ch07.pdf [accessed on December 12th 2016]

Aluminium honeycomb has in general the best strength to weight properties and has relatively low cost. Aluminium 5056 honeycomb is available in a wide range of densities from 32 to 128 kg/m^3. Next to the conventional hexagonal configuration it is also available in flex-core in order to make it useful in curved elements of the aircraft. Therefore it can for instance be used on curved skin panels, leading and trailing edge elements. The minimum thickness that is available is 6 mm. [51]

Aramid Fibre Reinforced Honeycomb
Suitable options for aramid fibre reinforced honeycomb core are HexWeb HRH-10 and HexWeb HRH-49. HexWeb HRH-10 is fabricated from Nomex aramid fibres. It has a high strength and toughness and though a low stiffness. Its density range is from 24 kg/m^3 till 144 kg/m^3, with a minimal thickness of 3 mm. The maximum service temperature is 175 °C and besides that it is fire resistant. The coefficient of thermal expansion (CTE) of HRH-10 is in the range of 33-36 *10$^-$6 m/m ° C. HexWeb HRH-10 is available in the hexagonal core, OX-core and flex-core. It can therefore be applied to both structural and non-structural parts in the aircraft. Most of the interior parts are made out of HexWeb HRH-10 because of its fire resistance and the relatively low density. Examples of exterior parts that are often manufactured with HexWeb HRH-10 are flaps and fairings. This is mainly because of the low density, high strength and its damage resistance.[52]

HRH-49 is made of Kevlar aramid fibres. It has a very good thermal stability and a low coefficient of thermal expansion, the (CTE) is in the range of 4 - 8 $\cdot 10^{-}6 m/m°C$. HRH-49 is a lightweight honeycomb, its density is 34 kg/m^3 with a thickness of 3 mm. It is only available in the hexagonal configuration.

Fibreglass Reinforced Honeycomb
HexWeb HRP is a good option for structural parts and fairings. It has a high strength and a moderate stiffness and is available in hexagonal core, OX-core and flex-core. The density varies from 35 to 192 kg/m^3. Minimal thickness to work with in this case is 3 mm. Furthermore HRP has tailorable shear properties by layup, good insulating properties and a good formability. [53]

Table 11.4: Mechanical properties of a honeycomb core

Material	ρ (kg/m^3)	σ_{cu} (MPa)	K (MPa)	τ_L (MPa)	G_L(MPa)	τ_W (MPa)	G_W (MPa)
Al 5056	32 - 128	0.76 - 13	207 - 3,000	0.62 - 65	138 - 986	0.41 - 3.9	72 - 325
HRH-10	24 - 144	0.62 - 14.48	41 - 621	0.48 - 3.55	21 -121	0.24 - 2.07	9 - 76
HRH-49	34	0.90	172	0.59	19	0.28	9.0
HRP	35 - 192	1.2 - 17	90 - 1,793	0.62 - 5.62	41 - 303	0.31 - 3.62	21 - 193

- σ_{cu} = ultimate compression strength [MPa]
- K = compression modulus [MPa]
- τ_L = Shear stress, L-direction [MPa]
- τ_W = Shear stress, W-direction [MPa]
- G_L = Shear modulus, L-direction [MPa]
- G_W = Shear modulus, W-direction [MPa]

11.4.3. Sandwich Facing

For the facing materials of the sandwich construction, Table 11.2 can be referred to. In general, the facing material will be either CFRP or AFRP. The choice between CFRP and AFRP is dependent on the location in the aircraft fuselage and the properties of both materials. Since AFRP has better impact properties, this can be used on locations where the risk of impact is high. This means that AFRP will be chosen as a facing material for the nose cone and the radome. For the fuselage itself CFRP will be chosen. CFRP has a better strength to weight ratio and has yet a higher specific E-modulus. This is beneficial because the CFRP facings will carry mainly tensile stresses. Next to that, it has an excellent fatigue resistance which makes it suitable for a pressurised fuselage.

11.5. Cost Estimation

In Table 11.6 the material costs can be found. The cost is divided into two main components: the raw material and the manufacturing (energy, labour and equipment) cost. The last one has been calculated for the materials by estimating that this cost will be 22% higher than the raw material cost. This estimation is based on the data in Table 11.5, which shows the manufacturing cost, in percentages, compared to raw material cost.

Table 11.5: Cost ratio of manufacturing costs over raw material cost [11]

Number of aircraft	200	1,000	7,500	50,000
Difference	+ 60%	+ 30%	+ 22%	- 20%

Table 11.6: Cost of materials

Material	Total cost(USD/kg)	Raw material cost (USD/kg)	Manufacturing cost(USD/kg)
Aluminium 7075-T6	26	12	14
Steel (Fe D6AC)	2	1	1
Titanium 6Al-4V	99	45	54
CFRP H-IM6	109	49	60
AFRP	69	31	38
GFRP S-glass	29	13	16
GLARE	17	8	9
AIREX C71	60	27	33
AIREX R82	300	135	165
HexWeb Al5056	225	101	124
HexWeb HRH-10	450	203	247
HexWeb HRH-49	450	203	247
HexWeb HRP	225	101	124

11.6. Trade-off: Concept Materials for the Fuselage

Because material selection is really dependent on application and location, it has been performed differently with the structure kept in mind. It is possible that different materials for different locations and different elements in the aircraft were chosen.

In Table 11.7 a comparison of different structural solutions to the structures and materials problem is shown. A clear conclusion that can be drawn from the results presented in this table is that a honeycomb sandwich construction is the best solution. The relative strength and stiffness have the highest scores compared to the other options and it has only 3% of the relative weight. Although structural extrusion is not a real possibility, it is included in this table for comparison. Although the mechanical characteristics of foam are not as good as honeycomb, foam is still considered due to the lower costs.

Table 11.7: Structural comparison of structures with equivalent weight[54]

	Relative strength	Relative stiffness	Relative weight	Relative costs
Honeycomb sandwich	100%	100%	++	-
Foam sandwich	26%	68%	+	++
Structural extrusion	62%	99%	-	-
Sheet and stringer	64%	86%	–	++

The concept materials, which follow from the research and trade-off before, are described by concepts 1 to 4. The core materials for the concepts are not specified here yet, because they are dependent on different loca-

[11] https://www.infosys.com/engineering-services/white-papers/Documents/carbon-composites-cost-effective.pdf

tions in the aircraft. Therefore the core materials will be specified later on for their specific applications.
As described in subsection 11.4.3 the facing materials will be either CFRP or AFRP. Therefore the concept materials that are still left for the fuselage are described below in Table 11.8.

Table 11.8: Composition of fuselage concept materials

Concept	Facing material	Core material
1	CFRP H-IM6	Honeycomb
2	CFRP H-IM6	Foam
3	AFRP	Honeycomb
4	AFRP	Foam

The honeycomb and foam core materials can be further subdivided into different materials. For the honeycomb core this will be: Al5056, Aramid HRH-10, Aramid HRH-49 and Fibreglass HRP. For the foam core this will be: AIREX R82 and AIREX C71. Further specification of the particular materials applied on different parts of the aircraft will be done in Section 11.7.

11.7. Application of Aircraft Materials

The materials selection for the fuselage is described in Section 11.7.1. The remainder materials, described in this chapter, can be used for the non-fuselage aircraft components. These material decisions will mainly be taken from reference aircraft, as can be read in Section 11.7.2.

From Figure 11.4 a general analysis of all kinds of different stresses can be performed. With this knowledge a final material selection can be done on the aircraft. Materials selection is dependent on whether a section is mainly in tension, compression, bending, torsion or shear. These main load conditions of different components determine the property requirements on which the design is based.

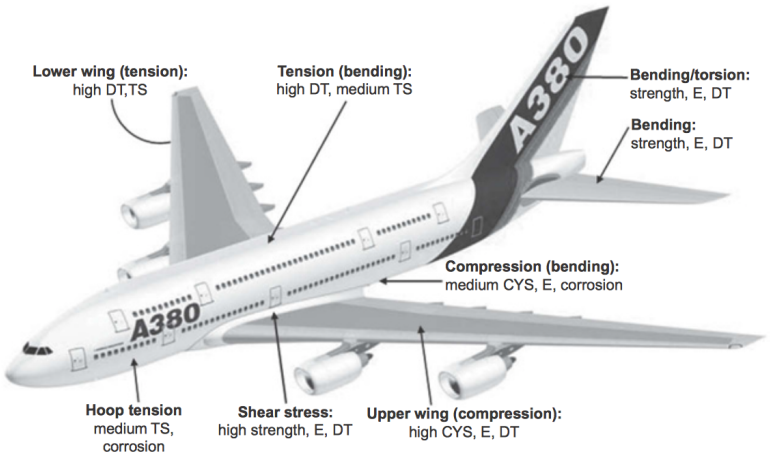

Figure 11.4: Typical load conditions and property requirements [55]

A few abbreviations are used in Figure 11.4, these are described in Table 11.9 below.

Table 11.9: Description of abbreviations used in Figure 11.4

Abbreviation	Description
DT	Damage tolerance
TS	Tensile strength
E	Elastic modulus
CYS	Compressive yield strength

11.7.1. Fuselage Materials

From Section 11.6 it follows that a sandwich construction is used for the fuselage. The structures department has developed a tool which provides the thickness of the core and facings as an output. This tool can simulate different load cases in order to figure out all the stresses that will be carried by the structure. Since composites are used, superposition of the load cases can be applied in order to find the facing lay-up that is necessary to carry all the stresses.

Fuselage: Sandwich Lay-Up
The materials that will be used for the sandwich are HexWeb HRH-49 aramid honeycomb core and CFRP H-IM6 for the laminate facings. The (C_{TE}) of CFRP H-IM6 is in the range of 0 to 3 $10^{-6} m/m°C$. The (C_{TE}) of HRH-49 is in the range of 4 to 8 10^{-6} m/m ° C [12]. This is one of the reasons that it is decided to use HRH-49 as a core material. Next to that, it is the most lightweight solution and has the best relative strength and stiffness compared to other materials. For the laminate facing, HexPly M92 epoxy will be used. This is the only Hexcel prepreg material with an aerospace grade. It will be built up from CFRP H-IM6 layers, with different orientations of the fibers.

In order to cope with all the stresses that will be on the aircraft fuselage, a certain sandwich construction and lay-up is needed. The thickness of the facings and the core will vary with location in the cross-section, in order to optimize the structure and save weight and costs. The lay-up is already discussed in Subsection 10.5.6.

Interior
For the interior, GFRP is used as facing material. This is preferred over AFRP and CFRP, since GFRP is less expensive in the first place. Next to that, interior panels do not have to withstand relatively high impacts. Interior doors, galleys, lavatories etc. sandwich constructions can be used in order to save weight and costs. A sandwich construction has the advantage that it will increase the strength and stiffness of a component and save weight, when compared to a full GFRP element for instance. Foam cores are usually applied to interiors, since they are well suited for non-structural elements. Therefore a sandwich core material AIREX C71 is used. It has less strength and stiffness compared to honeycomb, but it has way lower cost. An additional advantage of AIREX C71 is that it is temperature resistant. It will remain its structural properties at elevated temperatures. Though it will have an extra safety margin against fire because it is self-distinguishing.

The cabin floor is composed of CFRP H-IM6 facing material and HexWeb HRH-49 core material. Here HRH-49 honeycomb is used, since this material is better able to deal with stresses. Therefore, the cabin floor can be used as a primary structural element. Next to that, it will save more weight over using foam core material in this case.

Nose cone - radome
The nose cone, in particular the radome, of the aircraft has to have radar transparency and withstand impact loads at the same time. Therefore AFRP should be used as facing material, since this has excellent impact properties. As a core material AIREX R82 foam has to be used, since this is a well-suited material for radar transparency.

APU exhaust
For the APU exhaust part of the tail cone titanium is used, since this part can become relatively hot due to the

[12] https://upcommons.upc.edu/bitstream/handle/2099.1/20260/memoria.pdf [accessed on December 12th 2016]

APU exhaust. Titanium is able to withstand these high temperatures due to its excellent temperature resistance. Next to that, it is well-suited to combine with CFRP because it is also resistant against corrosion caused by CFRP, which makes it a good addition to a composite aircraft.

11.7.2. Non-Fuselage Materials

The materials that are applied on the so-called non-fuselage components of the aircraft are specified in Table 11.10. The decision on these materials is partly based on reference aircraft and partly based on other materials used in the aircraft. Except for the landing gear, this is retrieved from other research. Namely, Fokker and NLR have already been doing quite a lot of research and development on composite (CFRP) landing gears [56], [57]. The fact that the aircraft has to be in operative in the next 50 years is kept in mind here. The materials specification is not too detailed, since that is out the scope of this Design Synthesis Exercise. A top level specification of the materials is given here, in order to make sure that other components are also compatible with the fuselage.

Table 11.10: Description of non-fuselage materials

Aircraft component	**Materials used**
Wings	CFRP
Empennage	CFRP, GFRP
Landing gear	CFRP [], []
Engines	CFRP, Titanium (Pylon)

11.8. Conclusions

Today's single aisle 200 passenger aircraft are dominated by an aluminium fuselage. Most of it are composed of advanced aluminium alloys, such as aluminium-lithium. The most commonly used metals are aluminium alloys, aluminium-lithium is becoming more and more popular. Next to that, steel and titanium are used in aircraft components. Steel is becoming less popular due to its high weight and lower specific properties.

Composites are becoming more and more popular due to its high specific properties and low density. Mainly CFRP will be used for the fuselage, in addition AFRP will be used for impact resistant components. GFRP is a very suitable materials for interior, non load bearing, structures. Sandwich constructions improve the relative strength and stiffness, hence are a good solution to aircraft structural elements. As core materials mainly aramid honeycomb and foam will be used. Foam is heavier, but has lower cost.

The fuselage sandwich exist of CFRP H-IM6 facing material used with prepreg. As a core material aramid HRH-49 honeycomb is used here, since the (C_{TE}) values are more or less the same.

11.9. Recommendations

The materials that are chosen to be used on the non-fuselage components are relatively general now. They have to be specified in more detail and also the lay-up has to be explained in detail. For this more research has to be performed on reference aircraft. Next to that, a structural analysis has to be performed for all the aircraft components and sub-components. This should be done in order to optimise the material composition with its material thickness. For the fuselage material lay-up optimisation a FEM tool should be used that can simulate different load cases for the entire fuselage including interior. In this way a more accurate sandwich lay-up can be defined and optimised.

12. Aerodynamics

In this chapter the fuselage effect on the aerodynamic properties will be described. First, the initial numerical model is described. This model is used to determine the total drag and lift of the aircraft. As the available software version did not allow for enough elements to compute accurate drag values, another approach had to be used. The second approach involved simulating pressure over the model to analytically calculate the drag along the fuselage.

12.1. Problem Analysis

The goal of the aerodynamics department is to optimise the fuselage shape for $(\frac{L}{D})_{max,\,cruise}$. These can be compared and translated into direct operating costs. In order to find the influence of the fuselage on drag and lift, nose and tail are kept the same. The connection to the fuselage is tangent as sharp edges can have a big influence on the aerodynamic properties.

To derive these properties, a numerical and analytical model can be used. In the analytical model, it would be possible to compute the drag caused by the wetted area. However, there are no sources or formulae able to describe the effects of sharp angles in the direction parallel to the flow accurately. It would result in less freedom in making small changes to the fuselage dimensions and find the effects. Therefore, a numerical model is chosen which is based on Computational Fluid Dynamics (CFD) simulation software. The program named ANSYS was already installed on the available desktops, which was also found to be most user friendly.

The cruise flight is the most fuel consuming flight phase, therefore only this phase has been modelled. The three geometry concepts which are described in Chapter 9 are used in the simulations for the numerical model. The following general assumptions have been made for the aircraft model:

- After running the simulations without the wings and tail wings, those systems were added in order to compute lift over drag ratio that can be validated with real aircraft.
- The angle of attack of the aircraft was set to 3° simulating cruise conditions, which is the most fuel intensive flight.
- The velocity was set to correspond to 0.7 Mach to make use of the Karman Tsien rule. This implies that the lift coefficient of cruise needs to be higher and the lift over drag will increase, as can can be seen in Figure 12.1
- Steady symmetric flight conditions are considered, e.g. no side wind.

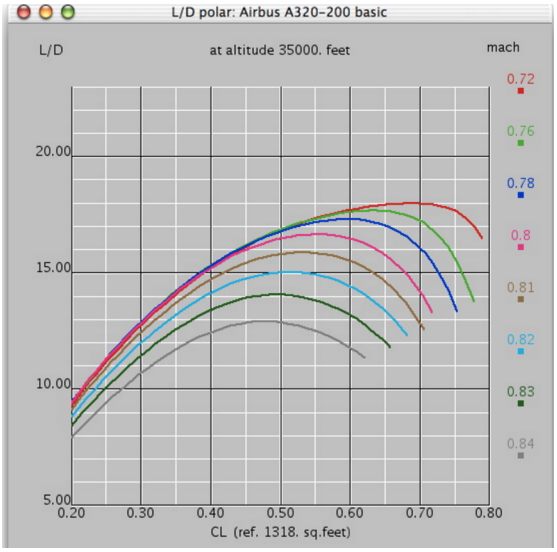

Figure 12.1: Lift over Drag polar for the A320ceo [58]

12.2. Initial Numerical Model

This section describes the pre-processing and post-processing actions of the initial CFD model. Pre-processing consists of the generation of a 3D CAD model, determination of the size of the flow domain and the model choice. The one-equation Spalart-Allmaras model is reviewed and compared to the two-equation Shear Stress Transport (SST) model. Hereafter, post-processing is performed which involves data handling of the results and a description of the verification and validation procedures. During these procedures, the model did not produce accurate and reliable results. Though it gave valuable insights about CFD software and computational modelling, which is the reason to present it in this report.

12.2.1. CAD Model Geometry

The 3D geometry used in the CFD software is made in CATIA. The nose has a length of 4.7 m, the fuselage has a length of 31.42 m, and the tail has a length of 7.841 m. An automatic generated fill has been used, which follows guides between drawings. Four drawings form this boundary and are based on a quadratic formula in both vertical and horizontal direction. The most forward drawing is a circle which makes the nose end in a sphere. The nose is connected to the fuselage without curved edges. The same approach was used for the tail. The tip of the tail has the same height as the fuselage and it ends in a cone.

The client advised to focus on the fuselage and use wing design from reference aircraft. The wing dimensions are based on the Airbus A320neo, which is the newest aircraft on the market with an approximately equal amount of passengers. The following dimensions were set for the model:

- Wing profile is NACA 23015
- Wing span is 33.9 m; root chord length is 5.8 m; wingtip chord length is 1.4 m; dihedral angle is 5 ° ; chord to chord sweep is 25 °
- Winglets chord length is 0.66; winglets height is 2.3 m
- Horizontal tail wing is 12.46 m; root chord length is is 3.9 m; wingtip chord length is 1.0 m; chord to chord sweep is 33.9 °
- Vertical tail wing height is 5.5 m; root chord length is 3.7 m; wingtip chord length is 1.13 m; chord to chord sweep is 41.8 °

12.2.2. Size and Grid of the Flow Domain

In order to use the continuous set of partial differential equations, PDEs discretisation of the flow domain must be performed. The size of the flow domain strongly influences the accuracy of the model. In this study, only steady symmetric flight conditions are considered. Therefore, only half of the model is needed for computations. This means the mesh size is also halved which increases the amount of elements available in this section. Figure 12.2 displays the aircraft and the flow domain. As can be seen in this figure, one side of the rectangular box is a symmetry plane of the aircraft. This has no implications on the drag and lift calculations, as the reference area of a single wing is taken. The aircraft is placed under an angle of attack of 3° to simulate cruise conditions. The size of the flow domain is determined by looking at mass in-balance between the inlet and outlet as well as the pressure distribution on the sides of the box. This is done by making a visual representation of the pressure distribution along the surfaces of the flow domain. If this distribution is not constant, the flow domain should be extended. Note that increasing the flow domain implies larger element sizes due to software constraints. Inside the domain, an unstructured tetrahedral mesh is generated automatically. To increase accuracy, the element size in vicinity of predefined sections has been decreased. To reach highest accuracy for the discretisation of the model, all meshes contained around 500,000 elements as the limit is 512,000 elements. This depends on both the element size and the size of the flow domain.

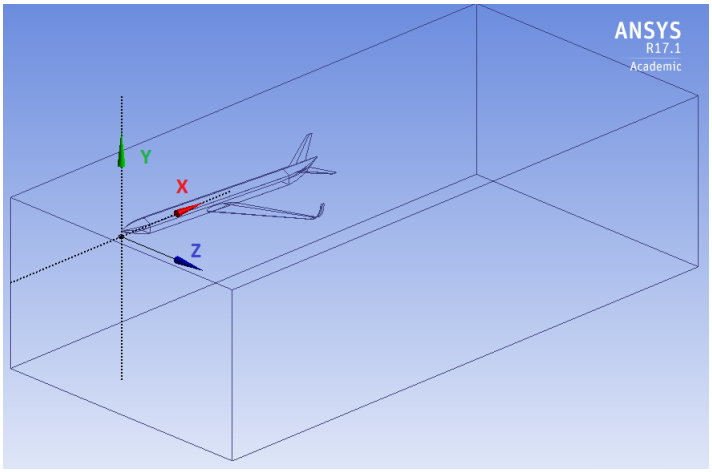

Figure 12.2: Example of the computational domain used in this study. Note that this figure is not to scale

12.2.3. Model Choice

No single turbulence model is universally accepted as being superior for a large variety of flows. Before any further simulations were performed, the accuracy of the previously used Spalart-Allmaras model was reviewed. A one-equation model was used in the conceptual project phase, due to the large amount of simulations that had to be performed. For the development of the final design, a higher accuracy of the turbulence model was desired. The accuracy of the Spalart-Allmaras model was analysed by comparing it to the Shear Stress Transport (SST) model. The Spalart-Allmaras model is a one-equation model, whereas the SST simulation has two-equations. It combines the k-ω model near the boundary layer and the k-ϵ model in the free shear flow. The k-ω model is able to accurately simulate near wall flows and boundary layer transitions. However, it lacks accuracy when simulating flows with pressure induced separation. This compensates for the lack of sensitivity to adverse pressure-gradients of the k-ϵ model [59] [60]. Subsequently, it combines the characteristics of both models to improve accuracy while still having an acceptable amount of computational effort. Due to the advantages of using both models, it is one of the most popular non-algebraic turbulence models [61]. The SST model does produce higher turbulence levels in regions with large normal strain, such as stagnation regions. Though this tendency is much less noticeable than with a single k-ϵ model [62]. Near convergence of the lift coefficient, a difference of 74.8%is measured for the two models. Furthermore, computational times deviate with 5.4%. Note that it is important to validate these results first, since the experimental lift coefficient is still unknown. The most accurate model is chosen after validation.

12.2.4. Discrepancies

This section describes the discrepancies of the initial model and explains why a new model had to be made to ensure sufficient accuracy of the results of the simulation.

The overview of a computational modelling process including the respective errors and uncertainties is shown in Figure 12.3. On the left, the modelling starts with defining one or more PDEs and boundary conditions which represent a physical system. Since this is done by approximations, model errors are introduced. These PDEs are continuous functions, which have to be discretised to solve the set of equations for the given problem. This inevitably introduces deficiencies called discretisation errors. Many of these systems are solved using iterative methods. Once the residuals are below a predefined value, the simulation is completed. This introduces the third error in the system, called the nonlinear iteration error. By applying time efficient iterative solvers, the solution is guessed, corrected and solved again. This is done until the corrections are sufficiently small. This last step described the linear iteration error, which is the error that remains due to discontinuing the iteration process.

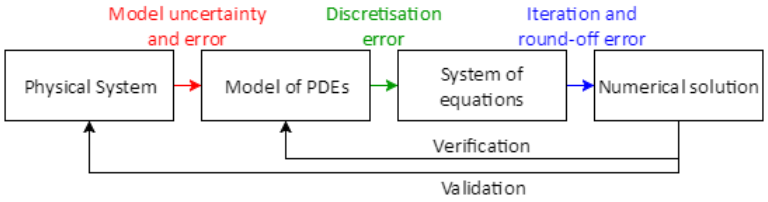

Figure 12.3: Diagram showing the numerical modelling process, adapted from [63]

This system can directly be applied to find the discrepancies in the initial numerical model. Initial stages in the conceptual design process showed promising results for the drag and lift coefficients. In the CFD model, the maximum nu mber of elements is used. Hence, the discretisation error is assumed to be small. As a consequence, the error was thought to be a modelling error. This is why the accuracy of the Spalart-Allmaras model was reviewed. Yet the limited number of elements are found to be too low to model a 3D aircraft. For 2D analysis, around 2-3 million elements are desired for sufficient accuracy of the model. This is around 20 times higher for a 3D simulation [1]. Subsequently, discretisation errors are too high to predict model and iteration errors. The mesh is too coarse for modelling the turbulent boundary layer. With the maximum settings, one element is larger than the thickness of the boundary layer. This meant that the system of PDEs is not solved at all in the boundary layer, but only for the flow at a greater distance from the aircraft. The results of drag calculations are therefore unreliable and cannot be simulated.

A new model had to be designed to determine the aerodynamic properties of different fuselage shapes. This resulted in a renewed model, described in Section 12.3.

12.3. Renewed Model

The renewed model is presented in this section. After reviewing the discrepancies of the previous model, a new model has been made, displayed in Figure 12.4. This model is based on the pressure calculations performed by CFD software. Drag calculations are subsequently performed by an empirical model, which requires the outputs of the numerical model. This new approach does not require a detailed discretisation of the thin boundary layer, as the empirical model uses boundary layer approximations. The aim of this model is to find a qualitative relationship between drag and the shape of the fuselage. Drag can be approximated using derived equations for boundary layers together with an inviscid model, which does not take boundary layers into account.

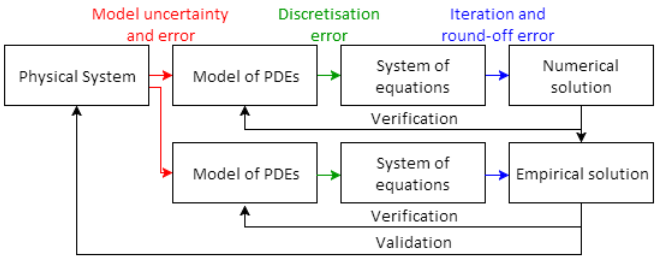

Figure 12.4: Diagram showing the renewed modelling process, adapted from [63]

Besides pressure distributions, the renewed model is also able to determine the lift coefficient of the aircraft. It is valid to determine the lift with an inviscid model due to the following. Aerodynamic forces acting on the aircraft arise from two causes. A normal force due to pressure on the surface and a shear force due to viscous effects. From basic aerospace theory it is known that the lift acts perpendicular to the flow. Moreover, drag acts parallel to the flow. This means that when neglecting viscosity of the flow, drag calculations are invalid. Yet, lift calculations are not effected by this assumption in the ideal case. Since the aircraft is at an angle of attack, the lift determined for inviscid flow is expected to be lower than the actual value [64].

[1] Dr. S.J. Hulshoff, personal communication, January 2017

With the renewed model it is possible to calculate the L/D ratio of the designed aircraft. The total drag is dependent on $D_{profile,fuselage}$, $D_{profile,non\text{-}fuselage}$ and $D_{induced}$. $D_{induced}$ is determined by the lift coefficient obtained from the numerical model. Statistical data is used for the Oswald factor and the aspect ratio is acquired from the aircraft wing geometry, see Equation 12.1. The profile drag of all non-fuselage components, such as wings is obtained from statistical data [58]. Subsequently, $D_{profile,fuselage}$ is obtained by the empirical model which used the pressure distributions along the fuselage as simulated by the numerical model. Dividing the total drag over the total lift force results in the L/D ratio.

$$C_{D_{induced}} = \frac{C_L^2}{\pi A e} \tag{12.1}$$

- A = Wing aspect ratio [-]
- e = Oswald factor [-]

12.3.1. Numerical Model

The renewed numerical model is based on pressure calculations of the different aircraft geometries as described in Chapter 9. Pressure measurements are performed using the same flow domain, but with an updated mesh. A so-called body of influence is used to decrease the element size of the mesh surrounding the fuselage. This body of influence has a rectangular shape which spans across the entire flow domain. Moreover, to improve the accuracy of the lift calculations, a face sizing has been added. The main wing, horizontal and vertical tail have a decreased element size. Further mesh sizing techniques that have been applied are identical to the previous model, as described in Section 12.2.2. Details of the flow domain and the mesh can be found in Table 12.1.

Table 12.1: Description of the mesh details

Size	Amount [m]
Length	65
Width	25
Height	20

After mesh generation is completed, the model must be chosen. As described in the previous section, an inviscid model is selected. This will provide the empirical model with the correct values for the flow above the boundary layer. If a viscid model is chosen, the pressure distribution will also include boundary layer effects. Since the mesh is not able to accurately simulate these effects, calculations will be invalid.

Figure 12.6 depicts the measurement locations of the pressure calculations. Three lines projected along the fuselage are used to determine the drag of the top, side and bottom of the fuselage. Since the effect of the pressure difference due to the nose section should be minimised, the lines start after this section. Furthermore, wing fuselage interactions are to be avoided for these calculations. Therefore, pressure calculations are performed between the nose and the tail section. From Figures 12.6 and 12.5, it can be seen that the three projections on the fuselage remain mostly unaffected by these sections since the distribution of both parameters does not change.The same simulations are performed to approximate the lift coefficient of the aircraft.

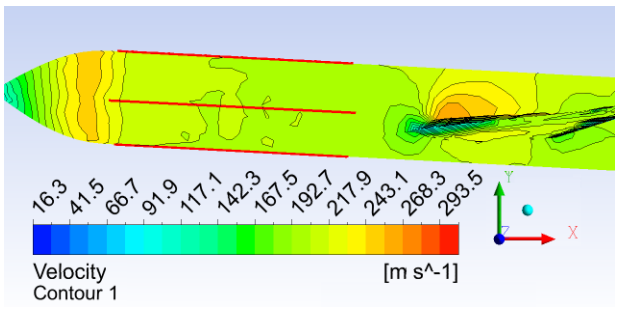

Figure 12.5: Velocity contours of the aircraft including measurement lines (red)

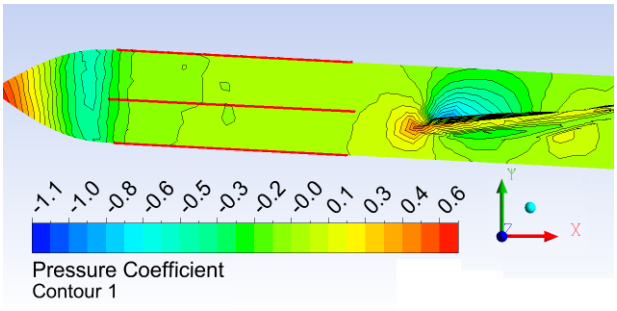

Figure 12.6: Pressure coefficient contours of the aircraft including measurement lines (red)

The same simulations are performed to approximate the lift coefficient of the aircraft.

12.3.2. Numerical Assumptions

Representing the physical system by approximations and assumptions influences the systems behaviour. This will introduce modelling errors to the solution. Hence it is important to give a clear overview of the assumptions for the numerical model, which are stated below.

- The fluid is assumed to be air with ideal gas properties.
- The gauge pressure is 22632.1 Pa.
- The temperature of the flow is 216.65 K.
- The flow in the model is inviscid.
- The simulation is converged once residuals fall below $1e^{-3}$.

Assuming ideal gas properties for air simplifies the set of equations. Ideal gas law is valid since $V_{air} \gg V_{molecules}$ and forces acting on the molecules are negligible due to the low pressure at cruising altitude [65]. The Mach number is derived from stakeholder requirements. Moreover, the atmospheric conditions are calculated at cruising altitude, which is 11 km as described in Section 15.1. Validity of the inviscid model and tolerance level of the residuals is described in Section 12.5.

12.3.3. Empirical Model

The empirical model translates the pressure coefficient (side, upper and lower) for the line of the fuselage to drag of these lines. First, the compressible pressure coefficient is translated into an incompressible pressure coefficient. Second, the incompressible pressure coefficient is translated into the velocity profile over the part of the fuselage. Third, the velocity and velocity differential are calculated. Fourth, the velocity is used to calculate the starting boundary layer shape and momentum thickness due to a flat plate. Fifth, the start will be used to determine the skin friction using the Head's method [66]. Finally, the skin friction can be translated into drag using the wetted area and boundary layer.

To calculate the velocity from the pressure coefficient, the C_P should be calculated as a form of incompressible flow, which can be translated using Bernoulli [2], see Equation 12.3. As the Mach number is set to 0.7, the compressibility factor can be derived using the Karman-Tsien correction [3]. The compressibility factor can be seen in Equation 12.2.

$$C_{P_{incompressible}} = \frac{\sqrt{1-{M_\infty}^2}\cdot C_{P_{compressible}}}{1-\frac{M_\infty^2}{2(1+\sqrt{1-M_\infty^2})}\cdot C_{P_{compressible}}} \tag{12.2}$$

- C_P = Pressure coefficient [-]
- M_∞^2 = Mach number without influence structure [-]

$$C_{P_{incompressible}} = 1-(\frac{Ve}{V_\infty})^2 \tag{12.3}$$

- Ve = Local velocity outside the boundary layer [m/s]
- V_∞ = Velocity without influence structure [m/s]

Knowing the velocity, the velocity differential is based on the numerical differentiation of the velocity over the x-position, see Equation 12.4, where i is the element analysed and x the length coordinate over the fuselage. Notice that the Δ x is determined from the input of the numerical model.

$$\frac{\Delta Ve}{\Delta x} = \frac{Ve[i]-Ve[i\text{-}1]}{x[i]\text{-}x[i\text{-}1]} \tag{12.4}$$

[2] http://www.aerostudents.com/files/introductionToAerospaceEngineering/AerodynamicsPressureCoefficients.pdf [accessed on January 19th 2017]

[3] https://www3.nd.edu/ātassi/Teaching/ame%2060639/Notes/compressible.pdf [accessed on Janurary 19th 2017]

- $\frac{\Delta Ve}{\Delta x}$ = Velocity differential [1/s]
- x[i] = Local point [m]
- x[i-1] = Previous point [m]

The Reynolds number is $2.8 \cdot 10^8$, based on the fuselage length and cruise conditions (speed is Mach 0.7 and density and viscosity are based on 11km altitude). For this value, it can be seen that the flow is completely turbulent, see 12.7, [4] . Therefore Head's method is chosen as it deals with complete turbulent flows [66].

For Head's method, the initial conditions of the flat plate (shape factor flow H, boundary layer thickness δ and momentum thickness θ) are known from literature. These are implemented with the velocity and velocity differential. Head's method allows to calculate the boundary layer shape factor and the momentum thickness along the length of the fuselage[66]. The flow over a profile and according parameters can be seen in Figure 12.8 [5]. All equations will be further based on Head's method, described in Moran [66].

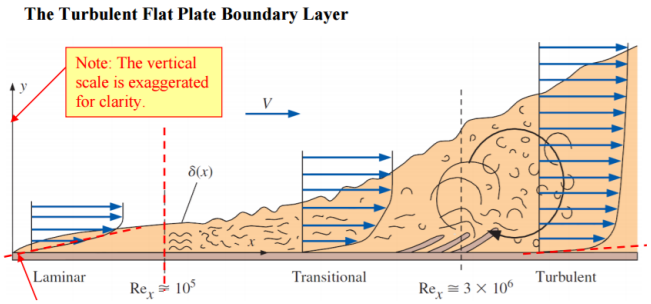

Figure 12.7: Boundary layer flow as function of Reynolds numbers [6]

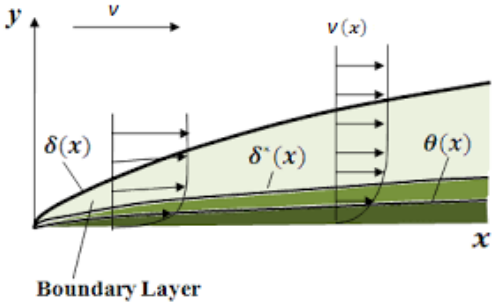

Figure 12.8: Parameters of turbulent flow [7]

Head's method is based on four equations , which form an integral system. One formula is the Von Karman integral relations. Equation two and three are based on statistical data by Cebeci-Bradshaw. The fourth equation based on statistical data, the skin-friction "law" from Ludwig-Tillman (see Equation 12.5, will be used to calculate the skin friction. From this integral system different boundary layer characteristics can be deduced, based on numerical extrapolation from initial conditions.These equations can be found in Moran [66]. The system is based on 4 variables: momentum thickness θ, shape factor flow H , entrainment shape factor H1 and friction coefficient, C_f.

$$C_f = 0.246 \cdot 10^{-0.676 \cdot H} * Re_\theta{}^{-0.268} \tag{12.5}$$

$$Re_\theta = \frac{\rho \cdot Ve \cdot \theta}{\mu} \tag{12.6}$$

- Re_θ = Reynolds number for momentum thickness [-]
- ρ = Density [kg/m^3]
- μ = Viscosity [kg/(s · m)]

As $\frac{\Delta Ve}{\Delta x}$ is calculated before, as well as Δx is determined from the numerical model and the initial θ is known from flat plate, Re_θ can be calculated using 12.6 and then the integral model can be solved. Notice the Reynolds number based on θ is an indication of the flow behaviour inside the boundary, just as the normal Reynolds number indicates the flow characteristic over the profile.

Once the integral system is known, more quantities about the boundary layer can be computed. The next step is to calculate the displacement thickness δ^* and boundary layer thickness δ, see Figure 12.8. The equations are given in Equations 12.7 and 12.8.

[4] http://www.mne.psu.edu/cimbala/me320web_Spring_2015/pdf/Flat_plate_turbulent_BL.pdf [accessed on 26-01-17]
[5] http://nptel.ac.in/courses/101103004/module5/lec9/4.html [accessed on 26-01-17]
[6] http://www.mne.psu.edu/cimbala/me320web_Spring_2015/pdf/Flat_plate_turbulent_BL.pdf [accessed on 26-01-17]
[7] http://nptel.ac.in/courses/101103004/module5/lec9/4.html [accessed on January 30th 2017]

$$\delta^* = H \cdot \theta \tag{12.7}$$

$$\delta = H1 \cdot \theta + \delta^* \tag{12.8}$$

- δ^* = Displacement thickness [m]
- δ = Boundary layer thickness [m]

Now all the flow parameters are known for the local point on x and the characteristics of the next point can be calculated by linearly extrapolating the data, using Equation 12.9 and 12.10. The $\Delta\theta$ and Δ H1 and are given by the integral system from Head's method [66].

$$\theta[i+1] = \theta[i] + \frac{\Delta\theta}{\Delta x} \cdot \Delta x \tag{12.9}$$

$$H1[i+1] = H1[i] + \frac{\Delta H1}{\Delta x} \cdot \Delta x \tag{12.10}$$

The average profile skin-drag can be calculated by integrating the profile skin drag over the distance and divide this sum by the distance, see Equation 12.11.

$$C_{f,average} = \frac{\int_0^x C_f dx}{x} \tag{12.11}$$

The total drag coefficient from the body is then

$$C_{D_{0,fuselage}} = C_f \cdot \frac{S_{wet}}{S} \tag{12.12}$$

- $C_{D_{0,fuselage}}$ = profile skin drag coefficient from fuselage
- S_{wet} = Wetted area (area effected by flow) [m^2]
- S = wing area

The total drag of the fuselage is estimated by assigning weights for different body lines according to their geometry (upper, side, body) and multiplying this by the wetted area corresponding to the body line. The wetted area is estimated in Equation 12.13 [67].

$$S_{wet} = \pi \cdot D_{eff} \cdot l_{fuselage}(1 - \frac{2}{\lambda})^{3/2}(1 + \frac{1}{\lambda^2}) \tag{12.13}$$

- D_{eff} = Effective diameter (surface divided by $\sqrt{\frac{\pi}{4}}$) [m]
- $l_{fuselage}$ = Length of the fuselage [m]
- l_{nose} = Length of the nose [m]
- λ = Fuselage ratio (length divided by effective diameter) [-]

12.4. Results

The aerodynamics coefficients that need to be provided by CFD computations are the lift and pressure coefficients. Also known as C_L and C_p, respectively. In this section however C_p is not discussed as the lift coefficient is a direct consequence of this parameter. Moreover, together with the empirical model, results of the drag coefficient, C_L are given. Finally, the L/D ratio will be presented for the different fuselage sections. A comparison with the different fuselage shapes and the Airbus A320ceo can be found in Table 12.2. Moreover, a visual representation of the normalised results can be found in Figure 12.9.

Table 12.2: Results of the renewed model vs the A320ceo [58]

Fuselage shape	C_L [-]	C_D [-]	L/D [-]
Circle	0.427	0.0225	19.0
Ellipse	0.429	0.0221	19.4
Rounded rectangle	0.408	0.0214	19.1
A320ceo	0.493	0.0277	17.8

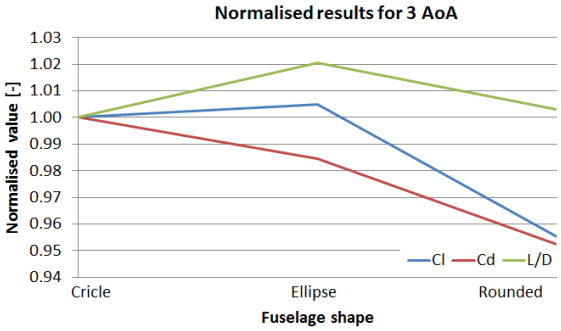

Figure 12.9: Normalised results for different fuselage shapes

It is expected that the lift calculations for the rounded rectangle are higher than expected in reality. Spiral vortices due to the sharp edges are a major drag contributor [68]. These vortices decrease the amount of lift generated by the fuselage. Models that are inviscid do not simulate vortices as in reality, which could decrease C_L and increase C_L.

The average L/D ratio of the three cross-sections is 7% higher than the L/D of an Airbus A320ceo. A main contributor of this discrepancy is the induced drag, which differs with 49%. This difference can be attributed to the difference in C_L and aspect ratio, which is 13% and 40%, respectively. The Airbus A320ceo has an aspect ratio of 10, while in preliminary design stages of the A342 the aspect ratio is 14.

The L/D ratio of all three cross-sections comply with requirement CFSM-ALC-12 The aircraft shall have a comparable or higher Lift over Drag ratio, compared to state-of-the-art aircraft, stated in Section 21. Requirement CFSM-S-04 Wings provide enough lift is met taken into account low angle of attack, airfoil characteristics, current CL from ANSYS, wing area and speed.

12.5. Verification

This section presents an overview of the verification processes of the CFD simulations and Head's method. The general objective is to determine the accuracy of the solutions by reviewing the levels of uncertainties and errors. This is done by determining the consistency of the numerical and empirical model with the model of equations.

12.5.1. Numerical Model

The verification assessment process starts with examining the computer programming code. Ansys does not allow users to change the source code. Extensive verification and validation of different models has been performed by Ansys and third parties. The results can be reviewed in [8]. Accuracy of different test cases range from 0.95 to 0.98 compared to experimental results. It is therefore assumed that the code contains no programming errors and the uncertainty is very small.

Next, model uncertainties are determined. For inviscid flows, ANSYS approximates a solution to the Euler equations. The mass conservation equation is the same as for a laminar flow, though the energy and momentum conservation equations are simplified due to the absence of molecular diffusion. An inviscid model does not reflect reality because any viscous effects are neglected. Yet this does not imply the pressure distributions or lift calculations are inaccurate. As explained in Section 12.3.1, normal forces due to pressure are still simulated and accounted for. The continuity and momentum equations compute velocity and pressure fields simultaneously. Due to extensive verification of ANSYS by other parties, consistency of the numerical model with the model equations is said to be confirmed.

Model errors can also be estimated by doing an artificial boundary study. This method can only be applied if the mesh is smoothly varying the element size. Solutions are computed and compared on domains of different

[8] https://www.sharcnet.ca/Software/Ansys/16.2.3/en-us/help/fbu_vm/fbu_vm.html [accessed on January 11th 2017]

sizes. Unfortunately, the mesh in the numerical model is unstructured due to the numerous geometry changes and interactions. Moreover, the mesh used in the simulations cannot be increased without increasing the element size in the flow domain, which results in an invalid comparison. This is due to the element constraint set by ANSYS software.

The errors that arise from discretisation can be estimated by doing a grid convergence study. By performing numerous simulations with different element sizes, convergence of the pressure coefficient is examined. If the pressure coefficient converges to the same value for multiple meshes, the element size is small enough and discretisation errors are low. The outcome of the convergence study is presented in Figure 12.10. Grid convergence is confirmed as the results of the grids with element sizes 0.385 m, 0.5 m and 0.55 m do not differ significantly from each other in comparison to the other grids.

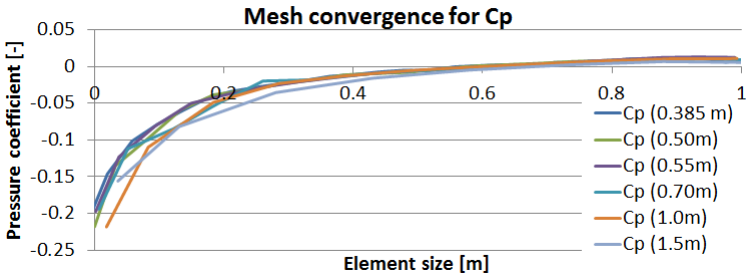

Figure 12.10: Pressure coefficients of the grid convergence study.

Grid convergence can also be verified by studying the correlation of lift coefficient and the element size of the mesh. This correlation is displayed in Figure 12.11. As the element size of the mesh decreases, the lift coefficient tends to reach a final value. Results of the lift coefficient are therefore assumed to have small discretisation errors.

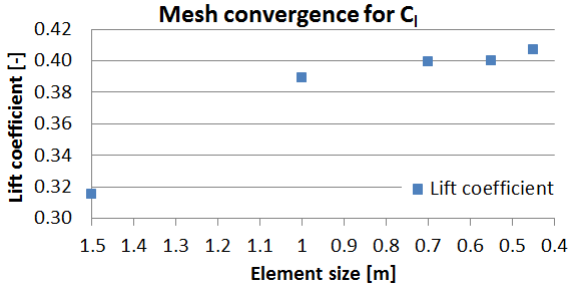

Figure 12.11: Lift coefficients of the grid convergence study.

Furthermore, iteration and round-off errors are estimated. Round-off errors are predicted by examining convergence of the residuals. This is a measure of the error magnitudes for the governing, continuity and energy equations. It is a crucial measure of convergence as it is directly related to whether the equations have been solved accurately. The simulation is finished when the residuals fall below $1e^{-3}$, which also indicates the round-off error. Figure 12.12 depicts the convergence of the residuals and the convergence criteria. It can be seen that at this value, the residuals level-off which indicate iterative convergence. Moreover, the results of the simulations are monitored to check if they remain unchanged with respect to the number of iterations.

Table 12.3: Blocktest and output verification Head's method

Shape	H	H normalised	θ	θ normalised	C_f	C_f normalised
Flat plate	1.29	1.00	0.0676	1.00	0.00212	1.00
Circle	1.33	1.04	0.00670	1.03	0.00196	0.926
Ellipse	1.33	1.03	0.00743	1.10	0.00199	0.940
Rectangle	1.33	1.03	0.00735	1.09	0.00199	0.940

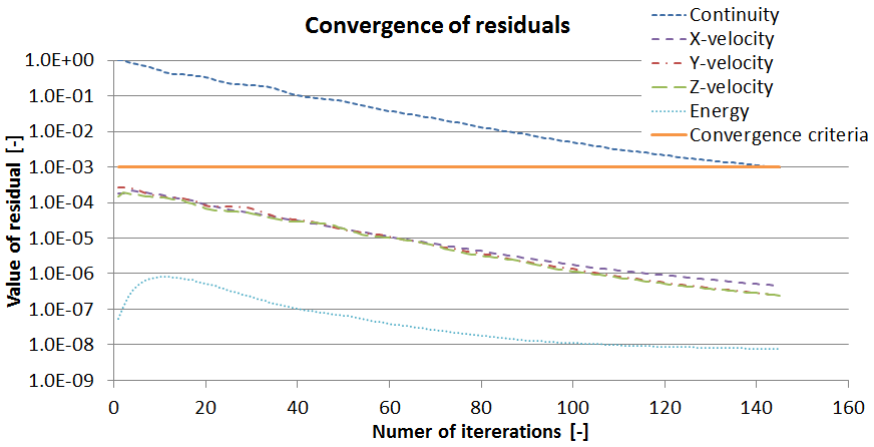

Figure 12.12: Convergence of the residuals of a simulation.

The CFD solutions must also be consistent with the conservation equations. A mass balance is made by determining the mass flux of the inlet and outlet. It has been determined that the difference is 0.23 percent.

Finally, a unit test is performed by placing the model at 0° angle of attack. Figure 12.13 displays the results. It is noticeable that the pressure distribution of the top and bottom sides is almost equal to each other for the zero angle of attack case. This confirms expectations since the aircraft is symmetric along the projected lines.

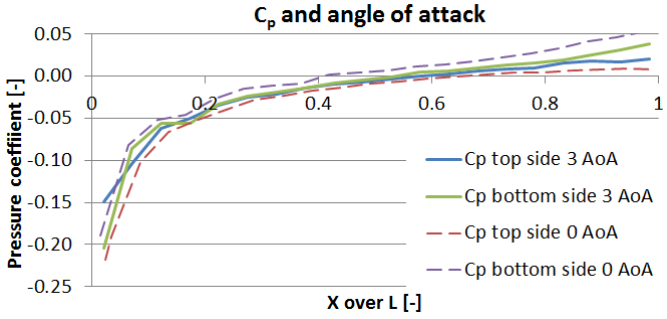

Figure 12.13: Pressure coefficients for 0 and 3 angle of attack. For clarity, only the top and bottom lines are displayed.

12.5.2. Empirical Model

The verification assessment process starts with examining the customised python code. The output C_f should be tested, as well as the extrapolated data H and θ. According to Whittington [69] the accuracy should be up to 10%. The output using Head's method from the python code confirms this, see Table 12.3.

The next step for the empirical model verification is to look for the discretisation error. However the input from the empirical model depends on the numerical model. Also, no further discretised input is used. Hence the verification of the model inputs (verification of numerical model) suffices. The model uses no iterations, hence this step can also be skipped.

The verification of the the empirical model will be based on the empirical friction coefficient plot versus Reynolds number, see Figure 12.14 discussed by Roskam [67]. The Reynolds number looked at is $2.8 \cdot 10^8$. The C_f is estimated at 0.017, so it is 15% off in comparison to the friction coefficient of the modelled circle.

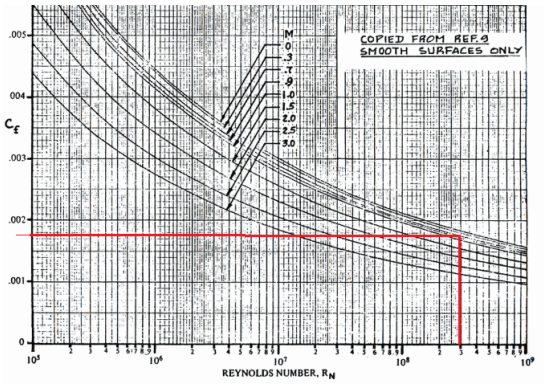

Figure 12.14: Friction coefficient as a function of Reynolds number

The wetted area could not be verified, but can be validated by comparing to other aircraft for skin friction coefficient and zero lift drag of the fuselage. For the comparison of zero lift drag of the fuselage, the values from Chapter 5 for fuselage drag will be used. The drag budget states that the zero lift drag contribution of the fuselage is a maximum of 0.011, while the maximum of the zero lift drag contribution of the fuselage from the model (circle) has a value of 0.0077. This concludes that the values of the model are in range of the budget. The $\frac{L}{D}$ was compared to compared to a typical jet transport, for which the values are in range of 12 to 20 [9]. Hence the $\frac{L}{D}$ is in the expected range.

12.6. Validation

This section presents an overview of the validation processes of the CFD simulations and Head's method. During validation, the outputs of the numerical and empirical are directly compared with the output of the physical model, as presented in Figure 12.4. This can provide estimates for the model uncertainty and error.

The results of the validation procedures can be seen in Table 12.4. First, the skin friction coefficient, C_f is compared. The largest difference, 10.3%, can be observed at the circular fuselage. Second, the friction coefficient of the fuselage only is compared to that of the A320ceo. Results vary from 9.15% for the circle to 16.8% for the rounded rectangle. This discrepancy can be attributed to the fact that nose, wing and tail interferences on the fuselage drag are not simulated. Though notice that for the circular cross-section, the difference is within the proposed uncertainty of 10%. Third, the lift coefficient of the whole aircraft is analysed. Finally, the L/D will be compared to that of the A320ceo. The circle and ellipse differ with 7.2% and 9.10%, respectively. A noticeable difference is the change of lift coefficient of the different fuselages compared to the A320. These vary from 12.9% for the circle and to 17.2% for the rounded rectangle. This can be explained by the wing setting and angle of attack. Though it could also mean that the simulations performed in Ansys require a more detailed mesh to increase accuracy regarding validation.

12.7. Sensitivity analysis

As the solution of the model might exhibit different behaviour to changing input data, a sensitivity analysis must be performed. This ensures that the system behaves optimal, even under slightly changed circumstances.

The empirical model has an accuracy of ±10%. Therefore the output C_f will be varied between -10% and +10% to see the impact of the change on the L/D. Also interesting is to vary the wetted area between ±10%, the effect of a 10% bigger or smaller fuselage. This corresponds to second biggest market for passenger capacity, namely

[9] http://faculty.dwc.edu/sadraey/Chapter%204.%20Preliminary%20Design.pdf [accessed on 29-01-2017]

Table 12.4: Validation of multiple parameters of Head's method and the A320ceo [58]

Shape	C_f	C_f normalised	$C_{D,0_{fuselage}}$	$C_{D,0_{fuselage}}$ normalised	C_L	C_L normalised	L/D	L/D normalised
A320ceo	0.00218	1.00	0.00852	1.00	0.493	1.00	17.8	1.00
Circle	0.00196	0.897	0.00774	0.909	0.4273	0.867	19.1	1.07
Ellipse	0.00199	0.909	0.00738	0.866	0.4294	0.871	19.4	1.09
Rectangle	0.00199	0.909	0.00709	0.832	0.4082	0.838	19.1	1.07

200-249 seats, see Figure 3.2. This has the exact same impact on the zero lift drag coefficient of the fuselage, hence in the sensitivity Table 12.5 it is left out. Furthermore, it is investigated what will change by incorporating a newer airfoil, which will produce less wing profile skin drag. Based on a small Javafoil analysis, this gain will be in the order of 10 to 20%. Finally the lift coefficient is set higher, corresponding to the A320 and the new L/D is calculated. The results can be seen in Table 12.5.

Table 12.5: Sensitivity analysis lift over drag aircraft

Shape	Circle		Ellipse		Rectangle	
Parameters	(L/D)min	(L/D)max	(L/D)min	(L/D)max	(L/D)min	(L/D)max
Original	19.09	19.09	19.42	19.42	19.05	19.05
C_f ± 10%	-3.3%	3.3%	-3.2%	3.2%	-3.2%	3.2
Cd0, wing [-10,-20]%	4.7%	9.9%	4.8%	10.0%	5.0%	10.5%
CL = 0.496	8.4%	8.4%	8.0%	8.0%	11.2%	11.2%

Notice that the effect of the fuselage is rather small (3.3%), while the real profit for the L/D (up to 10%) can be obtained in increasing the lift coefficient (higher angle of attack) and/or decreasing the wing profile skin drag coefficient (other airfoil)

12.8. Conclusions

Of all shapes, the ellipse shows the best results for lift over drag ratio. The circle performs 2% less and is also considered an option. The results for the rectangle look promising. However, as described in section 12.4, these results are not accurate. Especially the corners where flow separation is expected, should reduce the performance.

Therefore, from aerodynamic point of view the ellipse is preferred over the circle. The rectangle is not an option without further research into the impact of the corners. Using the ellipse in predefined conditions, the L/D of the aircraft will be 19.42 in cruise.

12.9. Recommendations

The research performed has lead to several recommendations regarding the approach, methods used and further research.
For the 3D CAD Model, the nose and tail should be designed and optimised for each fuselage shape, so that a fuselage shape is not rejected due to nose and tail design. Also, the Catia model should include all subsystems that will be present in the real aircraft. Nacelles, high lift devices, and manufacturing inaccuracies should be added in the Catia model.

If the constrains set by Ansys were removed, drag and lift calculations could be performed with the numerical model only. The empirical model would than be used as a verification method. Though this would also require more computational resources.

Supposing that the number of elements was infinite, a lift drag polar for different Mach numbers could also be made. This would give valuable insights in the aerodynamic characteristics of the aircraft. This is not possible with the empirical model, since application of the Karman-Tsien correction is valid for 0.7 Mach.

For the verification of the data, the lift vs angle of attack curve could be used. Placing the model at -3°, 0° and 3° results in the linear part of this curve. Moreover, 2D data and the Datcom method could provide the stall characteristics which are needed to finish the curve.

Finally, for each fuselage shape, wing fuselage interactions should be investigated. According to Hoerner [70] and Torenbeek [71], interference drag varies considerably with different wing positions. This will also be different for unsymmetrical fuselage shapes, such as the rounded rectangle. Moreover, the wing fuselage fairing must be optimised for each cross-sectional shape.

13. Fuselage Trade-off

In this chapter the trade-off for the fuselage shape is performed. While the other aircraft subsystems are trade-off in their respective chapters, aerodynamics and structures departments are performing one together. The reason for that is the fact that both of the departments are analysing the same thing - the fuselage shape.

13.1. Trade-Off Logic, Weights & Criteria

Normally, the technical parameters such as weight and drag would be connected to the driver requirements. However, in this case an alternative is taken. First, another look into the assignment is taken:

1. Challenge the circular cross section of the fuselage as being the optimum.
2. Find the optimum cross-section with optimum space usage, maximising payload per volume while maintaining the pressurisation requirement.
3. Analyse the impact of the adapted fuselage shape at overall aircraft level.
4. Optimise the fuselage shape to maximise product payload performance.

The item number one of the list above does not require a graphical trade-off. Referring back to the structures Chapter 10 it was found that flat areas on the fuselage are incapable of dealing with the pressurisation stresses, at least without the supporting structures. Even with supporting structures the aircraft would be heavier, which is not desired by anyone in a commercial aviation. The ellipse with a perfect fit for a given internal layout has been proven to be 4% more efficient with respect to the circumferential area, hence wetted area. However, the stress is increased by almost 100% with respect to the circle. Assuming a near linear relationship between the stress and the structural mass one can prove that the mass of the ellipse will still be higher than the one of a circle, at a very small gain in the reduction of the wetted area. Hence, it is proven that the circular shape is optimal when it comes to pressurising a structure for the commercial passenger transport. From aerodynamics point of view, the ellipse has an L/D of 19.4, while the circle has 19, which is an improvement of around 2%. Comparison of the ellipse and the rounded rectangle indicates a 1.5% improvement. However, rectangle analysis was not accurate enough to provide a definitive number. In any case, one can draw a conclusion with the given data. The rectangle is not feasible structurally. The ellipse, has a tremendous increase in structural mass, with only a small improvement in L/D ratio. Hence, one can derive that the optimal shape is an ellipse.

The second item is the more complicated case. Here, the actual trade-off has to be performed, given the current fuselage shape concepts. For the trade-off, the same methodology is applied as in the Mid-term Report [72]. This means, that the weights and criteria have to be chosen, based on this the fuselage shape can be selected.

For the criteria the following were chosen:

- **Volumetric Efficiency**, this follows directly from the client requirements.
- **Wetted Area**, to indicate the drag performance, which has a direct influence on the fuel consumption and hence direct operating costs.
- **Friction Coefficient**, to indicate the drag performance, which has a direct influence on the fuel consumption and hence direct operating costs.
- **Stress**, since higher stresses generally lead to the heavier structure, which has a direct influence on the direct operating costs.

The following weights were assigned:

- **Volumetric Efficiency = 1**, since this does not cause large implications on the Direct Operating Costs.
- **Wetted Area = 5**, it is assumed that the wetted area and friction coefficient combined should carry as much weight as the stress.
- **Friction Coefficient = 5**, it is assumed that the wetted area and friction coefficient combined should carry as much weight as the stress.
- **Stress = 10**, it is assumed that the wetted area and friction coefficient combined should carry as much weight as the stress.

13.2. Sensitivity Considerations

Weight assignment is usually a procedure where one operates under some form of uncertainty. Hence a sensitivity analysis is performed. The procedure is the same as in the Mid-term Report - different scenarios with different weight distributions are created.

First, it is assumed that the volumetric efficiency carries more weight than initially anticipated, and is increased to 5. Then, it is assumed that the drag carries more weight than predicted. Since the drag is comprised of the wetted area and the friction coefficient, both of these are increased to 10. Finally, it is assumed that the mass carries more weight than initially assigned. This means that the stress weight in the trade-off table is increased to 20.

Trade-off and Results

The results of the trade-off are presented in the Figure 13.1.

Weights - Modified 3	1	5	5	20	31					
Weights - Modified 2	1	10	10	10	31					
Weights - Modified 1	5	5	5	10	25					
Weights - Normal	1	5	5	10	21					
	Volumetric Efficiency	Wetted Area	Friction Coefficient	Stress	Results 1	Results 2	Results 3	Results 4	MIN	MAX
Circle	0.5	0.5	0.5	0.5	50.00	50	50.00	50.00	50.00	50.00
Ellipese	0.75	0.75	0.75	0.25	51.19	55	58.87	42.74	42.74	58.87
Rectangle	1	0.5	0.5	0	28.57	40	35.48	19.35	19.35	40.00

Figure 13.1: Fuselage trade-off

The scores were assigned in a same way as during the Mid-term Report trade-off. As it can be seen the elliptical fuselage has the higher maximum. Circle has a stable score, however, it is not allowed due to the shape requirement. Hence, elliptical fuselage is chosen.

14. Propulsion

This chapter discusses the different design options considered for the propulsion system. Then, the trade-off of the type of propulsion system is presented and explained. After, a sensitivity study is performed in order to evaluate the influence of specific fuel consumption on aircraft mass. Finally, recommendations for further development of the propulsion system are given.

14.1. Type of Engine

A literature study was performed in order to investigate the type of the engines available as well as trends for the future. The engine options were narrowed down to two general types of engines: the turbofan and the open rotor engine. This was due to the client's requirement regarding the cruise speed, fuel efficiency, and the service ceiling of the aircraft. Several different concepts of the turbofan and open rotor are considered. Advantages and disadvantages of the two engine types are discussed below.

High Bypass Turbofan

Propulsive efficiency is increased if the ratio of exhaust velocity to free stream velocity decreases. Reducing the fan pressure ratio, FPR, decreases the acceleration given to the air. In order to provide the same thrust the bypass ratio, BPR, has to be increased. In this manner, the specific fuel consumption, SFC, is reduced. This results in a reduction of CO_2 emission, but also in a reduction of the amount of noise generated by the engine. Current high bypass turbofan engines are operating in a BPR of 5 to 10 [73]. However, Rolls Royce predicts this will increase to numbers as high as 50 [74].

There are drawbacks to ever increasing BPR, as it leads to a lower velocity of the fan. In a direct drive turbofan the fan is directly connected to the low pressure compressor and turbine. Increasing BPR will lead to increasing the number of stages needed to get the same overall pressure ratio, OPR. This increases the engine mass. A geared turbofan engine provides a solution, however this increases the complexity of the engine. Also increasing BPR means increasing the nacelle, this increases the drag and weight of the configuration.

The large frontal area of the high bypass turbofan introduces additional drag. A counter-rotating turbofan concept provides a solution to reduce high frontal drag. The counter-rotating turbofan has a two stage fan, rotating in opposite directions. This divides the total aerodynamic load of the fan stage. Subsequently, it leads to a reduction of tip speed if FPR and BPR are kept constant for the same net thrust and engine size. It can also allow for a reduced fan diameter, giving mass and drag benefits. However, this is at the cost of a slight increase in FPR and decrease in propulsive efficiency. A trade-off is necessary to see if the decrease in mass and drag matches the decrease in propulsive efficiency. An additional benefit is the reduction in perceived noise level [21].

NASA estimates the SFC of an advanced direct drive turbofan to be $8.2 \cdot 10^{-6}$ kg/Ns at sea level, static thrust conditions, and $1.49 \cdot 10^{-5}$ kg/Ns for cruise conditions[75]. These values correspond with the 14% SFC improvement of the LEAP engines as compared to the CFM56-5B[76] [1][2]. NASA estimates the SFC of a geared turbofan to be $7.3 \cdot 10^{-6}$ kg/Ns at sea level, static thrust conditions, and for cruise at $1.43 \cdot 10^{-5}$ kg/Ns[75]. These value correspond with the 15% reduction in SFC of the GTF GEN1 engines developed by Pratt & Whitney and NASA over the V2500[76] [3]. The GTF GEN1 was then further developed into the PW1000G and was set as the baseline for the A320neo. The V2500 engine and CFM56-5B engine both were engine options of the A320ceo. A counter-rotating turbofan has the same SFC as a geared one[21].

[1] https://janes.ihs.com/Janes/Display/1342548 [accessed on January 27th 2017]
[2] http://www.boeing.com/commercial/737max/#/design-highlights/characteristics/ [accessed on January 27th 2017]
[3] http://www.cleansky.eu/sites/default/files/inline-files/Jean-Francois%20BRouckaert%20ENGINES-Aerodays-2015_final.pdf [accessed on January 27th 2017]

Advantages

- Low engine mass
- Nacelle protects against noise and provides blade containment
- Low SFC
- Already in production, performance parameters can be estimated for the upcoming 5 years

Disadvantages

- Nacelle introduces additional mass, drag and pressure losses
- Large frontal area introduces drag

Open Rotor

Advanced open rotor engines have been developed that are able to fly efficiently at altitudes and Mach numbers around 40,000 ft and 0.80, respectively[74]. The advanced propellers are designed so they are able to operate with relative supersonic Mach numbers at the tip without stalling[73].

To ensure maximum propulsive efficiency, the pitch of the propeller blades can be changed individually. A second row of counter rotating propellers can be added to eliminate the swirl angle of the exit flow. At a cruise Mach number of 0.8 this is estimated to add 7.5% points in efficiency [77]. Advanced open rotor engines are not yet in production, the TRL is 6[4]. The SFC is $4.47 \cdot 10^{-6}$ kg/Ns at sea level, static thrust conditions, and at cruise the value is $1.25 \cdot 10^{-5}$kg/Ns[75].

Advantages

- Low SFC
- No extra drag and weight due to nacelle
- High propulsive efficiency and thermal efficiency

Disadvantages

- High engine mass
- Difficult to place due to large propellers
- High noise level
- No blade containment due to lack of nacelle

14.2. Trade-Off: Propulsion

In this section a trade-off of the engine type is performed. The engine types considered for the trade-off are the direct-drive turbofan, geared turbofan and open rotor engine. The engine location will be assumed podded under the wing. Due to client wishes focus has been put on assessing the structural and aerodynamic performance of the aircraft by changing the fuselage shape and keeping a conventional layout for other subsystems.

Weights and Criteria

The criteria assigned are based the engine parameters that influence the aircraft performance the most. Engine type has an effect on direct operating cost through fuel burn. Therefore the direct operating cost increases as SFC, mass or drag increase. Noise characteristics do not have an influence on the direct operating cost, but it is important for the overall performance of the aircraft, see Chapter 3. Complexity is included in the trade-off, as this will likely have an effect on the maintenance costs.

The weights are assigned according to the effect on direct operating cost. Fuel costs will increase directly with SFC, therefore this has a weight of 20. Mass and drag directly influence the thrust required to comply with all performance requirements. Increasing the thrust required will increase the amount of fuel burned, if SFC and block time are assumed constant. Therefore both these criteria are assigned a value of 10. Noise is very important, if the aircraft does not confirm to future noise regulations there is no market for it. Therefore this will get a value of 15. Complexity is considered less important since maintenance costs are a smaller percentage of the direct operating costs than fuel costs. A value of 5 is assigned to this category.

Sensitivity Considerations

As discussed in the section before, the weights are assigned according to relative influence on the direct operating costs. However, there is an uncertainty in this, since the direct operating costs are computed using statistical data[78]. Therefore 3 additional scenarios are considered in order to mitigate this uncertainty.

[4] http://www.rolls-royce.com/about/our-technology/research/research-programmes/sustainable-and-green-engine-sage-itd.aspx#open-rotor-technology [accessed on December 15th 2016]

The first the time weights are modified, the importance of mass is increased, and the importance of noise is reduced by 5 points. This is in order to account for the fact that mass and drag might not be equal in importance. During the second modification, the drag is considered more important than the mass. Finally the complexity of the engine is ignored, and the importance of the SFC is increased. The scenarios are given in Figure 14.1.

Weights - Modified 3	30	15	10	5	0
Weights - Modified 2	20	10	15	10	5
Weights - Modified 1	20	15	10	10	5
Weights - Normal	20	10	10	15	5

	SFC	Mass	Drag	Noise	Complexity	Results 1	Results 2	Results 3	Results 4	MIN	MAX
Direct Drive Turbofan	0.50	0.75	0.25	0.50	0.75	52.08	54.17	50.00	52.08	50.00	54.17
Geared, Turbofan	0.75	0.50	0.50	0.75	0.50	64.58	62.50	62.50	64.58	62.50	64.58
Geared, Counter-rotating Open Rotor	1.00	0.00	0.75	0.25	0.50	56.25	54.17	60.42	64.58	54.17	64.58

Figure 14.1: Trade-off table propulsion

Trade-Off and Results

In the trade-off, each concept will be awarded a score from 0 to 1 for the criteria. Using this and the weights per criteria the total score for each engine type is computed. In Figure 14.1 the trade-off is presented. A 0 is awarded when the engine performs very bad and a 1 is awarded when it performs very well.

According to [75], the open rotor has the lowest value for SFC, the geared turbofan is slightly higher, and the direct drive turbofan is higher than that. This is translated into the scores for SFC as seen in Figure 14.1 .

The mass of a geared turbofan is higher than the mass of a direct drive turbofan engine. This is including the nacelle[75]. The mass of the open rotor engine is by far the highest[79]. In addition extra structural measures have to be taken in order to ensure passenger safety in case a blade breaks off. Therefore this engine receives 0 points for mass.

The drag of the geared counter-rotating turbofan is slightly less than the drag of the direct drive turbofan[21]. The open rotor engine performs even better because it has no nacelle and therefore less wetted area[1].

Considering noise the geared, counter rotating turbofan scores better than the direct drive turbofan[21]. The open rotor performs the worst in this trade-off according to [80]. However, the open rotor, if designed correctly can still perform better than today's standard. Therefore it was decided to give this a score of 0.25, rather than 0.

The last criteria is the complexity of the engine. The direct drive turbofan is the least complex because it is the only engine without a gearbox. It is assumed that there is no difference in complexity for the gearboxes for the geared counter rotating turbofan and open rotor, they have the same score.

The results can be seen in Figure 14.1. The geared turbofan and counter rotating geared open rotor have the same maximum score. This is due to the high weight of the SFC criteria in the last sensitivity scenario. However, it can also be concluded that the variation of the score of the open rotor engine is much higher than the turbofan. Therefore, the geared turbofan is chosen as the winning concept.

14.3. Engine Selection

With the required take-off thrust known from performance calculations, the engines can be selected. Since the focus of this project is put on challenging the shape and material of the fuselage design, the engine will be assumed as bought from an engine company. Therefore only engine characteristics will be assumed here.

It is assumed that the SFC will improve with 1% per year [5]. Using a reference value of $1.43 \cdot 10^{-5}$ kg/Ns[75] with baseline year 2012 and assuming that the engine will be produced in 2020 an SFC of $1.32 \cdot 10^{-5}$ kg/Ns has been calculated. This value corresponds with the predicted SFC of the Gen2 engine being developed by Pratt & Whitney[6]. The bypass ratio of this engine is estimated to be in the range of 15 to 20.

Since the aircraft performance is very dependent on this value, sensitivity studies have been performed to identify the effects of changing the SFC on aircraft parameters. The sensitivity study of the SFC on aircraft mass is presented in Section 14.4. The sensitivity study of the SFC on direct operating cost has been presented in Section 19.1.3.

Using data of reference aircraft and their engines the engine mass was estimated. The reference values are obtained from [75][76] [7] . No clear correlation was found between engine thrust and engine mass, based on the reference data. Therefore, engine mass was estimated using a linear regression of mass and bypass ratio. This resulted in an engine dry mass of 3,300 kg to 3,700 kg, depending on the bypass ratio. This is an conservative estimate, the use of the gearbox allows the reduction of the number of stages in the compressor and turbine. Therefore up to 180 kg of airfoil mass can be saved per engine[8].

14.4. Sensitivity Study

In this section a sensitivity study has been done to investigate the effect the SFC on the take-off mass, empty mass, and fuel mass. The results are based on a class I weight estimation method and presented in Table 14.1.

	1% SFC Increase	5% SFC Increase	7.5% SFC Increase
Increase in take-off mass	0.48 %	2.4%	3.7%
Increase in empty mass	0.39 %	2.0 %	3.0%
Increase in fuel mass	1.1 %	5.4%	8.2 %

Table 14.1: Sensitivity study SFC on mass

It can be seen that an 1% increase results in a 1.1% increase in fuel mass. To accommodate for this increase in mass, the structural mass needs to be increased as well, resulting in a 0.39% increase in empty mass. This corresponds to a total increase of take-off mass of 0.48%. In the Table 14.1 also an SFC increase of 7.5% is described. This would correspond to the SFC of today's advanced geared turbofan engines.

14.5. Recommendations

In this section the recommendations for further developing the propulsion system will be presented. It is highly recommended that the further investigation is performed into the engine parameters. So that these can be estimated more accurately. Furthermore, in addition to the engine type, engine location could be optimised as well. The engines could be embedded into the top aft part of the fuselage. The engines will ingest the boundary layer that develops over the aircraft fuselage. This technique, BLI, re-energises the wake of the aircraft, hence can reduce the drag of the aircraft by 5% to 10%. Also the ingestion of the slower air can increase propulsive efficiency[81].

[5] Personal correspondence with Airbus
[6] http://www.sustainableaviation.co.uk/wp-content/uploads/2015/09/SBAC-Aviation-and-Environment-Briefing-Paper-%E2%80%93-Open-Rotor-Engines.pdf [accessed on January 27th 2017]
[7] http://www.safran-aircraft-engines.com/ [accessed on January 19th 2017]
[8] https://www.flightglobal.com/news/articles/us-engine-makers-gear-up-for-2025-and-beyond-354207/ [January 27th 2017]

15. Performance

In this chapter the performance of the aircraft will be evaluated. First, the flight profile diagram will be presented. Then, the performance will be presented for every phase of flight. Then the matching plot based on these requirements is generated. Results will be compared with state-of-the-art aircraft.

15.1. Flight Profile

In Figure 15.1 the flight profile diagram is presented. The performance calculations will be based on this. The flight altitude is assumed to be 11 km, based on the flight altitude of the A320ceo [1]. In the sections below, the performance in several phases of flight are explained. On these requirements a matching plot is based. The input values are given in Table 15.1.

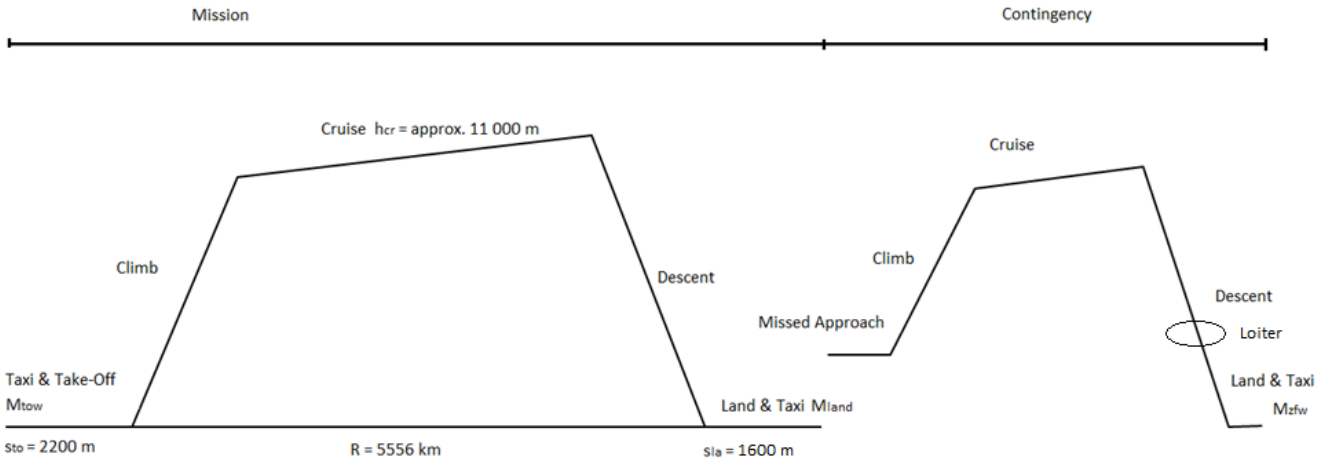

Figure 15.1: Flight profile diagram

Table 15.1: Input data matching plot

ρ_0 [kg/m^3]	1.225	C_{D_0} [-]	0.02
ρ_{1500m} [kg/^{3}]	0.974	$\Delta C_{D_{0_{toflaps}}}$ [-]	0.015
ρ_{11000m} [kg/m^3]	0.364	$\Delta C_{D_{0_{landflaps}}}$ [-]	0.065
ρ_{11887m} [kg/m^3]	0.321	$\Delta C_{D_{0_{landinggear}}}$ [-]	0.02
$V_{s_{clean}}$ [m/s]	150	e [-]	0.85
$V_{s_{land}}$ [m/s]	65	$\Delta e_{toflaps}$ [-]	0.05
$s_{land}[m]$	1,600	$\Delta e_{landflaps}$ [-]	0.1
$\frac{W_{land}}{W_{to}}$ [-]	0.8	$\Delta e_{landinggear}$ [-]	0
c [m/s]	0.5	$C_{L_{max_{clean}}}$	1.7
$\frac{c}{V}$ [-]	0.024	$C_{L_{max_{to}}}$ [-]	3.2
TOP [lb/ft^2]	190	$C_{L_{max_{land}}}$ [-]	3.4
σ [-]	1	A [-]	14
N_e [-]	2		

[1] http://booksite.elsevier.com/9780340741528/appendices/data-a/table-1/table.htm [accessed on December 15th 2016]

15.1.1. Stall Performance

First stall speed was considered. Lowering the stall speed makes the aircraft more safe and attractive. However, a higher C_L is needed, resulting in higher induced drag. Using Equation 15.1[5], the wing loading was determined for landing configuration at sea level and at 1.5 km altitude, and in clean configuration at the same altitudes. The values for the stall speed are given in Table 15.2 These values are for 1g flight.

$$\frac{W}{S} = \frac{1}{2}\rho V_s^2 C_{Lmax} \tag{15.1}$$

- $\frac{W}{S}$ = Wing Loading [N/m^2]
- ρ = Density [kg/m^2]
- V_s = Stall Speed [m/s]
- $C_{L_{max}}$ = Maximum Lift Coefficient [-]

Table 15.2: Stall speeds

Altitude	Configuration	Stall Speed [m/s]
Sea level	Landing Configuration	65
Cruise altitude	Clean Configuration	150

15.1.2. Take-Off Performance

The take-off length is a stakeholder requirement and cannot exceed 2,200 m. Other regulations that are considered for this part of the flight phase are CS25.101 and CS25.107. This was addressed using the TOP relation, Equation 15.2[41]. Four values for $C_{L_{max_{to}}}$ were considered, for which $C_{L_{to}}$ was computed using Equation 15.3. The take-off length requirement was evaluated for an airport at sea level altitude. At higher altitudes the take-off length will vary. The values are presented in Table 15.3. These values are comparable to the A320ceo and A321ceo[2].

$$TOP = \frac{W}{S}_{to} \frac{W}{T}_{to} \frac{1}{C_{L_{to}}} \frac{1}{\sigma} \tag{15.2}$$

$$C_{L_{to}} = \frac{C_{L_{max_{to}}}}{1.1^2} \tag{15.3}$$

- TOP = Take Off Parameter [N/m^2]
- $\frac{T}{W}_{to}$ = Thrust Loading at Take-Off [-]
- σ = Density ratio [-]
- $C_{L_{to}}$ = Take-Off Lift Coefficient [-]
- $C_{L_{max_{to}}}$ = Maximum Take-Off Lift Coefficient [-]

Table 15.3: Take-off runway Length

Altitude	Required Runway Length [m]
Sea level	2,200
1.5 km altitude on a hot day	3,050

[2] http://booksite.elsevier.com/9780340741528/appendices/data-a/table-1/table.htm [accessed on January 23rd 2017]

Table 15.4: Climb gradients CS25

Phase of Flight	Flaps	Landing Gear	Engines		Flight Speed	Minimum Climb Gradient OEI[%]	Minimum Climb Gradient N_e = 2[%]
Lift-off	Take-off configuration	Down	OEI	Take-off	Lift off	0	0.3
Take-off Flight Path	Take-off configuration	Up		Take-off	V_2	2.4	2.7
	Clean configuration	Up		Max. continuous power	1.25 V_s	1.2	1.5
Approach Climb	Approach configuration	Up	All Engines	Take-off	1.5 V_s	2.1	2.4
Landing Climb	Landing configuration	Down			1.3 V_s	3.2	3.2

15.1.3. Climb

The stakeholder requirement concerning the service ceiling of 39,000 ft also specifies a climb requirement, c, of 0.5 m/s at this altitude. This value was calculated using Equation 15.4 [5]. C_L and C_D are evaluated at maximum rate of climb according to Equations 15.5 and 15.6.

$$\frac{T}{W} = \frac{c}{\sqrt{\frac{W}{S}\frac{2}{\rho}\frac{1}{C_L}}} + \frac{C_D}{C_L} \tag{15.4}$$

$$C_L = \sqrt{3C_{D_0}\pi Ae} \tag{15.5}$$

$$C_D = 4C_{D_0} \tag{15.6}$$

- c = Climb speed [m/s]
- C_L = Lift Coefficient [-]
- C_D = Drag Coefficient [-]
- C_{D_0} = Zero-Lift Drag Coefficient [-]
- A = Aspect Ratio [-]
- e = Oswald Factor [-]

The climb gradients, $\frac{c}{V}$, are specified by CS25, Table 15.4. This is evaluated using Equation 15.7[5]. The critical case was the landing climb, for the one engine inoperative, OEI, case.

$$\frac{T}{W} = \frac{N_e}{N_e - N_{io}}\left(\frac{c}{V}2\sqrt{\frac{C_{D_0}}{\pi Ae}}\right) \tag{15.7}$$

- N_e = Number of Engines [-]
- N_{io} = Number of Engines Inoperative [-]
- $\frac{c}{V}$ = Climb Gradient [-]

15.1.4. Cruise

The cruise speed is specified by Airbus. This is translated into $\frac{W}{S}_{to}$ and $\frac{T}{W}_{to}$ using Equation 15.8[5].

$$\frac{T}{W}_{to} = \frac{\rho_0}{\rho_{cr}}^{\frac{3}{4}}\left(\frac{C_{D_0}\frac{1}{2}\rho_{cr}V^2}{\frac{W}{S}} + \frac{W}{S}\frac{1}{\pi Ae\frac{1}{2}\rho V^2}\right) \tag{15.8}$$

- ρ_0 = Density at sea level altitude[kg/m^3]
- ρ_{cr} = Density at cruise altitude[kg/m^3]
- V = Cruise Speed [m/s]

Payload-Range Diagram

The payload-range diagram was generated according to the outputs of the Class II Weight Estimation. These masses and other inputs are presented in Table 15.5. The fuel mass takes into account the design range of 5,556 km, plus an additional range of 400 km to fly to another airport and an additional 45 minutes of loitering time.

Table 15.5: Inputs payload-range diagram

MTOW [kg]	98,000
OEW [kg]	51,500
$M_{Fuel_{max}}$ [kg]	26,500
$C_{j_{cr}}$ [kg/N·s]	$1.36 \cdot 10^{-5}$
V_{cr} [m/s]	230
L/D_{cr} [-]	19

The range is computed using Equation 15.9. The resulting payload-range diagram is presented in Figure 15.2. The range at a maximum payload mass of 23,000 kg is 5,880 km. At the payload mass of 21,000 kg, for 200 passengers, the range is 6,650 km. This can be justified due to the fact that additional fuel is taken on board for additional range and loiter. The ferry range is computed to be 9,800 km.

$$R = \frac{V}{g \cdot c_{j\ cr}} \cdot \frac{L}{D_{cr}} \cdot ln \frac{W_{cr,begin}}{W_{cr,end}} \tag{15.9}$$

- R = Range [m]
- g = Gravitational Acceleration [m/s^2]
- c_j = Specific Fuel Consumption [kg/Ns]
- $\frac{L}{D_{cr}}$ = Lift over Drag Ratio at Cruise [-]
- $W_{cruise,begin}$ = Aircraft Weight at Start of Cruise [N]
- $W_{cruise,end}$ = Aircraft Weight at End of Cruise [N]

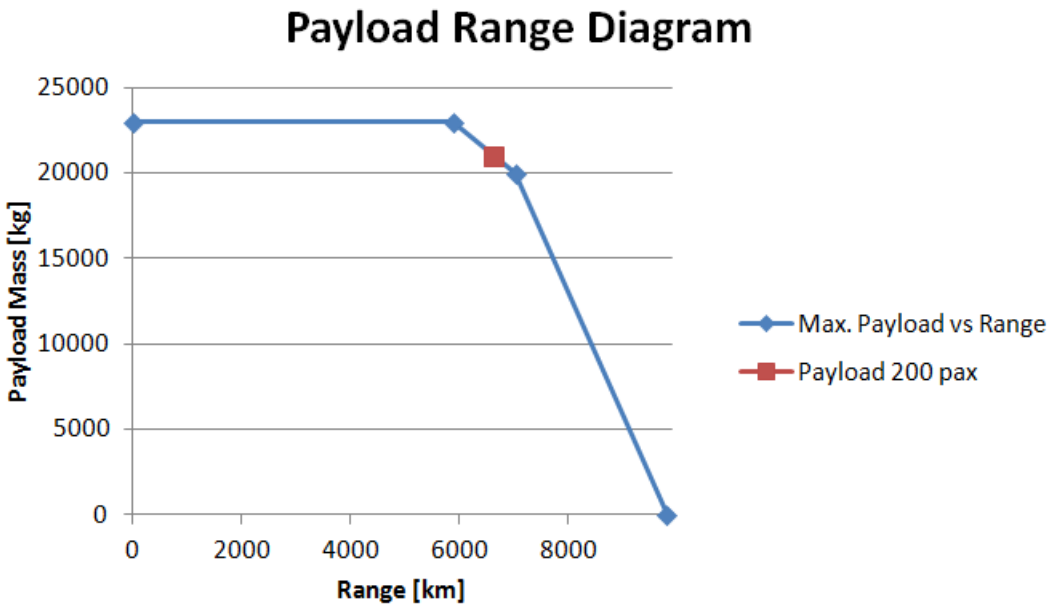

Figure 15.2: Payload-range diagram

Verification & Validation

The payload-range diagram is verified with hand calculations. The results matched 100%. For validation the values of the A320-200 and A380-800 were put into the program and the results compared with known payload-range diagrams. The input values and payload-range diagrams were found in the work by Élodie Roux [76]. Using this data the design range and ferry range computed were compared to the actual data, Table 15.6. There are slight discrepancies, these could be due to the simplifying assumptions, namely constant speed, L/D, and C_j, inherent in the Brequet range equation 15.9. Another explanation is that the L/D parameter was unknown for both aircraft and therefore approximated using reference data. The values used are 16 for the A320-200 and 18 for the A380-800, as the latter is a newer and likely more efficient aircraft.

Table 15.6: Validation payload-range diagram

	A320-200	Computed Value	Error[%]	A380-800	Computed Value	Error [%]
Design Range [km]	4,774	4,754	0.4	14,816	14,069	0.5
Ferry Range [km]	6,609	6,630	0.3	17,668	17,573	0.6

15.1.5. Landing Performance

The landing runway is evaluated using Equation 15.10 [5] at sea level and also at 1.5 km. The results for our aircraft are specified in Table 15.7. These values are comparable to the A320ceo and A321ceo[3].

$$\frac{W}{S}_{to} = \frac{C_{l_{max}} \rho \frac{s_{land}}{0.5847}}{2\frac{W_{land}}{W_{to}}} \tag{15.10}$$

- $C_{L_{max}}$ = Maximum Lift Coefficient at Landing [-]
- S_{land} = Landing Runway Distance [m]
- V = Cruise Speed [m/s]
- W_{land} = Landing Weight [N]
- W_{to} = Take-Off Weight [N]

Table 15.7: Landing performance

Altitude	Required Runway Length [m]
Sea level	1,600
1.5 km altitude at a hot day	1,900

15.2. Matching Plot

A matching plot was generated to ensure that the preliminary design complies with stakeholder requirements and that it is able to compete with existing state-of-the-art aircraft. This way the wing loading and thrust loading were estimated. The values of $C_{L_{max_{to}}}$, $C_{L_{max_{land}}}$ and A were varied, in order to estimate their effect on wing loading and thrust loading. Landing and take-off requirements constrain the wing and thrust loading. For $\frac{W}{S}$ a value of 6,900 $\frac{N}{m^2}$ can be obtained if a $C_{L_{max_{land}}}$ of 3.4 is used. If a $C_{L_{max_{to}}}$ of 3.2 is reached, a $\frac{T}{W}$ of 0.28 is possible. These values were computed with the input values found in Table 15.1. In Figure 15.3 the values for wing and thrust loading are compared to reference aircraft.

[3] http://booksite.elsevier.com/9780340741528/appendices/data-a/table-1/table.htm [accessed on January 23rd 2017]

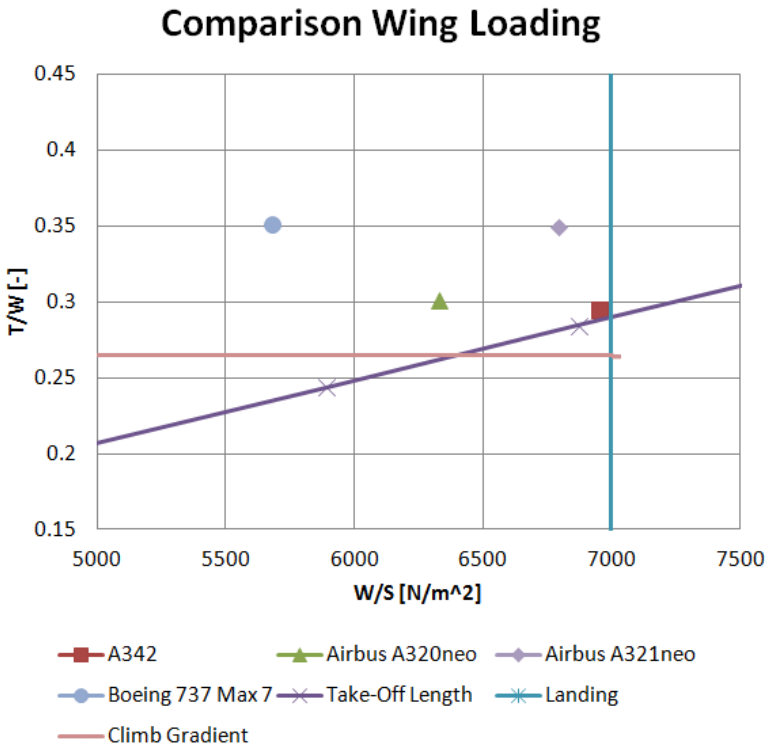

Figure 15.3: Matching Plot

15.2.1. Verification & Validation

The matching plot was verified by computing the equations by hand and comparing the results. The results matched. For the validation a matching plot of the A320ceo was created, and then compared to the values of wing loading and thrust loading computed using reference values. The results are presented in Table 15.8. Slight discrepancies can be observed. For the thrust loading this can be explained by the inaccuracy in calculating the take-off length using the TOP Take-off Parameter relation, Equation 15.2. For the wing loading the inaccuracy can be explained by the inaccuracy in estimation of $C_{l_{max}}$ values.

Table 15.8: Validation matching plot

	Estimated Value	A320ceo	Error margin [%]
T/W [-]	0.30	0.29	3.5
W/S [N/m^2]	6,000	6,250	4.0

16. Aircraft Subsystem Characteristics

In this chapter, the subsystems of the aircraft will be discussed. First the fuel tank layout will be presented, followed by the updated secondary power estimate. Then the hardware and software block diagrams, as well as the block diagrams of communication and data handling will be shown.

16.1. Secondary Power Estimate

In the Mid-term Review a secondary power estimate based on scaled up values from conventional reference aircraft was presented. The method that was used to get this estimate is not very accurate for All Electric Aircraft, AEA. Therefore, the power estimate has now been updated using a more precise method. The method that was used to gain the updated estimate is the one described by Chakraborty et al [7] [82].

Using this method, an Excel tool has been made in order to calculate the different subsystem loads based on estimated parameters. The electric loads for each flight phase and each subsystem were calculated separately in this Excel sheet.

16.1.1. Flight Control Surfaces

For the flight control surfaces, first the hinge moments were calculated. Based on those moments, it was possible to calculate the torque required by an electric motor to rotate or move the surface by a predetermined amount.The electric motor is usually connected to the surface via kinematic linkages, ball-screw mechanisms, and/or gearboxes. For the control surfaces powered by electro-hydrostatic actuators, there will also be a hydraulic cylinder and the electric motor will power a pump instead of powering the mechanical linkages directly. These components had to be accounted for as well of course, since they have their own efficiencies and gearing ratios.

The calculations for the primary control surfaces were done for each flight phase separately, in order to get the results for the different air densities, maximum surface deflections, airspeed and so on. The results gained this way still were based on the assumption that all the primary control surfaces are deployed by the maximum deflection over and over again as fast as possible. In Table 16.1 [7] a more realistic representation of the control surface usage is shown. Using this information, the ratio between necessary deployment frequency and maximum possible deployment frequency was calculated for each flight phase. Finally, the power estimates for repeated full deployment were multiplied with the calculated ratios in order to scale them down to the frequencies specified in Table 16.1.

Table 16.1: Control surface usage by flight phase [7]

	Aileron		Elevator		Rudder		Flt. Spoiler	
Phase	$+\delta/-\delta$	f [Hz]	$+\delta/-\delta$	f [Hz]	$+\delta/-\delta$	f [Hz]	$+\delta/-\delta$	f [Hz]
Ground	+1 / -1	0.4	+1 / -1	0.4	+1 / -1	0.4	1	0.4
Take-off	+0.12 / -0.2	0.4	+0.2 / -0.2	0.4	+0.2 / -0.2	0.4	0.12	0.4
Climb	+0.12 / -0.2	0.2	+0.2 / -0.2	0.2	+0.2 / -0.2	0.2	0.12	0.2
Cruise	+0.5 / -0.5	0.4	+0.3 / -0.3	0.4	+0.3 / -0.3	0.4	0.5	0.4
Descent	+0.12 / -0.2	0.3	+0.2 / -0.2	0.3	+0.2 / -0.2	0.3	0.12	0.3
Landing	+0.4 / -0.53	0.3	+0.53 / -0.53	0.3	+0.53 / -0.53	0.3	0.4	0.3

16.1.2. Landing Gear, Electric Taxi System and Nose Wheel Steering

The calculations made for the landing gear, the electric taxi system and the nose wheel steering are very similar to the calculation done for the flight control surfaces. First the torque or force required were calculated, and kinematic linkages gearboxes and such were taken into account. This again lead to the torque the electric motor needs to produce, which then could be used to calculate the sub-system power consumption.

The landing gear was assumed to be retracted at some point of time during the take-off phase, and deployed during the landing phase. The electric taxi system would be used during ground operations only, just as for the nose wheel steering.

16.1.3. Braking

For the braking system, first the torque required to decelerate the aircraft was calculated. From this it was possible to calculate the axial force required in order to produce that braking torque. Then, using the same method as for the other subsystems, the torque and power required by the electric motor were calculated. Braking was assumed to only be required during the landing phase. This is due to the fact that the landing is the only phase that is demanding on the braking system.

16.1.4. Environment Control System

For the Environment Control System, ECS, it was the goal to calculate the power required by the electric motor in order to operate the system. First the thermal loads on the cabin had to be calculated. The heat loss through the skin of the fuselage was calculated as well as the heat addition to the cabin by the metabolic heat of the passengers. The heat addition to the cabin due to energy losses of subsystems inside the cabin were also included. This resulted in a total amount of heat added to the cabin per time unit. From this it was possible to find the required mass airflow into the cabin. There are also regulations stating a minimum amount of airflow. Between those and the calculated values, the maximum was used as design value. Using this it was then possible to calculate the compressor work required to move the calculated amount of air, taking into account the pressure difference between the outside and the inside of the cabin. Finally, this lead to the power required by the electric motor.

The ECS uses power throughout all of the phases of flight, however the power it requires is different for ground operations than for flight. This is mainly due to the fact that on ground, the pressure difference between the outside and the inside of the cabin is almost zero. This reduces the amount of power required. However, the outside temperature is usually higher, which raises the required power again.

16.1.5. Ice Protection System

For an AEA the Ice Protection System (IPS) works by the principal of melting the ice off the surfaces. In order to reduce the power required, the IPS is split into zones, which then are heated one after another for a short time each. The total amount of power required was found by assuming a certain ice layer thickness, and then calculating the power required for the heating elements to melt off all of the ice in the heated zone within the specified zone heating time. The IPS was assumed to operate during ground operation, take-off, descent and landing. From the calculations it became clear that during climb and cruise, the airspeed is high enough to produce the energy required for melting the ice through aerodynamic friction alone.

16.1.6. Result

The total secondary power required for the whole aircraft was calculated based on the different operations phases. For the flight control surfaces, the maximum deflections and deployment frequencies found in the works of Chakraborty et al. [7] were used as base for the different flight phases. For the rest of the subsystems, the total power required by the electric motor was used, but those values were only added in the flight phases during which the subsystems are actually operated. Adding the power consumptions of the subsystems for each flight phase, the total power consumption was obtained, Table 16.2. The total power consumption is around 1523 kW, and it occurs during the descent phase.

Table 16.2: Total power consumptions per flight phase

Phase	Power [kW]	Phase	Power [kW]
Ground	1424	Cruise	531
Take-off	1211	Descent	1113
Climb	907	Landing	1523

16.2. Fuel Tank Layout

Fuel weight is a large part of an aircraft. Because of that, a lot of storage space for the fuel has to be reserved.

The wings of an aircraft are a suitable place for fuel storage, since the shape of the wings makes it difficult to use that space for storage of payload and most subsystems. Storing fuel in the wings also has the advantage of a bending relief. Furthermore, the location of the fuel tank has a significant influence on the centre of gravity of the aircraft. Therefore, aircraft often have small fuel tanks in the tail section. This makes a larger centre of gravity shift possible, by only pumping fuel from one tank into the other. In case the wing section does not provide enough space for all the fuel necessary to reach the design range, more fuel tanks can be stored within the fuselage. The fuel distribution system can be seen in Figure 16.1, which had been made for the Mid-term Review.

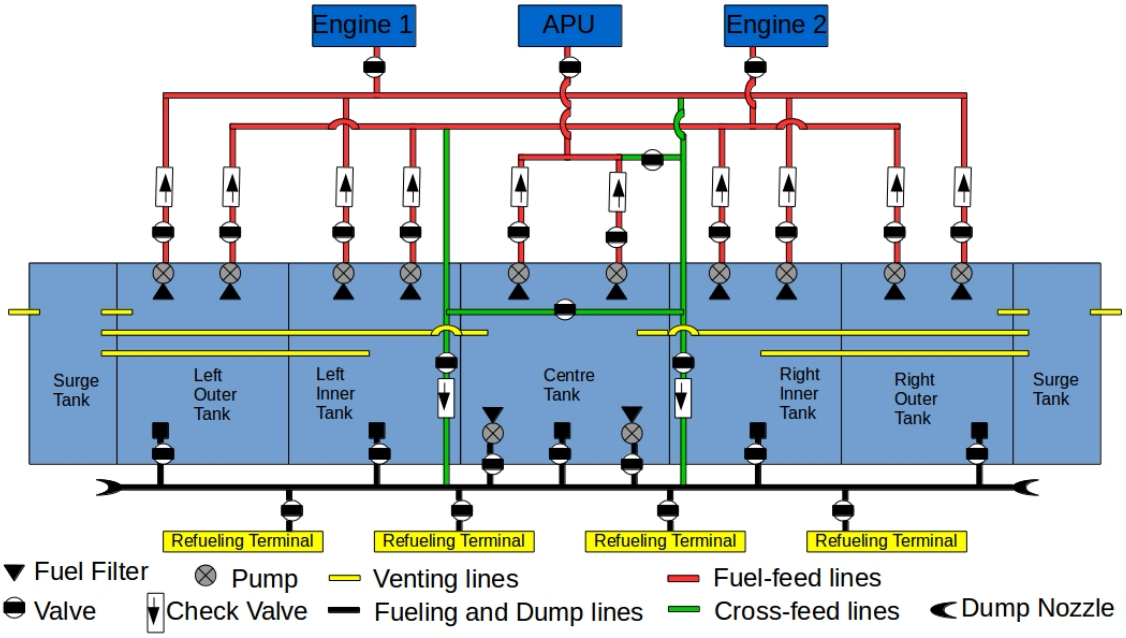

Figure 16.1: Fuel system layout

The fuel volume that can be stored within the wings is limited by the location of the spars. The calculations were done assuming the spars are located at 15% of chord and at 65% of the chord from the leading edge [83]. Also, only 85% of the span can usually be used for fuel storage. Furthermore, 5% of the volume has to be subtracted in order to account for fuel expansion due to temperature changes. Another 4% has to be subtracted to account for systems and structures that use up some of the space. The maximum fuel amount that could be stored in the wings was calculated using Equations 16.1 to 16.3 [83]. The data presented in Table 16.3 was used for the calculations.

$$V_{fuel} = \frac{L}{6} \cdot (S_1 + S_2 + \sqrt{S_1 + S_2 + S_1 \cdot S_2}) \tag{16.1}$$

$$S_1 = \frac{1}{2} \cdot (h_{r1} + h_{r2}) \cdot w_r \tag{16.2}$$

$$S_2 = \frac{1}{2} \cdot (h_{t1} + h_{t2}) \cdot w_t \tag{16.3}$$

Table 16.3: Inputs fuel volume calculations

L	43.47 m	$\rho_{kerosene}$	810 $\frac{kg}{m^3}$
h_{r1}	0.743 m	h_{t1}	0.238 m
h_{r2}	0.637 m	h_{t2}	0.204 m
w_r	5.175 m	w_t	1.656 m

The total volume available for fuel storage was calculated to be 34.98 m^3. Assuming a fuel density of 810 $\frac{kg}{m^3}$ [1], the fuel mass that can be stored in the wings was calculated to be 28,338 kg. This is well above the 26,000 kg that are needed to reach the design range. The result gained from equations 16.1 to 16.3 is valid for the whole wing, since the total span was used as input instead of the half span. Since the wing profile that is being used is rather thick (NACA 63A518), it is possible to store a lot of fuel within the wings.

16.3. Electrical Block Diagram

The electrical power systems of aircraft are quite complex, in order to facilitate the design process block diagrams are used. As the design progresses, the block diagram will be updated, and slowly transform into an actual schematic diagram of the whole electric power system.

In order to make a diagram of any kind, it is necessary to know which type of system will be designed. There are mainly three different types of power distribution systems for large commercial aircraft. Those are the split-bus power distribution system, the parallel distribution system and the split-parallel distribution system. In recent years also solid-state power distribution systems have become feasible. In a solid-state power distribution system thermal-mechanical circuit breakers are replaced by solid-state circuit boards. The basic layout of a such a solid-state system is very similar to a split-system.

16.3.1. Split Bus Power Distribution Systems

In an aircraft with a split bus power distribution system one engine driven alternator only powers one AC power bus during normal condition. In fact no bus can be powered by more than one alternator at a time in order to avoid damaging components. This is due to the fact that the phase of the alternator output is not regulated. It is however possible to let one alternator power more than one bus at a time in case of an emergency. In a modern split bus system, the APU can also be started during flight in order to provide power to one or more bus systems in case one of the engines or alternators fail. In case all alternators fail, including the Ram generator, the essential systems can also be powered by the batteries, through an inverter.

16.3.2. Parallel Power Distribution System

In a parallel power distribution system all alternators driven by the main engines are connected to the sync bus which then distributes power to the different AC loads. In order for this to be possible, the output of the different alternators have to be phase synchronised before being fed into the bus. The main advantage of this power system is that in case of failure of one alternator, the others are already connected to the bus.

16.3.3. Split-Parallel Bus Power Distribution System

A split-parallel bus power distribution system operates the same as a parallel system in normal operation, however if needed each alternator can power a single bus, as is the case in a split power distribution system. This type of system is rarely used. I can typically be found on aircraft with three engines.

16.3.4. Solid-State Power Distribution System

The solid-state power distribution system uses solid-state control units to distribute power to the different subsystems. The solid-state power distribution usually is a split system, where the thermo-mechanical switches have been replaced by solid-state electronics. Compared to more conventional systems, the solid-state type increases flexibility, safety, performance and maintainability. Using solid-state technology, it is also possible to monitor the whole electrical system during operation. Another advantage of solid-state electronics is that

[1] http://physics.info/density/ [accessed on January 19th 2017]

the Secondary Power Distribution Units, SPDU, can be located closer to the loads, which means the majority of the cables can be shorter compared to conventional systems. Problems that prevented usage of this type of systems, such as high power dissipation or the inability to interrupt a short circuit without damage, have been solved in recent years [8], which means now it is a viable design option. In fact aircraft that have recently been designed, such as the Boeing 787, already use solid-state circuit breakers and relays [2].

16.3.5. Power Distribution System Choice

It was decided to use Variable Frequency Starter Generators (VFSG). This implies that the only possible design options for the power distribution system are the split bus type and the solid-state type.In the parallel and split-parallel bus power distribution systems the alternators have to be synchronised in phase, which is only possible if they operate at exactly the same frequency, which is not the case with VFSG.

In order to decide which one of those two types of systems to use, a trade-off table was made. The table can be seen in Figure 16.2. For each criterion a score of between 0 and 1, in 0.25 steps, was given. The value of 1 being the best possible score and 0 being the worst possible score. Weights were also assigned to each criterion. The most important criteria received the highest weights. Besides the normal weights, also modified weights were used in order to see the effects different design priorities have on the result of the trade-off. In each of the weighted cases the solid-state technology won the trade-off. From this it became clear that the solid-state type is a better choice than the conventional split bus system. When also considering the fact that with split bus systems, one alternator first has to be disconnected before another alternator can be connected, this choice becomes even more clear. Solid-state systems can switch between generators faster, and they can produce a smooth transition while switching from on generator to another. In conventional split distribution systems, the transition is rather harsh on the electric components.

Weights - Modified 7	5	3	5	4	5	1	23
Weights - Modified 6	5	5	10	10	10	5	45
Weights - Modified 5	10	5	15	10	10	5	55
Weights - Modified 4	15	10	20	5	20	10	80
Weights - Modified 3	10	15	15	5	15	10	70
Weights - Modified 2	15	15	15	10	10	5	70
Weights - Modified 1	20	15	20	10	15	5	85
Weights - Normal	20	10	15	15	10	5	75

	Reliability	TRL	Weight	Number of additional functions	Cost	Complexity	Results 1	Results 2	Results 3	Results 4	Results 5	Results 6	Results 7	Results 8	MIN	MAX
Thermo-Mechanical System	0.5	1	0.5	0.5	0.5	0.5	56.67	58.82	60.71	60.71	56.25	54.55	55.56	56.52	54.55	60.71
Solid-State System	1	0.75	0.75	1	0.75	0.75	86.67	83.82	83.93	80.36	81.25	84.09	83.33	84.78	80.36	86.67

Figure 16.2: Power distribution network: Trade-off table

Using this information and looking at drawings of aircraft electrical systems in literature, a block diagram was created. This block diagram can be found in Figure 16.3. In order to increase reliability, any generator can power any SPDU, while any other (up to three) generators power the other 3 SPDUs independently. The generators in this system produce AC current. While many of the subsystems work fine with AC current, some subsystems need DC current. In Figure 16.3 it is assumed that the Primary Power Distribution Units (PPDU) as well as the SPDUs include the transformers, rectifiers and inverters necessary to supply the loads with the right type of current.

It should be noted that Generator 1 and 2 are connected to the same main engine, while generators 3 and 4 are powered by the second main engine. This means that the start batteries do not need to be connected to every generator, however being able to use either generator to start the engine will make an engine start possible even if one generator fails. The APU can be started by either using power from one of the buses, or by using power from the emergency battery.

[2] http://www.boeing.com/commercial/aeromagazine/articles/qtr_4_07/article_02_3.html [accessed on January 13th 2017]

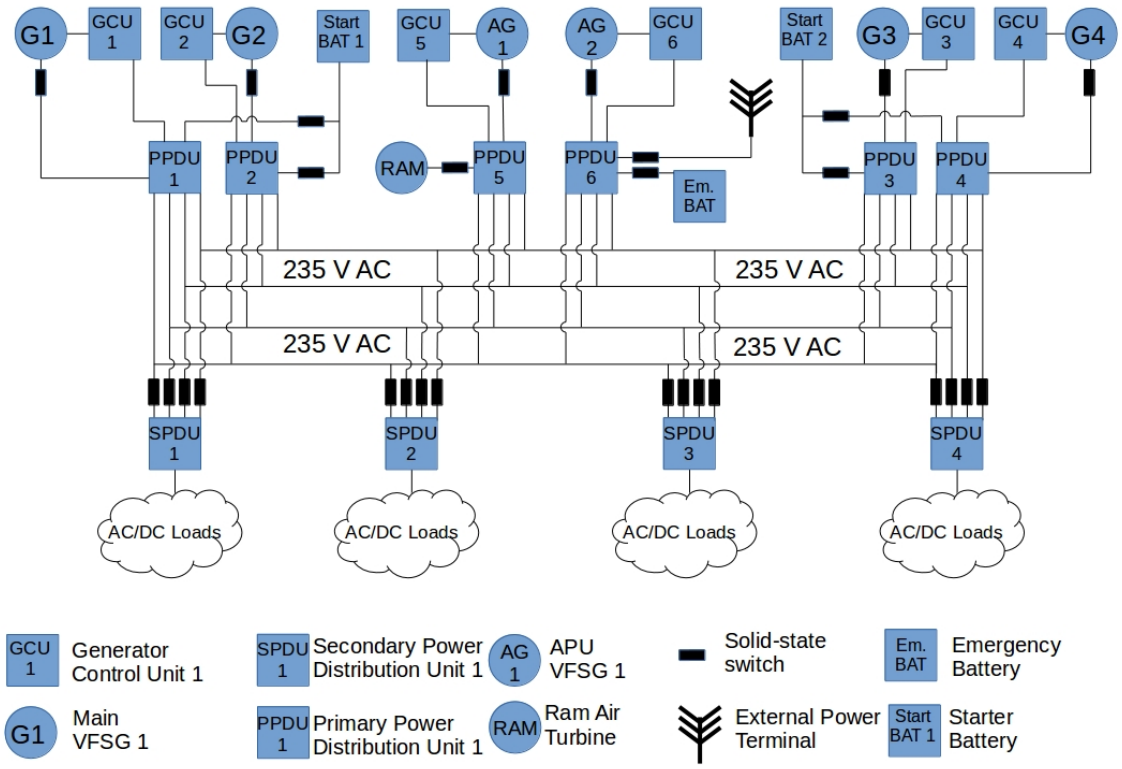

Figure 16.3: Electrical block diagram

16.4. Data Handling Block Diagram

The data handling block diagram shows the flow of data within the aircraft in an easily comprehensible way.

In order to reduce the amount of cables necessary for data handling, aircraft manufacturers have moved away from the independent avionics architecture, towards bus systems. One of the newer bus types that can be used in aircraft is the Avionics Full-Duplex Ethernet, AFDX, protocol. It is based on IEEE 802.3 10/100 Mbit Ethernet hardware, but was modified in order to increase reliability. Compared to the Ethernet protocol the loss of single frames is less likely. Due to the larger data handling capabilities of AFDX, when compared to more traditional bus systems, it is well suited for applications that require a lot of bandwidth. AFDX systems also increase flexibility, since adding new systems to a AFDX bus is a simple task. [84]

In Figure 16.4 the data handling block diagram is shown. For the bus systems the AFDX type will be used. The avionics systems have a separate bus. The same counts for the flight control systems. Separating the network into several sub-networks has the advantage that most cables can be made shorter, since a switch can be located close to the systems connected to it, with only one cable per channel going to each other switch it is directly connected to.

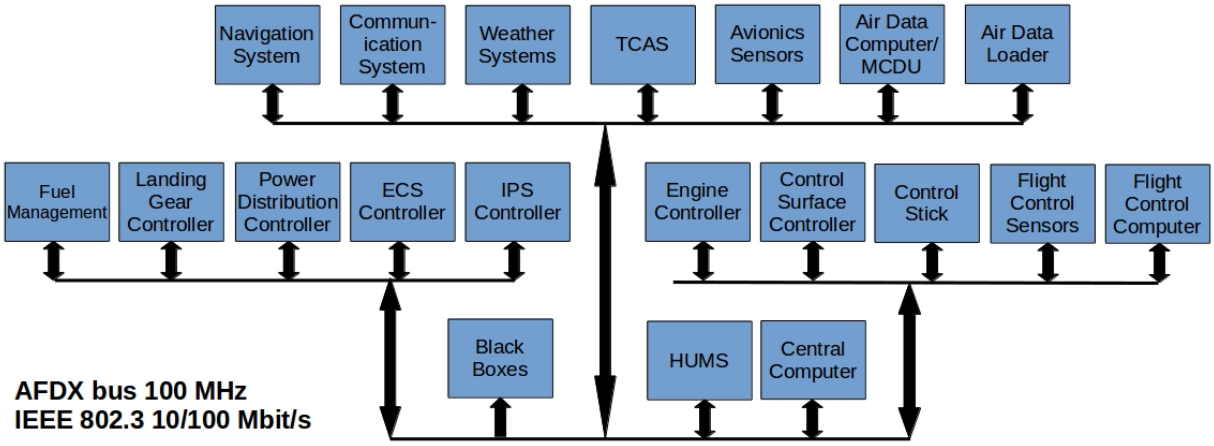

Figure 16.4: Data handling block diagram

16.5. Hardware Block Diagram

The hardware block diagram shows in a simple way how the different hardware components are related and connected to each-other.

The protocol to be used for data handling also determines part of the hardware layout. Since the AFDX protocol will be used, the logical hardware bus layout is star shaped, with a switch at the centre. Several of those star shaped sub-networks can be connected into one larger network. Figure 16.5 shows the hardware block diagram that was created for the aircraft.

The avionics main computer includes the autopilot. The air data computer has more than one task as well. It manages the systems connected to aux switch. It also manages the Multifunction Control Display Unit, MCDU. Assigning more than one task to one of the computers if favourable since it reduces the amount of CPUs necessary, which means less weight and less power consumption.

In order to increase reliability, the network will be redundant. This is not shown in Figure 16.5, but the network will be designed with two channels per connection. In case one of the channels fails, communication can still flow over the second channel. The safety critical computers also need to be redundant [84]. Usually three computers do the exact same calculations. The results are then compared, and in case of disagreement the faulty results are discarded [85]. All these redundancies, and the fact that each network node has its own controller, reduce the risk of single-point failure [84].

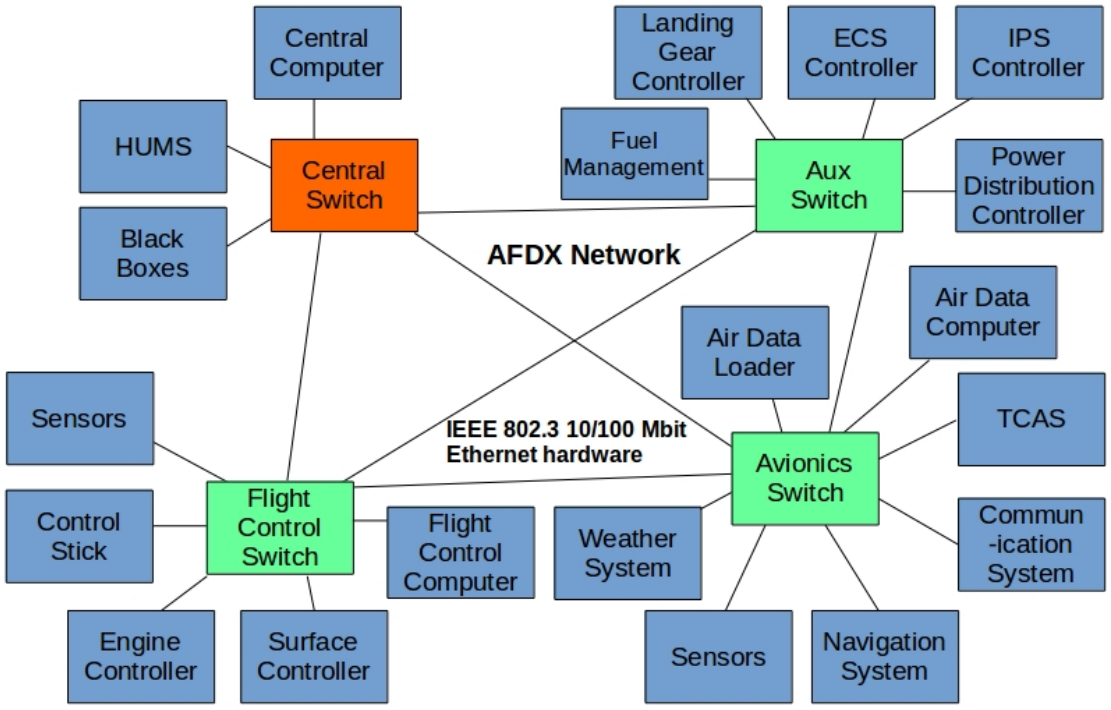

Figure 16.5: Hardware block diagram

16.6. Software Block Diagram

The software block diagram presents how the aircraft data network operates from a software point of view.

Figure 16.6 shows the software block diagram. It illustrates the interaction of the different pieces of software, and it includes a short description of the main tasks the different software blocks have to fulfil.

Figure 16.6: Software block diagram

16.7. Communication Flow Diagram

The Communication Flow Diagram depicts the flow of communications between the aircraft and the outside world, as well as the communication between the pilot and the systems, and the communication between the crew and passengers on board. The communications flow diagram can be found in Figure 16.7.

The pilot is central to the data/information flow. However, most of the input the pilot gets is from the flight computer. Flight computer receives both, communications from the ground, and signals from navigation and other systems. It is also used to provide the control commands and send out data. For internal communications, the flight attendant becomes a central figure. Passengers can not directly communicate to the pilot, but can with the flight attendants. Flight attendants can communicate with both, the passengers and the pilots. Pilots can communicate with everyone in the aircraft.

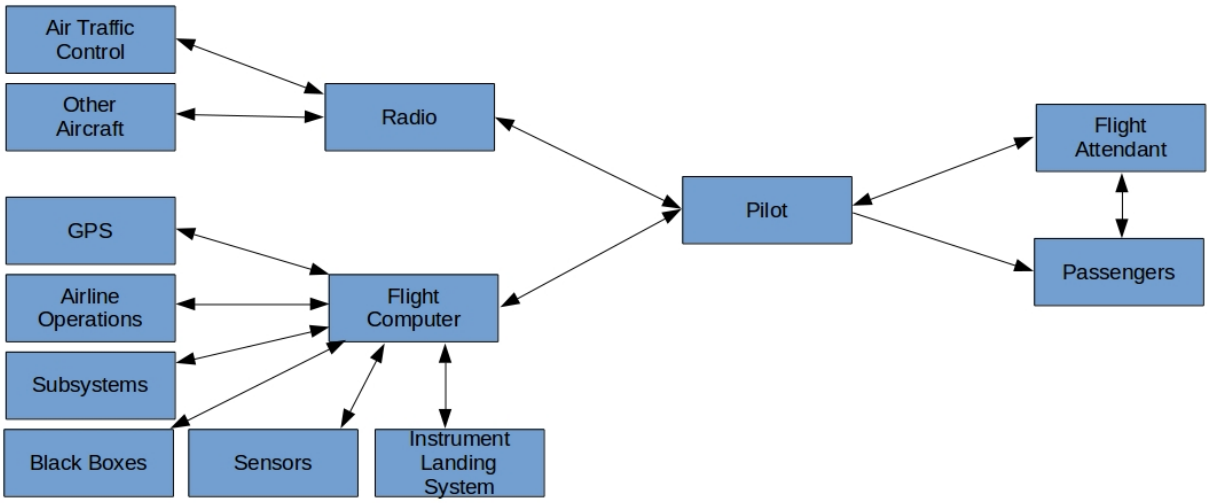

Figure 16.7: Communication flow diagram

17. Control & Stability

In this chapter, the control & stability of the aircraft will be presented. Changes in the standard fuselage design should not affect the stability and controllability to detrimental extent. To make a substantiated assessment a tool was developed, verified and validated. With the tool the tailplane could be sized. In the end of this chapter the tailplane trade-off is discussed as well as recommendations for the tail design and overall stability assessment.

17.1. Centre of Gravity

The location of centre of gravity is essential for assessing the stability. The centre of gravity was calculated by determining the aircraft component weight and their location with a class II weight estimation [41] (p.403, for cargo/transports). Combined with the operational items and dry engine weight this yields the OEW (Operational Empty Weight). Raymer's weight estimation is rather optimistic compared to other class II weight estimations from Roskam [86] and Torenbeek [71]. Therefore it was adapted to yield more conservative values. Furthermore the use of composites and an increased fuselage weight are taken into account. Therefore the design has a heavier fuselage than the A320ceo fuselage. Table 17.1 shows the global input results from the initial weight estimation, the global output results from the class II weight estimation and the individual aircraft component weights and their percentage of MTOW (Maximum Take-Off Weight).

Table 17.1: Class II results [kg]

Weight [kg]	Class I	Class II
MTOW	95,799	97,853
OEW	50,714	50,426
Fuel	26,384	26,385
Payload	21,000	21,042
Components	%MTOW	Weight
Wing	9.7%	9,462
Horizontal tail	0.7%	694
Vertical tail	0.4%	415
Fuselage	15.2%	14,879
Main landing gear	2.8%	2,729
Nose landing gear	0.4%	389
Nacelle	1.3%	1,241
Engine	6.8%	6,616
Engine control	0.03%	31
Engine starter	0.1%	90
Fuel system	0.2%	218
Flight controls	1.1%	1,098
APU	0.2%	220
Instruments	0.2%	194
Hydraulics	0.2%	163
Electronics	2.1%	2,096
Avionics	1.0%	971
Furnishing	2.1%	2,093
Air conditioning	1.0%	973
Anti icing	0.2%	209
Handling gear	0.03%	31
Operational items	5.74%	5,612

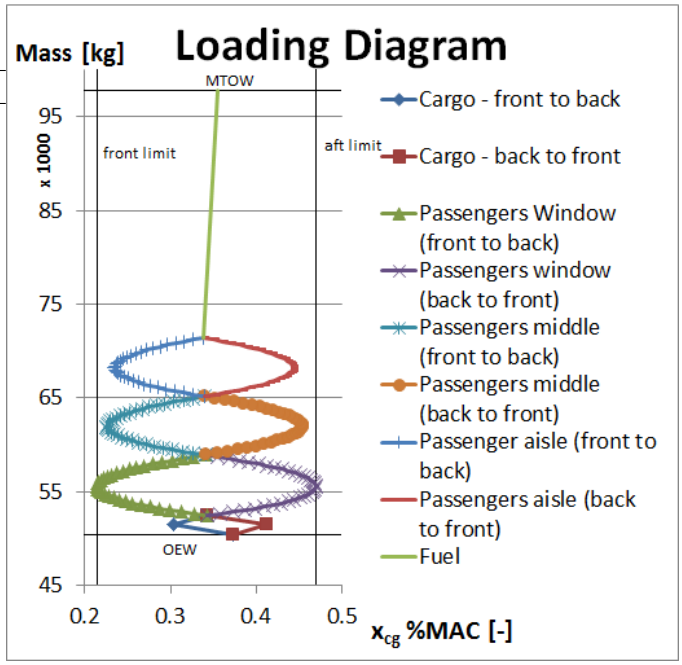

Figure 17.1: Loading diagram

By making estimations for the locations, the centre of gravity can be calculated. This can be varied by changing the the longitudinal wing position. The loading diagrams were created for 200 passengers with an assumed weight of 95 kg per passenger. This is accounting for increased carry-on luggage per passenger. The front and

aft limits of the centre of gravity are used in the next section for sizing the tailplane. They also give indications for the landing gear longitudinal location, although it does put some restrictions on the loading of the aircraft (e.g. all window seats are filled first). From the loading diagram in Figure 17.1 the centre of gravity range can be extracted. This serves as an input for the tailplane design.

17.2. Control

Controlling a large aircraft is a complicated matter and its careful investigation takes up quite some time. The aircraft is controlled by its control surfaces. The elevator for pitch control and trim, the rudder for yaw control and the ailerons for roll control, as can be seen in Figure 17.2. The main focus of this section lies on designing for static longitudinal stability and the elevator design.

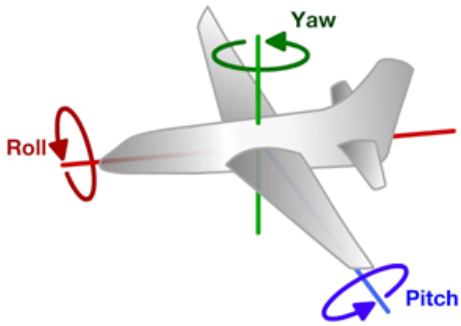

Figure 17.2: Aircraft axis system [1]

17.2.1. Horizontal Tailplane

The tailplane is essential for longitudinal stability and control. A scissors plot was created by plotting two curves for varying $\bar{x}_{c.g.}$ for different S_h/S: the controllability curve and the stability curve. This plot requires a lot of data regarding the aerodynamic centre, the zero-lift moment coefficients and the lift coefficients. Some of these calculated values are shown in Table 17.2 and the resulting scissors plot can be found in Figure 17.3.

Another requirement from the tailplane flows from the rotation on lift-off[2]. At least 8% of the aircraft weight should be carried by the nose wheel to provide acceptable traction for steering. This also implies that the main landing gear should be positioned $0.08 \cdot \Delta_{lg}$ behind the centre of gravity. Combined with the centre of gravity plot, the tail was designed on $S_h/S = 0.17$, which yields an horizontal tailplane area $S_h = 23\ m^2$.

Table 17.2: Values for stability and controllability

	x_{LEMAC} [m]	$\Delta\bar{x}_{ac_{fuselage}}$	$\Delta\bar{x}_{ac_{nacelles}}$	$\bar{x}_{ac}$	c_{m0}
Airbus A320ceo	16.3	-0.053	-0.05	0.211	-0.251
Airbus A342	19.3	-0.097	-0.029	0.314	-0.275

Trim

When the aircraft is trimmed, it is non-rotating. Figure 17.5 and Figure 17.6 show the elevator trim curve and the aircraft moment coefficient respectively for different angle of attack α. To trim the aircraft the elevator deflection δ_e decreases with increasing angle of attack α. The negative moment also increases with increasing angle of attack α, which is important for stability.

17.2.2. Vertical Tailplane

For designing the vertical tailplane of the multi-engine A342 the most critical requirement flows from the one engine inoperative scenario. In that case the Airbus A342 should be able to cope with asymmetric thrust.

[1] http://theboredengineers.com/WordPress3/wp-content/uploads/2012/05/PitchRollYaw.png [accessed on January 18th 2017]
[2] http://adg.stanford.edu/aa241/stability/taildesign.html [accessed on January 22nd 2017]

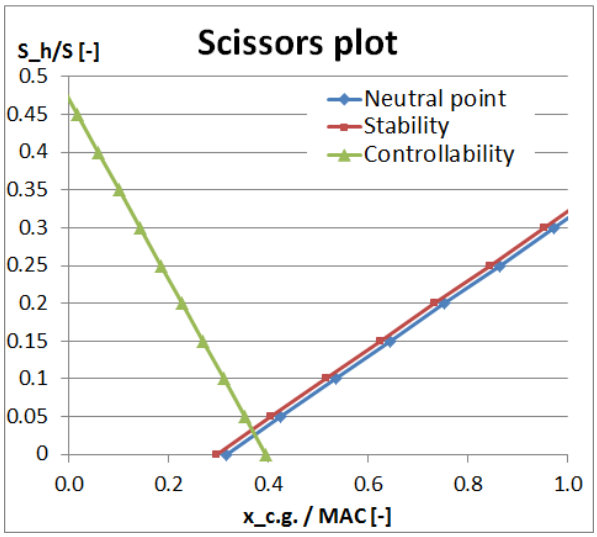

Figure 17.3: Scissors plot

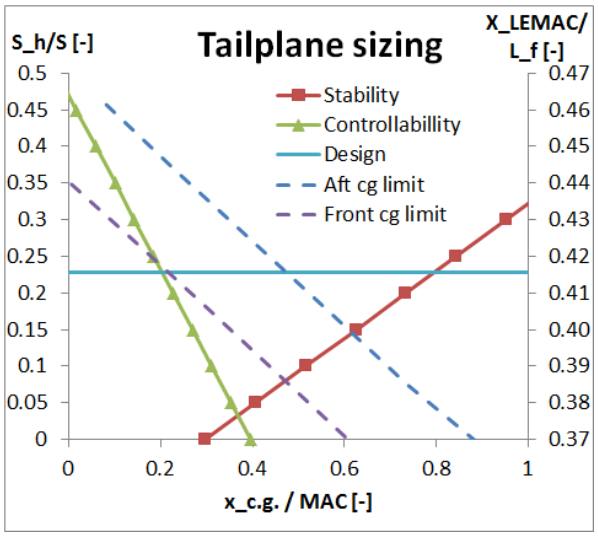

Figure 17.4: Combining with the c.o.g. limits

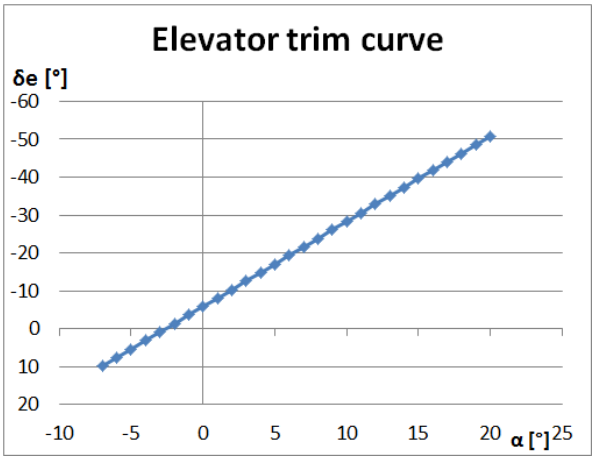

Figure 17.5: Elevator trim curve

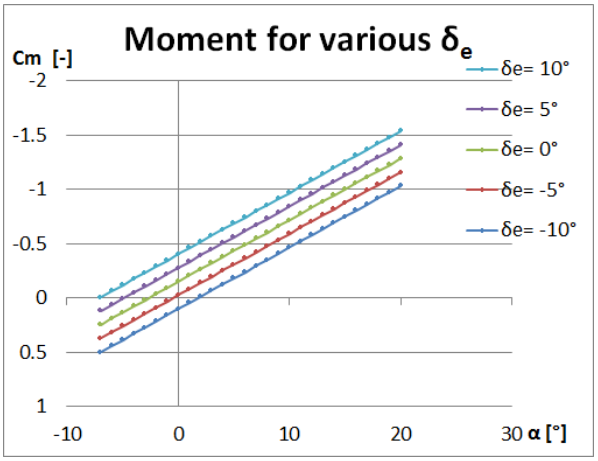

Figure 17.6: Moment for varying elevator deflection

Calculating $C_{L_{v\beta}}$ and $C_{n\beta}$ using Torenbeek[71] and Sadraey [3] and assuming rudder and aileron deflection to be zero, the maximum side slip angle $\beta = 24^o$ for take-off. Although this is larger than $\beta = 15^o$ (recommended by CS-25 regulations), it is with the rudder influence neglected. Further calculations for the rudder and overall dynamic stability (e.g. Dutch roll damping) were not conducted at this stage. The final values for the tail volume coefficients are shown in Table 17.3.

17.2.3. CONTROL SYSTEMS

The actual control of the aircraft will be executed by several flight computers. These computers can far better control the aircraft and minimise trim drag. The Airbus A342 is designed with a small static margin of 0.02 %MAC. Therefore it is still stable, as is required for the CS25 regulations. It also makes the aircraft flyable by the pilot, might a failure occur within the flight computer system. This also implies the absence of a trim tab.

[3] http://faculty.dwc.edu/sadraey/Rudder%20Design.pdf [accessed on January 22nd 2017]

Table 17.3: Tail volume coefficients

	S[m^2]	$\bar{c}$[m]	b[m]	S_H[m^2]	l_H[m]	S_V[m^2]	l_V[m]	$\bar{V}_H$[-]	$\bar{V}_V$[-]
Airbus A320ceo	122.4	4.29	33.91	31.0	13.53	21.5	12.53	0.799	0.0648
Airbus A342	136	3.22	44.46	23.0	18	21.5	17	0.94	0.06

Since the computer regulates the elevator, it is no longer required. Also all the stick forces felt by the pilot are but computer generated stick forces to create a controllable and stable feel, as is required for the CS-25 regulations as well.

For the flight control system fly-by-optics might be a future replacement for the current fly-by-wire systems. This is because of having a lower weight, an increased shielding against EMI (electronic magnetic interference) and an increased bandwidth compared to fly-by-wire systems. However, since this system is not flight proven yet, it is decided for now to incorporate a fly-by-wire control system.

17.3. Verification & Validation

The Airbus A320ceo data are used to verify and validate the class II weight estimation. In Table 17.4 the discrepancies between the model and the real life data are presented. The initial values of the wing weight and empennage weight and therefore the operational weight were lower. These values have been increased with a factor of 1.3, to generate values that lie in line with other weight estimation methods [67] and with the validation data of the component weights [87]. The discrepancies between the subsystem weights is because the class II weight estimation are calibrated on the total Operational Empty Weight and not on each individual subsystem.

Table 17.4: Verification & validation

Component Weights [kg]	Value	Verification	Discrepancy	Validation	Discrepancy
Wing	8,354.8	8,354.8	0%	8,801	5.1%
Horizontal tail	697	697	0%	625	-11.5%
Vertical tail	523.1	523.1	0%	462	-13.2%
Fuselage	9,251.6	9,251.6	0%	8,938	-3.5%
Main landing gear	2,353.5	2,353.5	0%	2,275	-3.4%
Nose landing gear	352.8	352.8	0%	-	-
Nacelle	1,376.8	1,376.8	0%	907	-51.8%
Engine	6,602.3	6,602.3	0%	6,621	0.3%
Engine control	31	31	0%	29	-6.9%
Engine starter	90.2	90.2	0%	-	-
Fuel system	217.8	217.8	0%	299	27.2%
Flight controls	1,053	1,053	0%	772	-36.4%
APU	199.6	199.6	0%	223	10.5%
Instruments	165.3	165.3	0%	71	-132.9%
Hydraulics	141.5	141.5	0%	866	83.7%
Electronics	1,657.6	1,657.6	0%	1,375	-20.6%
Avionics	971.3	971.3	0%	702	-38.4%
Furnishing	1,195.5	1,195.5	0%	2,431	50.8%
Air conditioning	952.5	952.5	0%	664	-43.5%
Anti icing	157.3	157.3	0%	30	-424.5%
Handling gear	23.6	23.6	0%	-	-
Operational items	4,795.1	4,795.1	0%	3,215	-49.1%
OEW	41,163.4	41,163.4	0%	41,500	-0.8%
Fuel	17,756.3	17,756.3	0%	17,750	0
Payload	14,143.3	14,143.3	0%	14,250	0.7%
MTOW	73,063	73,063	0%	73,500	0.6%
Stability & Tail Sizing					
x_{LEMAC} [m]	16.301	16.301	0%	16.310 [88]	0.055%
$\Delta\bar{x}_{ac_{fuselage}}$ [-]	-0.053	-0.053	0%	-0.06 [4]	11.7%
$\Delta\bar{x}_{ac_{nacelles}}$ [-]	-0.050	-0.050	0%	-0.06 [4]	16.7%
$\bar{x}_{ac}$ [-]	0.211	0.211	0%	-	-
$\bar{V}_H$ [-]	0.799	0.799	0%	0.799 [5]	0%
$\frac{S_h}{S}$ [-]	0.2	0.2	0%	0.253 [5]	20.9%

Weights - 5	10	10	7	7	5	5	10	54
Weights - 4	10	7	10	10	5	5	7	54
Weights - 3	7	7	7	7	10	7	10	55
Weights - 2	7	5	7	7	7	7	5	45
Weights - 1	10	5	10	10	7	10	10	62

	Weight	Ease of design & manufacturing	Provide Stability	Provide Controllability	Lifespan	Safety	Drag	Results 1	Results 2	Results 3	Results 4	Results 5
Conventional Tail	0.5	0.5	0.5	0.5	0.5	0.5	0.5	50.00	50	50.00	50.00	50.00
T-Tail	0.25	0.25	0.75	0.75	0.75	0.25	0.25	46.77	48.333	46.82	48.15	42.59
V-Tail	0.5	0	0.5	0.5	0.5	0.25	0.5	41.94	40.556	40.45	41.20	38.43
Canard	0.5	0	0.5	0.25	0.5	0.75	0.75	50.00	47.222	48.18	44.44	44.44

Figure 17.7: Tailplane trade-off

17.4. Trade-Off: Tailplane

In this section the tailplane is traded off. The options are limited to the conventional tail, the T-tail, the V-tail and the canard. The trade-off was conducted using engineering sense and information from the reference below.[6]

17.4.1. Weights and Criteria

The criteria are divided in weight, ease of design and manufacturing process, providing stability & controllability, lifespan, safety and drag. The conventional tailplane, mounted on the A320ceo is taken as reference at 0.5 weight. For the weight most tail planes are comparable. All non-conventional tail planes actually have lower ease of design & manufacturing. For the aerodynamics the weights are harder to assign correctly. Since a T-tail has higher efficiency, it will have better stability and controllability. It also has increased lifespan, because it is less prone to vibrations from the wing wake. The canard is even more complicated, but, if designed properly, it might have a lower trim drag. It also has the advantage of avoiding deep stall, which can be a fatal factor for aircraft.

17.4.2. Sensitivity Considerations

The weight, stability, controllability, safety and drag criteria have weight 10 for the first case, since they are assumed most critical for the direct operating costs. For the first case, the conventional tail and the canard produce similar results, mainly due to the above average safety and drag weights. For all other variations the conventional tailplane actually scores best. The complete overview can be seen in Figure 17.7.

17.4.3. Trade-Off and Results

It can be seen that for most cases the conventional tail plane is the best choice. The canard could be a possible alternative, but will create a significantly harder design process. Furthermore the drag advantages are not proven for large transport aircraft yet. Therefore it is decided to choose a conventional tailplane.

17.5. Conclusions & Recommendations

The stability and controllability can still be achieved for another fuselage shapes. That is the most important conclusion. Because the fuselage might generate more lift, deviations can occur in the resulting aerodynamic centre and the moment around the aerodynamic centre. This could potentially lead to instability. This is compensated for by the longer fuselage which is very beneficial for the stability.

Future developments would comprise of more detailed aircraft design, producing better results for the centre of gravity calculation and the tailplane sizing. Furthermore, the dynamic stability of the aircraft should be assessed in the next design phase.

[4] http://naca.central.cranfield.ac.uk/reports/1942/naca-report-751.pdf [accessed on January 20th 2017]
[5] http://booksite.elsevier.com/9780340741528/appendices/data-a/table-1/table.htm [accessed on January 20th 2017]
[6] http://faculty.dwc.edu/sadraey/Chapter%206.%20Tail%20Design.pdf [accessed on January 20th 2017]

18. Manufacturing, Assembly, Integration Plan

In this chapter, the production plan will be discussed. A production plan is of great importance to build and deliver an aircraft in a specific time span. It contains the manufacturing, assembly and integration plan. A production plan on all the aircraft components will be presented. Major components such as wings, empennage and fuselage are internally produced and assembled according to the production plan (see Figures 18.1, 18.2). Expensive parts such as engines are added last and produced externally. Since a major part of the A342 consists of composite materials, the production of this sort of materials will be discussed in Section 18.2

18.1. Manufacturing & Assembly

Before assembling the entire aircraft, the separate components have to be manufactured. Wings, control surfaces, empennage and fuselage are internally developed and manufactured. Fokker and NLR have been developing a composite landing gear, so the landing gear will be retrieved by Fokker Landing Gear. As mentioned before the engines are the most expensive parts, therefore these will be ordered from an external company and assembled at last. Next to that, the auxiliary power unit and the avionics will be externally out-sourced.

The flow chart in Figures 18.1 and 18.2 is divided into twelve separate stages, indicated by the light-grey arrows. In each stage some aircraft components are assembled or integrated together. It starts with the fuselage and the wings assembled to it, the more smaller aircraft components were assembled later on. The engines will be assembled at one of the latest stages, since these are the most expensive parts of the aircraft.

For every stage of the assembly line, a time duration of 1 week is planned. The throughput time is the time duration of twelve successive stages. In this time span one entire aircraft is assembled together. This means, the throughput time is 84 days (12 stages of 1 week).

18.2. Production of composite materials

The majority of the A342 components will be made out of carbon fibre reinforced plastics, CFRP, namely the wings, empennage and interior components of the aircraft. For the fuselage skin, sandwich construction with honeycomb core will be used. Manufacturing techniques for CFRP and sandwich constructions will therefore be discussed in this section.

The main elements of the cost of a composite are manufacturing procedures and processes. One of the main features of composite components is that they are made of fewer parts than metal components and need a reduced number of mechanical fasteners, leading to cost reductions [35].

Carbon fibres are processed in solid state and the fibre orientation allows for shape tailoring. The resin provides the desired transverse stiffness. The carbon fibre composite will be finished by curing processes. It should be noted that the machinery required for carbon composites is cheaper compared to the one needed for metals. This is because lower forces are needed to form carbon composites; in fact, shaping by hand is possible.

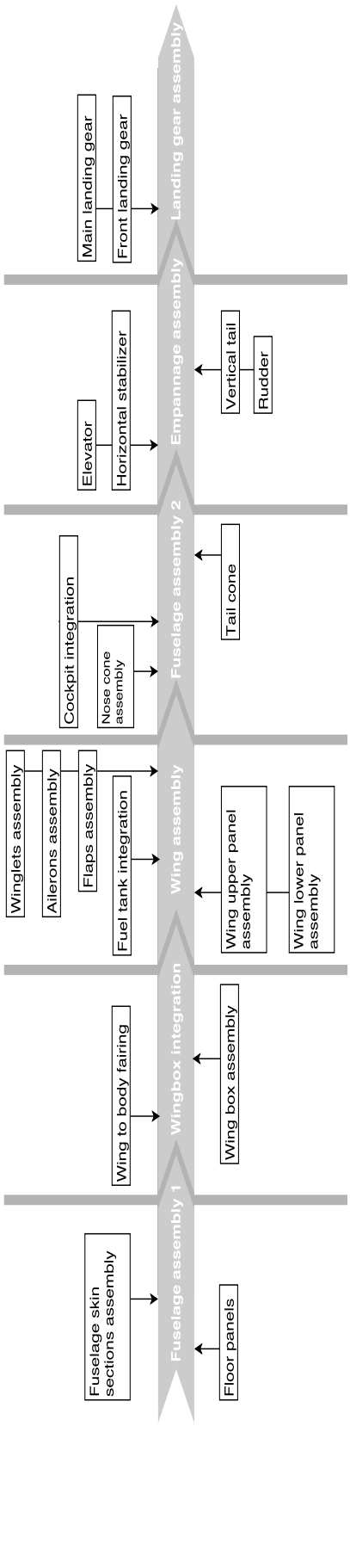

Figure 18.1: Flow chart: manufacturing, assembly and integration - part 1

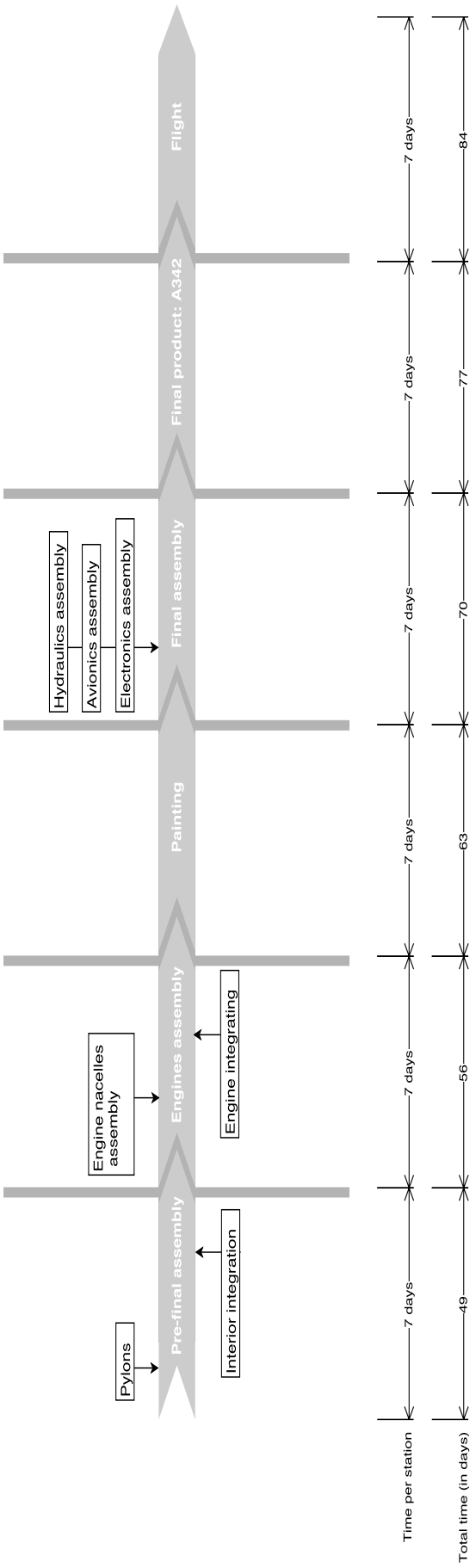

Figure 18.2: Flow chart: manufacturing, assembly and integration - part 2

19. Manufacturer & Airliner Economics

In this chapter the manufacturer and airliner economics are presented. It is important to analyse these in order to know how viable an aircraft is from business point of view. First, the cost breakdown, with the development, manufacturing and acquisition, direct operating, indirect operating, disposal and total life cycle costs are presented. Then, the profitability aspects of the aircraft are presented.

19.1. Cost Breakdown

In this section the cost breakdown structure is presented. During the design process special attention was paid to the direct operating cost of the aircraft. This is because the direct operating cost is a stakeholder requirement and directly related to the performance of an aircraft. The costs are estimated using the method of Roskam [86]. All costs and prices are shown in USD and corrected for the year 2017, unless specified otherwise.

19.1.1. Development Cost

The development costs consist of all the cost involving aircraft development. It accounts for all the activities from planning and conceptual design stages up to certification. The development costs is broken down into the cost categories each described below. The total development cost is estimated at 7.24 billion USD.

Table 19.1: Inputs development cost calculation in USD, corrected for 2017 [78] [1]

Engineering salary [USD/manhr]	117
Manufacturing salary [USD/manhr]	65
Tooling salary [USD/manhr]	65
Engine price [million USD]	13.1
Avionics system price [million USD]	7.5

Airframe Engineering and Design Cost

The activities that are included in the airframe engineering and design cost are:

- Planning, conceptual design and associated cost studies.
- Preliminary design and system integration studies, including associated cost studies.
- Engineering and design for wind tunnel models, mock-ups and engine tests.
- Design and construction of dedicated test facilities, conduct of developmental tests and static tests including system tests.
- Detailed design and development.
- Release and maintenance of drawings and specifications.
- Liaison with manufacturing and with vendors.
- Incorporation and analysis of design changes.
- Development of specifications for materials, processes and for items purchased from vendors.
- Analysis of reliability, maintainability and accessibility.

The total engineering man hours needed to complete all these tasks are based on a statistical relationship relating the take-off weight, cruise speed, number of prototype aircraft produced, a complexity factor and CAD factor. The complexity factor is an estimation of how complex the aircraft is w.r.t. conventional aircraft, the CAD factor indicates to what extend CAD methods are used in the design. Then, using the engineering USD rate per hour the total cost is computed. The engineering USD rate per hour includes direct labour, overhead, general and administrative costs and miscellaneous direct charges.

The take-off weight is provided by the Class II Weight estimation, the cruise speed based on stakeholder requirements. The number of prototype aircraft was based on the number of prototype aircraft of the A380,

[1] https://www.cfmaeroengines.com/press-articles/ryanair-to-purchase-200-cfm-leap-1b-engines-at-a-value-of-more-than-1-3b/776/ [accessed on January 14th 2017]

which was 5 in total, 2 for static tests, 3 for flying[2]. The complexity factor was assumed the highest level, at 2, which is consistent with 'aggressive use of advanced technology'. This complexity factor was chosen because the aircraft challenges the shape and material of the fuselage. The CAD factor is assumed as 0.8, since CAD methods are widely used in the design process. The engineering USD rate per hour was taken from Roskam [86], and can be found in Table 19.1 adjusted to 2017 USD.

Development Support and Testing Cost

This category of costs comprises the following activities:

- Windtunnel testing.
- Systems testing.
- Structural testing.
- Propulsion testing.
- Simulation for development support testing.

This cost is also based on a statistical relationship relating the cost to the take-off weight, cruise speed, number of prototype aircraft produced and complexity factor.

Flight Test Aircraft Cost

The flight test aircraft cost can be broken down into five different components:

- Cost of engine and avionics as acquired from vendors.
- Manufacturing labour costs.
- Manufacturing material cost.
- Tooling cost.
- Quality control cost.

The cost per engine, see Table 19.1, is based on the A320neo engines [3]. For the cost of the avionics system the value suggested by Roskam[86] was used, this amounts to approximately 5% of the aircraft list price.

The number of manufacturing man-hours required to build the prototype aircraft is based on a statistical relationship using the take-off weight, cruise speed, number of prototype aircraft produced and complexity factor. The cost of materials to manufacture the test aircraft is found using a statistical relationship relating the cost to the take-off weight, cruise speed, number of prototype aircraft produced and material factor. The material factor is assumed to be 3, based on the extensive use of composite materials.

The tooling cost is also based on a statistical relationship relating the cost to the take-off weight, cruise speed, number of prototype aircraft produced and complexity factor. Finally, the quality control cost is assumed to be a factor 0.13 of the manufacturing labour costs of the prototype aircraft.

Flight Test Operations Cost

The activities included in this cost category are flight testing and simulation activities associated with flight testing. This cost is also based on a statistical relationship relating the cost to the take-off weight, cruise speed, number of prototype aircraft used for flying produced and complexity factor.

Test and Simulation Facilities Cost

The test and simulation facilities cost estimates the cost of the facilities build for testing the new aircraft. In this stage of the design this is calculated as a factor of the total development costs. The factor used is 0.2 [86].

Cost to Finance Research & Development Phase

It is assumed that Airbus will borrow at least a part of the money to finance the development costs. The interest costs of this is calculated as a factor of the total development costs. The factor used is 0.1 [86].

[2] https://janes.ihs.com/Janes/Display/1343880 [accessed on January 18th 2017]
[3] https://www.cfmaeroengines.com/press-articles/ryanair-to-purchase-200-cfm-leap-1b-engines-at-a-value-of-more-than-1-3b/776/ [accessed on January 14th 2017]

Table 19.2: Sensitivity of development cost to variation in take-off weight

Development Cost	1% take-off weight increase	5% take-off weight increase	10% take-off weight increase
7.24 billion USD	7.29 billion USD (+0.7%)	7.48 billion USD (+3.3%)	7.71 billion USD (+6.1%)

Verification & Validation & Sensitivity Analysis

The program to calculate the development costs was verified using an example printed in [86]. The outputs matched 100%. After this the program was validated, using data from the A380. The development cost of this aircraft is estimated to be 10.7 billion USD [4].

The input parameters that were adjusted were the take-off weight, cruise speed, number of engines, engine cost and avionics cost[4] [5] [86]. Furthermore, the development cost was expressed in 2001 USD, therefore all values were adjusted to this year. This resulted in a model output of 10.6 billion USD. This is a 0.9% difference with the reference value found earlier. The model is therefore assumed to give outputs in the required range. However it cannot be said the model is validated, because the different components of the model are not validated. It is recommended to validate the model for the different components and also for aircraft closer to the designed aircraft size. Due to lack of reference data this was however not possible.

A sensitivity analysis is performed in order to estimate the variation of development cost with take-off weight. The variation of development cost per change in take-off weight is shown in Table 19.2.

19.1.2. Manufacturing Costs and Acquisition Costs

This section explains the manufacturing and acquisition costs calculation. The acquisition cost consists of the manufacturing costs and the manufacturers profit. The last will be discussed in Section 19.2.1. It is important to note that these costs are program costs. The price paid by an airliner for one aircraft can vary due to negotiations on the profit margin of the manufacturer, which is common practice.

The total manufacturing costs are estimated at 1,379 billion USD. This will translate into 58.7 million USD per aircraft produced. The manufacturing costs can be divided into the categories described below.

Airframe Engineering and Design Cost

This cost includes activities such as:

- Engineering design work required for problems uncovered after the research and development phase.
- Design studies to account for special customer wishes.
- Engineering work due to errors or changes made in manufacturing processes.
- Release and maintenance of drawings and specifications.
- Liaison engineering with manufacturing and vendors.

The total program cost of all these activities is estimated using the required engineering man-hours and the engineering man-hour rate, see Table 19.1. The required engineering man-hours is estimated using the take-off weight, cruise speed, number of aircraft produced, the complexity factor and the CAD factor. The number of aircraft produced is estimated using information from the market analysis. Airbus estimates the total deliveries of single aisle aircraft to be 23,500 over the next 20 years, see Chapter 3.

Aircraft Production Cost

The aircraft production cost consists of several cost components. They are each described in the paragraphs below.

The cost of the engines and avionics as acquired from vendors are assumed to be the same as in Section 19.1.1. The cost of the aircraft interior includes items such as seats, partitions, cabin walls, ceiling and floors, galleys, lavatories etc. The cost for interior is estimated at 8,000 USD per passenger[6].

[4] https://janes.ihs.com/Janes/Display/1343880 [accessed on January 18th 2017]

[5] http://www.rolls-royce.com/media/press-releases/yr-2015/pr-170415rolls-royce-wins-largest-ever-order-from-emirates.aspx [accessed on January 18th 2017]

[6] http://www.aircraftmonitor.com/uploads/1/5/9/9/15993320/commercial_aspects_of_aircraft_customization___v1.pdf [accessed on January 19th 2017]

Table 19.3: Sensitivity of manufacturing cost per aircraft

	Man. cost	1% increase	5% increase	10% increase
Take-off weight	58.7 mil. USD	58.8 mil. USD (+0.1%)	59.2 mil. USD (+0.9%)	59.7 mil. USD (+1.7%)
Number of aircraft	58.7 mil. USD	58.6 mil. USD (−0.1%)	58.5 mil. USD (−0.4%)	58.3 mil. USD (−0.7%)

The manufacturing labour man hours and the tooling man hours are both estimated using a statistical relationship using take-off weight, cruise speed, number of aircraft built and the complexity factor. The manufacturing material cost is estimated based on a statistical relationship using take-off weight, cruise speed, number of aircraft built and the material factor. Finally the quality control cost is estimated to be a factor 0.13 of the total manufacturing cost.

Production Flight Test Operations Cost

This cost includes the flight testing of the produced aircraft. It is based on the number of aircraft, the number of flight test hours, operating costs and a factor for overhead. It is assumed that each aircraft is tested for 10 hours. The overhead factor is assumed to be 2.

Cost of Financing the Manufacturing Program

It is assumed that Airbus will borrow at least a part of the money to finance the development costs. The interest costs of this is calculated as a factor of the total development costs. The factor used is 0.1 [86].

Verification, Validation and Sensitivity Analysis

The program to calculate the development costs was verified using an example printed in [86]. The outputs matched 100%. The program was validated using estimated manufacturing cost data. As aircraft manufacturers are very secretive about manufacturing cost it had to be estimated ourselves using revenues and profit margins published by Airbus [7].
This way the total costs Airbus makes are estimated. Dividing this by the gross number and net number of orders of the A320ceo will result in two estimates for the cost per aircraft. It has to be noted that these costs combine manufacturing costs and research, development and testing costs.
A third estimate for the cost per aircraft is to use the estimated market price for the A320ceo [8]. When the computed profit margin is deducted from this, the total cost per aircraft remains. This approach resulted in aircraft cost ranging from 43.3 million USD to 80.9 million USD, the average is 59.5 million USD.

The model was run for the A320ceo, adjusting the following input parameters: the take-off weight, cruise speed, number of engines, engine cost and avionics cost[9]. The cost per aircraft was computed by adding the development cost and manufacturing cost. This resulted in a model output of 59.5 million USD. This is the same as the average reference value found earlier. However, it is recognised that the reference values are very imprecise, and therefore this model is not fully validated. It is highly recommended to validate the program with more accurate values. It is however shown that the program gives costs in the appropriate range.

The manufacturing cost per aircraft is mainly based on the take-off weight and the number of aircraft built. Therefore, a sensitivity analysis into these parameters is performed in Table 19.3.

19.1.3. Direct Operating Costs

The direct operating cost includes crew costs, fuel costs, maintenance costs and cost of ownership. For the direct operating cost the Roskam method [86] was only partially followed. During validation it was concluded that the model output for most costs matched very well with the reference data, however maintenance costs had large deviations. Therefore, it was not decided to follow this method one to one, but rather adjust it for maintenance cost as described in the section below.

The direct operating cost is evaluated at a block range of 3,000 km. Using the performance characteristics this results in a block time of 7.3 hours, and a block speed of 413 kts. The daily utilisation is estimated at 10.6 block

[7] http://www.airbusgroup.com/int/en/news-media/press-releases/Airbus-Group-9M-2016-Results.html [accessed on January 19th 2017]
[8] https://airinsight.com/2016/05/16/aircraft-pricing-list-vs-market/ [accessed on January 19th 2017]
[9] https://janes.ihs.com/Janes/Display/1342548 [accessed on January 18th 2017]

hours per day[89]. The direct operating costs are estimated based on these values. It should be noted that the aircraft utilisation is dependent on the block time of the flight and the efficiency of the airline, therefore these values are only an indication.

Crew Cost

Crew cost is defined as the cost of the pilots and co-pilots. The cost of cabin crew is considered in the indirect operating cost. The method of Roskam [86] is used to compute crew cost. The crew cost is based aircraft characteristics and airline characteristics. Therefore it can differ per airline. Input values can be found in Table 19.4.

Table 19.4: Inputs direct operating cost

	A342 BBB	A320neo
Block range [nm]	3,000	3,000
Block time [hrs]	7.3	7.3
Block speed [kts]	416	416
Take-off mass [kg]	88,500	79,000
Cruise altitude [m]	11,000	11,000
Take-off thrust loading [-]	0.28	0.3
Take-off wing loading [N/m^2]	6,950	6,330
Aspect ratio [-]	14	9.6
Oswald factor [-]	0.85	0.85
L/D ratio [-]	19.4	17.8
C_{d_0} [-]	0.020	0.022
Annual salary pilot [USD/year]	224,000	224,000
Annual salary co-pilot [USD/year]	134,000	134,000
Number of flight hours [fl.hr/year]	3,870	3,870
Cost factor [-]	0.26	0.26
Travel expense factor [USD/bl.hr]	20	20
SFC [kg/Ns]	$1.32 \cdot 10^{-5}$	$1.43 \cdot 10^{-5}$
Fuel price [USD/gallon]	1.58	1.58
Fuel density [lbs/gallon]	6.73	6.73
Number of Engines [-]	2	2
Oil price [USD/gallon]	42.8	42.8
Oil density [lbs/gallon]	7.74	7.74
Estimated List Price [USD]	$127.5 \cdot 10^6$	$109 \cdot 10^6$
Estimated Market Price [USD]	$63.8 \cdot 10^6$	$54.5 \cdot 10^6$
Residual Value [USD]	$9.6 \cdot 10^6$	$8.2 \cdot 10^6$
Depreciation Period [USD]	20	20

Fuel and Oil Cost

The fuel and oil costs are based on the method of Roskam [86]. The amount of fuel used is calculated with the Breguet range equation 15.9. The amount of oil is estimated using the block time and the number of engines. The input values can be found in Table 19.4.

Maintenance Cost

The maintenance cost consists of labour cost, material cost and maintenance burden. It was first estimated using the Roskam method and the method was verified. However after comparison with reference data it was found that the discrepancy between the results was unacceptable.

Therefore another approach was considered, by estimating the maintenance cost as a percentage of the total direct operating cost. It was found that the percentage of total maintenance cost over the total direct cost varies

from 15% to 23% depending on the reference[89][10][11]. However as an average 18% was computed, therefore this value was used.

Cost of Ownership

The cost of ownership is defined as the sum of the depreciation costs and hull insurance costs. The depreciation costs are calculated using linear depreciation, using Equation 19.1. The input values can be found in Table 19.4. The residual value is assumed to be 15% of the original value and the depreciation period is 20 years. The list price was estimated using a linear regression of take-off weight and list prices[12]. The market price is assumed to be half this value [13]

$$Cost of Depreciation = \frac{OriginalMarketPrice - ResidualValue}{DepreciationPeriod \cdot YearlyUtilisation} \tag{19.1}$$

The hull insurance cost is calculated as a fraction of the total direct operating costs. The fraction used is 0.05.

Landing Fees, Navigation Fees and Registry Taxes

The costs of landing fees, navigation fees and registry taxes are computed using the Roskam method [86]. It was chosen to include this in the direct operating cost, but there is no clear convention on whether this should be in the direct operating cost or indirect operating cost.

Verification, Validation & Sensitivity Analysis

The direct operating calculation tool was first verified by calculating an example from Roskam [86]. For the adjusted sections the equations were calculated by hand and compared. This resulted in a 100% match. The validation required more work. The outputs of the model was scaled to several reference years and compared to reference data. The results can be found in Table 19.5 and Table 19.6.

It is striking that the fuel and oil costs calculations are very close to the reference values, whereas the operational parameters that depend on the airline, differ along a range. the reason for this is that the airline has a big influence over the crew cost, maintenance cost and cost of ownership. Since these values were not published, it is very hard to validate the data. The fuel and oil cost could be validated, since the wholesale price is widely published [14].

Table 19.5: Validation direct operating cost tool A320ceo[89] in 2012 USD

	Model Output	Reference Value	Error Margin
Crew Cost [USD/block hr]	607	562	8.0%
Fuel & Oil Cost [USD/block hr]	2,571	2,578	-0.2%
Maintenance Cost [USD/block hr]	821	774	6.1%
Cost of Ownership [USD/block hr]	564	653	-14%
Total Direct Operating Cost [USD/block hr]	4,564	4,563	-0.02%

[10] https://www.faa.gov/regulations_policies/policy_guidance/benefit_cost/media/econ-value-section-4-op-costs.pdf [accessed on January 19th 2017]

[11] https://www.eurocontrol.int/eec/gallery/content/public/documents/projects/CARE/CARE_INO_III/DCI_TDD9-0_Airline_maintenance_marginal_delay_costs.pdf [accessed on January 19th 2017]

[12] http://www.airbus.com/presscentre/pressreleases/press-release-detail/detail/new-airbus-aircraft-list-prices-for-2016/ [accessed on January 14th 2017]

[13] https://airinsight.com/2016/05/16/aircraft-pricing-list-vs-market/ [accessed on January 14th 2017]

[14] https://www.eia.gov/dnav/pet/hist/LeafHandler.ashx?n=PET&s=EMA_EPPK_PWG_NUS_DPG&f=M [accessed on 23 January 2017]

Table 19.9: Direct operating cost A342 and A320neo

	A342	A320neo	Difference [%]
Crew Cost [USD cents/passenger-km]	0.42	0.44	-6
Fuel & Oil Cost [USD cents/passenger-km]	0.80	0.84	-5
Maintenance Cost [USD cents/passenger-km]	0.36	0.37	-2
Cost of Ownership [USD cents/passenger-km]	0.38	0.34	9
Cost of Landing Fees, Navigation Fees and Registry Taxes [USD cents/passenger-km]	0.04	0.04	8
Total Direct Operating Cost [USD cents/passenger-km]	1.99	2.04	-2

Table 19.6: Validation direct operating cost tool narrow body aircraft in 2013 USD [15]

	Model Output	Reference Value	Error Margin %
Crew Cost [USD/block hr]	617	724	-15%
Fuel & Oil Cost [USD/block hr]	2,397	2,394	0.1%
Maintenance Cost [USD/block hr]	785	715	9.8%
Cost of Ownership [USD/block hr]	562	555	1.3%
Total Direct Operating Cost [USD/block hr]	4,362	4,388	-0.6%

The sensitivity of the direct operating cost is also investigated in Table 19.7. A sensitivity analysis with respect to take-off weight, SFC, and L/D is conducted in order to investigate the effect of aircraft properties on the DOC. A sensitivity analysis of the daily block hour use will be conducted to calculate the sensitivity of the DOC on the way the airline is being run.

Table 19.7: Sensitivity of DOC per block hour

	DOC [USD/block hr]	1% increase	5% increase	10% increase
Take-off weight	3,240	3,257 (+0.5%)	3,326 (+2.7%)	3,413 (+5.3%)
SFC	3,240	3,251 (+0.3%)	3,297 (+1.8%)	3,352 (+3.5%)
L/D	3,240	3,229 (−0.3%)	3,186 (−1.7%)	3,137 (−3.7%)
Daily block hour utilisation	3,240	3,233 (−0.2%)	3,207 (−1.0%)	3,177 (−1.9%)

Comparison with A320neo

The output values of the model can be found in Table 19.8. In Table 19.9 the direct operating cost is presented in dollar cents per passenger-km. It can be seen that the A342 performs slightly better than the A320neo in terms of total direct operating cost, crew, fuel and oil costs and maintenance cost per block hour. The ownership cost is higher for the A342, because of the higher estimated market value.

Table 19.8: Direct operating cost A342 and A320neo

	A342	A320neo
Crew Cost [USD/block hr]	641	641
Fuel & Oil Cost [USD/block hr]	1,217	1,221
Maintenance Cost [USD/block hr]	548	531
Cost of Ownership [USD/block hr]	576	499
Cost of Landing Fees, Navigation Fees and Registry Taxes [USD/block hr]	64	58
Total Direct Operating Cost [USD/block hr]	3,0460	2,949

[15] https://www.faa.gov/regulations_policies/policy_guidance/benefit_cost/media/econ-value-section-4-op-costs.pdf [accessed on 23 January 2017]

19.1.4. Indirect Operating Costs

The indirect operating costs are assumed to include all costs related to passengers, ground facilities, aircraft service and control and general and administrative costs. These costs are extremely dependent on the airline, rather than a property of the aircraft. Therefore these are not computed, but rather a range will be indicated for these costs as a percentage of the total operating cost.

Two sources have been found for reference data on the indirect operating cost, [89] and [16]. The indirect operating cost as a percentage of the total operating costs ranges from 46% to 48%. Therefore the average value was taken. However, a side note must be made that the percentages have shifted over the years. The values here are based on 2013 and are the most recent that were found.

19.1.5. Disposal Costs

The disposal costs are calculated according to the method of Roskam [86]. In this method the disposal costs are assumed to be 10% of the total life cycle cost. Values can be found in Table 19.10

19.1.6. Life Cycle Costs

The total life cycle costs of the aircraft consist of the sum of the development, manufacturing, total operating costs and disposal costs per aircraft. These are presented in Table 19.10. In this case the operating costs are based on the daily block hour utilisation of 10.6 hours and 20 years of service life.

Table 19.10: Life cycle costs in USD

Cost	Total Cost [USD]	Cost per Aircraft [USD]
Development Cost	$7.24 \cdot 10^9$	$0.3 \cdot 10^6$
Manufacturing Cost	$1{,}380 \cdot 10^9$	$58.7 \cdot 10^6$
Total Direct Operating Cost	$5{,}540 \cdot 10^9$	$236 \cdot 10^6$
Total Indirect Operating Cost	$4{,}912 \cdot 10^9$	$214 \cdot 10^6$
Disposal Cost	$1{,}315 \cdot 10^9$	$56 \cdot 10^6$
Total Life Cycle Cost	$13{,}150 \cdot 10^9$	$590 \cdot 10^6$

19.2. Profitability

In this section the profitability and return on investment is calculated for the manufacturer and the airline acquiring the aircraft.

19.2.1. Manufacturer Profits

In order to prove profitability of the aircraft to the aircraft manufacturer, the possible profit and return on investment are calculated. For these calculations it is assumed that Airbus both develops and manufactures the aircraft. As very little is known about the profit margin in the aircraft industry a value of 10%, suggested by Roskam [86], is used.

Based on the development and manufacturing cost per aircraft the profit per aircraft is calculated. Multiplying this value by the total predicted orders (±23500) will result in the total profit. The total predicted orders is assumed to be the same as the total number of aircraft produced estimated in section 19.1.2. Cost is comprised of total program manufacturing costs and development costs. By filling in these values in Equation 19.2, the Return on Investment (ROI) of the total project was estimated to be 0.59%.

$$ROI = \frac{RevenueFromInvestment - CostOfInvestment}{CostOfInvestment} \tag{19.2}$$

The number of aircraft sold to break even can be approximated as follows. The number of aircraft sold is treated as a variable called N. Assuming that the total manufacturing costs are distributed evenly over the number of

[16] https://www.faa.gov/regulations_policies/policy_guidance/benefit_cost/media/econ-value-section-4-op-costs.pdf [accessed on January 12th 2017]

aircraft produced Equation 19.3 will hold.

$$N = \frac{TotalDevelopmentandManufacturingCost}{MarketValuePerAircraft} \tag{19.3}$$

The number of aircraft to break even is 17,000. However, it should be noted that the market value of the aircraft is based on reference data and includes some uncertainty.

Furthermore, the net present value was calculated for the year 2037, if 23,500 aircraft were sold. In order to calculate the total profit, the costs were split into recurring costs, such as materials and engines, and fixed costs, such as development costs. It is assumed that the fixed costs occurred in the year 2017, and that the recurring cost occur each year, they depend on the amount of aircraft sold. The aircraft sold per year are estimated over a 20 year period. The discount rate used was estimated at 1% [90]. The results are presented in Figure 19.1.

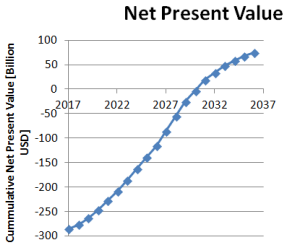

Figure 19.1: Net Present Value over 20 years

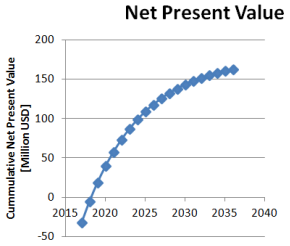

Figure 19.2: Net Present Value over 20 years

19.2.2. Operational Profit & Return On Investment

In order to prove profitability of the aircraft to the airlines it is important to calculate the return on investment. Airlines are interested in making profit, which in a very basic form can be described as in Equation 19.4.

$$GrossProfit = Revenue - Cost \tag{19.4}$$

The following strategy is used. First, the cost per nautical mile is estimated. Then, the revenue per nautical mile is estimated. Using the utilisation factor this will be transformed to profit per nautical mile. Then, since purchase cost of the aircraft is known, one can calculate the required miles of flight to break even. The approach is outlined mathematically in Equations 19.5 - 19.7. Here, $DOP_{\text{Per Nautical Mile}}$ is the direct operating costs per nautical mile, $IOC_{\text{Per Nautical Mile}}$ is the Indirect Operating Costs Per Nautical Mile, ATP is the average ticket price, PLF is the passenger load factor factor and PUC is the purchase cost.

$$\text{Cost} = DOP_{\text{Per Nautical Mile}} + IOC_{\text{Per Nautical Mile}} \tag{19.5}$$

$$\text{Revenue} = \frac{\text{ATP} * 200 * \text{PLF}}{\text{Average Trip Length}} \tag{19.6}$$

$$\text{Break Even Miles} = \frac{\text{PUC}}{\text{Revenue - Cost}} \tag{19.7}$$

$DOP_{\text{Per Nautical Mile}}$ is acquired from the developed tool, which was described verified & validated in Section 19.1.2 and results in USD 7.37. $IOC_{\text{Per Nautical Mile}}$ is acquired as described in Section 19.1.4 and results in USD 6.53. ATP is acquired from the available public records, and is equal to 349 USD [17]. Taking Lufthansa as an example airline, PLF is on average 79.3% [18]. Average trip length is assumed to be 1500 nautical miles, which is half the maximum distance of the design range. PUC is assumed to be USD 63.7 million. Substituting this into the the equations above yields that it is required to fly 2,770,000 nm to break even.

[17] https://www.rita.dot.gov/bts/airfares/programs/economics_and_finance/air_travel_price_index/html/AnnualFares.htm [accessed on January 18th 2017]

[18] https://investor-relations.lufthansagroup.com/fileadmin/downloads/en/financial-reports/interims-reports/LH-QR-2016-3-e.pdf [accessed on January 18th 2017]

It is known that the aircraft will fly about 1,600,000 nautical miles per year. This is around 4,350 nautical miles per day, assuming a year of 365 days. Now, one can estimate the days required to break even. For this, Equation 19.8 is used.

$$DaysToBreakEven = \frac{BreakEvenMiles}{MilesPerDay} \tag{19.8}$$

Substituting numbers yields that it takes 634 days to break even. Now, assuming that the aircraft will be in service for 20 years, one can say that the aircraft is profitable 91.3% of the service life. Putting this into a money perspective, the return on investment can be calculated using Equation 19.2. The return on investment is 1,055% or 670 million USD per aircraft per lifetime.
Furthermore, the net present value was calculated for the year 2037, if the aircraft were used 20 years. In order to calculate the total profit, the costs were split into operating cost, recurring per flight hour, and the acquisition cost of the aircraft. It is assumed that the aircraft was bought in the year 2017, and that the recurring cost occur each year, they depend on the amount of hours flown. The discount rate used was estimated at 10% [91]. The results are presented in Figure 19.2.

20. Design Integration

In this chapter the design integration is presented. It is divided into two main sections: research and design of a non-circular fuselage design. This chapter combines results of different research fields and provides an overview of the overall procedure and resulting product.

20.1. Research

Here, the research results of various parameters are presented and conclusions about the effects of several fuselage shapes are drawn. Referring back to the structures (Chapter 10) it was found that flat areas on the fuselage are incapable of dealing with the pressurisation stresses, at least without supporting structures. Even with supporting structures the aircraft would be heavier, which is not desired by anyone in commercial aviation.

The ellipse with a perfect fit for a given internal layout has been proven to be 6% more efficient with respect to the circumferential area, hence wetted area. However, the stress is increased by 70% with respect to the circle. Assuming a near linear relationship between the stress and the skin mass one can prove that the mass of the ellipse will still be higher than the one of a circle.

From aerodynamics, chapter 12 point of view, the ellipse has an L/D of 19.4, while the circle has 19, which is an improvement of around 2%. Comparison of the ellipse and the rounded rectangle indicates a 1.5% improvement of L/D. However, rectangle analysis was not accurate enough to provide a definitive number. In any case, one can draw a conclusion with the given data. The rectangle is not feasible structurally.

An interesting phenomena to visualise is how various parameters change when changing the shape from circle to rectangle or ellipse. As it can be seen in Figure 20.1, the skin weight increases when one deviates from the circle, which would mean that the circle outperforms the rest with respect to the other shapes. However, as it can be seen in the figure 20.2, L/D is actually higher in both, an ellipse and a rounded rectangle, than in a circle. So while structurally circle performs best, aerodynamically it is an ellipse which wins.

It would be interesting to see what would these changes result in with respect to the direct operating costs and this is presented in the table 20.1. As it can bee seen, the direct operating costs and fuel burn are comparable when it comes to an elliptical and and circular fuselages. The L/D increase of the ellipse evidently compromises for the small weight increase in total take-off weight due to skin weight increase. Rectangular fuselage DOC's were not calculated since the models have not been accurate enough and even so indicate are worse performance than that of an ellipse.

Table 20.1: Direct operating cost and fuel burn comparison for different fuselage shapes

	Circle	Ellipse
Total Direct Operating Cost [USD/nm]	7.35	7.37
Total Fuel Cost [USD/nm]	2.94	2.96

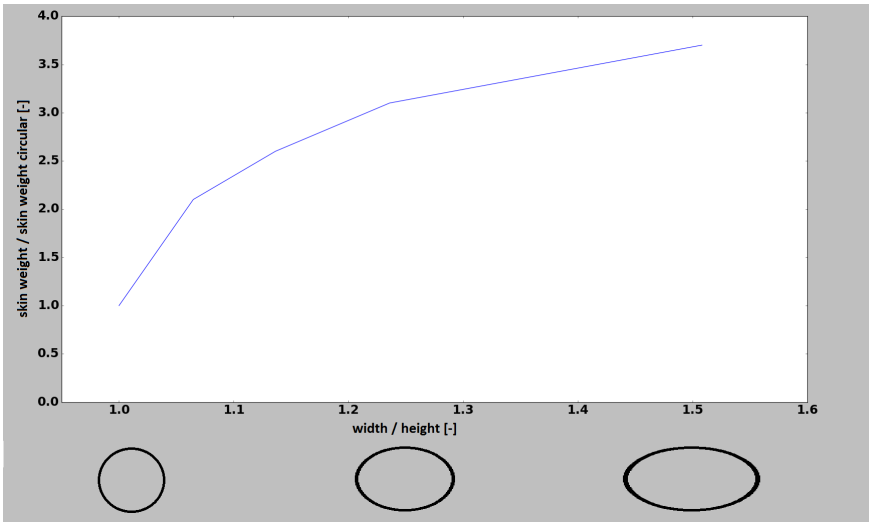

Figure 20.1: Skin weight change when varying the fuselage shape from ellpise to a circle

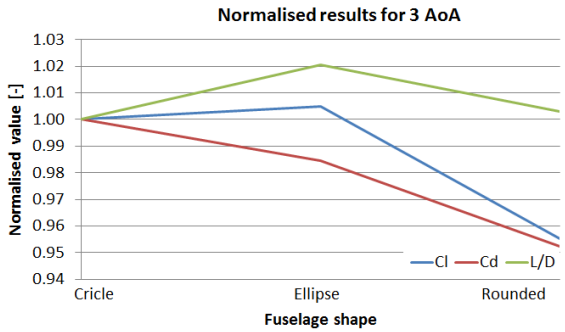

Figure 20.2: Normalised results for different fuselage shapes

20.2. Design Procedure & Results

Different departments worked on different aspects of the the aircraft. The design integration strategy is summed up in Figure 20.3. The large middle rectangle encapsulates the design integration. The right-most one provides the list of design output. Rectangles around the integration rectangle illustrate input information sources. The integrated design parameters are in Table 20.2, with an accompanying picture Figure 20.3.

In general, the design procedure was carried out as follows. The class 1 & 2 weight estimation tools were being built while the interior design department designed the inside of the aircraft. Once the inside of the aircraft was finalised, it was passed structures and aerodynamics departments to determine the outer fuselage & fuselage shape. The shape was chosen to be either rounded rectangle, ellipse or a circle. The dimensions were chosen such that there is a perfect i.e the wetted area is minimised while still fitting the interior shape. The reader is referred to Chapter 9 to read more about the interior choice and this procedure. Aerodynamic and structural analysis is then performed on those shapes and overall aircraft shape is known. At this point inputs are made into the middle rectangle of the 20.3. Stability & Control and Performance & Propulsion departments were developing tools in the mean time. Once all the tools have been verified & validated, the input parameters were tuned and finalised according to the flow of the Figure 20.3.

Table 20.2: A342 Beeblebrox characteristics

Parameter	Value
W_{OEW} [kg]	45600
W_{Fuel} [kg]	26000
$W_{Payload}$ [kg]	21000
W_{MTOW} [kg]	89000
L/D [-]	19.4
$C_{L_{max}}$ [-]	1.7
$C_{D_{cruise,\ design}}$ [-]	0.03
Take Off Length [m]	2,200
Fuel Consumption [kg/N·s]	$1.32 \cdot 10^{-5}$
Direct Operating Costs [USD per NM]	7.37
Manufacturing Cost Per Aircraft [million USD]	58.9
Cruise Altitude [m]	11,000
Secondary Power Consumption [MW]	1.5
Aspect Ratio [-]	14
Wing Span [m]	43.6
Aircraft Length [m]	44.5
Major Axis [m]	2.125
Minor Axis [m]	1.409
Seat Pitch [m]	0.71
Seat Width [m]	0.5
W/S [N/m^2]	6950
T/W [-]	0.28
Operational Time Per Day [block hr]	10.6
Life Cycle [year]	20
Recyclability	100%

Table 20.3: Integrated design - A342 Beeblebrox

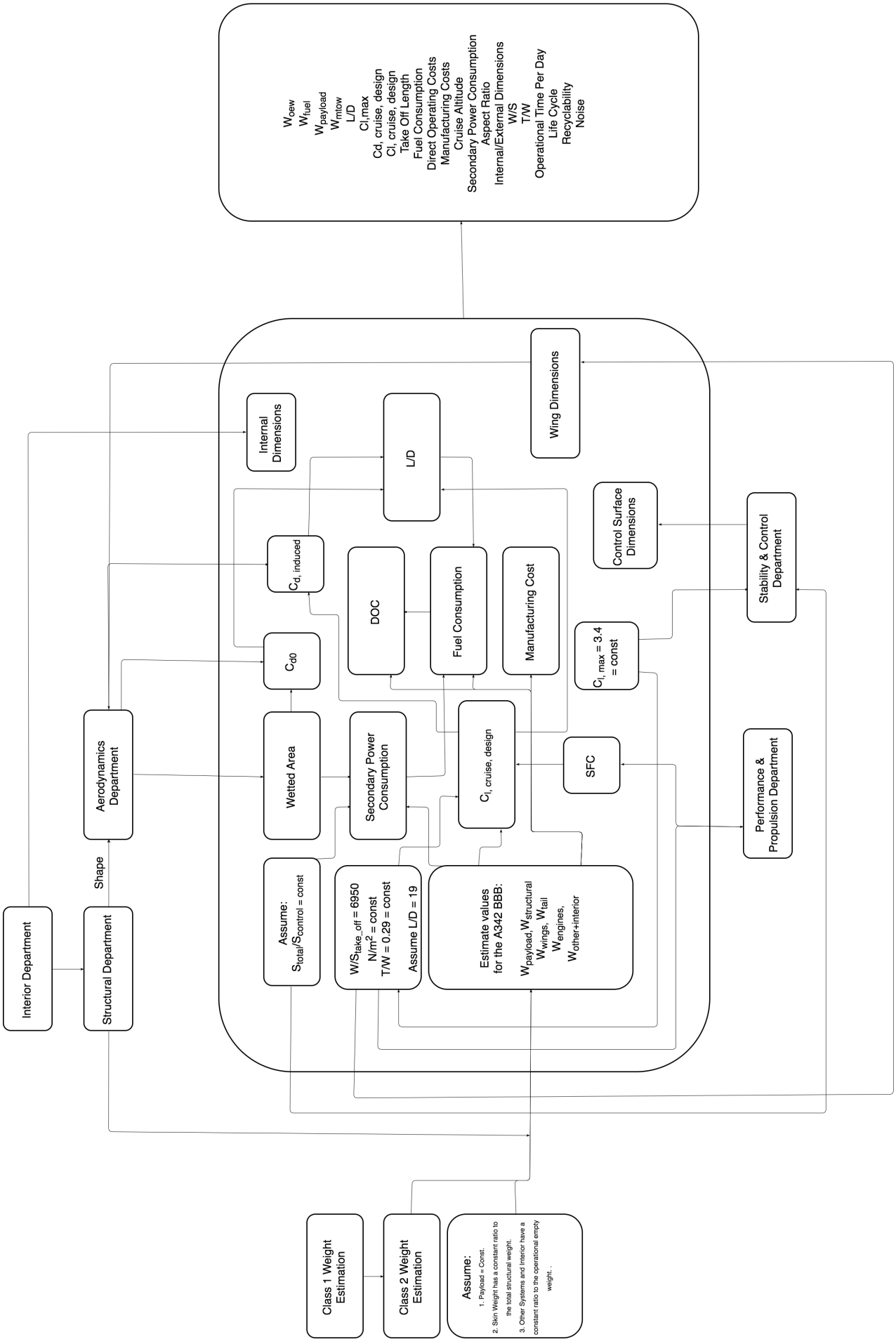

Figure 20.3: Design Integration Scheme

21. Compliance Matrix

In this chapter the compliance matrix is presented. Compliance matrix indicates which requirements are met and provides a traceable link to the proof. It can be found in the Tables 21.1 to 21.5. The first column indicates the requirement code, the second column indicates the Airbus A342 status against that requirement and the last column indicates where a proof can be found. Regarding the status, there are different codes the reader has to be familiar with: **C** means that design complies with the requirement, **C*** means that design complies with the updated requirement, **P** means that the design partially agrees with the requirement, **F** means that the design fails to meet the requirements, **NA** means that requirement was not yet addressed by the design and will be done in the preliminary or detailed design stage. All references are made to the chapters of this report. The requirements corresponding to the requirement codes can be found in the Baseline Report [2].

Table 21.1: Compliance matrix, part 1

Requirement	Status	Proof
CFSM-COC-01	NA	This requirement will be addressed in the later stages of design
CFSM-COC-02	NA	This requirement will be addressed in the later stages of design
CFSM-COC-03	NA	This requirement will be addressed in the later stages of design
CFSM-COC-04	NA	This requirement will be addressed in the later stages of design
CFSM-COC-05	NA	This requirement will be addressed in the later stages of design
CFSM-COC-06	NA	This requirement will be addressed in the later stages of design
CFSM-COC-07	NA	This requirement will be addressed in the later stages of design
CFSM-COC-08	NA	This requirement will be addressed in the later stages of design
CFSM-CAC-01	C	While seating is not decided on, budget and space is ready 9
CFSM-CAC-02	C	Interior has been designed, budget was set for improvements 9
CFSM-CAC-03	NA	This requirement will be addressed in the later stages of design
CFSM-CAC-04	NA	This requirement will be addressed in the later stages of design
CFSM-PAS-01	C	This has been designed and described in 9
CFSM-PAS-02	C	This has been designed and described in 9
CFSM-PAS-03	C	This has been designed and described in 9
CFSM-PAS-04	C	Structure has been prepared for this pressure 10
CFSM-PAS-05	NA	This requirement will be addressed in the later stages of design
CFSM-PAS-06	NA	This requirement will be addressed in the later stages of design
CFSM-PAS-07	C	Silent propulsion method has been chosen 15
CFSM-PAS-08	NA	This requirement will be addressed in the later stages of design
CFSM-PAS-09	NA	This requirement will be addressed in the later stages of design
CFSM-ALC-01	C	The aircraft is designed around this requirement 15
CFSM-ALC-02	C	This requirement has been exceeded 15
CFSM-ALC-03	C	This has been chosen as design speed 15, 12
CFSM-ALC-04	C	It has been designed for this requirement 15
CFSM-ALC-05	C	It has been designed for this requirement 15
CFSM-ALC-06	C	It has been designed for this requirement 15
CFSM-ALC-07	C	It has been designed for this requirement 8
CFSM-ALC-08	C	It has been designed for this requirement 15
CFSM-ALC-09	C	It has been designed for this requirement 15
CFSM-ALC-10	C	It has been designed for this requirement 7
CFSM-ALC-11	NA	This requirement will be addressed in the later stages of desig
CFSM-ALC-12	C	This requirement has been met and is described 12
CFSM-ALC-13	NA	his requirement will be addressed in the later stages of design

Table 21.2: Compliance matrix, part 2

Requirement	Status	Proof
CFSM-ACM-01	C	Non-toxic materials have been chosen 11
CFSM-ACM-02	C	This is designed for by default 18
CFSM-ACM-03	C	This is designed for by default 18
CFSM-ACM-04	C	This is designed for by default 18, 8
CFSM-ACM-05	C	This is designed for by default 18
CFSM-ACM-06	NA	This has not been confirmed
CFSM-ACM-07	F	Only the conceptual design has been performed
CFSM-ACM-08	C	The aircraft is conventional takes CS25 into consideration 7
CFSM-AGP-01	C	The aircraft has windows
CFSM-AGP-02	C	Span is determined 9.2
CFSM-AGP-03	C	It has been designed for this requirement 7
CFSM-AGP-04	NA	This requirement will be addressed in the later stages of design
CFSM-RMC-01	NA	This is up to an airline. Access is granted
CFSM-RMC-02	NA	This is up to an airline. Access is granted
CFSM-RMC-03	NA	This is up to an airline. Access is granted
CFSM-RMC-04	NA	This is up to an airline. Access is granted
CFSM-RMC-05	NA	This requirement will be addressed in the later stages of design
CFSM-GOV-01	NA	At this point it is not known if all 600+ of CS25 requirements are met
CFSM-GOV-02	C	Engine exceeds these requirements 14
CFSM-GOV-03	NA	Current regulations are met but future can imply new requirements
CFSM-GOV-04	C	Engine exceeds these requirements 14
CFSM-RCA-01	C	Engine exceeds these requirements 14
CFSM-RCA-02	C	Engine exceeds these requirements 14
CFSM-S-01	NA	At this point it is not known if all 600+ of CS25 requirements are met
CFSM-S-02	C	This is achieved through control surfaces and electronics 17, 16
CFSM-S-03	C	It has been allocated 9
CFSM-S-04	C	Wings provide enough lift 12
CFSM-S-05	C	This is designed for by default 7, 16
CFSM-S-06	NA	This is up to an airline
CFSM-S-07	C	Aisles and space are allocated 9
CFSM-S-08	NA	This is up to an airline
CFSM-S-09	C	Aisles and space are allocated 9
CFSM-S-10	C	200 seats have been allocated 9
CFSM-S-11	C	Performance calculations indicate that's exceeded 15
CFSM-S-12	C	Performance calculations indicate that's exceeded 15
CFSM-S-13	C	This speed was taken as a design speed 15
CFSM-S-14	C	Aerodynamic calculations indicate that's met 15
CFSM-S-15	C	Performance calculations indicate that's met 15
CFSM-S-16	NA	These numbers are subjects to change
CFSM-S-17	C	This altitude was used as a design altitude 15
CFSM-S-18	C	Fuel efficient engines have been chosen 14
CFSM-S-19	C	Fuel efficient engines have been chosen 14
CFSM-S-20	C	Reliable subsystems have been chosen 7
CFSM-S-21	C	Fuel efficient engines have been chosen 14
CFSM-S-22	C	Costs are shown in 19
CFSM-S-23	C	This is designed for be default
CFSM-S-24	NA	This requirement will be addressed in the later stages of design
CFSM-S-25	NA	This requirement will be addressed in the later stages of design

Table 21.3: Compliance matrix, part 3

Requirement	Status	Proof
CFSM-S-CGN-01	C	This has been designed and described in chapter 17
CFSM-S-CGN-02	NA	This requirement will be addressed in the later stages
CFSM-S-CGN-03	NA	This requirement will be addressed in the later stages
CFSM-S-CGN-04	NA	This requirement will be addressed in the later stages
CFSM-S-CGN-05	NA	This requirement will be addressed in the later stages
CFSM-S-CGN-06	NA	This requirement will be addressed in the later stages
CFSM-S-CGN-07	NA	This requirement will be addressed in the later stages
CFSM-S-CGN-08	NA	This requirement will be addressed in the later stages
CFSM-S-CGN-09	NA	This requirement will be addressed in the later stages
CFSM-S-CGN-10	NA	This requirement will be addressed in the later stages
CFSM-S-CGN-11	NA	This requirement will be addressed in the later stages
CFSM-S-CGN-12	NA	This requirement will be addressed in the later stages
CFSM-S-CGN-13	NA	This requirement will be addressed in the later stages
CFSM-S-CGN-14	NA	This requirement will be addressed in the later stages
CFSM-S-CGN-15	NA	This requirement will be addressed in the later stages
CFSM-S-CGN-16	NA	This requirement will be addressed in the later stages
CFSM-S-CGN-17	NA	This requirement will be addressed in the later stages
CFSM-S-CGN-18	P	This has been partly designed and described in chapter 17
CFSM-S-CGN-19	NA	This requirement will be addressed in the later stages
CFSM-S-CGN-20	NA	This requirement will be addressed in the later stages
CFSM-S-CGN-21	NA	This requirement will be addressed in the later stages
CFSM-S-CGN-22	NA	This requirement will be addressed in the later stages
CFSM-S-CGN-23	P	This has been partly designed and described in chapter 17
CFSM-S-CGN-24	NA	This requirement will be addressed in the later stages
CFSM-S-ADFI-01	P	This requirement was taken into account in Chapter 16 .
CFSM-S-ADFI-02	P	This requirement was taken into account in Chapter 16 .
CFSM-S-ADFI-03	P	This requirement was taken into account in Chapter 16 .
CFSM-S-ADFI-04	NA	This requirement will be addressed in the later stages of design.
CFSM-S-ADFI-05	P	This requirement was taken into account in Chapter 16 .
CFSM-S-ADFI-06	P	This requirement was taken into account in Chapter 16 .
CFSM-S-ADFI-07	P	This requirement was taken into account in Chapter 16 .
CFSM-S-ADFI-08	P	This requirement was taken into account in Chapter 16 .
CFSM-S-ADFI-09	P	This requirement was taken into account in Chapter 16 .
CFSM-S-ADFI-10	P	This requirement was taken into account in Chapter 16 .
CFSM-S-ADFI-11	P	This requirement was taken into account in Chapter 16 .
CFSM-S-ADFI-12	P	This requirement was taken into account in Chapter 16 .
CFSM-S-ADFI-13	P	This requirement was taken into account in Chapter 16 .
CFSM-S-ADFI-14	P	This requirement was taken into account in Chapter 16 .
CFSM-S-ADFI-15	P	This requirement was taken into account in Chapter 16 .
CFSM-S-ADFI-16	P	This requirement was taken into account in Chapter 16 .
CFSM-S-ADFI-17	P	This requirement was taken into account in Chapter 16 .
CFSM-S-ADFI-18	P	This requirement was taken into account in Chapter 16 .
CFSM-S-ADFI-19	P	This requirement was taken into account in Chapter 16 .
CFSM-S-ADFI-20	NA	This requirement will be addressed in the later stages of design.
CFSM-S-ADFI-21	NA	This requirement will be addressed in the later stages of design.
CFSM-S-ADFI-22	P	This requirement was taken into account in Chapter 16 .
CFSM-S-ADFI-23	NA	This requirement will be addressed in the later stages of design.
CFSM-S-PC-01	P	This is up to the airline. Seating spaces for flight attendants have been taken into account
CFSM-S-PC-02	C	This requirement is exceeded 9
CFSM-S-PC-03	C	This requirement has been met 9

Table 21.4: Compliance matrix, part 4

Requirement	Status	Proof
CFSM-S-PC-04	C*	This requirement has been met 9
CFSM-S-PC-05	NA	This requirement will be addressed in the later stages of design 9
CFSM-S-PC-06	C*	This requirement has been met 9
CFSM-S-PC-07	C	This requirement has been met 10
CFSM-S-PC-08	NA	This requirement will be addressed in the later stages of design
CFSM-S-PC-09	NA	This requirement will be addressed in the later stages of design
CFSM-S-PC-10	NA	This requirement will be addressed in the later stages of design
CFSM-S-PC-11	NA	This requirement will be addressed in the later stages of design
CFSM-S-PC-12	NA	This requirement will be addressed in the later stages of design
CFSM-S-PC-13	C	This requirement is exceeded 9
CFSM-S-PC-14	NA	This requirement will be addressed in the later stages of design
CFSM-S-PC-15	C	This requirement has been met 9
CFSM-S-PC-16	NA	This requirement will be addressed in the later stages of design
CFSM-S-PC-17	NA	This requirement will be addressed in the later stages of design
CFSM-S-PC-18	C	This requirement has been met 9
CFSM-S-PC-19	NA	This requirement will be addressed in the later stages of design
CFSM-S-PC-20	NA	This requirement will be addressed in the later stages of design
CFSM-S-PC-21	NA	This requirement will be addressed in the later stages of design
CFSM-S-PC-22	C	This requirement has been met 9
CFSM-S-PC-23	C	This requirement has been met 9
CFSM-S-LS-01	C*	This requirement has been updated and met 17
CFSM-S-LS-02	C*	This requirement has been updated and met 17
CFSM-S-LS-03	C*	This requirement has been updated and met 9.2
CFSM-S-LS-04	C*	This requirement has been updated and met 9.2
CFSM-S-LS-05	C	This requirement has been met 9.2
CFSM-S-LS-06	C	This requirement has been met 12
CFSM-S-LG-01	NA	This requirement will be addressed in the later stages of design
CFSM-S-LG-02	NA	This requirement will be addressed in the later stages of design
CFSM-S-LG-03	NA	This requirement will be addressed in the later stages of design
CFSM-S-LG-04	NA	This requirement will be addressed in the later stages of design
CFSM-S-P-01	C	This requirement has been met 15
CFSM-S-P-02	C	This requirement has been met 15
CFSM-S-P-03	C	This requirement has been met 14
CFSM-S-P-04	C	This requirement has been met 14
CFSM-S-P-05	NA	This requirement will be addressed in the later stages of design
CFSM-S-P-06	C	This requirement has been met 16
CFSM-S-P-07	C	This requirement has been met 15
CFSM-S-C-01	NA	This requirement will be addressed in the later stages of design
CFSM-S-C-02	NA	This requirement will be addressed in the later stages of design
CFSM-S-STR-01	NA	This requirement will be addressed in the later stages of design
CFSM-S-STR-02	NA	This requirement will be addressed in the later stages of design
CFSM-S-STR-03	C	This requirement has been met 10
CFSM-S-STR-04	P	The parts of structure that need regular inspections are accessible but not as easily as for the circular cross-section 10
CFSM-S-STR-05	NA	This requirement will be addressed in the later stages of design
CFSM-S-STR-06	NA	This requirement will be addressed in the later stages of design
CFSM-S-STR-07	P	The fuselage structure will be able to withstand a bending moment of TBD Nm around the pitch axis. However, this accounts only for pressurisation 10
CFSM-S-STR-08	C	This requirement has been met 10

Table 21.5: Compliance matrix, part 5

Requirement	Status	Proof
CFSM-S-STR-09	C	This requirement has been met since necessary space can be allocated 10
CFSM-S-STR-10	C	This requirement has been met since necessary space can be allocated 10
CFSM-S-STR-11	NA	This requirement will be addressed in the later stages of design
CFSM-S-STR-12	NA	This requirement will be addressed in the later stages of design
CFSM-S-STR-13	NA	This requirement will be addressed in the later stages of design
CFSM-S-STR-14	NA	This requirement will be addressed in the later stages of design
CFSM-S-STR-15	NA	This requirement will be addressed in the later stages of design
CFSM-S-STR-16	C	IPS was taken into account in the secondary power estimation in Chapter 16.

22. Conclusions

The purpose of this report was to provide a reasonable proof of the optimal fuselage shape. Additionally, the team was assigned to investigate effects of a more volumetrically efficient shape on the overall aircraft performance.

It was decided that the circular fuselage might be optimal when it comes to dealing with the pressure, however, an elliptical fuselage aircraft features a better L/D ratio. Also it was found that the increase in skin weight resulted in a smaller increase in empty weight than anticipated. This resulted in a direct operating costs which are comparable to each other. This conclusion proves that optimal fuselage shape does not necessarily has to be a circle - ellipse can perform and potentially even better.

It was found that the non-circular fuselage has a rather low impact on the overall performance of the aircraft with a conventional tube and wing planform. Propulsion system is influenced by the effects of the non-circular fuselage, fuel burn is reduced with 5% for our elliptical fuselage design with respect to the A320neo. Evidently an increase in L/D compromises for the increase in structural mass. Stability&control does not experience any major effects either, except for possible change in control surfaces due to changed lift over drag ratio. Operations would generally be carried out in a conventional manner, except that inspections should take place more often. The reason for that is because the chosen new shape and material have not been commercially flown before and uncertainties in reliability are present.

23. Recommendations

In this chapter, general recommendations for future investigations will be presented. For aerodynamic and structural analysis a perfect fit has been chosen for the selected interior which does not take into account the wingbox integration, hence investigation on the effects of including the wingbox is recommended. Since the direct operating costs of the A342-BBB are comparable with the state-of-the-art aircraft, to further increase the performance of the aircraft, structural efficiency can be improved by implementing different planform configurations such as blended-wing-body configurations. A blended-wing-body configuration would also allow for the implementation of engines embedded on top of the fuselage. This should be investigated since it could lead to noise reduction in proximity of airports and improved aerodynamic efficiency. The implementation of different wing configurations such as box-wing, should be investigated to achieve better aerodynamic efficiency. The introduction of bionic structures in the internal cabin, should be considered. Due to their lightweight and recyclable properties, bionic structure could prove to be beneficial in terms of load bearing structures. Recommendations on further investigations required to reach a complete design in terms of structures, aerodynamics, material choice, stability & control and propulsion have already been given in the specific chapters.

One of the main recommendations that goes beyond the scope of this project is the investigation of aircraft with non-pressurised non-circular fuselage shapes for optimal volumetric efficiency and maximised product payload performance. This recommendation implies the development of a cargo and not a passengers aircraft, which considering the current market outlook, might prove to be more beneficial in terms of profitability. In fact, logistics and transport business is of great actuality and predicted to continue expanding in the near future. Evidence for this is provided for instance by Amazon, the biggest world's online retailer, which is momentarily offering fast and free deliveries and trying to reduce costs. To support this aim, Amazon is looking to vertically integrate their whole business and hence presents aircraft manufacturers an opportunity in enhancing cargo transportation.

24. Work Division

In Table 24.1 the work division for this project is presented.

Table 24.1: Work Division

Group Member	**Chapters & Sections**
Y. M. Blommert	Section: 2.2, Chapter 11, 18
R. Bosch	Abstract, Chapter 5, Chapter 17
G. J. A. van den Eijnden	Chapter 10, 10.1, 10.3, 10.5
R. J. P. Giele	Chapter 12, Section 9.2
P. Goergen	Chapter 7, Chapter 16
J. M. Knepper	Chapter 3 & Chapter 5 & Chapter 12
L. Paskauskas	Chapter 1, Chapter 2, Chapter 3, Chapter 4, Chapter 10, Chapter 13, Chapter 19, Chapter 20, Chapter 21, Chapter 22
T. de Reijer	Chapter 4, Chapter 12
F. A. A. S. D. T. Rometsch	Chapter 3, Chapter 8, Chapter 9 Section 9.1, Chapter 10 Sections 10.2, 10.1, 10.3, 10.4, 10.5,10.9, Chapter 23
A. Takken	Chapter 1, Section 10.6
S. van der Velden	Chapter 6, Chapter 14, Chapter 15, Chapter 19, Section 5.2.2, Section 5.2.3, Section 8.2, Section 8.3

Bibliography

[1] M.Sadraey, *Aircraft Design - A Systems Engineering Approach* (Wiley, 2013).

[2] Y. Blommert *et al.*, *Baseline report: challenging fuselage shape and material,* (December 2016).

[3] Airbus, *Global market forecast - mapping demand 2016-2035,* (2016), [Online; accessed 23-November-2016].

[4] Boeing, *Current market outlook 2016-2035,* (2016), [Online; accessed 23-November-2016].

[5] R. Vos, J. Melkert, B. Zandbergen, drs. Z. Berdowski, *et al.*, *AE1222-II - Aerospace Design and Systems Engineering* (TU Delft, September 2016).

[6] I. Maragakis, *Bird population trends and their impact on Aviation safety 1999-2008 ,* (2009), [Online; accessed 24-November-2016].

[7] D. N. M.-M. E. Imon Chakraborty, David Trawick and A. Schneegans, *A requirements-driven methodology for integrating subsystem architecture sizing and analysis into the conceptual aircraft design phase,* (2014).

[8] D. M. D. F. Andrew Valko, Jason Petrella and K. Alves, *Solid-state secondary power distribution,* (2014).

[9] G. M. P. Simões, *Rams analysis of railway track infrastructure,* (2008).

[10] M. Li, *Temperature and moisture effects on composite materials for wind turbine blades,* (2000).

[11] C. de l'Union Europeenne et Parlement Europeen, *Directive 2000/53 ce du parlement europeen et du conseil du 18 septembre 2000 relative aux vehicules hors d'usage,* Journal officiel des Communautes Europeennes (2000), [Online; accessed 11-December-2016].

[12] G. Nilakantan, R. Olliges, R. Su, and S. Nutt, *Reuse strategies for carbon fiber-epoxy prepeg scrap,* (2016) [Online; accessed 12-December-2016].

[13] D.-J. van Heerden and R. Curran, *Value extraction from end-of-life aircraft,* in *Encyclopedia of Aerospace Engineering*, edited by R. Blockley and W. Shyy (John Wiley&Sons, Ltd., 2010) Chap. 306, pp. 716–3726.

[14] T. E. Parliament and the Council of the European Union, *Directive (eu) 2015/1513 the european parliament and the council of the european union,* Official Journal of the European Union (2015), [Online; accessed 14-December-2016].

[15] E. Commission, *Flightpath 2050 - europe's vision for aviation,* (2011), [Online; accessed 15-November-2016].

[16] K. G. Kyprianidis, *Future Aero Engine Designs: An Evolving Vision,* (2011), [Online; accessed 2-December-2016].

[17] ICAO, *ON BOARD A SUSTAINABLE FUTURE - ICAO Environmental Report 2016,* (2016), [Online; accessed 5-December-2016].

[18] EASA, EEA, and Eurocontrol, *European Environmental Aviation Report,* (2016), [Online; accessed 17-November-2016].

[19] S. Dron, *Toward acare 2020: Innovative engine architectures to achieve the environmental goals,* (2008), [Online; accessed 13-December-2016].

[20] L. Leylekian, M. Lebrun, and P. Lempereur, *An overview of aircraft noise reduction technologies,* (2014), [Online; accessed 13-December-2016].

[21] N. G. Diez, A. G. Rao, and J. van Buijtenen, *Conceptual study of counter-rotating turbofan engines,* (2010), [Online; accessed 11-December-2016].

[22] FAA, *Open rotor aeroacoustic technology, non-proprietary report,* (2013), [Online; accessed 1-December-2016].

[23] L. Yong, W. Xunnian, and Z. Dejiu, *Control strategies for aircraft airframe noise reduction,* Chinese Journal of Aeronautics **26**, 249 (2013), [Online; accessed 13-December-2016].

[24] D. E. V. Z. Christopher E. Hughes and J. D. Heidmann, *Aircraft Engine Technology for Green Aviation to Reduce Fuel Burn,* (2013), [Online; accessed 29-Januari-2017].

[25] D.Schiktanz and D.Scholz, *BOX WING FUNDAMENTALS - AN AIRCRAFT DESIGN PERSPECTIVE,* (Deutscher Luft- und Raumfahrtkongress, 2011) [Online; accessed 14-December-2016].

[26] Y. Yang, R. Boom, B. Irion, D.-J. van Heerden, P. Kuiper, and H. de Wit, *Recycling of composite materials,*

Chemical Engineering and Processing - Elsevier **51**, 53 (2011), [Online; accessed 14-December-2016].

[27] S. Das, J. Warren, D. West, and S. M. Schexnayder, *Global carbon fiber composites supply chain competitiveness analysis,* Contract (2016).

[28] M. Princaud, N. Perry, and D. L. Stephane Pompidou, *Recycling of carbon fiber. identification of bases for synergy between recyclers and designers,* (2012) [Online; accessed 11-December-2016].

[29] R. Huang *et al., Energy and emissions saving potential of additive manufacturing: the case of lightweight aircraft components,* Journal of Cleaner Production , 1559 (2016), [Online; accessed 12-December-2016].

[30] S. Dietrich, M. Wunderer, A. Huissel, and M. Zaeh, *A new approach for a flexible powder production for additive manufacturing,* Procedia Manufacturing , 88 (2016), [Online; accessed 12-December-2016].

[31] D. Howe, *Aircraft Conceptual Design Synthesis* (Professional Engineering Publishing, 2009).

[32] E. Torenbeek, *Synthesis of Subsonic Airplane Design* (Delft University Press Kluwer Academic Publisher, 1996) Chap. 3, pp. 68–75.

[33] drs. Z. Berdowski *et al., Survey on standard weights of passengers and baggage* (EASA, May 2009).

[34] I. D. Steenhuizen and D. A. Elham, *AE2111-II Aerospace Design and Systems Engineering Elements II* (TU Delft, September 2016).

[35] M. C. Niu, *Airframe Structural Design - Practical Design Information and Data on Aircraft Structures* (Hong Kong Conmilit Press Ltd., 1988).

[36] I. Sen, *Aircraft fuselage design study -,* (2010), [Online; accessed 23-December-2016].

[37] G. J. Ruijgrok, *Elements of Airplane Performance* (VSSD, 2007) Chap. 8.

[38] EASA, *Certification specifications for large aeroplanes cs-25,* (2007).

[39] *How to find deflection using castigliano theorem,* https://www.youtube.com/watch?v=-HfM-ZyH9Co (2016).

[40] J. Faupel, *Pressure vessels of noncircular cross section (commentary new rules for asme code),* Journal of Pressure Vessel Technology **101**, 255 (1979), [Online; accessed 12-December-2016].

[41] D. P. Raymer, *Aircraft Design : a Conceptual Approach* (Reston, Va.: American Institute of Aeronautics and Astronautics, 2006).

[42] J. T. H. Assler, *Design of aircraft structures under special consideration of ndt,* (2006), [Online; accessed 10-January-2017].

[43] A. mill products, *Alloy 2024 sheet and plate,* (2000), [Online; accessed 16-January-2017].

[44] A. mill products, *Alloy 7075 sheet and plate,* (2000).

[45] V. K. P. Rambabu, N. Eswara Prasad and R. Wanhill, *Aerospace materials and material technologies* (Springer Science Business Media Singapore, 2017).

[46] T. G. M. B. Roger Sauermann, Bernd Friedrich and Bührig-Polaczek, *Development of aluminum-lithium alloys processed by the rheo container process,* Trans Tech Publications (2006).

[47] S. D. A. Baker and D. Kelly, *Composite materials for aircraft structures,* (2004), [Online; accessed 11-January-2017].

[48] I. M. Daniel and O. Ishai, *Engineering Mechanics of Composite Materials* (Oxford University Press, 1994).

[49] A. Composites, *Airex r82 data sheet,* (2011), [Online; accessed 16-January-2017].

[50] A. Composites, *Airex c71 data sheet,* (2011), [Online; accessed 16-January-2017].

[51] Hexcel, *Hexweb cr-paa product data,* (2014), [Online; accessed 18-January-2017].

[52] Hexcel, *Hexweb hrh10 product data,* (2015), [Online; accessed 11-January-2017].

[53] Hexcel, *Hexweb hrp product data,* (2007), [Online; accessed 18-January-2017].

[54] T. Bitzer, *Honeycomb Technology: Materials, Design, Manufacturing, Applications and Testing* (Springer Science and Business Media, 2012).

[55] R. Wanhill, *Aerospace applications of aluminum lithium alloys,* (2014), [Online; accessed 26-January-2017].

[56] H. Thuis, *The development of composite landing gear components for aerospace applications,* (2004), [Online; accessed 27-January-2017].

[57] F. L. Gear, *The art of safe landings,* (2012), [Online; accessed 27-January-2017].

[58] D. D. Simos, *Piano User's guide* (Lissys, Ltd., 2012).

[59] B. E. Launder and D. Spalding, *The numerical computation of turbulent flows,* Computer methods in applied mechanics and engineering **3** (1974).

[60] F. R. Menter, *Two-equation eddy-viscosity turbulence models for engineering applications,* AIAA journal **32** (1994).

[61] F. R. Menter, *Zonal two equation k-turbulence models for aerodynamic flows,* AIAA paper **2906** (1993).

[62] F. R. Menter, *Improved two-equation k-omega turbulence models for aerodynamic flows,* (1992).

[63] H. S.J., *Computational Modelling* (TU Delft, 2016).

[64] H. Hurt, *Aerodynamics for Naval Aviators,* FAA Handbooks Series (Aviation Supplies & Academics, 1965).

[65] L. Bers, *Mathematical aspects of subsonic and transonic gas dynamics,* Surveys in applied mathematics (Wiley, 1958).

[66] J. Moran, *An introduction to theoretical and computational aerodynamics* (John Wiley and Sons, 1984).

[67] J. Roskam, *Airplane Design,* Airplane Design No. dl. 6 (DARcorporation, 2000).

[68] E. C. Polhamus, *A concept of the vortex lift of sharp-edge delta wings based on a leading-edge-suction analogy,* (1966).

[69] F. White, *Viscous fluid flow* (McGraw-Hill, 1974).

[70] S. F. Hoerner, *Fluid-dynamic drag: practical information on aerodynamic drag and hydrodynamic resistance* (Hoerner, S F, 1965).

[71] E. Torenbeek, *BLENDED WING BODY AND ALL-WING AIRLINERS* (EWADE, 2007).

[72] Y. Blommert *et al., Mid-term report: challenging fuselage shape and material,* (December 2016).

[73] S. Farokhi, *Aircraft Propulsion* (Wiley, 2014).

[74] J. Whurr, *Future Civil Aeroengine Architectures & Technologies,* (2013), [Online; accessed 2-December-2016].

[75] E. S. Hendricks and M. T. Tong, *Performance and weight estimates for an advanced open rotor engine,* (2012), [Online; accessed 21-November-2016].

[76] Élodie Roux, *Avions civils à réaction* (Éditions Élodie Roux, 2007).

[77] P. Schlimming, *Counter rotating fans - an aircraft propulsion for the future?* Journal of Thermal Science (2003).

[78] J. Roskam, *Airplane Design, Part VII: Determination of Stability, Control and Performance Characteristics,* Airplane Design (DARcorporation, 2002).

[79] C. L. Nickol and L. A. McCullers, *Hybrid Wing Body Configuration System Studies* (NASA, 2009).

[80] C. E. Hughes, *Nasa collaborative research on the ultra high bypass engine cycle and potential benefits for noise, performance, and emissions,* (2009), [Online; accessed 21-November-2016].

[81] A. P. Plas, M. A. Sargeant, V. Madani, D. Crichton, E. M. Greitzer, T. P. Hynes, and C. A. Hall, *Performance of a Boundary Layer Ingesting (BLI) Propulsion System,* (2007), [Online; accessed 12-December-2016].

[82] D. T. Imon Chakraborty, David Jackson and D. N. Mavris, *Development of a sizing and analysis tool for electrohydrostatic and electromechanical actuators for the more electric aircraft,* AIAA (2013).

[83] I. D. Steenhuizen, *AE2101: Aerospace Design and Systems Engineering Elements II, Wing Design Part 4 lecture slides* (TU Delft, 2013).

[84] A. Z. Nour El-Din Safwat, M. A. El-Dakroury, *The evolution of aircraft data networks,* International Journal of Computer Applications **94** (2014).

[85] R. E. S. Eric Fleischman and N. Multari, *Networked local area networks in aircraft: Safety, security, and certification issues, and initial acceptance criteria (phases 1 and 2),* (2008).

[86] J. Roskam, *Airplane Design, Part VIII: Airplane Cost Estimation: Design, Development, Manufacturing and Operating* (DAR corporation, 2002).

[87] E. Obert, *Aerodynamic Design of Transport Aircraft* (IOS press, 2009).

[88] A. Fillipone, *Advanced Aircraft Flight Peformance* (Cambridge University Press, 2012).

[89] P. Belobaba, *Airline Operating Costs* (Istanbul Technical University, March 2014).

[90] W. Gibson, *Airline finance and aircraft financial evaluation:evidence from the field,* (2005), [Online; accessed 29-Januari-2017].

[91] B. Vasigh *et al., Foundations of Airline Finance: Methodology and Practice* (Ashgate Publishing Group, 2010).